Automation of Jet function Calculations in Soft-Collinear Effective Theory

Dissertation

zur Erlangung des akademischen Grades eines Doktors
der Naturwissenschaften

vorgelegt von

M.Sc. Kevin Marc Brune

eingereicht bei der Naturwissenschaftlich-Technischen Fakultät
der Universität Siegen

Siegen
September 2022

Betreuer und erster Gutachter

Prof. Dr. Guido Bell

Universität Siegen

Zweiter Gutachter

PD Dr. Tobias Huber

Universität Siegen

Weitere Mitglieder der Promotionskommission

Prof. Dr. Markus Cristinziani

Universität Siegen

und

PD Dr. Matthias Kleinmann

Universität Siegen

Tag der mündlichen Prüfung

30.11.2022

Abstract

The occurrence of large Sudakov logarithms, associated with soft and collinear radiation, in the calculation of cross sections in Quantum Chromodynamics (QCD) spoils the perturbative expansion in the strong coupling constant. This breakdown of perturbative QCD is a bottleneck for achieving precise predictions for a large class of observables at the Large Hadron Collider (LHC). Therefore, these logarithms must be resummed to all orders to preserve the predictive power of perturbation theory. A convenient way to achieve this resummation uses methods from effective field theory. Currently, most observables are calculated analytically case-by-case, but for some observables a numerical approach is the only feasible way.

This thesis is focused on developing a formalism that automates the calculation of two-loop jet functions, which are an essential ingredient for the resummation of Sudakov logarithms to next-to-next-to-leading logarithmic (NNLL) accuracy in Soft-Collinear Effective Theory (SCET). In particular, we developed a systematic strategy based on sector decomposition, selector functions, non-linear transformations, and suitable phase-space parametrisations to evaluate the quark and gluon jet functions to next-to-next-to-leading order (NNLO) in perturbation theory. The strategy allows one to completely factorise all the phase-space singularities associated with the jet functions in terms of master formulae. We furthermore transformed the master formulae into a computational parametrisation to improve the convergence of the numerical routines and to obtain reliable uncertainty estimates. The master formulae were finally implemented into the publicly available code `pySecDec`, which performs the expansion in the dimensional and rapidity regulators and which provides an interface to the `CUBA` library for the numerical integrations.

The novel framework allows us to compute two-loop results for quark and gluon jet function for a broad class of collider observables. We have verified our framework against the known results for thrust and obtained new results for several e^+e^- event-shape variables both for SCET_I and SCET_II.

This thesis represents the next step towards a complete automatic resummation tool for generic collider observables to NNLL accuracy in SCET.

Zusammenfassung

Bei der Berechnung von Wirkungsquerschnitten in der Quantenchromodynamik (QCD) treten große Sudakov-Logarithmen auf, welche mit softer und kollinearer Strahlung verbunden sind. Diese Logarithmen führen zu einem Zusammenbruch der Störungsreihe in der starken Kopplungskonstante. Dieses Scheitern der perturbativen QCD ist ein Engpass für das Erreichen präziser Vorhersagen für eine große Klasse von Observablen am Large Hadron Collider (LHC). Daher müssen diese Logarithmen auf alle Ordnungen zusammengefasst werden, um die Vorhersagekraft der Störungstheorie zu erhalten. Ein geeigneter Weg, diese Resummierung zu erreichen, sind Methoden aus der effektiven Feldtheorie. Gegenwärtig, werden die meisten Observablen explizit analytisch berechnet, aber für einige Observablen ist ein numerischer Ansatz der einzig mögliche Weg.

Diese Arbeit konzentriert sich auf die Entwicklung eines Formalismus, der die Berechnung von Jetfunktionen automatisiert, die ein wesentlicher Bestandteil für die Resummierung von Sudakov-Logarithmen mit nächst-zu-nächst-zu-führender logarithmischen (NNLL) Genauigkeit in der Soft-Collinear Effective Theory (SCET) sind. Insbesondere haben wir eine systematische Strategie entwickelt, die auf Sektorenzerlegung, Selektorfunktionen, nichtlinearen Transformationen und geeigneten Phasenraum-Parametrisierungen basiert, um die Quark- und Gluonen-Jetfunktionen in der Störungstheorie bis zur nächst-zu-nächst-zu-führender Ordnung auszuwerten. Diese Strategie ermöglicht es, alle mit den Jetfunktionen verbundenen Phasenraum-Singularitäten vollständig in Form von Masterformeln zu faktorisieren. Darüber hinaus haben wir die Masterformeln in eine numerisch günstigere Parametrisierung umgewandelt, um die Konvergenz der numerischen Routinen zu verbessern und zuverlässige Fehlerabschätzungen zu erhalten. Die Masterformeln wurden schließlich in den öffentlich verfügbaren Code `pySecDec` implementiert, der die Expansion in Dimensionalitäts- und Rapiditätsregulatoren durchführt und eine Schnittstelle zur `CUBA` Bibliothek für die numerischen Integrationen bietet.

Das neuartige Rahmenwerk ermöglicht die Berechnung von Zweischleifenergebnissen für Quark- und Gluonen-Jetfunktionen für eine breite Klasse von Observablen an Teilchenbeschleunigern. Wir haben unser Programm durch die Berechnung mit dem

bekannten Ergebnis für Thrust verifiziert und neue Ergebnisse für mehrere e^+e^- Event-shape Variablen sowohl für $\mathrm{SCET_I}$ als auch für $\mathrm{SCET_{II}}$ erhalten.

Diese Arbeit ist der nächste Schritt auf dem Weg zu einem vollständigen automatischen Resumierungswerkzeug für generische Observablen an Teilchenbeschleunigern mit NNLL-Genauigkeit in SCET.

Contents

Chapter 1

Introduction

This year we celebrated the 10th anniversary of the discovery of the Higgs boson [1, 2] at the Large Hadron Collider (LHC) at CERN near Geneva. Besides the discovery of the Higgs boson, the LHC aims at searching for New Physics, from Supersymmetry to Dark Matter, and new sources of CP-violation. After gathering data during the successful LHC Runs 1 and Run 2 [3] we are currently right at the start of the next LHC Run 3 [4]. This will result in more data at a higher luminosity and higher collision energy until the LHC will shutdown for its High Luminosity upgrade [5] in 2029 for both precision measurements of Higgs properties and the continued search for New Physics.

Currently, the Standard Model (SM) is our best attempt to describe the interactions and forces we observe in collider experiments like the LHC. The SM is a gauge theory of spin-$\frac{1}{2}$ fermions, a spin-0 Higgs boson, and spin-1 gauge bosons which mediate the interactions according to the gauge group $\mathrm{SU}(3)_C \times \mathrm{SU}(2)_L \times \mathrm{U}(1)_Y$. The $\mathrm{SU}(2)_L \times \mathrm{U}(1)_Y$ subgroup describes the electroweak interactions, and the $\mathrm{SU}(3)_C$ represents Quantum Chromodynamics (QCD), the relevant gauge group on how we model the strong interactions.

While particles that interact solely via the electroweak interaction like the electron or muon can be directly detected in the experiments, this is not true in QCD. Instead we observe that particles that are charged under the $\mathrm{SU}(3)_C$ gauge group are never found as asymptotic states in nature, but only colour-singlet states like mesons and baryons. This behaviour of QCD was explained by the introduction of asymptotic freedom [6, 7]. Asymptotic freedom can be considered as the opposite of screening in electromagnetism; the strong force gets weaker at higher energies and stronger as particles are further apart if the energy decreases. However, the coupling strength

increases until we are left with colour-neutral bound states composed of colour charged objects.

At a proton-proton (pp) collider like the LHC, it is crucial to understand the primary force that governs the collisions, the strong interaction, because, without precise knowledge of the strong dynamics, it is neither possible to make accurate measurements of the properties of the Higgs boson, nor to find any signs of potential New Physics signatures.

From the theory side, we want to predict or confirm experimental observations. The essential tool for these calculations in Quantum Field Theory is perturbation theory, which handles all interactions as small perturbations around the free-field theory. This approach breaks down when the interaction strength is too large for the interactions to be considered as perturbations around the free field. In the case of QCD, the energy scale at which the perturbative regime breaks down and the non-perturbative regime overshadows it is at $\sim 1\,\text{GeV}$, far below the current LHC center-of-mass energy of 13.6 TeV. We could expect that perturbative QCD has no predictivity as we can only describe the interactions of weakly coupled systems of colour-charged quarks and gluons. Finally, we only measure colour-neutral mesons and baryons, or collimated collections of particles known as jets, in the detector. The transition between the partonic regime of colour-charged particles and the hadronic regime of colour-neutral mesons and baryons is precisely the transition between the perturbative and the non-perturbative regime, where no model-independent description exists.

However, QCD has a way out of this dilemma because it tends to factorize at high center-of-mass energies. This means that the cross section for hadronic collisions can be decomposed into a partonic cross section, which we can calculate within perturbation theory, convoluted with universal parton distribution functions. In the end, it is equipped with some hadronisation model to arrive at a purely hadronic final state. Technically, QCD factorisation has only been proven for a few observables [8]; however, it is assumed to hold for a larger class under specific conditions [9].

Sadly, it is not as simple as it appears at first glance. It is possible to calculate the partonic cross section at high energies in QCD. However, the coupling is still comparatively large; for example, the world average for the strong coupling is $\alpha_s(M_Z^2) \sim 0.118$ while $\alpha_{\text{EM}} \sim 0.008$, thus the convergence rate of the perturbative series is much smaller. Furthermore, in some regions of phase space, the perturbative series breaks down entirely due to the radiation of soft or collinear particles. This break-down of perturbation theory manifests itself in form of logarithms of small τ, where τ represents

a generic measurement scale. It takes the form of Sudakov double logarithms $\alpha_s^n \ln^{2n} \tau$ at n-loop order and additional lower logarithmic terms. If τ becomes small enough, the value of the logarithm diverges, and the product of the logarithm and the small perturbation parameter α_s tend to diverge. This effect ripples through the complete perturbative series, thus spoiling its convergence.

In the regions of phase space where the perturbative series converges slowly, the computation of higher loop orders can be used to address this problem. However, this comes at the cost of an increasing number of complicated Feynman diagrams. In the regions where the perturbative series breaks down, the large logarithms must be resummed to *all* orders in perturbation theory. Finally, the two calculations must be matched to arrive at a physical cross section. These procedures are highly complex, and computer-aided tools are indispensable for them.

The increase of loop order of any perturbative computation can be performed by different tools that automate the calculation of next-to-leading order (NLO) corrections [10–17]. They are often combined with Monte Carlo event generators [18–22] to include parton showers to model collinear and soft QCD radiation. Additionally, they are interlaced with some hadronisation model. Finally, the NLO calculation and parton showers are matched [23, 24] to avoid double counting real emissions.

At first glance, this strategy sounds relatively straightforward; however, there are still challenges. The matching between fixed-order calculations and parton showers is a non-trivial procedure. The probabilistic nature of the showers makes it hard to resum more than the leading logarithm (LL) in the Sudakov region. Though progress is being made in this direction [25] no shower has yet achieved full next-to-leading logarithmic (NLL) accuracy for generic collider observables.

The inclusion of higher logarithmic accuracy is usually addressed with analytic resummation methods, which are generally implemented on a case-by-case basis for inclusive observables, like e^+e^- event-shapes. Some computational tools which automate the resummation of generic observables are `CAESAR` [26] for NLL resummation and `ARES` [27] for resummation to NNLL accuracy. Both tools use the so-called direct QCD framework [28] to resum the large logarithms. Here the soft and collinear emissions are described by universal splitting functions, which can be iterated to resum logarithms to all orders.

Instead of using the direct QCD framework, effective field theories (EFT) provide a different framework of handling large logarithms. In EFTs, systematic scale separations ultimately lead to large logarithms; however, they are taken as a justification to further

factorise the partonic cross section into different contributions that describe the physics at the different scales. Therefore we expect EFTs to become better approximations of the full theory in the region where the Sudakov problem worsens.

One EFT which is able to resum Sudakov logarithms in QCD is Soft-Collinear Effective Theory (SCET) [29–32], whose different degrees of freedom are soft and collinear modes, which give rise to large logarithms. We can derive all order factorisation theorems within SCET, which factorise the partonic cross section into contributions that describe only the hard, soft, and collinear dynamics. The connection between full QCD and SCET is then performed by matching between the two theories.

The resummation of Sudakov logarithm in SCET proceeds in the typical EFT framework via the renormalisation group flow. In perturbation theory, the different contributions in the factorisation theorem are evaluated at their natural scale, where there are no large logarithms. Then they are evolved to some common scale, and the logarithms are resummed in the renormalisation group evolution kernel. This procedure has achieved $\mathrm{N^3LL}$ and $\mathrm{N^4LL}$ resummation accuracy for some observable [33–40].

Even though SCET has proven to be able to resum these large logarithms to high accuracy, no complete automated setup exists for calculating all factorisation ingredients. The hard contributions are calculated via the matching relation to QCD. They contain the underlying partonic hard-scattering diagrams, prior to the collinear branching and soft radiation encoded in the jet and soft functions. On the other hand, the soft and collinear contributions depend on the measured observable. In the case of the soft contributions there exists an automated approach `SoftSERVE` [41–43], which provides the necessary ingredients for NNLL[1] resummation. In the case of the collinear contribution, automated tools exist only for the computation of the NLL ingredients [44, 45].

In this thesis, we follow the ideas proposed for the automation of the soft functions and apply them to the final-state collinear contribution to arrive at a similar setup that allows the calculation of the necessary resummation ingredients for the collinear sector. Compared to the soft functions, the jet functions have a more complicated matrix element and more involved singularity structure at NNLO because of the three-particle phase space. For the first time we present an automated approach to calculate the two-loop quark and gluon jet functions. This framework has been validated against the known results from the literature, and we obtain new results for several e^+e^- event-shapes [46]. In parallel a similar setup has been developed for the initial-state collinear

[1] And NNLL′, which involves the two-loop matching correction.

radiation, the beam functions [47, 48].

The thesis is structured as follows, in section 2 we first give a short review of the Standard Model and perturbative QCD, followed by a review of event-shapes as a brief introduction to the observables we have in mind in our computation in section 3. In section 4 we take a closer look into the SCET approach to resummation. In section 5 we determine the necessary ingredients for NNLL resummation and outline the general strategy of our approach, followed by a detailed discussion about the underlying matrix-element calculations and suitable phase-space parametrisations at both NLO and NNLO in section 6. In section 7 we outline the setup for the numerical integration and give insight into the technical difficulties of our approach. Section 8 lists results calculated with our approach. Finally, in the appendix A, we collect all required anomalous dimensions. We state the decomposition of the collinear splitting functions in App.B, list the explicit master formulae in our parametrisation in App.C, and provide the necessary steps to completely disentangle the overlapping singularities in App.D.

Chapter 2

Brief introduction to the Standard Model and perturbative QCD

In this chapter, we briefly introduce the Standard Model of particle physics and introduce QCD, in particular, lay out the basics of perturbative QCD.

2.1 The Standard Model

The Standard Model (SM) of particle physics is the theory that successfully describes three of the four fundamental interactions known in nature: electromagnetic, strong, and weak interactions. However, it is apparent that the SM cannot be the final theory of nature.[1] In the following, we introduce the main features of the SM without any intent to give a complete and self-contained introduction to the subject. For a more detailed introduction to the SM, we refer to standard textbooks (e.g [50], [51]).

The interactions within the SM are described by gauge symmetries, where quantum fields transform locally under the gauge group elements. To maintain gauge symmetry, two field configurations at different space-times must be connected by covariant derivatives, which contain the gauge fields as minimal couplings. The interaction between field configurations is thus propagated through the gauge fields. The gauge group of the SM is

$$\mathcal{G}_{\mathrm{SM}} = \mathrm{SU}(3)_C \times \mathrm{SU}(2)_L \times \mathrm{U}(1)_Y, \tag{2.1.1}$$

In eq. (2.1.1), $\mathrm{SU}(3)_C$ is the colour symmetry group of the strong interactions with coupling constant g_s; this theory of QCD involves three colour charges and has eight

[1] As an example, the SM is not able to incorporate gravity, dark matter, dark energy etc [49].

mediators, the gluons. The $\mathrm{SU}(2)_L$ is the weak isospin group with coupling constant g and involves three gauge fields, W^a_μ. The $\mathrm{U}(1)_Y$, in eq. (2.1.1), is the group of the weak hypercharge. The gauge group is mediated by one gauge boson B_μ, with coupling g'.

In the unbroken gauge group of the SM, the theory consists of massless fields. The gauge group of the SM is spontaneously broken by the Higgs potential to

$$\mathcal{G}_{\mathrm{SM}}^{\mathrm{SSB}} = \mathrm{SU}(3)_C \times \mathrm{U}(1)_Q. \tag{2.1.2}$$

As a result of spontaneous symmetry breaking (SSB), the Higgs field acquires a non-zero vacuum expectation value and the fermions obtain masses through the Yukawa couplings to the Higgs field. The weak gauge fields become massive after SSB where massless Goldstone bosons are absorbed by the gauge fields to give the mass, which appear as a result of the SSB of the Higgs field. The massive gauge bosons in the broken phase are the charged $W^\pm$ and the neutral Z^0. The massless photon is the gauge boson of the unbroken $\mathrm{U}(1)_Q$ of electromagnetism. The massless photon field is constructed as linear combinations of the W^3_μ and B_μ fields. Thus, the coupling constant of $\mathrm{U}(1)_Q$ is given as $e = gg'/\sqrt{g^2 + g'^2}$.

The particle content of the SM is shown in figure 2.1.1, including their mass, charge and spin. In the SM there are six types of quarks: up (u), down (d), strange (s), charm (c), bottom (b), top (t); and six types of leptons: electron (e), muon (μ), tau (τ) and their respective neutrinos (ν_e,ν_μ, ν_τ). Quarks and leptons are organised in three families, where the left-handed fields

$$Q^i_L \equiv \left(\begin{pmatrix} u_L \\ d_L \end{pmatrix}, \begin{pmatrix} c_L \\ s_L \end{pmatrix}, \begin{pmatrix} t_L \\ b_L \end{pmatrix} \right),$$
$$L^i_L \equiv \left(\begin{pmatrix} \nu_{eL} \\ e_L \end{pmatrix}, \begin{pmatrix} \nu_{\mu L} \\ \mu_L \end{pmatrix}, \begin{pmatrix} \nu_{\tau L} \\ \tau_L \end{pmatrix} \right)$$

are $\mathrm{SU}(2)_L$ doublets and the right-handed fields

$$e^i_R \equiv \{e_R, \mu_R, \tau_R\},$$
$$u^i_R \equiv \{u_R, c_R, t_R\}, \quad d^i_R \equiv \{d_R, s_R, b_R\},$$

are $\mathrm{SU}(2)_L$ singlets. Under $\mathrm{SU}(3)_C$, leptons are colour singlets while quarks, which have colour charge, are $\mathrm{SU}(3)_C$ triplets. Besides the twelve fermions, there exists four gauge bosons that mediate the different interactions. The final piece of the SM is the

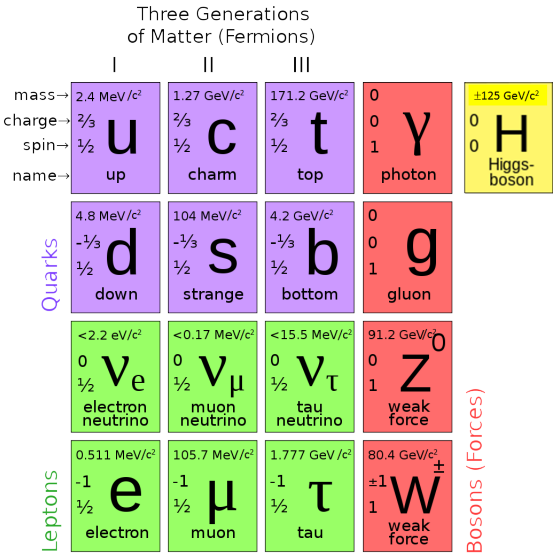

Figure 2.1.1: Elementary particles of the SM. Image from ref. [52]

Higgs scalar field , which is an $SU(2)$ doublet and has a non-zero vacuum expectation value

$$\langle H \rangle = \frac{1}{\sqrt{2}} \begin{pmatrix} 0 \\ v \end{pmatrix}. \tag{2.1.3}$$

The SM Lagrangian is the most general Lagrangian which contains all terms that fulfill the conditions of field content, the gauge group $\mathcal{G}_{\text{SM}}$ and renormalizability.[2] Schematically, it reads

$$\mathcal{L}_{\text{SM}} = \mathcal{L}_{\text{QCD}} + \mathcal{L}_{\text{EW}} + \mathcal{L}_{\text{Yukawa}} + \mathcal{L}_{\text{Higgs}}. \tag{2.1.4}$$

The explicit form of $\mathcal{L}_{\text{QCD}}$ is

$$\mathcal{L}_{\text{QCD}} = \sum_{\psi} \bar{\psi} \left(i \not{D} - m_{\psi} \right) \psi - \frac{1}{2} \text{Tr} \left\{ \tilde{G}_{\mu\nu} \tilde{G}^{\mu\nu} \right\}, \tag{2.1.5}$$

with the covariant derivative and field strength tensor

$$\begin{aligned} D_{\mu}\psi &= (\partial_{\mu} - i g_s \tilde{A}_{\mu})\psi, \\ \tilde{G}_{\mu\nu} &= \partial_{\mu}\tilde{A}_{\nu} - \partial_{\nu}\tilde{A}_{\mu} + i g_s \left[\tilde{A}_{\mu}, \tilde{A}_{\nu} \right] = \frac{i}{g_s} \left[D_{\mu}, D_{\nu} \right]. \end{aligned}$$

[2] Dropping the renormalizability one obtains a more general Lagrangian, called the Standard Model Effective Field Theory(SMEFT) Lagrangian [53].

Here we abbreviate

$$\tilde{A}_{\mu(\nu)} = A^a_{\mu(\nu)} \frac{\lambda_a}{2},$$

where λ_a are the Gell-Mann matrices. In eq. (2.1.5) the sum runs over the different quark flavours. Additionally, we included the mass term of the quarks in $\mathcal{L}_{\text{QCD}}$ to separate it completely from the rest of the SM Lagrangian. Technically, the mass term is part of the Yukawa Lagrangian. The explicit forms of the electroweak ($\mathcal{L}_{\text{EW}}$), Yukawa ($\mathcal{L}_{\text{Yukawa}}$) and Higgs-Lagrangian ($\mathcal{L}_{\text{Higgs}}$) are not used in this work and thus we refer to [54] for their explicit forms.

2.2 Perturbative QCD

Our modern understanding of the high-energy behavior of the strong interactions was conceived with the idea of the parton model in the late 1960s [55–57]. In the early 1970's it was born with the introduction of asymptotic freedom [6, 7]. From there, it became clear that hadrons are made up of smaller particles, named partons, which are nothing but the excitations of quantum fields which occur in the theory of quark and gluons interacting via strong coupling. Asymptotic freedom allows one to consider quarks as free quanta at short distances and over short times, thus connecting with the idea of a parton as a non-interacting constituent of a hadron on these scales. In high energy processes involving large momentum transfer, one separates (factorises) the process into one part, which involves the hard interactions and which is computable using perturbative QCD (pQCD), and a second part which involves non-perturbative physics [8]. The non-perturbative part mostly involves parton dynamics at low scales where the perturbative approach fails. These non-perturbative parts are encoded in parton distribution functions which describe the probability for finding a parton with a certain energy fraction of the proton within the proton. We refer to [58–60] for further information on this topic.

Before revisiting $\mathcal{L}_{\text{QCD}}$ in eq. (2.1.5), we perform an excursion into group theory and summarise useful relations satisfied by the fundamental and adjoint representation matrices of SU(N) [61]. The associated algebra of the SU(N) Lie Group is the $\mathfrak{su}(N)$ Lie Algebra. The N^2-1 generators in the fundamental representation of $\mathfrak{su}(N)$, labeled by T^a, serve as a basis for the set of traceless Hermitian $N \times N$ matrices. The Lie algebra is defined through its commutation relations:

$$\left[T^a, T^b\right] = i f_{abc} T^c, \quad a, b, c = 1, 2, \ldots, N^2 - 1, \tag{2.2.1}$$

where f_{abc} are known as structure constants. In this work, we employ the following normalisation convention for the generators in the fundamental representation

$$\mathrm{Tr}\{T^a T^b\} = \frac{1}{2}\delta_{ab}. \tag{2.2.2}$$

In this convention, the structure constants are totally antisymmetric under the exchange of any pair of indices. We define the quadratic Casimir $C_2(R)$ by

$$T_R^a T_R^a = C_2(R)\mathbb{I}, \tag{2.2.3}$$

where R is the appropriate representation and $\mathbb{I}$ the corresponding identity matrix. Starting from eq. (2.2.3) we define the following quadratic Casimirs for the fundamental and adjoint representation

$$\begin{aligned} C_F &\equiv C_2(\text{fund.}) = \frac{N^2-1}{2N}, \\ C_A &\equiv C_2(\text{adj.}) = N. \end{aligned}$$

The main relations we will use in following chapters are

$$\begin{aligned} \mathrm{Tr}\{T^a T^b\} &= T_F \delta_{ab}, \\ (T^a T^a)_{ij} &= C_F \delta_{ij}, \\ f^{acd} f^{bcd} &= C_A \delta_{ab}, \end{aligned} \tag{2.2.4}$$

with $T_F = \frac{1}{2}$. In particular, we find for the SU(3) group the following quadratic Casimirs $C_F = \frac{4}{3}$ and $C_A = 3$.

Now that we have familiarised ourselves with the SU(N), we will derive the explicit form of $\mathcal{L}_{\mathrm{QCD}}$ in eq. (2.1.5). In the previous section, we have stated that the only particles charged under colour are the quarks and gluons. Quarks are described by a Dirac spinor field $\psi_i(x)$ that transforms under the fundamental representation of SU(3)

$$\psi_i(x) \underset{U}{\longrightarrow} U_{ij}\psi_j(x), \qquad U \in \mathrm{SU}(3). \tag{2.2.5}$$

In the following we will suppress the indices i, j for the fundamental representation and write $\psi(x) \to U\psi(x)$ to shorten the notation. Thus we are able to transform the antiquark field as $\bar{\psi}(x) \to \bar{\psi}(x)U^\dagger$, with $UU^\dagger = 1$. The gluons are represented by $\tilde{A}_\mu(x)$

that transform under the adjoint representation of SU(3),

$$\tilde{A}_\mu(x) \underset{U}{\longrightarrow} U\tilde{A}_\mu(x)U^\dagger. \tag{2.2.6}$$

In eqs. (2.2.5) and (2.2.6) we have assumed that U is a global colour rotation, which implies conservation of the total colour charge. Therefore, we can ask to what degree this assumption has already determined the QCD Lagrangian's form. The operators that can appear in it should be polynomials of the fields and derivatives, with a total mass dimension of four. In addition, the operators must be Lorentz scalars to preserve Lorentz invariance. Thus we have the following operators

$$\mathcal{L}_{\text{QCD}} \supset \bar{\psi} i\partial\!\!\!/ \psi, \quad \bar{\psi}\tilde{A}\!\!\!/\psi, \quad \text{Tr}\left[\partial^n \tilde{A}^{4-n}\right], \tag{2.2.7}$$

where the last expression represents any Lorentz scalar contraction of derivatives and gluon fields. These operators can appear with arbitrary coefficients. We could set eliminate two operators by choosing a normalisation for the quark and gluon fields. The resulting Lagrangian is however still undetermined, especially in the gluon sector.

The dynamics of QCD follows instead from elevating eqs. (2.2.5) and (2.2.6) to a local gauge symmetry under a transformation $U(x)$,

$$\psi(x) \underset{U(x)}{\longrightarrow} U(x)\psi(x), \quad \tilde{A}_\mu(x) \underset{U(x)}{\longrightarrow} U(x)\tilde{A}_\mu(x)U^\dagger(x) + U(x)\left[\frac{i}{g_s}\partial_\mu U^\dagger(x)\right], \tag{2.2.8}$$

where g_s in the last term is the gauge coupling parameter associated with QCD. This transformation behaviour of the gluon field allows us to write down the covariant derivative in the form defined in eq. (2.1.5).

The covariant derivative then satisfies

$$D_\mu \underset{U(x)}{\longrightarrow} U(x)D_\mu(x)U^\dagger(x). \tag{2.2.9}$$

D_μ is the only possible combination in which derivatives and the gauge field could appear in the Lagrangian to make it gauge invariant. Therefore, this requirement uniquely fixes all terms in the Lagrangian which act on quark fields such that

$$\mathcal{L}_{\text{QCD}} \supset \bar{\psi} iD\!\!\!/\psi. \tag{2.2.10}$$

Additionally, the only other operators built out of D_μ that may appear in the remaining

terms of the Lagrangian are those that satisfy

$$\mathcal{O}(D_\mu)f(x) = [\mathcal{O}(D_\mu)]\, f(x), \tag{2.2.11}$$

for any test function $f(x)$, the brackets on the LHS of the equation denote the commutator. To identify these operators in a simple way, we rewrite all derivatives of the gauge field as commutators acting on test functions,

$$\left[\partial_\mu \tilde{A}_\nu\right] f(x) = \partial_\mu \left[\tilde{A}_\nu f(x)\right] - \tilde{A}_\nu \partial_\mu f(x) = \left[\partial_\mu, \tilde{A}_\nu\right] f(x). \tag{2.2.12}$$

By demanding gauge invariance, it follows that all operators $\mathcal{O}(D_\mu)$ that satisfy eq. (2.2.11) depend on D_μ only through the field strength tensor $\tilde{G}_{\mu\nu}$ defined in eq. (2.1.5). Thus, at mass dimension four, we find exactly three operators that are invariant under local gauge transformations

$$\mathcal{L} = \bar{\psi} i \not{D} \psi - \frac{1}{2} \mathrm{Tr}\left\{\tilde{G}_{\mu\nu}\tilde{G}^{\mu\nu}\right\} + \theta_{QCD} \frac{g_s^2}{32\pi^2} \epsilon_{\mu\nu\rho\sigma} G^{a,\rho\sigma} G^{a,\mu\nu}. \tag{2.2.13}$$

To match the QCD Lagrangian in eq. (2.1.5), we note two modifications to the Lagrangian stated in eq. (2.2.13). The first modification is that quarks carry an additional quantum number called flavour, which is conserved in QCD. The different flavoured quarks are distinguishable by their respected masses m_ψ; this can be seen in figure 2.1.1. The masses enter the QCD Lagrangian as the dimensionful coefficients of the $\bar{\psi}\psi$ operator which is not gauge invarient, and is induced in the SM via the Higgs mechanism. The second modification concerns the third term in eq. (2.2.13). The coefficient of this term introduces an additional free parameter θ_{QCD} into the theory, with a conventional factor pulled out. However, it is proportional to a total derivative; thus, it never contributes to perturbative computations because the fields are assumed to vanish asymptotically at infinity. It could contribute to non-perturbative calculations where the fields do not vanish on the boundary. The phenomenological significance in these cases is that this term explicitly breaks the CP symmetry that is otherwise conserved in QCD. Experimental searches for permanent electric dipole moments of neutrons and mercury atoms [62, 63] set strong limits on the strong CP angle, with $|\theta_{QCD}| \leq 10^{-11}$. Theoretically, there has been much speculation as to why θ_{QCD} should be zero [64].

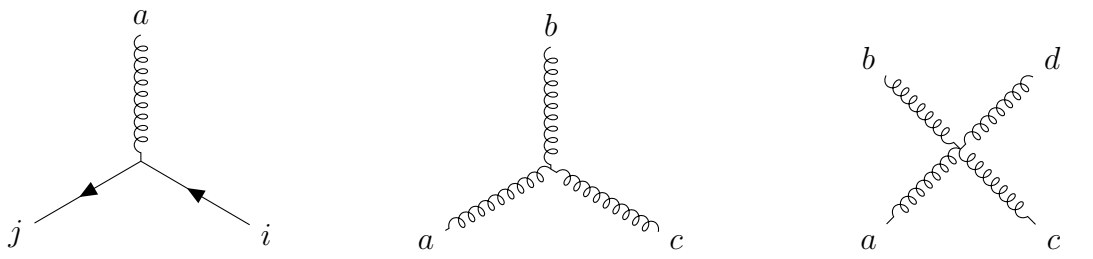

(a) $g_s\,(T^a)_{ij}$ **(b)** $g_s f^{abc}$ **(c)** $g_s^2 f^{abe} f^{cde}$+perm.

Figure 2.2.1: Elementary interaction vertices of QCD, their colour structure, and scaling with g_s. The Lorentz and spin structure of the vertices is suppressed but can be taken, for example, from [51]. In general gauges, additional ghost interactions need to be added.

After performing the two modifications to eq. (2.2.13) we arrive at

$$\mathcal{L}_{QCD} = \sum_{\psi} \bar{\psi} \left(i \not{D} - m_{\psi} \right) \psi - \frac{1}{2} \mathrm{Tr} \Big\{ \tilde{G}_{\mu\nu} \tilde{G}^{\mu\nu} \Big\} \tag{2.2.14}$$

which is the same as eq. (2.1.5). Now that we have derived the QCD Lagrangian, we state the QCD Feynman rules used throughout this work.

The interaction vertices that arise from the Lagrangian are illustrated in figure 2.2.1. To write down the propagator for the gluon, we first note the following: In a path integral over the gluon field $\tilde{A}_\mu$, many configurations only differ by pure gauge transformations, which leave the action unchanged. This overcounting of physical degrees of freedom cancels between numerator and denominator in the normalized partition function when calculating gauge-invariant quantities. However, this cancellation is also required for gauge-dependent quantities like the gluon propagator in perturbative computations. This can be achieved by inserting a gauge constraint $\delta \left[G(\tilde{A}_\mu) \right]$, with a suitable Jacobian, into the functional integral over the gluon field, where G is some functional of the field strength. In the Faddeev-Popov procedure [65], the Jacobian is represented as a functional integral over the Grassmann-valued fields $c^a(x)$, called ghosts. This allows the gauge constraint to be written as a simple modification of the action, leading to additional Feynman rules that fix the overcounting of degrees of freedom in the sum over diagrams at any given order in the perturbation theory. The precise definition of the ghost action depends on $G(\tilde{A}_\mu)$. Another way to fix the overcounting issue is to work in an axial gauge [66]. In this class of gauges, where one picks some reference vector r^μ and imposes $G(\tilde{A}_\mu) = r \cdot \tilde{A} = 0$, the ghosts do not propagate and also decouple from the gluon field. This, however, comes at the cost of explicitly breaking Lorentz invariance by r^μ. However, Lorentz invariance is restored

after calculating physical observables because the dependence on the reference vector drops out. In this thesis, we will work explicitly in the light-cone gauge [67] which is a special case of the axial gauge with $r^2 = 0$. In light-cone gauge, there are only two physical polarizations of the gluon: those transverse to the momentum and the gauge direction. Since only two polarizations are being propagated, we do not need ghosts to cancel the unphysical polarizations, which explains why they decouple [68]. In this gauge, the gluon propagator is given by

$$\nu, A \underset{p}{\sim\!\sim\!\sim} \mu, B \; = \frac{i}{p^2 + i\epsilon}\left(-g^{\mu\nu} + \frac{r^\mu p^\nu + r^\nu p^\mu}{rp}\right)\delta^{AB}, \tag{2.2.15}$$

where p is the momentum label, A, B are colour indices, μ, ν are Lorentz indices, and r^μ is the lightlike direction. The propagators for coloured fermions are the same as for QED but with an additional δ^{ij} factors, where i, j refer to fundamental colour indices. In this thesis, we work exclusively in the limit where we can assume the quarks to be massless. Therefore, the quark propagator is given by

$$j \xrightarrow[p]{} i \; = \frac{i\delta^{ij}}{p^2 + i\epsilon}\not{p}. \tag{2.2.16}$$

Chapter 3

Event-shape Observables

Theoretical predictions generally address differential cross sections that describe parton-level physics. Once we turn to collider experiments, however, we see that we measure distributions of individual leptons and hadrons. One possible way of linking the rift between theoretical predictions and experimental measurements is through event-shape observables. These observables describe the geometrical information of hadronic final states in collider experiments. They can typically be computed in perturbation theory with minor non-perturbative corrections; and, in particular, they can also be measured [69–71].

The main applications of event-shape observables can be divided into two different classes: First, we want to point out that even though QCD correctly describes the strong interactions, it is necessary to investigate the QCD dynamics precisely. On top of that, some SM constants, like the coupling constants and masses, cannot be determined by the underlying formulation of the SM and thus have to be determined via measurements. As a concrete example we point to the determination of the strong coupling $\alpha_s \equiv \frac{g_s^2}{4\pi}$. The world average of α_s [72] is formed out of many different measurements, and among them are extractions from event-shape observables [35, 73, 74] because of their clean signatures.

The other application of event-shapes involves the search for beyond the SM (BSM) physics. Since event-shapes describe final-state geometries and topologies, they can be used in BSM searches, where cuts on their values can be used to restrict phase-space region to reduce background noise [75, 76]. Additionally, it is also possible to design specific event-shapes for the searches of BSM physics [77–79].

3.1 Thrust

Event-shapes are a class of observables which can be defined both at lepton [80] and hadron colliders [81]. They were used starting from the early days of QCD [82, 83] until now [77, 84]. A few of them like thrust [83] have gained popularity over the years due to their simple structure. This broad field makes it comparatively difficult to pinpoint an exact set of criteria that specifies what is and is not an event-shape observables. For this work, we take the definition that an event-shape observable is an infrared and collinear safe[1] continuous measure of the energy and momentum flow of hadrons in the final state. For the didactic purpose, we will use an example, thrust [83], to construct an understanding of event-shapes and their intricacies without seeking to arrive at a more precise definition.

At the beginning of this section, we stated that event-shapes describe the geometry of the final state in collider experiments; this information must somehow be translated into a number. Thus, it should not rely on the exact quantum numbers of individual particles but the global structure of the event. Thrust obeys this principle. Its definition in terms of momenta is given by

$$\begin{aligned} T &= \max_{\vec{n}} \frac{\sum_i |\vec{n} \cdot \vec{p}_i|}{\sum_i |\vec{p}_i|} \\ &= \max_{\vec{n}} \frac{\sum_i |\vec{n} \cdot \vec{p}_i|}{Q}, \end{aligned} \tag{3.1.1}$$

where the sum runs over all particles in the final state. In the second line of (3.1.1) we have taken into account that $\sum_i |\vec{p}_i| = Q$ in the centre-of-mass (CoM) frame for massless particles. The unit vector $\vec{n}$ that maximizes the right-hand side of (3.1.1) defines the thrust axis, for later convenience we label the thrust axis as $\vec{n}_T$.

Before we turn our attention to the computation of thrust, we would first like to understand what we are measuring. From eq. (3.1.1) it is evident that if a particle's momentum projection onto the thrust axis is close to its total momentum, then the thrust value is more sizeable. So we can identify large thrust events as those where this is true for all particles in the final state. The thrust axis is the same for all particles, thus pencil-like events as seen on the left in figure 3.1.1 take $T \approx 1$. On the other hand, more uniformly distributed events have lower thrust values.

[1] Later in this chapter we determine what infrared and collinear safe means.

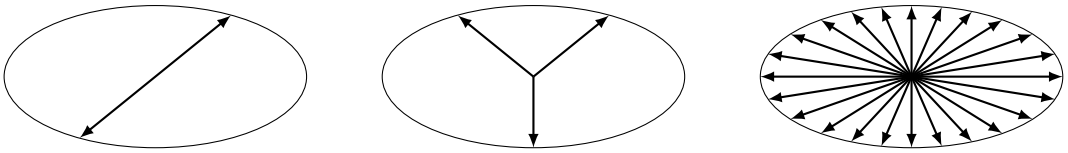

$T = 1$ $T = \frac{2}{3}$ $T \approx \frac{1}{2}$

Figure 3.1.1: Thrust values for various event geometries.

3.1.1 Fixed-order calculation

Now that we understand what we are measuring, we want to improve our understanding of thrust from a theoretical point of view. As we have a definition in terms of momenta, we can start calculating the expected distribution for thrust in perturbation theory.

Starting from the matrix element, the differential cross section is proportional to the square of the matrix element: $\mathrm{d}\sigma \sim |\mathcal{M}|^2 \mathrm{d}\Phi_n$, where $\mathrm{d}\Phi_n$ is the n-particle Lorentz-invariant phase space. In order to compute event-shape distributions we include the measurement as a phase-space constraint of the form $\delta(\tau - \tau(\{p_i\}))$. Hence we write the differential cross section with respect to our measurement as

$$\frac{\mathrm{d}\sigma}{\mathrm{d}\tau} \sim |\mathcal{M}|^2 \delta(\tau - \tau(\{p_i\})) \mathrm{d}\Phi_n. \tag{3.1.2}$$

In principle, we could now start to calculate the thrust distribution by inserting (3.1.1) into the previous equation. However we limit this calculation to the hadronic final state which is of interest here. The leading-order contribution to this process is $\gamma^* \to q\bar{q}$, and momentum conservation in the CoM frame fixes the quarks to be in a back-to-back configuration, so the thrust value is $T = 1$.[2] In general, it is more useful to define $\tau \equiv 1 - T$. Thus, the leading order is

$$\frac{1}{\sigma_0} \frac{\mathrm{d}\sigma}{\mathrm{d}\tau} = \delta(\tau) + \mathcal{O}(\alpha_s), \tag{3.1.3}$$

where σ_0 is the tree-level contribution to the total cross section. At one-loop order, three diagrams contribute at $\mathcal{O}(\alpha_s)$, one virtual correction where a gluon is exchanged between the quark and antiquark and two real-emission corrections where a gluon is emitted from either the quark or the antiquark. Thus the complete QCD one-loop

[2] We are neglecting the leptonic initial-state $e^+e^- \to \gamma^*$ as this is irrelevant for the thrust distribution.

correction for the thrust distribution [33] is

$$\frac{1}{\sigma_0}\frac{\mathrm{d}\sigma}{\mathrm{d}\tau} = \delta(\tau) + \frac{\alpha_s}{2\pi}C_F\Bigg\{\left(\frac{\pi^2}{3}-1\right)\delta(\tau) - \left[\frac{4+6\tau(\tau-1)}{1-\tau}\right]\left[\frac{\ln(\tau)}{\tau}\right]_+ + \left[3(1+\tau)(3\tau-1) + \frac{(4+6\tau(\tau-1))\ln(1-2\tau)}{1-\tau}\right]\left[\frac{1}{\tau}\right]_+\Bigg\} + \mathcal{O}\left(\alpha_s^2\right), \tag{3.1.4}$$

where we used

$$\int_0^1 \mathrm{d}z\ [g(z)]_+ f(z) = \int_0^1 \mathrm{d}z\ (f(z)-f(0))\, g(z), \tag{3.1.5}$$
$$[g(z)]_+ = g(z) \quad \text{for} \quad z \neq 0,$$

as definition for the plus distributions. To get rid of the distributions, we can work with the integrated version of the thrust distribution:

$$\int_0^{\tau'} \mathrm{d}\tau\ \left(\frac{1}{\sigma_0}\frac{\mathrm{d}\sigma}{\mathrm{d}\tau}\right)_{\text{sing}} = 1 + \frac{\alpha_s}{2\pi}C_F\Bigg\{-2\ln^2(\tau') - 3\ln(\tau') + \frac{\pi^2}{3} - 1\Bigg\} + \mathcal{O}(\tau', \alpha_s^2), \tag{3.1.6}$$

where we expanded eq. (3.1.4) around $\tau \sim 0$ before performing the integration as indicated by the subscript "sing". By integrating over the $\left[\frac{\ln(\tau)}{\tau}\right]_+$-term we arrive at a term $\ln^2(\tau')$ in eq. (3.1.6). This double or Sudakov [85] logarithm is a common feature in many event-shape distributions. It signals the incompleteness of perturbation theory in this region. This can also be seen in figure 3.1.2. In the high τ region, the theoretical prediction matches the experimental data fairly well; however, in the region $\tau \sim 0$, the calculation loses its predictivity due to the appearance of these large Sudakov logarithms.

3.2 Origin of Sudakov logarithms

We have seen in figure 3.1.2 that for the thrust distribution in the dijet limit, $\tau \sim 0$, large logarithms appear that spoil the perturbative calculation. To address this problem, we first need to understand the origin of these logarithms.

Let us revisit the structures that appear in the thrust distribution at one-loop order in QCD. One contribution arises from the virtual correction, where we are left with a $q\bar{q}$-pair in the final state. On the other hand, the real corrections have a $q\bar{q}g$ final state, so overall, we have contributions from two and three-particle final-states. In the case of the two-particle final-state, momentum conservation requires $\tau = 0$. Thus, we need

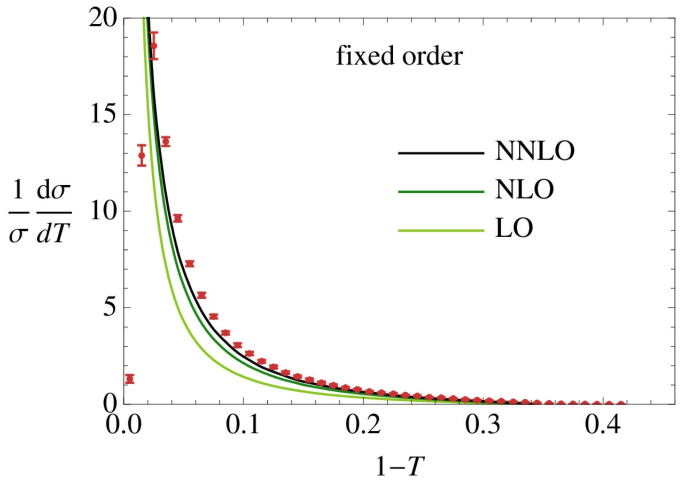

Figure 3.1.2: Convergence of fixed-order distribution. ALEPH(red) data at 91.2 GeV is included for reference. The figure is from [33] and uses $\alpha_s(M_Z) = 0.1168$.

at least a three-particle final-state to achieve non-zero thrust values; however, not all configurations give rise to contributions in the $\tau \sim 0$ region, for example, the second geometry in figure 3.1.1. Instead, the sum of the projected momenta onto the thrust axis must be close to the total scalar momenta of the final state. So consequently, the third particle must be approximately parallel to the thrust axis or be so low-energetic that its contribution is irrelevant to generating contributions in the $\tau \sim 0$ region. To rephrase it, the third particle must be either soft in comparison or collinear to the primary partons.

In a more general way, we can consider the occurrence of the Sudakov logarithms as the consequence of an incomplete cancellation [86] of infrared divergences between real and virtual corrections. It is well established that the one-loop virtual corrections to $q\bar{q}$ pair production feature soft and collinear divergences which cancel against the analogous divergences in the $q\bar{q}g$ cross section [87], thus the inclusive cross section at NLO is altogether finite. The inclusive cross section covers the integration over the entire three-particle phase space; however, from eq. (3.1.2) it is visible that we restrict the phase space when calculating event-shape distributions at small values of the observable. Thus, the result is not fully inclusive over the final state, and so soft and collinear divergences appear in the form of large Sudakov logarithms.

3.3 Infrared and collinear safety

Now that we understand where the large logarithms arise from, we want to introduce the concept of infrared and collinear (IRC) safe observables.

Previously, we mentioned that we measure distributions of individual leptons and hadrons in collider experiments. However, the calculations are done on a purely partonic level, and no hadronisation model describes this transition from first principles, only in model-dependent ways [88]. So to produce a model-independent prediction of QCD, we want to look at observables that are not particularly sensitive to hadronisation effects. However, due to the structure of QCD, partons will undergo many collinear splittings as part of the fragmentation process, and additionally, there is always some emission of soft particles. Thus infrared-collinear safety is the property that if one modifies an event by a collinear splitting or the addition of a soft emission, the value of the event-shape variable should remain unchanged.

Now we want to convince ourselves that thrust is an IRC safe observable. Thus the thrust values have to be invariant under the following momentum branching

$$\begin{aligned} &\text{i)} \quad \vec{p}_m \to 0, \\ &\text{ii)} \quad \vec{p}_m \to \lambda \vec{p}_m + (1-\lambda)\vec{p}_m, \end{aligned}$$

where λ is the momentum fraction of the m-th particle with respect to its mother momentum $\vec{p}_m$. The first case corresponds to the soft-emission case. Inserting this into the thrust definition of eq. (3.1.1), we find the following:

$$\begin{aligned} T &= \max_{\vec{n}_T} \frac{\sum_i^k |\vec{n}_T \cdot \vec{p}_i|}{\sum_i^k |\vec{p}_i|} = \max_{\vec{n}_T} \frac{|\vec{n}_T \cdot \vec{p}_1| + \ldots + |\vec{n}_T \cdot \vec{p}_m| + \ldots + |\vec{n}_T \cdot \vec{p}_k|}{|\vec{p}_1| + \ldots + |\vec{p}_m| + \ldots + |\vec{p}_k|} \\ &\underset{\text{i)}}{\to} \max_{\vec{n}_T} \frac{|\vec{n}_T \cdot \vec{p}_1| + \ldots + 0 + \ldots + |\vec{n}_T \cdot \vec{p}_k|}{|\vec{p}_1| + \ldots + 0 + \ldots + |\vec{p}_k|} = \max_{\vec{n}_T} \frac{|\vec{n}_T \cdot \vec{p}_1| + \ldots + |\vec{n}_T \cdot \vec{p}_k|}{|\vec{p}_1| + \ldots + |\vec{p}_k|} \\ &= \max_{\vec{n}_T} \frac{\sum_j^{l=k-1} |\vec{n}_T \cdot \vec{p}_j|}{\sum_j^{l=k-1} |\vec{p}_j|} = T, \end{aligned}$$

where

$$j = \begin{cases} i, & \text{if } j < m \\ i+1, & \text{otherwise .} \end{cases}$$

Similarly inserting the collinear splitting into the definition leads to:

$$\begin{aligned} T &= \max_{\vec{n}_T} \frac{\sum_i |\vec{n}_T \cdot \vec{p}_i|}{\sum_i |\vec{p}_i|} = \max_{\vec{n}_T} \frac{|\vec{n}_T \cdot \vec{p}_1| + \ldots + |\vec{n}_T \cdot \vec{p}_m| + \ldots + |\vec{n}_T \cdot \vec{p}_k|}{|\vec{p}_1| + \ldots + |\vec{p}_m| + \ldots + |\vec{p}_k|} \\ &\underset{\text{ii)}}{\to} \max_{\vec{n}_T} \frac{|\vec{n}_T \cdot \vec{p}_1| + \ldots + \lambda|\vec{n}_T \cdot \vec{p}_m| + (1-\lambda)|\vec{n}_T \cdot \vec{p}_m| + \ldots + |\vec{n}_T \cdot \vec{p}_k|}{|\vec{p}_1| + \ldots + \lambda|\vec{p}_m| + (1-\lambda)|\vec{p}_m| + \ldots + |\vec{p}_k|} \\ &= \max_{\vec{n}_T} \frac{\sum_i |\vec{n}_T \cdot \vec{p}_i|}{\sum_i |\vec{p}_i|} = T, \end{aligned}$$

thus thrust is invariant under both types of splittings and consequently an IRC safe observable.

In conclusion, IRC safety constrains observables in various nontrivial fashions. However, we will require precisely that for the observables in our approach.

3.4 Resummation

Now that we understand where the large logarithms in eq. (3.1.6) arise from; we want to handle them systemically.

In the case of the one-loop cumulant thrust distribution, we note that the leading term appears as $\alpha_s \ln^2 \tau$. If we now compute higher n-loop order corrections to the distribution, we would find the leading behaviour to be $\alpha_s^n \ln^{2n} \tau$. So in the singular thrust limit we find a power series in $\alpha_s \ln^2 \tau$. In the case of large values of τ, this would not be problematic because the series still converges. However, for small values of τ, it is unacceptable because higher corrections, in general, scale now similarly to lower-order corrections, and thus the expansion fails as can be seen in figure 3.1.2. Therefore the straightforward way out of the problem would be to use a different expansion parameter, where perturbation theory is valid, or to find a workaround without the expansion in the first place, i.e., without perturbation theory.

The commonly taken option is to work with the standard fixed-order calculation but to systematically construct an all-order expression, which resums the critical terms [28]. The accuracy of the resummed expression is usually written as $\mathrm{N}^n\mathrm{LL}$, compared to the fixed-order $\mathrm{N}^n\mathrm{LO}$ loop counting. The construction of the logarithmic counting is as follows:

Let us define a fixed-order expansion of some observable $O(\tau)$, where large logarithms in τ must be resummed. Then, in loop counting, it has the subsequent expres-

sion,

$$\begin{aligned} O(\tau) = x_{00} & \\ &+ \alpha_s \left(x_{12}L^2 + x_{11}L + x_{10}\right) \\ &+ \alpha_s^2 \left(x_{24}L^4 + x_{23}L^3 + x_{22}L^2 + x_{21}L + x_{20}\right) \\ &+ \dots \\ &+ R(\alpha_s, \tau), \end{aligned} \tag{3.4.1}$$

where $L = \ln \tau$ stands for the logarithms of the generic observable $O(\tau)$. Resummation is required for small τ values. The x_{ij}'s are plain numbers accompanying the logarithms and $R(\alpha_s, \tau)$ contains all terms that vanish in the limit $\tau \to 0$.

We are now able to rearrange the generic expression in eq. (3.4.1) into an exponentiated version, which reduces the difficulty of the problem to $\alpha_s^n \ln^{n+1} \tau$ for leading terms:

$$\begin{aligned} O(\tau) \coloneqq & C(\alpha_s) e^{\bar{E}(\alpha_s, L)} + R(\alpha_s, \tau) \\ = & \left(1 + C_1 \alpha_s + C_2 \alpha_s^2 + \dots\right) \\ & \times \exp\Big\{ \alpha_s \left[c_{12}L^2 + c_{11}L\right] + \\ & \qquad \alpha_s^2 \left[c_{23}L^3 + c_{22}L^2 + c_{21}L\right] + \\ & \qquad \alpha_s^3 \left[c_{34}L^4 + c_{33}L^3 + c_{32}L^2 + c_{31}L\right] + \dots \Big\} + R(\alpha_s, \tau), \end{aligned} \tag{3.4.2}$$

where $R(\alpha_s, \tau)$ contains all terms that vanish in the limit $\tau \to 0$. We follow the notation used in [28, 89]. Thus, we can group the terms in different α_s powers together and end up with[3]

$$\bar{E}(\alpha_s, L) = L g_1(\alpha_s L) + g_2(\alpha_s L) + \frac{1}{L} g_3(\alpha_s L) + \dots, \tag{3.4.3}$$

where the functions g_i resum towers of $\alpha_s L$. Constructing an expression for $\bar{E}(\alpha_s, L)$ up to g_n is equivalent to achieving resummation to (next-to)$^{n-1}$-leading logarithmic accuracy. This counting in eq. (3.4.3) is natural in a regime where the logarithms are large enough so that $L \sim \frac{1}{\alpha_s}$. Then LL sums all terms of order $\frac{1}{\alpha_s}$, NLL all terms of order 1, etc. In this counting, the fixed-order terms in $C(\alpha_s)$ are counted as C_1 being NNLL, C_2 being N^{3}LL, etc. Often, the fixed-order coefficients are included to one higher order in α_s, yielding the so-called 'prime' counting [35]. The N^{n}LL counting is summarized in table 3.1.

[3] We will give a precise definition of $\bar{E}$ in terms of anomalous dimensions in a later section.

Accuracy	g_n	C_n
LL	g_1	–
NLL	g_2	–
NNLL	g_3	C_1

Accuracy	g_n	C_n
LL	g_1	–
NLL′	g_2	C_1
NNLL′	g_3	C_2

Table 3.1: Convention for counting $\mathrm{N}^n\mathrm{LL}$ and $\mathrm{N}^n\mathrm{LL}'$ order. The g_n from eq. (3.4.3) and the C_n from eq. (3.4.2) are the highest terms included to achieve (next-to)^n-leading logarithmic accuracy. In the primed counting, the fixed-order coefficient C_n are computed to one higher order in α_s.

There are two distinct ways of setting up a framework capable of achieving resummation. Their final result is essentially the same [89]; however, their origin is very different.

The first approach is based on iterative soft and collinear emissions. The idea of this approach is that because the double logarithms arise only from the emission of a gluon becoming soft and collinear, higher powers of the Sudakov logarithms are connected to multiple emissions of soft and collinear gluons. However, the structure of soft and collinear emissions are universal in QCD and can be described using DGLAP-splitting kernels. Thus a suitable iteration approach can be used to calculate contributions from arbitrary high orders of α_s for any observable which requires resummation.

The basic approach for this kind of resummation framework is usually denoted as the CTTW scheme [28] and forms the framework for the resummation techniques in direct QCD. This approach has found computational realisation in the form of the state of the art programs of `CAESAR` [26] (NLL resummation) and `ARES` [27] (NNLL resummation).

The second approach is based on the use of effective field theories (EFT). In event-shape observables we know that only certain momentum modes contribute to the phase-space region where the Sudakov logarithms appear. In that case, we can use the EFT approach in which only these modes are dynamical. This can be backed by the observation that we can reorganize the observable, which requires resummation as a ratio of scales. As example, for thrust the scales would be $\max_{\vec{n}_T} \sum_i |\vec{n}_T \cdot \vec{p}_i|$ and Q. The critical region is the region where effective theories use this ratio as its expansion parameter and thus are expected to shine.

The advantage of the EFT approach over the direct QCD method is that the effective Lagrangian allows one to derive all-order factorisation theorems and to systematically resum logarithmically enhanced contributions at all orders. The effective Lagrangian also provides a systematic way to write down higher power corrections, by

including subleading terms in the effective Lagrangian.

The effective field theory that will be the underlying framework of this thesis and which we will construct in the next section is called Soft-Collinear Effective Theory (SCET). SCET allows one to derive factorisation theorems which divide the theoretical description for processes into different structures describing physics at different scales. Resummation in SCET is then achieved by the renormalization group (RG) evolution of these structures to a common scale. Finally, the RG evolution shifts these large logarithms into the exponent of the evolution kernels, where they can not spoil perturbation theory anymore.

Now that we have a systematic way of dealing with the large logarithms in the small τ region, the connection to the fixed-order results is re-established by matching. The matching is constructed as

$$O(\tau)_{\text{matched}} = O(\tau)_{\text{resummed}} - O(\tau)_{\text{expanded resummed}} + O(\tau)_{\text{fixed-order}}, \tag{3.4.4}$$

where $O(\tau)$ is some observables. The idea here is that in the vicinity of the critical region the fixed-order expansion breaks down, so $O(\tau)_{\text{resummed}}$ and $O(\tau)_{\text{expanded resummed}}$ are different, but the singular parts of $O(\tau)_{\text{expanded resummed}}$ and $O(\tau)_{\text{fixed-order}}$ match. Therefore the remaining terms in $O(\tau)_{\text{matched}}$ are the resummed term $O(\tau)_{\text{resummed}}$ and the non-singular remainder of $O(\tau)_{\text{fixed-order}}$. In the rest of the region, where fixed-order calculations are adequately defined, $O(\tau)_{\text{resummed}}$ equals $O(\tau)_{\text{expanded resummed}}$ and thus cancels, leaving only $O(\tau)_{\text{fixed-order}}$ to contribute to the final expression.

Chapter 4

Soft-Collinear Effective Theory

In this chapter, we will construct the effective theory briefly described in the last section. We will apply it in the derivation of factorisation theorems, followed by a short overview of the technicalities of resummation within a SCET context. In terms of literature, there exists a lot of different introductions to SCET, ranging from redefining basic concepts of QFT within SCET to various complications that can arise in its application. Here we will only focus on the bare minimum necessary to understand the basics upon which this thesis is built. As a starting point for more information, we point to different lecture notes [90], books [91] and, the original papers [29–32].

4.1 The method of regions

A critical conceptual aspect of SCET is the method of regions [92]. It is a technique that allows to construct asymptotic expansions of loop integrals in dimensional regularisation (DR) by separating the integration domain into different regions and expanding the integrands appropriately in each one of them. The different integration regions correspond to different fields in the effective field theory. The expanded integrals obtained by the method of regions are in a one-to-one correspondence to the Feynman diagrams of the effective field theories regularized in DR.

In order to illustrate the main idea of the method of regions, we start by considering a simple toy integral:

$$I = \int_0^\infty \mathrm{d}k \frac{k}{(k^2+m^2)(k^2+M^2)} = \frac{\ln \frac{M}{m}}{M^2-m^2}. \tag{4.1.1}$$

This type of integral appears in the one-loop self-energy of a two-dimensional theory,

with two different masses. We will assume a hierarchy between the masses of the form $m^2 \ll M^2$, and we will discuss the expansion of the integral in the limit of small m. Through asymptotically expanding the r.h.s. of eq. (4.1.1) in the small m limit we find

$$I = \frac{\ln \frac{M}{m}}{M^2} \left(1 + \frac{m^2}{M^2} + \frac{m^4}{M^4} + \mathcal{O}\left(\frac{m^6}{M^6}\right)\right). \tag{4.1.2}$$

The method of regions gives a prescription on how to recover this asymptotic result when expanding the integrand before integration. To begin with, we have to identify all the momentum modes involved in the problem; here, there are two modes: I) $k \sim m \ll M$ and II) $k \sim M \gg m$. After identifying the modes, one expands the integrand in these regions and integrates them over the entire phase space. One subtlety is the necessity of a regulator because the expansion of the integral was asymptotic when performed after the integration. Thus the result was not analytic in the limit around which we expanded. Hence, divergences in the integral must occur upon expanding before performing the integration. Now we will expand the integral in both regions and integrate; as a regulator, we introduce $k^{-\epsilon}$, and we will eventually send $\epsilon \to 0$ at the end of the computation. In the first region, we find

$$\begin{aligned} I_{\mathrm{I})} &= \int_0^\infty \mathrm{d}k \frac{k^{1-\epsilon}}{(k^2+m^2)M^2} \left(1 - \frac{k^2}{M^2} + \frac{k^4}{M^4} + \mathcal{O}\left(\frac{k^6}{M^6}\right)\right) \\ &= \frac{\pi}{2M^2} m^{-\epsilon} \csc\left\{\frac{\pi\epsilon}{2}\right\} \left(1 + \frac{m^2}{M^2} + \frac{m^4}{M^4} + \mathcal{O}\left(\frac{m^6}{M^6}\right)\right) \\ &= \frac{1}{M^2}\left(\frac{1}{\epsilon} - \ln m\right)\left(1 + \frac{m^2}{M^2} + \frac{m^4}{M^4} + \mathcal{O}\left(\frac{m^6}{M^6}\right)\right) + \mathcal{O}(\epsilon), \end{aligned} \tag{4.1.3}$$

and for the second region

$$\begin{aligned} I_{\mathrm{II})} &= \int_0^\infty \mathrm{d}k \frac{k^{1-\epsilon}}{k^2(k^2+M^2)} \left(1 - \frac{m^2}{k^2} + \frac{m^4}{k^4} + \mathcal{O}\left(\frac{m^6}{k^6}\right)\right) \\ &= -\frac{\pi}{2M^2} M^{-\epsilon} \csc\left\{\frac{\pi\epsilon}{2}\right\} \left(1 + \frac{m^2}{M^2} + \frac{m^4}{M^4} + \mathcal{O}\left(\frac{m^6}{M^6}\right)\right) \\ &= \frac{1}{M^2}\left(-\frac{1}{\epsilon} + \ln M\right)\left(1 + \frac{m^2}{M^2} + \frac{m^4}{M^4} + \mathcal{O}\left(\frac{m^6}{M^6}\right)\right) + \mathcal{O}(\epsilon). \end{aligned} \tag{4.1.4}$$

Finally we add up the contributions, set $\epsilon \to 0$ and arrive at

$$I_{\mathrm{I})} + I_{\mathrm{II})} = \frac{\ln \frac{M}{m}}{M^2} \left(1 + \frac{m^2}{M^2} + \frac{m^4}{M^4} + \mathcal{O}\left(\frac{m^6}{M^6}\right)\right), \tag{4.1.5}$$

the same expression as in eq. (4.1.2). The logarithm $\ln \frac{M}{m}$ is the remnant of explicit divergence cancellation. One subtlety is that even though we are integrating both contributions over the whole phase-space, there is no double counting. The reason is that the two pieces scale differently. The low-energy integral can never produce a term $M^{-\epsilon}$ since they depend analytically on the large scale, and vice-versa. We can show explicitly that there is no double counting by calculating $I_{\mathrm{I})}$ in the limit $k \sim M \gg m$ and $I_{\mathrm{II})}$ in the limit $k \sim m \ll M$. In both cases we end up with an integral which scales as $k^{-1-\epsilon}$ at leading power which is a scaleless integral and vanishes in DR. This feature of the method of regions is non-trivial and leads to more subtleties in more involved scenarios.

4.2 Momentum modes in SCET

In the previous toy example, it was straightforward to identify the different momentum modes as there were only two regions in the problem. In general, however, it is not as clear. The modes depend on the problem one wants to investigate. In our approach, we consider two different momentum mode scalings. The options are that the soft and collinear modes have different virtualities, which we call $\mathrm{SCET_I}$, and where their virtualities are the same, $\mathrm{SCET_{II}}$.

4.2.1 $\mathrm{SCET_I}$ mode analysis

As an example for a $\mathrm{SCET_I}$ process, we turn again to thrust. Before we start, however, let us first fix the notations and conventions:

We denote the CoM energy as Q, and the parent partons in the dijet case to be emitted along the lightlike vectors n and $\bar{n}$. They are defined as

$$n_\mu = (1, 0, 0, 1), \quad \text{and} \quad \bar{n}_\mu = (1, 0, 0, -1), \tag{4.2.1}$$

so that

$$n^2 = \bar{n}^2 = 0, \tag{4.2.2}$$

$$n \cdot \bar{n} = 2. \tag{4.2.3}$$

We can thus decompose any four-vector p^μ into light-cone components as

$$\begin{aligned} p^\mu &= (p\cdot\bar{n})\,\frac{n^\mu}{2} + (p\cdot n)\,\frac{\bar{n}^\mu}{2} + p_\perp^\mu \\ &= p_-\frac{n^\mu}{2} + p_+\frac{\bar{n}^\mu}{2} + p_\perp^\mu, \end{aligned} \tag{4.2.4}$$

where $p_\perp^\mu$ is a four-vector related to the two-dimensional vector $\vec{p}_T$ which is transverse to n^μ and $\bar{n}^\mu$. We will often shorten this notation to

$$p^\mu = (p_-, p_+, p_\perp)\,. \tag{4.2.5}$$

In this notation the scalar products can then be written as $p\cdot q = \frac{1}{2}p_+q_- + \frac{1}{2}p_-q_+ + p_\perp\cdot q_\perp$ and in the special case of $p = q$ we find $p^2 = p_-p_+ + p_\perp^2$.

Near the dijet limit, thrust simplifies to [28]

$$\tau \sim \frac{p_L^2 + p_R^2}{Q^2}, \tag{4.2.6}$$

where the two hemispheres are defined by the directions n^μ and $\bar{n}^\mu$. Here, p_L^2 and p_R^2 are the invariant masses of the coloured particles in each hemisphere.

The highest energy scale, which eventually we integrate out of the theory, should arise from the virtual effects in the production of the quark-antiquark pair at the CoM energy Q. This implies that this mode should be independent of the small thrust value and only depends on Q. Thus we can identify the hard scale as

$$k_h^\mu = (1,1,1)Q. \tag{4.2.7}$$

Next we consider additional emissions, and we choose p_L to be in the n direction and p_R in the $\bar{n}$ direction in the dijet region. We know that the only possible radiation is collinear or soft, so if we emit collinear radiation into any hemisphere, we find that

$$p_{L/R}^2 \sim \tau Q^2. \tag{4.2.8}$$

Momentum conservation imposes that the large light-cone component must be of order Q, which means that $p_{L/R}^2 \sim \tau Q^2$ fixes the scaling of the on-shell collinear modes to

be

$$k_c^\mu = (1, \tau, \sqrt{\tau})Q, \tag{4.2.9}$$

$$k_{\bar{c}}^\mu = (\tau, 1, \sqrt{\tau})Q, \tag{4.2.10}$$

where $k_{c/\bar{c}}$ is the momentum scaling in the region collinear to $n/\bar{n}$. The scaling of additional soft emissions can be explained similarly. First, note that soft emissions do not have a preferred direction; thus, the emission in either direction n and $\bar{n}$ must scale the same. Secondly, we can not introduce terms in $p^2_{L/R}$ which are bigger than $Q^2\tau$, which would change the invariant mass in the hemisphere. Thus we arrive at the following soft scaling[1]

$$k_s^\mu = (\tau, \tau, \tau)Q. \tag{4.2.11}$$

4.2.2 $\mathbf{SCET_{II}}$ mode analysis

Now let us look at another observable, namely recoil-free broadening [93]. This observable is the recoil-free version of broadening, which is the scalar sum of transverse momentum measured with respect to the thrust axis. In order to avoid recoil effects, the broadening is measured here with respect to the broadening axis $\hat{b}$. The broadening axis $\hat{b}$ is the direction that minimizes the scalar sum of the transverse momentum within a hemisphere.

In the limit for small τ_b values, we find that the measurement function simplifies to

$$\tau_b \sim \frac{|\vec{p}_\perp|^L}{Q} + \frac{|\vec{p}_\perp|^R}{Q}, \tag{4.2.12}$$

where $|\vec{p}_\perp|^{L,R}$ is the scalar sum of transverse momentum in each hemisphere along the broadening axis.

For the hard scale, the same arguments as before are still valid. Thus, we can directly declare eq. (4.2.7) as the hard scale.

Next, we will consider collinear emissions and assume only radiation into the left hemisphere. Thus τ_b simplifies further to

$$\tau_b \sim \frac{|\vec{p}_\perp|^L}{Q}. \tag{4.2.13}$$

Here we can see directly that $p_\perp^L \sim \tau_b Q$ and because of momentum conservation of the

[1] In the literature often denoted as ultra-soft modes to distinguish them from soft modes in $\mathrm{SCET_{II}}$.

Modes	Thrust	Broadening
Hard	$(1,1,1)Q$	$(1,1,1)Q$
n-collinear	$(1,\lambda^2,\lambda)Q$	$(1,\lambda^2,\lambda)Q$
$\bar{n}$-collinear	$(\lambda^2,1,\lambda)Q$	$(\lambda^2,1,\lambda)Q$
soft	$(\lambda^2,\lambda^2,\lambda^2)Q$	$(\lambda,\lambda,\lambda)Q$

Table 4.1: Momentum modes for thrust and broadening. Here we relabeled $\tau = \lambda^2$ and $\tau_b = \lambda$ for a better comparison.

on-shell collinear modes we find that

$$k_c^\mu = (1, \tau_b^2, \tau_b)Q. \tag{4.2.14}$$

Through the same logic we find similar modes in the right hemisphere, namely

$$k_{\bar{c}}^\mu = (\tau_b^2, 1, \tau_b)Q. \tag{4.2.15}$$

In the end, we turn again to the soft modes. In eq. (4.2.12) we see that the soft modes scale as $p_\perp \sim \tau_b Q$, similar to the collinear modes. Additionally, we once more state that soft emissions have no preferred direction and thus scale the same in all directions. Therefore we find the following scaling for the soft modes

$$k_s^\mu = (\tau_b, \tau_b, \tau_b)Q. \tag{4.2.16}$$

4.2.3 SCET_I vs SCET_II

Let us now recap what we have learned from the last two sections by comparing them side by side, which can be seen in table 4.1.

We see that, first of all, the difference in the two cases is only the scaling of the soft modes. In the thrust case, the soft modes scale as the smaller of the two collinear $\pm$-components, while for broadening, they scale as the $\perp$-component of the collinear scale. As previously pointed out, we now have two different theories of SCET depending on the observable. One where the virtuality of the soft and collinear modes is different: SCET_I (or thrust-like) and where the virtuality is equal: SCET_II (or broadening-like). This is also illustrated in figure 4.2.1.

For SCET_I we are able to derive factorisation theorems because the soft and collinear modes scale differently. In the case of SCET_II this causes problems since similar scaling of soft and collinear modes make it challenging to isolate the two sec-

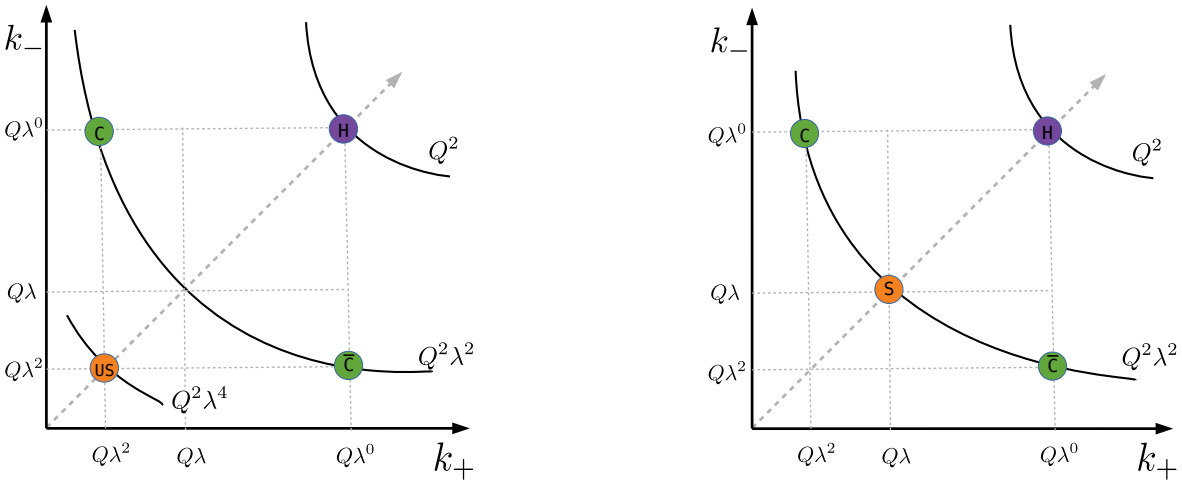

(a) SCET_I **(b)** SCET_II

Figure 4.2.1: Different momentum scalings and their classification, using $\lambda \ll 1$ as the expansion parameter. $H, C, \bar{C}, S, US$ denote the hard, collinear, anticollinear, soft and ultrasoft scaling.

tors. So virtuality alone is not adequate to classify an emission as being either soft or collinear. Thus we have to include a second quantity to disentangle them explicitly. A straightforward example would be the rapidity, which corresponds to the ratio between the $+$ and $-$ components of an emission. The rapidity of the soft modes would then be ~ 1 compared to the collinear modes, which would either be λ^2 or $\sim 1/\lambda^2$ depending on the precise definition of the rapidity. The problem of not being able to separate soft and collinear modes also has a manifestation in the computations as we will see below.

One approach to solve this problem proceeds by introducing an additional regulator, e.g., an analytic regulator [94], into the collinear and soft regions. The dependence on this additional regulator cancels when the soft and collinear contributions are, in the end, put together. However, new large logarithms remain as a residue of this cancellation. These remaining logarithms are of a similar type as the logarithm in eq. (4.1.5).

One can resum these new large logarithms by the Collinear Anomaly approach [95], where the product of collinear and soft functions can be brought into a form that directly exponentiates the rapidity logarithms.

4.3 SCET Lagrangian

As we now understand the underlying momentum scalings of SCET; we are now in the position to construct the SCET Lagrangian to learn about the dynamics and interactions of the theory. We will use this knowledge later to see how we can derive factorisation theorems.

In the previous chapter, we have seen that we need two variants of SCET in our project. However, as the Lagrangian is similar in both cases, we will only consider the $\mathrm{SCET_I}$-type here. We will point to the differences between $\mathrm{SCET_I}$ and $\mathrm{SCET_{II}}$ later.

In order to keep the construction of the Lagrangian as simple as possible, we will only deal with one soft and one collinear sector with the scaling $p_s^\mu = (\lambda^2, \lambda^2, \lambda^2)Q$ and $p_c^\mu = (1, \lambda^2, \lambda)Q$ in a generic expansion parameter λ, respectively. We will include an additional anticollinear sector later where it is needed. We follow the presentations in [90, 91].

To start we split the QCD fields for quarks and gluons into soft and collinear modes:

$$\begin{aligned} \psi(x) &= \psi_s(x) + \psi_c(x), \\ \tilde{A}^\mu(x) &= \tilde{A}_s^\mu(x) + \tilde{A}_c^\mu(x). \end{aligned} \tag{4.3.1}$$

From the QCD Lagrangian from eq. (2.1.5) we see that we have to transform two structures in the massless case: the gluonic piece $\left(\sim \mathrm{Tr}\left\{\tilde{G}_{\mu\nu}\tilde{G}^{\mu\nu}\right\}\right)$ and the quark piece $\left(\sim \bar{\psi} \not{D} \psi\right)$.

4.3.1 $\mathcal{L}_{\mathbf{SCET}}^{\mathbf{Gluon}}$

The gluonic structure of the SCET Lagrangian is obtained by simply including the splitting of regions in $\mathrm{Tr}\left\{\tilde{G}_{\mu\nu}\tilde{G}^{\mu\nu}\right\}$. The structure decomposes into three parts: the kinetic, the triple, and the quartic interaction. In the kinetic part, we simply have copies of the full QCD structure for each mode because momentum conservation forbids mixing between the fields. In the case of the interactions, we can see a similar story. We have a full soft and collinear part again; however, now, some mixing is allowed. For example, in the triple interaction, the mixing of collinear-collinear-soft(ccs) is allowed while collinear-soft-soft(css) is forbidden due to momentum conservation. Therefore

we find for the gluonic structure the following expression

$$\mathcal{L}_{\text{SCET}}^{\text{Gluon}} = \mathcal{L}_s + \mathcal{L}_c + \mathcal{L}_{c+s}, \tag{4.3.2}$$

where $\mathcal{L}_{c,s}$ are identical to the QCD structure only for pure soft or collinear modes. The soft-collinear mixing structure $\mathcal{L}_{c+s}$ is not given explicitly as it can be eliminated at a later step.

4.3.2 $\mathcal{L}_{\text{SCET}}^{\text{Quark}}$

Let us now look at the quark structure $\bar{\psi}\not{D}\psi$ and include the splitting into different modes. When the quark field is soft, the covariant derivative can not contain any collinear modes because the soft fields can not interact with the large momentum component because of momentum conservation. Thus, we find a copy of the QCD structure with the subscript s for soft for the soft quark field.

On the other hand, the collinear quark sector can contain mixing between the sectors because the suppressed momentum component of the collinear fields is of the same order as the corresponding soft gluon fields. In the case of the collinear quark field, we can further split it into two different components:

$$\psi_c(x) = \xi(x) + \eta(x), \tag{4.3.3}$$

where

$$\begin{aligned} \xi(x) &= P_+\psi_c(x) = \frac{\not{n}\bar{\not{n}}}{4}\psi_c(x), \\ \eta(x) &= P_-\psi_c(x) = \frac{\bar{\not{n}}\not{n}}{4}\psi_c(x). \end{aligned} \tag{4.3.4}$$

As the next step, we want to determine the power of λ with which the different field components scale such that we can determine the dominant component. This information can be obtained by looking at the two-point correlators. We start with the $\xi(x)$

component:

$$\begin{aligned}\langle 0|\, T\left\{\xi(x)\bar{\xi}(0)\right\}|0\rangle &= \frac{\not{n}\bar{\not{n}}}{4}\langle 0|\, T\left\{\psi_c(x)\bar{\psi}_c(0)\right\}|0\rangle\frac{\bar{\not{n}}\not{n}}{4}\\ &= \int\frac{\mathrm{d}^4k}{(2\pi)^4}\frac{i}{k^2+i\epsilon}e^{-ik\cdot x}\underbrace{\frac{\not{n}\bar{\not{n}}}{4}\not{k}\frac{\bar{\not{n}}\not{n}}{4}}_{\sim\lambda^0}\\ &\sim \lambda^4\frac{1}{\lambda^2}\lambda^0\sim\lambda^2,\end{aligned}\tag{4.3.5}$$

where we used the identity

$$\frac{\not{n}\bar{\not{n}}}{4}\not{k}\frac{\bar{\not{n}}\not{n}}{4} = k_-\frac{\not{n}}{2}.\tag{4.3.6}$$

Therefore we see that $\xi(x)\sim\lambda$. The correlator for the $\eta(x)$ component is very similar; the only difference is that we have to employ the identity

$$\frac{\bar{\not{n}}\not{n}}{4}\not{k}\frac{\not{n}\bar{\not{n}}}{4} = k_+\frac{\bar{\not{n}}}{2}\sim\lambda^2.\tag{4.3.7}$$

Thus we find that $\eta(x)\sim\lambda^2$. So the $\eta(x)$ component is suppressed by one power of λ with respect to the $\xi(x)$ component. Therefore in the collinear quark Lagrangian we can integrate out the $\eta(x)$ fields.

In order to integrate out the $\eta(x)$ fields, we start from the collinear quark Lagrangian:

$$\begin{aligned}\mathcal{L}_c &= \bar{\psi}_c(x)i\not{D}\psi_c\\ &= \left(\bar{\xi}(x)) + \bar{\eta}(x)\right)\left[i\bar{n}\cdot D\frac{\not{n}}{2} + in\cdot D\frac{\bar{\not{n}}}{2} + i\not{D}_\perp\right](\xi(x)) + \eta(x))\\ &= \bar{\xi}(x)in\cdot D\frac{\bar{\not{n}}}{2}\xi(x) + \bar{\xi}(x)i\not{D}_\perp\eta(x) + \bar{\eta}(x)i\not{D}_\perp\xi(x) + \bar{\eta}(x)i\bar{n}\cdot D\frac{\not{n}}{2}\eta(x),\end{aligned}\tag{4.3.8}$$

where we used the relations $\not{n}\xi(x) = \bar{\not{n}}\eta(x) = 0$ and $\{\not{n},\not{D}_\perp\} = \{\bar{\not{n}},\not{D}_\perp\} = 0$. A simple way to determine the Lagrangian after integrating out the $\eta(x)$ field is to employ the equations of motion from the Lagrangian in eq. (4.3.8). We find the following solution from the equations of motion for η and $\bar{\eta}$:

$$\eta(x) = -\frac{\bar{\not{n}}}{2\bar{n}\cdot D}\not{D}_\perp\xi(x),\tag{4.3.9}$$

$$\bar{\eta}(x) = -\bar{\xi}(x)\overleftarrow{\not{D}}_\perp\frac{\bar{\not{n}}}{2\bar{n}\cdot\overleftarrow{D}},\tag{4.3.10}$$

where the arrow indicates that the covariant derivative is acting to the left. Finally, we can plug the solutions for η and $\bar{\eta}$ back into the Lagrangian and arrive at:

$$\mathcal{L}_c = \bar{\xi}(x) i n \cdot D \frac{\not{\bar{n}}}{2} \xi(x) + \bar{\xi}(x) i \not{D}_\perp \frac{1}{i\bar{n} \cdot D} \frac{\not{\bar{n}}}{2} \xi(x), \tag{4.3.11}$$

where we used the previously stated relations and on top $P_+ \not{D}_\perp \xi(x) = \not{D}_\perp P_+ \xi(x) = \not{D}_\perp \xi(x)$. Furthermore, only the $n \cdot \tilde{A}_s$ component of the soft gluon field[2] is not power suppressed with respect to the corresponding component of the collinear quark field; thus, only this component enters the leading soft-collinear interactions. We arrive at the following Lagrangian for the collinear quark field

$$\begin{aligned} \mathcal{L}_c &= \underbrace{\bar{\xi}(x) i n \cdot D_c \frac{\not{\bar{n}}}{2} \xi(x) + \bar{\xi}(x) i \not{D}^c_\perp \frac{1}{i\bar{n} \cdot D_c} \frac{\not{\bar{n}}}{2} \xi(x)}_{\hat{\mathcal{L}}_c} - g \bar{\xi}(x) n \cdot \tilde{A}_s(x_+) \frac{\not{\bar{n}}}{2} \xi(x) \\ &= \hat{\mathcal{L}}_c + \mathcal{L}_{c+s}, \end{aligned} \tag{4.3.12}$$

where we performed a multipole expansion of the soft fields to achieve a consistent EFT power counting. The first part of eq. (4.3.12) is the pure collinear quark field Lagrangian, while the second term is still a soft-collinear interaction term. In the end we are able to write $\mathcal{L}^{\text{Quark}}_{\text{SCET}}$ in the following form:

$$\mathcal{L}^{\text{Quark}}_{\text{SCET}} = \mathcal{L}_s + \hat{\mathcal{L}}_c + \mathcal{L}_{c+s}, \tag{4.3.13}$$

where $\mathcal{L}_s$ is identical to the QCD structure with only soft fields and $\hat{\mathcal{L}}_c$ and $\mathcal{L}_{c+s}$ are the collinear and soft-collinear interaction terms.

4.3.3 Decoupling Transformation

We noted in $\mathcal{L}^{\text{Gluon}}_{\text{SCET}}$ and $\mathcal{L}^{\text{Quark}}_{\text{SCET}}$ that there are terms that still allow interactions between the soft and collinear modes even at leading power in the EFT expansion. These interactions must be eliminated if we want to derive an all-order factorisation theorem. Before doing so, we have to introduce the concept of Wilson lines.

In order to understand Wilson lines, it is easiest to see where they come from based on an example; here, we choose the vector current operator J^μ. At the tree level, the

[2] From the two-point correlator for the gluon we find that the gluon field scales like its momentum, thus $\tilde{A}^\mu_s(x) \sim p^\mu_s$ and $\tilde{A}^\mu_c(x) \sim p^\mu_c$.

QCD diagram can be reproduced by a SCET operator

$$J^\mu = \bar{\psi}\gamma^\mu\psi \longrightarrow \bar{\xi}_{\bar{c}}\gamma_\perp^\mu\xi_c, \tag{4.3.14}$$

where we decomposed γ^μ into light-cone coordinates and used the projection relations. However, the above operator is insufficient beyond tree-level or for processes involving collinear gluons. One problem with the operator is that usually, operator derivatives are power suppressed. However, in SCET, the derivatives corresponding to the large momentum component of the collinear fields $\bar{n}\cdot\partial\xi_c \sim \xi_c$ are not suppressed since the collinear momentum has a large component $p_c^- \sim Q$. Thus we need to include operators with an arbitrary number of such derivatives.

The expansion of a collinear field along the direction associated with the large momentum component can be written in terms of an infinite sum over non-power suppressed derivatives,

$$\xi_c(x + t\bar{n}) = \sum_{k=0}^{\infty} \frac{t^k}{k!} \left(\bar{n}\cdot\partial\right)^k \xi_c(x). \tag{4.3.15}$$

Therefore, including terms with arbitrary high derivatives is equivalent to allowing non-locality of the collinear fields along the collinear direction. However, when combining operators at different points in gauge theory, we must be careful to maintain gauge invariance. In a gauge theory, a product of fields at different space-time points is only invariant if the fields are connected by Wilson lines, defined as

$$[x + t\bar{n}, x] = \mathbf{P}\exp\left(ig\int_0^t \mathrm{d}t'\bar{n}\cdot A(x + t'\bar{n})\right), \tag{4.3.16}$$

where $\mathbf{P}$ is the path ordering operator and A is a generic gauge field. In SCET, it is useful to work with Wilson lines which run from infinity along $\bar{n}^\mu$ to the point x^μ:

$$W(x) \equiv [x, -\infty\bar{n}] = \mathbf{P}\exp\left(ig\int_{-\infty}^0 \mathrm{d}t'\bar{n}\cdot A(x + t'\bar{n})\right). \tag{4.3.17}$$

The Wilson line along a finite segment can be written as a product of two Wilson lines extending to infinity:

$$[x + t\bar{n}, x] = W(x + t\bar{n})W^\dagger(x). \tag{4.3.18}$$

We notice that since in the SCET Lagrangian, there are two types of gauge fields, the collinear and the soft ones; it is necessary to consider two types of Wilson lines,

which will be denoted as follows:

$$W_c(x) = \mathbf{P} \exp\left(ig \int_{-\infty}^{0} \mathrm{d}s\, \bar{n} \cdot \tilde{A}_c(x + s\bar{n}) \right), \tag{4.3.19}$$

$$S_n(x) = \mathbf{P} \exp\left(ig \int_{-\infty}^{0} \mathrm{d}s\, n \cdot \tilde{A}_s(x + sn) \right), \tag{4.3.20}$$

where $W_c(x)$ is the collinear and $S_n(x)$ the soft Wilson line. The collinear Wilson lines are useful to construct operators, while the soft Wilson lines are useful because of the structure of the soft interactions.

Now we turn our attention once more to the soft-collinear interactions in $\mathcal{L}_{\mathrm{SCET}}$. One can show that one can eliminate these interactions at leading power in $\lambda \ll 1$ by making use of field redefinitions called decoupling transformations. To that end, we redefine the collinear fields as

$$\xi(x) \to S_n(x_-)\xi^0(x), \tag{4.3.21}$$

$$\tilde{A}_n(x) \to S_n(x_-)\tilde{A}_n^0(x)S_n^\dagger(x_-), \tag{4.3.22}$$

where S_n is a soft Wilson line along the n-direction. Let us start with the soft-collinear interactions in the quark Lagrangian $\mathcal{L}_{\mathrm{SCET}}^{\mathrm{Quark}}$. With this definition we have

$$\begin{aligned} in \cdot D\xi(x) &\to \left(in \cdot \partial + gn \cdot S_n(x_-)\tilde{A}_n^0(x)S_n^\dagger(x_-) + gn \cdot A_s(x_-) \right) S_n(x_-)\xi^0(x) \\ &= \left(\underbrace{(in \cdot D_- S_n(x_-))}_{=0} + S_n(x_-) in \cdot \partial + S_n(x_-) gn \cdot \tilde{A}_n^0(x) \right) \xi^0(x) \\ &= S_n(x_-) \left(in \cdot \partial + gn \cdot \tilde{A}_n^0(x) \right) \xi^0(x) \\ &\equiv S_n(x_-) in \cdot D_c^0 \xi^0(x). \end{aligned}$$

Here we used that $S_n(x_-)S_n^\dagger(x_-) = 1$, that the derivative acting on $S_n(x_-)$ pulls the gauge field out of the exponential and that the covariant derivative of a Wilson line vanishes along its integration contour. Thus for the collinear quark Lagrangian, we

find,

$$\begin{aligned}\mathcal{L}_{\text{SCET}}^{\text{Quark}} &\sim \bar{\xi}(x)\frac{\bar{n}\!\!\!/}{2} in\cdot D\xi(x)\\ &\to \bar{\xi}^0(x)S_n^\dagger(x_-)\frac{\bar{n}\!\!\!/}{2}S_n(x_-) in\cdot D_c^0\xi^0(x)\\ &= \bar{\xi}^0(x)\frac{\bar{n}\!\!\!/}{2} in\cdot D_c^0\xi^0(x).\end{aligned} \tag{4.3.23}$$

So we find that the soft gluon field no longer appears in the collinear quark Lagrangian. We can use the same decoupling transformation to eliminate the soft-collinear interactions in the gluonic structure. This is because the transformations of the covariant derivative implies that the field strength tensor transforms as $\tilde{G}_{\mu\nu} \to S_n(x_-)\tilde{G}^0_{\mu\nu}S_n^\dagger(x_-)$. In the Lagrangian, the field strength tensor appears within a trace, so via its cyclic property, we can eliminate $\tilde{A}_s$ from the collinear gluon Lagrangian.

We want to emphasize that even though we have shown that the soft and collinear interactions decouple, this is only true at leading power in the expansion parameter λ. At subleading power, soft and collinear interactions are still present in the Lagrangian even after applying the decoupling transformation.

4.3.4 Gauge-covariant building blocks

In the previous section, we brushed aside the notion that $\xi(x)$ and $\tilde{A}_n(x)$ are not gauge invariant. However, now we will come back to this and define gauge-invariant building blocks. We already stated that by including Wilson lines, we can maintain gauge invariance.

The Wilson lines extending to infinity transform as follows under gauge transformations

$$W(x) \to V(x)W(x)V^\dagger(-\infty\bar{n}), \tag{4.3.24}$$

where $V(x)$ is either a soft or a collinear gauge transformation. If one considers gauge functions vanishing at infinity, such that $V^\dagger(-\infty\bar{n}) = 1$, the combinations

$$\chi(x) \equiv W^\dagger(x)\xi(x), \tag{4.3.25}$$

$$\bar{\chi}(x) \equiv \bar{\xi}(x)W(x), \tag{4.3.26}$$

are gauge invariant and can be used as building blocks to construct non-local operators. Similarly, we can introduce a gauge-invariant operator $\mathcal{A}_\perp^\mu(x)$ for the collinear gluon

fields, which we define as follows:

$$\mathcal{A}_\perp^\mu(x) \equiv W^\dagger(x)\left(iD_c^\mu W(x)\right). \tag{4.3.27}$$

The gauge independence of $\chi(x)$ and $\mathcal{A}_\perp^\mu(x)$ follows directly from the behaviour of the collinear fields, the Wilson lines, and the covariant derivatives under collinear gauge transformations.

4.4 Factorisation

After decoupling the soft and collinear modes in the Lagrangian, we are in the position to derive factorisation theorems. As a helpful example, we will derive now the factorisation theorem for the thrust distribution in the dijet region.

We will use [51] as a guide to derive the factorisation theorem; we will, however adapt the notation in order to be consistent with the rest of this work and to highlight key points.

In the Standard Model, the cross section for $e^+e^- \to$ dijets produces partons in the final state via an electroweak current, either from a photon or a Z-boson. In order to keep the discussion as simple as possible, we assume that there is only a photon. The differential cross section averaged over the incoming e^+e^- spins is written as

$$\frac{1}{\sigma_0}\mathrm{d}\sigma = \frac{-2\pi}{NQ^2}\sum_X \mathrm{d}\Pi_X (2\pi)^4\delta^4\left(q - p_X\right)\langle 0|\, J_\mu^\dagger(0)\,|X\rangle\,\langle X|\, J^\mu(0)\,|0\rangle\,, \tag{4.4.1}$$

where σ_0 is the tree-level cross section, N is the number of colours, q^μ is the total momentum of the photon in the centre-of-mass frame $q^\mu = (Q,0,0,0)$, and $J^\mu = \bar{\psi}\gamma^\mu\psi$ is the electromagnetic current operator for one quark flavour. In dijet production, any radiation apart from the primary partons must be either collinear or soft. Thus SCET is the appropriate effective theory. In SCET, the electroweak current operator is replaced by

$$J^\mu(x) = \int \mathrm{d}s\,\mathrm{d}t\, C(s,t,\mu)\bar{\chi}_{\bar{n}}(x+sn)S_{\bar{n}}^\dagger(x_+)\gamma^\mu S_n(x_-)\chi_n(x+t\bar{n}), \tag{4.4.2}$$

where $C(s,t,\mu)$ is the Wilson coefficient from matching QCD onto SCET. Finally, X are the QCD states, which will be restricted or weighted by the definition of thrust. However, in SCET there are no interactions between soft, collinear, and anticollinear sectors because of the decoupling at leading power. Thus the sum over the states $|X\rangle$

decomposes into a sum over individual soft, collinear, and anticollinear final-states:

$$\sum_X \to \sum_{X_s,X_c,X_{\bar{c}}}$$
$$|X\rangle \to |X_s\rangle \otimes |X_c\rangle \otimes |X_{\bar{c}}\rangle\,. \tag{4.4.3}$$

Hence, we are able to decompose $\langle 0|\, J_\mu^\dagger(0)\,|X\rangle\,\langle X|\, J^\mu(0)\,|0\rangle$ to

$$\begin{aligned}\langle 0|\, J_\mu^\dagger(0)\,|X\rangle\,\langle X|\, J^\mu(0)\,|0\rangle \to \int \mathrm{d}s'\,\mathrm{d}t'\,\mathrm{d}s\,\mathrm{d}t\, C^*(s',t',\mu)C(s,t,\mu)\\ \times \langle 0|\left[S_n^\dagger(0)S_{\bar{n}}(0)\right]_{ab}|X_s\rangle\,\langle X_s|\left[S_{\bar{n}}^\dagger(0)S_n(0)\right]_{cd}|0\rangle\\ \times \langle 0|\left[\bar{\chi}_{n,k}(t'\bar{n})\right]_a|X_c\rangle\,\langle X_c|\left[\chi_{n,j}(t\bar{n})\right]_d|0\rangle\,\gamma^\mu_{kl}\\ \times \langle 0|\left[\chi_{\bar{n},l}(s'n)\right]_b|X_{\bar{c}}\rangle\,\langle X_{\bar{c}}|\left[\bar{\chi}_{\bar{n},i}(sn)\right]_c|0\rangle\,\gamma_{\mu,ij},\end{aligned} \tag{4.4.4}$$

where we used $a,...,d$ for colour indices and $i,...,l$ for spinor indices, allowing us to rearrange the structures containing collinear and anticollinear fields.

In order to simplify eq. (4.4.4) further, we first notice that the collinear structures describe the propagation of only one sector because there are no interactions between sectors; the structures must be colour diagonal. Thus we can average over the colour. Secondly, Lorentz invariance dictates the proportionality of the collinear and anticollinear structures to $\bar{n}\!\!\!/$ and $n\!\!\!/$, respectively. Finally, we write eq. (4.4.4) as,

$$\begin{aligned}\langle 0|\, J_\mu^\dagger(0)\,|X\rangle\,\langle X|\, J^\mu(0)\,|0\rangle = \int \mathrm{d}s'\,\mathrm{d}t'\,\mathrm{d}s\,\mathrm{d}t\, C^*(s',t',\mu)C(s,t,\mu)\,\mathrm{Tr}\left[\gamma_\mu\frac{n\!\!\!/}{8}\gamma^\mu\frac{\bar{n}\!\!\!/}{8}\right]\\ \times \mathrm{tr}\{\langle 0|\left[S_n^\dagger S_{\bar{n}}\right]_{ab}(0)\,|X_s\rangle\,\langle X_s|\left[S_{\bar{n}}^\dagger S_n\right]_{cd}(0)\,|0\rangle\}\\ \times \frac{\delta_{ad}}{N}\,\mathrm{Tr}\{\langle 0|\,\bar{\chi}_n(t'\bar{n})\,|X_c\rangle\,\langle X_c|\,\bar{n}\!\!\!/\chi_n(t\bar{n})\,|0\rangle\}\\ \times \frac{\delta_{bc}}{N}\,\mathrm{Tr}\{\langle 0|\,\chi_{\bar{n}}(sn)\,|X_{\bar{c}}\rangle\,\langle X_{\bar{c}}|\,n\!\!\!/\bar{\chi}_{\bar{n}}(s'n)\,|0\rangle\},\end{aligned} \tag{4.4.5}$$

where Tr is a Dirac trace and tr is a colour trace. Additionally we have used a Fierz rearrangement for the spinor indices.

In order to avoid explicit non-locality, we introduce the Fourier transform of $C(s,t,\mu)$:

$$C(s,t,\mu) = \int \mathrm{d}k\,\mathrm{d}l\, e^{iks}e^{ilt}\tilde{C}(k,l,\mu). \tag{4.4.6}$$

By applying the translation operator in either the collinear or anticollinear sector we

find that

$$\langle X_c|\,\mathcal{O}(t\bar{n})\,|0\rangle = \langle X_c|\,e^{i\mathcal{P}t\bar{n}}\mathcal{O}(0)e^{-i\mathcal{P}t\bar{n}}\,|0\rangle = e^{it\bar{n}p_{X_c}}\,\langle X_c|\,\mathcal{O}(0)\,|0\rangle\,. \tag{4.4.7}$$

We can find a similar result for the anticollinear sector. By substituting $C(s,t,\mu)$ in terms of its Fourier transform and using the translation operator, we can perform the integrations over s, s', t, t', which results in δ-distributions, fixing k and l to the large components of the collinear and anticollinear momenta: $\bar{n}\cdot k = n\cdot l = Q$.

Let us now turn to the δ-distribution which enforces momentum conservation in eq. (4.4.1). Here we note that p_X is simply the sum of the radiated momenta from all relevant sectors, i.e. $p_X = p_s + p_c + p_{\bar{c}}$. As we know the typical scaling of these modes, we can write the δ-distribution in light-cone components in the following way. For the n-component we find $\delta(\bar{n}\cdot q - \bar{n}\cdot p_X) = \delta(Q - \underbrace{\bar{n}\cdot p_s}_{\sim\lambda^2} - \underbrace{\bar{n}\cdot p_c}_{\sim\lambda^0} - \underbrace{\bar{n}\cdot p_{\bar{c}}}_{\sim\lambda^2}) = \delta(Q - \bar{n}\cdot p_c)$, which fixes the $\bar{n}\cdot p_c$ component. Similarly, for the $\bar{n}$-component we find $\delta(Q - n\cdot p_{\bar{c}})$. In the case of the $\perp$-component, we know that $\vec{q}_\perp = \vec{0}$, and $\vec{p}_{s,\perp} \sim \lambda^2 \sim \lambda\vec{p}_{\{c,\bar{c}\},\perp}$, so the $\perp$-component is determined by $\delta^{(2)}(\vec{p}_{c,\perp} + \vec{p}_{\bar{c},\perp})$. This can be further simplified by recognising that we integrate over the relative direction between incoming leptons and outgoing hadrons when calculating the cross section, which means that the final result cannot depend on our choice of axis. We can thus choose our coordinate system for a collinear sector in a way that the z-axis points along $\vec{n}$. This forces the transverse component to vanish, which we have to compensate by introducing a new constraint $\pi Q^2\delta^{(2)}(\vec{p}_{c,\perp})$. Overall the momentum conservation thus reads

$$\delta^{(4)}(q - p_X) \to 2\pi Q^2\delta(Q - \bar{n}\cdot p_c)\delta(Q - n\cdot p_{\bar{c}})\delta^{(2)}(\vec{p}_{c,\perp})\delta^{(2)}(\vec{p}_{\bar{c},\perp}), \tag{4.4.8}$$

where the additional factor 2 emerges due to the transition to light-cone coordinates. We can see from the previous expression that we have constraints for three out of the four components for both collinear and anticollinear sectors. Next, we insert the identity

$$1 = \int \mathrm{d}x_c\,\mathrm{d}x_{\bar{c}}\,\delta(x_c - n\cdot p_c)\delta(x_{\bar{c}} - n\cdot p_{\bar{c}}) \tag{4.4.9}$$

where we define x_c and $x_{\bar{c}}$ via the following vectors

$$r_c^\mu = \frac{n^\mu}{2}Q + \frac{\bar{n}^\mu}{2}x_c, \qquad r_{\bar{c}}^\mu = \frac{\bar{n}^\mu}{2}Q + \frac{n^\mu}{2}x_{\bar{c}}, \tag{4.4.10}$$

which obey the same constraints from the momentum conservation. The insertion of

the redundant constraint of the small component yields

$$\delta^{(4)}(q-p_X)=\frac{1}{2}\pi Q^2\int \mathrm{d}x_c\,\mathrm{d}x_{\bar{c}}\,\delta^{(4)}(r_c^\mu-p_c^\mu)\delta^{(4)}(r_{\bar{c}}^\mu-p_{\bar{c}}^\mu). \tag{4.4.11}$$

For the final step we use that $r^2_{\{c,\bar{c}\}}=Qx_{\{c,\bar{c}\}}$, and hence $\mathrm{d}r^2_{\{c,\bar{c}\}}=Q\mathrm{d}x_{\{c,\bar{c}\}}$, and thus we are able to write the thrust distribution as

$$\begin{aligned}\frac{1}{\sigma_0}\frac{\mathrm{d}\sigma}{\mathrm{d}\tau}=&|\tilde{C}(Q,Q,\mu)|^2\int \mathrm{d}r_c^2\,\mathrm{d}r_{\bar{c}}^2\,\delta(\tau-\tau(p_X))\\
&\times\sum_{X_s}\frac{1}{N}\mathrm{tr}\{\langle 0|\left[S_n^\dagger S_{\bar{n}}\right](0)\,|X_s\rangle\,\langle X_s|\left[S_{\bar{n}}^\dagger S_n\right](0)\,|0\rangle\}\\
&\times\sum_{X_c}\frac{1}{N}\frac{(2\pi)^4}{4\pi Q}\delta^{(4)}(r_c^\mu-p_c^\mu)\,\mathrm{Tr}\{\langle 0|\,\bar{\chi}_n(0)\,|X_c\rangle\,\langle X_c|\,\frac{\bar{n}\!\!\!/}{2}\chi_n(0)\,|0\rangle\}\\
&\times\sum_{X_{\bar{c}}}\frac{1}{N}\frac{(2\pi)^4}{4\pi Q}\delta^{(4)}(r_{\bar{c}}^\mu-p_{\bar{c}}^\mu)\,\mathrm{Tr}\{\langle 0|\,\chi_{\bar{n}}(0)\,|X_{\bar{c}}\rangle\,\langle X_{\bar{c}}|\,\frac{n\!\!\!/}{2}\bar{\chi}_{\bar{n}}(0)\,|0\rangle\}.\end{aligned} \tag{4.4.12}$$

This is the extent to which we can get with the scaling information. Before we continue, a few words about the different structures are in order. The Wilson coefficient $|\tilde{C}|^2$ in the first line encodes the matching between QCD to SCET and is the square of the vector form factor. It includes virtual corrections at all loop orders. The natural scale of this function is the hard scale Q, which is reasonable as it is determined by integrating out the hard modes. It is typically referred to as the *hard function*. The second line gives rise to the *soft function*, which describes the emission of soft isotropic radiation from the colour-charged particles in the process. Here the sum over X_s implicitly contains phase-space integrations for any emissions off the Wilson lines enclosed by the bras and kets. Finally, the last two structures are the *jet functions*, which describe the collinear radiation off the energetic, outgoing primary particles. The sum includes the phase-space integrations, and a sum over all colours is assumed.

In the following, we leave the general discussion and specialise the calculation to thrust. So we turn to the definition as it enters into eq. (3.1.2) in detail: In the dijet limit, thrust reduces to $\tau=\frac{p_L^2+p_R^2}{Q^2}$, where $p_{L,R}$ is the total 4-momentum into the left or right hemisphere defined by the thrust axis $\vec{n}_T$. All particles in X_c go into the left hemisphere and thus contribute to p_L, and those in $X_{\bar{c}}$ contribute to p_R and thus are in the right hemisphere. On the other hand, soft emissions can go either way depending if $(\bar{n}\cdot p_s>n\cdot p_s)$ or $(\bar{n}\cdot p_s<n\cdot p_s)$. Let us assume that the total soft momentum of

the left hemisphere is given by k_L and thus

$$p_L^2 = (p_c + k_L)^2 = \underbrace{p_c^2}_{\sim\lambda^2} + \underbrace{2p_c k_L}_{\sim\lambda^2} + \underbrace{k_L^2}_{\sim\lambda^4} \sim r_c^2 + Qn\cdot k_L, \tag{4.4.13}$$

where we used the relative scaling of the collinear and soft modes to eliminate the subleading contributions from k_L^2 and $p_c k_L$, we also used the form of p_c as we have previously written it down in the thrust distribution for the dijet cross section. For the emission into the right hemisphere, we find a similar form:

$$p_R^2 = (p_{\bar{c}} + k_R)^2 \sim r_{\bar{c}}^2 + Q\bar{n}\cdot k_R. \tag{4.4.14}$$

Combing these two, we find

$$\tau = \sum_{L,R} \frac{p_L^2 + p_R^2}{Q^2} \sim \frac{r_c^2 + Qn\cdot k_L + r_{\bar{c}}^2 + Q\bar{n}\cdot k_R}{Q^2} = \tau_c + \tau_{\bar{c}} + \tau_s, \tag{4.4.15}$$

where in the last equality, we emphasize that the observable decomposes into a sum of contributions from the different regions. This decomposition into independent contributions to the observables from the individual functions is required for any observables to allow factorisation. Substituting this into the factorisation theorem, we find that the phase-space integrations in X_s and $X_{c,\bar{c}}$ are now related. We, therefore, adapt eq. (4.4.12) by inserting an additional integral and δ-functions into our cross section. Furthermore, as $\tau \ll 1$, $r_c, r_{\bar{c}}, k_L$ and k_R must be small, thus we can extend the sum over just collinear, anticollinear, and soft states to all states. In the end, we arrive at the factorisation theorem for thrust:

$$\begin{aligned}\frac{1}{\sigma_0}\frac{\mathrm{d}\sigma}{\mathrm{d}\tau} &= |\tilde{C}(Q,Q,\mu)|^2 \int \mathrm{d}r_c^2\,\mathrm{d}r_{\bar{c}}^2\,\mathrm{d}k\,\delta\left(\tau - \frac{r_c^2 + r_{\bar{c}}^2 + Qk}{Q^2}\right)\\
&\times \sum_X \frac{1}{N}\mathrm{tr}\{\langle 0|\left[S_n^\dagger S_{\bar{n}}\right](0)\,|X\rangle\,\langle X|\left[S_{\bar{n}}^\dagger S_n\right](0)\,|0\rangle\}\delta(k - n\cdot k_L - \bar{n}\cdot k_R)\\
&\times \sum_X \frac{1}{N}\frac{(2\pi)^4}{2\pi Q}\delta^{(4)}(r_c^\mu - p_c^\mu)\,\mathrm{Tr}\{\langle 0|\,\bar{\chi}_n(0)\,|X\rangle\,\langle X|\,\frac{\bar{n}\!\!\!/}{2}\chi_n(0)\,|0\rangle\}\\
&\times \sum_X \frac{1}{N}\frac{(2\pi)^4}{2\pi Q}\delta^{(4)}(r_{\bar{c}}^\mu - p_{\bar{c}}^\mu)\,\mathrm{Tr}\{\langle 0|\,\chi_{\bar{n}}(0)\,|X\rangle\,\langle X|\,\frac{n\!\!\!/}{2}\bar{\chi}_{\bar{n}}(0)\,|0\rangle\}.\end{aligned} \tag{4.4.16}$$

We can again identify $|\tilde{C}|^2$ as the hard function, the second line as the soft function for thrust, and the final two structures as the jet functions.

Each of these functions can be computed individually in perturbation theory and subsequently convoluted with the others to arrive at the singular part of the thrust distribution. Assigning the standard notation to the different contributions, the factorisation theorem takes the simple form

$$\frac{1}{\sigma_0}\frac{\mathrm{d}\sigma}{\mathrm{d}\tau} = H(Q,\mu)\int \mathrm{d}r_c^2\,\mathrm{d}r_{\bar{c}}^2\,\mathrm{d}k\,\delta\left(\tau - \frac{r_c^2 + r_{\bar{c}}^2 + Qk}{Q^2}\right) J(r_c^2,\mu)\bar{J}(r_{\bar{c}}^2,\mu)S(k,\mu). \tag{4.4.17}$$

4.5 Resummation in SCET

Before we turn to the resummation of the factorisation ingredients, let us highlight some details by inspecting the jet function more thoroughly.

As in any perturbative computation, the jet function, similar to the hard and soft function, is ill-defined in the absence of a suitable regularisation and renormalisation procedure. In dimensional regularisation, the bare jet function for thrust can be evaluated, and the one-loop result reads [96]

$$\begin{aligned} J(r_c^2,\mu) = \delta(r_c^2) + \frac{\alpha_s C_F}{4\pi}\Bigg[&\left(\frac{4}{\epsilon^2} + \frac{3 + 8\ln\frac{\mu}{Q}}{\epsilon} + 8\ln^2\frac{\mu}{Q} + 6\ln\frac{\mu}{Q} + 7 - \pi^2\right)\delta(r_c^2) \\ &- \left(\frac{4}{\epsilon} + 3 + 6\ln\frac{\mu}{Q}\right)\left[\frac{1}{r_c^2}\right]_\star + 4\left[\frac{\ln r_c^2}{r_c^2}\right]_\star\Bigg], \end{aligned} \tag{4.5.1}$$

where the $\star$-distribution is a generalisation of a $+$-distribution for dimensional variables. At $\mathcal{O}(\alpha_s)$ in the $\overline{\mathrm{MS}}$ scheme, renormalisation proceeds via the introduction of a counterterm Z, which at this order has the same effect as dropping the ϵ-poles. The anticollinear jet function will read the same, the only difference being that $r_c^2 \to r_{\bar{c}}^2$.

The occurrence of δ and $\star$-distributions in eq. (4.5.1) is a minor nuisance for two reasons. First, renormalising the jet-, hard-, and soft functions requires the convolution with an appropriate Z-factor, which in the end leads to non-local renormalisation group equations (RGE). The non-locality makes the solution of the RGEs cumbersome. Second, considering we want to calculate the jet function numerically, distribution-valued results are inconvenient; we prefer regular functions.

One way of dealing with this is switching from momentum space to Laplace-space,

where each function f has an associated Laplace space version:

$$\mathcal{L}\{f\}(s) = \int_0^\infty f(t)e^{-st}\mathrm{d}t. \tag{4.5.2}$$

In order to shorten the notation we will use $\tilde{f}(s) = \mathcal{L}\{f\}(s)$ for the Laplace-transformed functions. We find that the factorisation theorem becomes in Laplace space

$$\int_0^\infty \mathrm{d}\tau\, e^{-\tau Q s}\frac{1}{\sigma_0}\frac{\mathrm{d}\sigma}{\mathrm{d}\tau} = H\left(\frac{\mu}{Q}\right)\tilde{J}\left(\frac{\mu\sqrt{s}}{Q}\right)\tilde{\tilde{J}}\left(\frac{\mu\sqrt{s}}{Q}\right)\tilde{S}\left(\frac{\mu s}{Q}\right), \tag{4.5.3}$$

where the objects on the right-hand side are regular functions and do not contain any distributions.

Multiplicative renormalisation for any function F leads to a RGE of the form

$$\frac{\mathrm{d}F(\mu)}{\mathrm{d}\ln\mu} = \gamma_F F(\mu), \tag{4.5.4}$$

where γ_F is the anomalous dimension of F. The anomalous dimension contains information about the deviations from the classical scaling behaviour of F.

In the case of the renormalised and Laplace-transformed jet function in eq. (4.5.1) we find:

$$\begin{aligned}\frac{\mathrm{d}\tilde{J}_R\left(\frac{\mu\sqrt{s}}{Q}\right)}{\mathrm{d}\ln\mu} &= \frac{\mathrm{d}}{\mathrm{d}\ln\mu}\left[1+\frac{\alpha_s C_F}{4\pi}\left(8\ln^2\frac{\mu\sqrt{s}}{Q}+6\ln\frac{\mu\sqrt{s}}{Q}+7-\frac{2\pi^2}{3}\right)\right]+\mathcal{O}\left(\alpha_s^2\right)\\ &= \left[\frac{\alpha_s C_F}{4\pi}(16)\ln\frac{\mu\sqrt{s}}{Q}+\frac{\alpha_s C_F}{4\pi}(6)+\mathcal{O}\left(\alpha_s^2\right)\right]\tilde{J}_R\left(\frac{\mu\sqrt{s}}{Q}\right)\\ &= \gamma_{\mathrm{jet}}\tilde{J}_R\left(\frac{\mu\sqrt{s}}{Q}\right).\end{aligned} \tag{4.5.5}$$

So from eq. (4.5.5) we find that the anomalous dimensions for the jet function is

$$\gamma_{\mathrm{jet}} = \left(\frac{\alpha_s C_F}{4\pi}\right)16\ln\frac{\mu\sqrt{s}}{Q}+\left(\frac{\alpha_s C_F}{4\pi}\right)6+\mathcal{O}\left(\alpha_s^2\right) \tag{4.5.6}$$

which is the first perturbative order of

$$\gamma_{\mathrm{jet}} = 4\Gamma_{\mathrm{Cusp}}\left(\alpha_s\right)\ln\frac{\mu\sqrt{s}}{Q}+\gamma_J\left(\alpha_s\right), \tag{4.5.7}$$

where we defined the Cusp anomalous dimension $\Gamma_{\mathrm{Cusp}}\left(\alpha_s\right)$ and the jet anomalous

dimension $\gamma_J(\alpha_s)$. $\Gamma_{\text{Cusp}}(\alpha_s)$ is related to the renormalisation of Wilson lines with a cusp or kink [97], and thus universal for all observables. The circumstance that $\Gamma_{\text{Cusp}}(\alpha_s)$ is accompanied by a $\ln \frac{\mu\sqrt{s}}{Q}$ is the reason why we can resum double logarithm using RGE techniques. On the other hand, γ_J is observable-dependent and in general different from its soft and hard counterpart γ_S and γ_H. However, they can all be related to each other via a consistency relation, which we will state later. If we define the perturbative expansion for both anomalous dimensions as

$$\Gamma_{\text{Cusp}}(\alpha_s) = \sum_{n=0}^{\infty} \left(\frac{\alpha_s}{4\pi}\right) \Gamma_n \tag{4.5.8}$$

$$\gamma_J(\alpha_s) = \sum_{n=0}^{\infty} \left(\frac{\alpha_s}{4\pi}\right) \gamma_n^J, \tag{4.5.9}$$

we can directly read off $\Gamma_0 = 4C_F$ and $\gamma_0^J = 6C_F$.

We are now able to solve the RGE in eq. (4.5.5) and allow the solution to run between any scales μ and μ_0 as:

$$\tilde{J}\left(\frac{\mu\sqrt{s}}{Q}\right) = U(\mu_0,\mu)\tilde{J}\left(\frac{\mu_0\sqrt{s}}{Q}\right), \tag{4.5.10}$$

where $U(\mu_0,\mu)$ is an evolution kernel which evolves the jet function from the scale μ_0 to μ. It can be written in the form

$$\begin{aligned} U(\mu_0,\mu) &= \exp\left[\int_{\mu_0}^{\mu} \mathrm{d}\ln\mu'\, \gamma_{\text{jet}}\left(\frac{\mu'\sqrt{s}}{Q}\right)\right] \\ &= \exp\left[\int_{\mu_0}^{\mu} \mathrm{d}\ln\mu' \left\{4\Gamma_{\text{Cusp}} \ln\frac{\mu'}{\mu_0} + \gamma_J + 4\Gamma_{\text{Cusp}}\ln\frac{\mu_0\sqrt{s}}{Q}\right\}\right] \\ &= e^{A_J(\mu,\mu_0)}\left(\frac{\mu_0\sqrt{s}}{Q}\right)^{4\int_{\mu_0}^{\mu}\mathrm{d}\ln\mu'\Gamma_{\text{Cusp}}}, \end{aligned} \tag{4.5.11}$$

where $A_J(\mu,\mu_0) = \int_{\mu_0}^{\mu} \mathrm{d}\ln\mu' \left(4\Gamma_{\text{Cusp}}\ln\frac{\mu'}{\mu_0} + \gamma_J\right)$.

We have shown the solution to the RGE of the jet function, there are however equivalent ones for the soft and hard functions:

$$H\left(\frac{\mu}{Q}\right) = H\left(\frac{\mu_0}{Q}\right) e^{A_H(\mu,\mu_0)}\left(\frac{\mu_0}{Q}\right)^{-4\int_{\mu_0}^{\mu}\mathrm{d}\ln\mu'\Gamma_{\text{Cusp}}}, \tag{4.5.12}$$

$$\tilde{S}\left(\frac{\mu s}{Q}\right) = \tilde{S}\left(\frac{\mu_0 s}{Q}\right) e^{A_S(\mu,\mu_0)}\left(\frac{\mu_0 s}{Q}\right)^{-4\int_{\mu_0}^{\mu}\mathrm{d}\ln\mu'\Gamma_{\text{Cusp}}}. \tag{4.5.13}$$

We can now observe why resummation is necessary in Laplace space. By transforming from momentum space to Laplace space the $r^2_{c,\bar{c}}$- and k-integrals fix the mass dimension of the different functions. Therefore it also fixes the relative power of s and μ. This is the reason why we find $\frac{\mu\sqrt{s}}{Q}$ as the dimensionless parameter in the evolution kernel of the jet function, and similarly, $\frac{\mu s}{Q}$ in the soft function evolution kernel.

Let us now assume that we did not run the renormalisation scale μ, i.e., if we set $\mu = \mu_0$, and choose to remove the large logarithms from the jet function $\mu_0 = \frac{Q}{\sqrt{s}}$. This will ensure that the logarithms in the jet function are $\sim \mathcal{O}(1)$, however in the hard function we will find logarithms $\sim \mathcal{O}\left(\frac{1}{\sqrt{s}}\right)$ and similar for the soft function $\sim \mathcal{O}\left(\sqrt{s}\right)$. So as long as we do not run the renormalisation scale μ, we can remove large logarithms only from one of the functions, while the others still exhibit large logarithms.

If, however, we allow the running of μ, and choose μ_0 to be $\mu_H \sim Q$ for the hard, $\mu_S \sim \frac{Q}{s}$ for the soft and $\mu_J \sim \frac{Q}{\sqrt{s}}$ for the jet function, the functions are evaluated at their natural scales and thus will be free of any large logarithms. The exponents in the different evolution kernel, for any choice of μ_0 away from their respective natural scales, will then ensure that we will resum all logarithms.

Previously, we have claimed that the cusp anomalous dimension is the same for all functions and that the non-cusp anomalous dimension can be related to each other; let us now verify this claim. We know that the left-hand side of eq. (4.5.3) must be independent of the renormalisation scale μ. Thus the product of hard, jet, and soft functions must be independent as well:

$$\frac{\mathrm{d}}{\mathrm{d}\ln\mu}\left[H\left(\frac{\mu}{Q}\right)\tilde{J}\left(\frac{\mu\sqrt{s}}{Q}\right)\tilde{\bar{J}}\left(\frac{\mu\sqrt{s}}{Q}\right)\tilde{S}\left(\frac{\mu s}{Q}\right)\right] = 0. \tag{4.5.14}$$

By performing the differentiation with respect to the renormalisation scale μ, one finds

$$\begin{aligned} 0 =& \frac{\mathrm{d}}{\mathrm{d}\ln\mu}\ln\left[H\left(\frac{\mu}{Q}\right)\tilde{J}\left(\frac{\mu\sqrt{s}}{Q}\right)\tilde{\bar{J}}\left(\frac{\mu\sqrt{s}}{Q}\right)\tilde{S}\left(\frac{\mu s}{Q}\right)\right] \\ =& \gamma_{\text{hard}} + \gamma_{\text{jet}} + \gamma_{\text{jet}} + \gamma_{\text{soft}}. \end{aligned} \tag{4.5.15}$$

Here we can see that the sum of the anomalous dimensions vanishes. If we write the anomalous dimensions in terms of cusp and non-cusp piece, this equation becomes

$$0 = -4\Gamma_{\text{Cusp}}\ln\frac{\mu}{Q} + \gamma_H + 4\Gamma_{\text{Cusp}}\ln\frac{\mu\sqrt{s}}{Q} + \gamma_J + 4\Gamma_{\text{Cusp}}\ln\frac{\mu\sqrt{s}}{Q} + \gamma_J - 4\Gamma_{\text{Cusp}}\ln\frac{\mu s}{Q} + \gamma_S. \tag{4.5.16}$$

In order for this cancellation to work, it is crucial that the scale dependence is logarith-

mic, with the same coefficient Γ_{Cusp} in all of the RGEs which enter eq. (4.5.14). Also, this relation forces the non-cusp anomalous dimension to obey the following consistency relation

$$\gamma_H + 2\gamma_J + \gamma_S = 0. \tag{4.5.17}$$

Finally, let us come back to the counting of logarithms. In eq. (3.4.2) we have established a scheme for the counting of logarithms; we expect that A_H, A_J, and A_S follow the scheme and resum the logarithms. Let us, therefore, take a closer look at A_J.[3] Any μ-dependence is either expressed directly as $\ln \mu$, or is hidden within $\alpha_s(\mu)$. Thus, if we know the QCD β-function, we can express $\alpha_s(\mu)$ in terms of $\alpha_s(\mu_0)$ at some other scale μ_0.

The QCD β-function is known to 5-loops [98, 99], but for our work fewer orders will be sufficient. In renormalisation-group improved perturbation theory, the β-function governing the scale dependence of the renormalised coupling α_s can be written as

$$\beta(\alpha_s(\mu)) = -2\sum_{n=0}^{\infty} \beta_n \left(\frac{\alpha_s(\mu)}{4\pi}\right)^{n+2}. \tag{4.5.18}$$

In order to find the running of α_s we solve eq. (4.5.18) to some fixed order and expand around its value at some reference scale μ_0. The solution up to $\mathcal{O}(\alpha_s^3(\mu_0))$ is then given by

$$\alpha_s(\mu) = \alpha_s(\mu_0) - \frac{\alpha_s^2(\mu_0)}{2\pi}\beta_0 \ln\frac{\mu}{\mu_0} + \frac{\alpha_s^3(\mu_0)}{8\pi^2}\left(2\beta_0^2 \ln^2\frac{\mu}{\mu_0} - \beta_1 \ln\frac{\mu}{\mu_0}\right) + \mathcal{O}(\alpha_s^4(\mu_0)). \tag{4.5.19}$$

We can observe from eq. (4.5.19) that the terms $\alpha_s^n L^{n-1}$ appear always in combination with β_0 and the term $\alpha_s^n L^{n-2}$ with β_1, this pattern generalises to higher orders. Thus, generally, we can say that terms of the form $\alpha_s^n L^{n-m}$ are always accompanied by a β_{m-1} term.

Finally, let us look at the evolution kernel A_J as a whole. To collect the logarithms,

[3] Similar considerations apply to A_H and A_S as well.

we write the first few terms of the expansion of the anomalous dimensions.

$$\begin{aligned}
A_J &\sim \int_{\mu_0}^{\mu} \mathrm{d}\ln\mu' \left\{ \Gamma_{\mathrm{Cusp}} \ln\frac{\mu'}{\mu_0} + \gamma_J \right\} \\
&= \int_{\mu_0}^{\mu} \mathrm{d}\ln\mu' \left[\frac{\alpha_s(\mu')}{4\pi}\Gamma_0 \ln\frac{\mu'}{\mu_0} + \frac{\alpha_s(\mu')}{4\pi}\gamma_0^J + \left(\frac{\alpha_s(\mu')}{4\pi}\right)^2 \Gamma_1 \ln\frac{\mu'}{\mu_0} + \left(\frac{\alpha_s(\mu')}{4\pi}\right)^2 \gamma_1^J \right. \\
&\qquad \left. + \left(\frac{\alpha_s(\mu')}{4\pi}\right)^3 \Gamma_2 \ln\frac{\mu'}{\mu_0} + \left(\frac{\alpha_s(\mu')}{4\pi}\right)^3 \gamma_2^J + \dots \right] \\
&= \int_{\mu_0}^{\mu} \mathrm{d}\ln\mu' \left[\left(\frac{\alpha_s(\mu_0)}{4\pi}\right) \left\{ \Gamma_0 \ln\frac{\mu'}{\mu_0} + \gamma_0^J \right\} + \left(\frac{\alpha_s(\mu_0)}{4\pi}\right)^2 \left\{ -2\beta_0\Gamma_0 \ln^2\frac{\mu'}{\mu_0} - 2\beta_0\gamma_0^J \ln\frac{\mu'}{\mu_0} \right. \right. \\
&\quad \left. + \Gamma_1 \ln\frac{\mu'}{\mu_0} + \gamma_1^J \right\} + \left(\frac{\alpha_s(\mu_0)}{4\pi}\right)^3 \left\{ \frac{\beta_0^2\Gamma_0}{2} \ln^3\frac{\mu'}{\mu_0} - \frac{\beta_1\Gamma_0}{4} \ln^2\frac{\mu'}{\mu_0} + \frac{\beta_0^2\gamma_0^J}{2} \ln^2\frac{\mu'}{\mu_0} - \frac{\beta_1\gamma_0^J}{4} \ln\frac{\mu'}{\mu_0} \right. \\
&\qquad \left. \left. -2\beta_0\Gamma_1 \ln^2\frac{\mu'}{\mu_0} - 2\beta_0\gamma_1^J \ln\frac{\mu'}{\mu_0} + \Gamma_2 \ln\frac{\mu'}{\mu_0} + \gamma_2^J \right\} + \dots \right].
\end{aligned} \tag{4.5.20}$$

In order to visualize the counting of logarithms let us perform the integration and collect the result in the same spirit as in eq. (3.4.3). Thus we arrive at the following ordering

$$\begin{aligned}
A_J \sim & \underbrace{\left(\Gamma_0 (\alpha_s L) + \beta_0\Gamma_0 (\alpha_s L)^2 + \beta_0^2\Gamma_0 (\alpha_s L)^3 + \mathcal{O}((\alpha_s L)^4)\right)}_{\mathrm{LL}} L \\
& + \underbrace{\left(\gamma_0^J (\alpha_s L) + \left(\beta_0\gamma_0^J + \Gamma_1\right)(\alpha_s L)^2 + \left(\beta_1\Gamma_0 + \beta_0^2\gamma_0^J + \beta_0\Gamma_1\right)(\alpha_s L)^3 + \mathcal{O}((\alpha_s L)^4)\right)}_{\mathrm{NLL}} \\
& + \underbrace{\left(\gamma_1^J (\alpha_s L)^2 + \left(\beta_1\gamma_0^J + \beta_0\gamma_1^J + \Gamma_2\right)(\alpha_s L)^3 + \mathcal{O}((\alpha_s L)^4)\right)}_{\mathrm{NNLL}} \frac{1}{L} + \mathcal{O}(\mathrm{N^3LL}),
\end{aligned} \tag{4.5.21}$$

where $L = \frac{\mu}{\mu_0}$. In eq. (4.5.21), it is obvious what ingredients we need to achieve a desired logarithmic accuracy. For example, to achieve leading logarithmic accuracy, we only need β_0 and Γ_0. On the other hand, if we want to capture the $\alpha_s^n L^n$ terms, then we need, in addition to the previous quantities, β_1, Γ_1, and γ_0^J.

To summarize: For LL resummation, we need only the 1-loop α_s running and 1-loop cusp anomalous dimension, NLL requires 2-loop α_s running and cusp anomalous dimension, and 1-loop non-cusp anomalous dimension. This can be generalized such that for $\mathrm{N^nLL}$ resummation we need the $(n+1)$-loop α_s running and cusp anomalous dimension and n-loop non-cusp anomalous dimension [100]. One thing to keep in mind is that for this work, we only looked at A_J. However, there are also contributions from

the soft and hard function, so any order of γ_J has to be matched by the same order of γ_S and γ_H. One upshot is that through eq. (4.5.17) only one of them is needed, besides γ_J.

As a final remark of this section, we consider the boundary conditions $\tilde{J}\left(\frac{\mu_0\sqrt{s}}{Q}\right)$, $\tilde{S}\left(\frac{\mu_0 s}{Q}\right)$ and $H\left(\frac{\mu_0}{Q}\right)$. As we count $\alpha_s L \sim \mathcal{O}(1)$, we can map the perturbative expansions of $\tilde{J}, \tilde{S}$, and H to the logarithmic counting. The series then starts at tree level, where no logarithmic enhancement is present, and gains inverse powers of logarithms as more and more orders of α_s are added. So we require for the boundary conditions α_s^n-terms for $\mathrm{N}^{n+1}\mathrm{LL}$ accuracy. From a computational point of view, it is reasonable to assume that if the anomalous dimension is known to a specific order in α_s, then the corresponding boundary condition is also known to the same order. Thus we can introduce a modified counting scheme: the $\mathrm{N}^n\mathrm{LL}'$ accuracy, which requires the renormalised functions to α_s^n-order.

4.6 $\mathrm{SCET_{II}}$ and the collinear-anomaly approach

Prior to laying out the framework of our project, we need to review $\mathrm{SCET_{II}}$ because of the additional complications arising from it.

We start by summarising what we know of $\mathrm{SCET_{II}}$-observables so far. These observables are those where the soft and collinear modes lie on the same virtuality hyperbola as shown in figure 4.2.1. This implies that contributions from the overlap regions between the two modes lead to essentially unconstrained integrations over the respective rapidities and thus result in divergences unregularised by dimensional regularisation. Therefore, $\mathrm{SCET_{II}}$ observables cannot be reasonably computed with just dimensional regularisation.

The solution consists in introducing a second regulator based on the rapidities to disentangle the soft and collinear modes. This allows the computation of soft and jet functions, which show divergences in the new regulator, in addition to the usual ϵ-divergences. This second regulator can be introduced in different ways, either by modifying the underlying matrix element [101–104], or by restricting the phase-space via additional factors [94, 105]. We choose the latter, where both jet and soft functions have explicit poles in the new regulator, usually denoted as α. As this regulator is artificially implemented, the α dependence cancels as soon as all soft and collinear contributions are added up. However, in the remainder, large logarithms remain in the expression.

Since the additional regulator is implemented on the phase-space level, an additional dimensionful factor must be introduced that breaks the equal scaling of the soft and collinear modes in the computation. This new 't Hooft scale associated with the analytic regulator is similar to the appearance of μ in dimensional regularisation. Therefore the product of the relevant jet and soft functions must be independent of the artificially introduced scale ν. Consequently, the quantity

$$P = \tilde{J}\left(s, Q, \mu, \nu\right) \tilde{\bar{J}}\left(s, Q, \mu, \nu\right) \tilde{S}\left(s, Q, \mu, \nu\right), \tag{4.6.1}$$

should satisfy the differential equation

$$\frac{\mathrm{d}}{\mathrm{d}\ln\nu} \ln P = \frac{\mathrm{d}}{\mathrm{d}\ln\nu} \left[\ln \tilde{J}\left(s, Q, \mu, \nu\right) + \ln \tilde{\bar{J}}\left(s, Q, \mu, \nu\right) + \ln \tilde{S}\left(s, Q, \mu, \nu\right)\right] = 0. \tag{4.6.2}$$

This implies that the terms within the square brackets in the equation above should be at most linear in $\ln\nu$ [95, 106]. One can then extract the terms depending on ν by

defining a remainder expression W as follows:

$$\begin{aligned} \ln P &\equiv \ln W(s,\mu) - F(s,\mu) \ln (sQ) \\ \Longrightarrow P &= (sQ)^{-F(s,\mu)} W(s,\mu), \end{aligned} \tag{4.6.3}$$

where $F(s,\mu)$ is the anomaly exponent. After this exponentiation, the remaining expressions are free from large logarithms associated with the rapidities, and the usual SCET procedure, described in the previous section, of running hard and remainder functions to a common scale can be set up.

Chapter 5

General considerations

In the previous section, we learned how the techniques for the resummation of large logarithms work within the SCET framework. Therefore we can now clearly state the boundaries, general considerations, and assumptions that define our project. Thus, we will list in this chapter all the properties we require to be compatible with our setup. In general the project can be thought of as a natural extension of the existing program `SoftSERVE` [41–43].

5.1 Logarithmic accuracy

First, we need to establish which accuracy we want to achieve and, therefore, to which perturbative order we have to calculate the jet function. We have shown in section 4.5 which ingredients are needed to achieve NNLL′ accuracy and outline what would be required to achieve $\mathrm{N}^n\mathrm{LL}'$ accuracy. The current state-of-the-art accuracy is NLL′, however some full and many partial results exist for NNLL resummation, and even $\mathrm{N}^3\mathrm{LL}$ and $\mathrm{N}^4\mathrm{LL}$ accuracy has been achieved for a few observables [33–36, 39, 40]. This work, alongside `SoftSERVE`, is supposed to provide the NNLO input for NNLL′ accuracy for a generic class of collider observables. Thus we first need to determine which quantities are known and which need to be calculated.

In order to achieve NNLL′ accuracy, we require the cusp anomalous dimension at $\mathcal{O}(\alpha_s^3)$. One approach to the calculation is based on evaluating the correlation function of a rectangular light-like Wilson loop with a Lagrangian insertion, normalised by the expectation value of the Wilson loop. With this approach the cusp anomalous dimension was calculated up to $\mathcal{O}(\alpha_s^4)$ [107–111]. Similarly, we require the same order of the QCD-β function. In the literature the function is currently known to 5-loop [98,

99] order. The hard anomalous dimension γ_H and matching coefficient c_H have to be known up to NNLO. As they are related to the Wilson coefficient, they do not depend on the measurement, only on the underlying hard-scattering process. The non-cusp anomalous dimension γ_H is therefore related to either quark or gluon form factors [112, 113], depending on the hard-scattering process. The coefficient c_H is either known [112] or can be extracted from tools that automate the calculation of hard scattering processes [114, 115]. The soft function, and collinear exponent in the case of $\mathrm{SCET_{II}}$, depend on the observable one is interested in; for some observables, these quantities are known to the desired order analytically. However, this is not true for generic observables; therefore, one has to use `SoftSERVE` to provide numerical values for γ_S, c_S and F at NNLO. The last ingredient required for NNLL$'$ accuracy is the 2-loop jet function[1] and the 2-loop remainder function for $\mathrm{SCET_{II}}$. Here we have a similar picture as in the soft function case; for some observables, the quantities are known analytically, but not for a generic class of observables.

To summarise: In order to resum observables to NNLL$'$-accuracy, we require a program, similar to `SoftSERVE`, which can calculate the 2-loop jet functions in order to obtain γ_J, c_J and with the combination of the soft function, the remainder function W in the case of $\mathrm{SCET_{II}}$ observables.

5.2 General principle

In this section we address the question how to set up a framework that covers generic collider observables.

Recall from the previous chapters that the starting point for the computation of event-shape measures is of the schematic form

$$\frac{\mathrm{d}\sigma}{\mathrm{d}\tau} \sim |\mathcal{M}|^2 \delta(\tau - \tau(\{p_i\}))\mathrm{d}\Phi_n, \tag{5.2.1}$$

which, following a factorisation theorem, gives rise to jet functions of a similar form

$$J(\tau) \sim |\mathcal{M}_{\mathrm{coll}}|^2 \delta(\tau - \tau_c(\{p_i\}))\mathrm{d}\Phi_n^c. \tag{5.2.2}$$

The underlying principle is now the fact that all divergences, either from virtual contributions or associated with real radiation, are contained in the matrix element $|\mathcal{M}_{\mathrm{coll}}|^2$.

[1] At hadron colliders beam functions, which describe initial-state collinear radiation, are also required. In this project, however, we will deal exclusively with final-state collinear radiation.

These divergences are the same for all observables because the jet functions are process independent. They only depend on the parton that initiate the jet. The observable-dependence only enters through the measurement function, which changes the weight of different phase-space points.

Therefore, in our approach, we first have to isolate all divergences in the matrix element analytically and make them explicit, followed by the expansion in the regulator. This approach can be used in principle for any observable. So, if all divergences are adequately treated, the remaining integrals are convergent and thus can be safely evaluated numerically.

5.3 The jet functions in detail

In eq. (4.4.16) we have shown the definition of the jet function in the specific case of thrust. However, since we want to calculate other observables, we need a more general definition of the jet function.

One comment is in order before writing down the definition, which we will use as the starting point in calculating jet functions. Namely there are two different jet functions depending on the parton which initiates the jet. If the parent parton is a quark, then we will use quark fields in the matrix element and calculate the quark jet function J_q; however, if the jet is initiated by gluon, we replace quark fields with gluon fields and adjust the prefactor accordingly. Thus we compute the gluon jet function J_g.

The precise definition of the quark jet function is given in [116] and has the form:

$$\frac{\not{n}}{2}\pi J_q(\tau,\mu,Q) = \sum_X (2\pi)^d \delta\left(Q - \textstyle\sum_i k_i^-\right) \delta^{d-2}\left(\textstyle\sum_i k_i^\perp\right) \\ \mathcal{M}\left(\tau;\{k_i\}\right) \langle 0|\, \chi(0)\, |X\rangle \, \langle X|\, \bar{\chi}(0)\, |0\rangle\,, \tag{5.3.1}$$

where $|X\rangle$ denotes all collinear particles in the final state. The δ-functions restrict part of the phase-space in such a way that the sum of the large components of the parton momenta are constrained by the total energy of the jet Q, and their transverse momenta must balance each other out so that the jet is aligned in the n-direction. In eq. (5.3.1) the observable only enters via $\mathcal{M}\left(\tau;\{k_i\}\right)$. In momentum space this is in general in the form of a δ-function. However, in Laplace space, on the other hand, this transforms into an exponential form. The final piece of J_q is the collinear matrix element $\langle 0|\, \chi(0)\, |X\rangle \, \langle X|\, \bar{\chi}(0)\, |0\rangle$. We discuss its computation in section 6.

Similarly we define the gluon jet function, given in [117], as

$$-g_\perp^{\mu\nu}\frac{\pi}{Q}\delta^{ab}g_s^2 J_g(\tau,\mu,Q) = \sum_X (2\pi)^d \delta\left(Q-\textstyle\sum_i k_i^-\right)\delta^{d-2}\left(\textstyle\sum_i k_i^\perp\right) \\ \mathcal{M}\left(\tau;\{k_i\}\right)\langle 0|\,\mathcal{A}_\perp^{\mu,a}(0)\,|X\rangle\,\langle X|\,\mathcal{A}_\perp^{\nu,b}(0)\,|0\rangle\,, \quad (5.3.2)$$

where the collinear gluon field is defined as

$$\mathcal{A}_\perp^\mu(x) = T^a\mathcal{A}_\perp^{\mu,a}(x), \quad (5.3.3)$$

and

$$g_\perp^{\mu\nu} = g^{\mu\nu} - \frac{n^\mu\bar{n}^\nu + n^\nu\bar{n}^\mu}{2}. \quad (5.3.4)$$

The rest of the structure is similar to the ones described for the quark jet function.

Before we turn our attention to the measurement function $\mathcal{M}\left(\tau;\{k_i\}\right)$ two comments are in order. The first comment concerns the anticollinear jet functions $\bar{J}_q, \bar{J}_g$. In order to compute the anticollinear jet functions, we can simply use the definitions in eq. (5.3.1) and eq. (5.3.2) and interchange n and $\bar{n}$ while also keeping in mind the scaling of the two regions. However, the collinear and anticollinear matrix elements and phase-space factors are generally symmetric under this exchange after a suitable phase-space parametrisation. Thus, the only asymmetry can arise in the measurement function. If the measurement function is symmetric under $n \leftrightarrow \bar{n}$, then the collinear and anticollinear jet functions will be equivalent. In this case we will only need to calculate the collinear jet function to extract the required ingredients for resummation. Suppose the measurement function is asymmetric under this exchange. In that case, we still only require a setup for the collinear jet function because then the anticollinear jet function is equivalent to the collinear jet function by exchanging the definition of the parton momenta, $k_i^+ \leftrightarrow k_i^-$, in the measurement function. The second comment is in regards to $\mathrm{SCET_{II}}$ observables. We have previously outlined how to regularise the occurring rapidity divergences. However, we never explicitly stated the form of the additional regulator. In this work, we will use a variant of the analytic regulator introduced in [94]. This regulator, as stated earlier, modifies the generic d-dimensional phase-space measure as

$$\int \mathrm{d}^d k\,\delta\left(k^2\right)\theta\left(k^0\right) \longrightarrow \int \mathrm{d}^d k \left(\frac{\nu}{k_- + k_+}\right)^\alpha \delta\left(k^2\right)\theta\left(k^0\right), \quad (5.3.5)$$

where α is the additional regulator and ν is the new 't Hooft scale. We can further use

the scaling behaviour between k_- and k_+, and therefore, we find that the phase-space measure in the $\mathrm{SCET_{II}}$ case is

$$\int \mathrm{d}^d k \left(\frac{\nu}{k_- + k_+}\right)^\alpha \delta\left(k^2\right) \theta\left(k^0\right) \underset{k_- \gg k_+}{\longrightarrow} \int \mathrm{d}^d k \left(\frac{\nu}{k_-}\right)^\alpha \delta\left(k^2\right) \theta\left(k^0\right), \tag{5.3.6}$$

for collinear emissions. So in order to calculate $\mathrm{SCET_{II}}$ observables we have to adjust the definitions in eq. (5.3.1) and eq. (5.3.2) by a factor of $\left(\nu/k_i^-\right)^\alpha$ for each additional emission to the tree-level process. In the gluon jet function we have to add this factor for each final-state particle. This is because at NLO we structure with two gluons in the final state. However, we cannot distinguish the tree-level and the additional emission from each other. So in order to have a consistent setup we include this factor for each final-state particle starting from the tree-level process. Therefore we find the following expansion for the quark(gluon) jet function at NNLO in terms of the additional scale ν,

$$J_q = 1 + \left(\frac{\nu}{Q}\right)^\alpha \left(J_q^{\mathrm{NLO}} + J_q^{\mathrm{NNLO,RV}}\right) + \left(\frac{\nu}{Q}\right)^{2\alpha} J_q^{\mathrm{NNLO,RR}}, \tag{5.3.7}$$

$$J_g = \left(\frac{\nu}{Q}\right)^\alpha \left(1 + \left(\frac{\nu}{Q}\right)^\alpha \left(J_g^{\mathrm{NLO}} + J_g^{\mathrm{NNLO,RV}}\right) + \left(\frac{\nu}{Q}\right)^{2\alpha} J_g^{\mathrm{NNLO,RR}}\right). \tag{5.3.8}$$

Although we want to be as generic with our approach as possible, we have to have some constraints on the measurement function $\mathcal{M}\left(\tau; \{k_i\}\right)$. We assume that the measurement function can be written in the form

$$\mathcal{M}\left(\tau; \{k_i\}\right) = \exp\left[-\tau \omega\left(\{k_i\}\right)\right]. \tag{5.3.9}$$

As previously stated, this can be achieved by taking a Laplace transform[2] of the momentum space jet function, with τ being the associated Laplace variable. In order to ensure that the phase-space integrals converge, we require that $\omega\left(\{k_i\}\right) > 0$. More specifically, the function $\omega\left(\{k_i\}\right)$ is allowed to vanish only for phase-space domains of measure zero, and as long as these zeroes do not interfere with any divergences from the matrix element. The next assumption is about the mass dimensions, we assume that τ has the mass dimension 1/mass, and the function $\omega\left(\{k_i\}\right)$, which only depends on the final-state momenta k_i and Q, has the dimension of mass, such that $\mathcal{M}\left(\tau; \{k_i\}\right)$ does not have a mass dimension. Currently, we assume that the jet function should

[2] In some cases, a Fourier transform might be required, or no transformation at all.

only depend on one variable τ apart from the renormalisation and rapidity scales μ and ν. This can be physically interpreted as that the observable is single-differential in one kinematic variable. $\omega(\{k_i\})$ should also be ϵ and α-independent, as with additional dependencies in the regulators, the expansion changes; however, we assume this to be fixed. The final assumption is based on the angular dependence in the transverse plane. We allow the observable to depend on only one angle θ_i per final-state particle in the transverse plane. Thus it implies that the measurement is taken with respect to an external reference vector v^ν, and the angle θ_i is then introduced as the angle between $\vec{v}_\perp$ and $\vec{k}_i^\perp$ in the plane transverse to n and $\bar{n}$. One subtlety of this assumptions is that from eq. (5.3.1) and eq. (5.3.2), we can see that the $(d-2)$-dimensional δ-function restricts the transverse component of the jet. Therefore we only have $i-1$ independent angles while θ_i is a function depending on the other angles.

Chapter 6

Calculation of jet functions

In this section, we cover the computation of the collinear matrix elements and apply suitable parametrisations to the jet functions such that we can transform them from the definitions in eq. (5.3.1) and eq. (5.3.2) to a form that is suitable for subtraction, regulator expansion, and the subsequent numerical integration.

6.1 The NLO case

We start by computing the collinear matrix element for the quark jet function J_q. The corresponding diagrams are shown in figure 6.1.1. We can now state one of the advantages of using light-cone gauge in our calculations. In this gauge, the collinear Wilson lines which multiply the fields χ and $\mathcal{A}_\perp^{\mu,a}$ become trivial; therefore, only the diagram in figure 6.1.1(a) contributes to the quark jet function at NLO. Similarly, only the diagrams in figure 6.1.1(e) and 6.1.1(i) will contribute to the gluon jet function to this order.

In order to simplify the calculations, we project out the contribution to the quark jet function via

$$\mathrm{Tr}\left[\frac{\not{n}}{2}\frac{\not{\bar{n}}}{4}J_q(\tau,\mu,Q)\right] = J_q(\tau,\mu,Q). \tag{6.1.1}$$

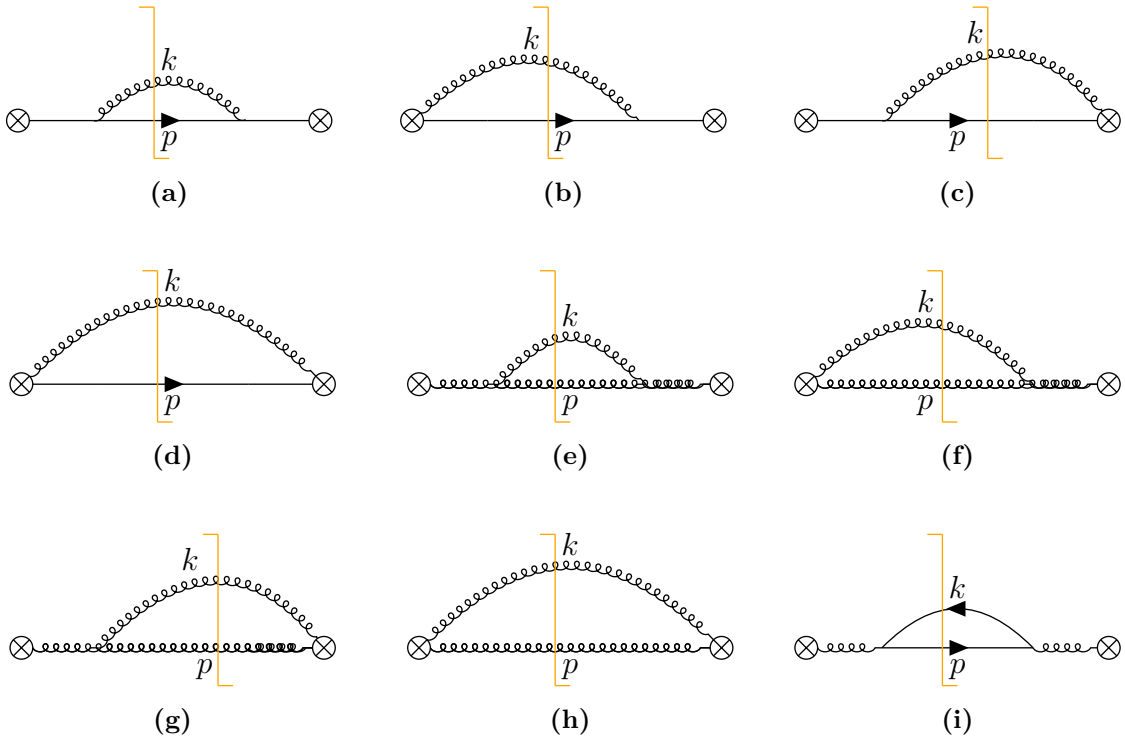

Figure 6.1.1: Cut 1-loop diagrams. Diagrams (a) to (d) correspond to the NLO quark jet function and diagrams (e) to (i) contribute to the gluon jet function. In light-cone gauge, only diagrams (a), (e) and, (i) yield non-vanishing results.

Thus we arrive at the following expression for the collinear matrix element

$$\mathcal{M}_a = \mathrm{Tr}\left[\frac{\not{\bar{n}}\not{n}}{4}\frac{i}{(k+p)^2}\left(\not{k}+\not{p}\right)\left(ig_s\tilde{\mu}^\epsilon T^a\gamma^\mu\right)\frac{i}{p^2}\not{p}\left(ig_s\tilde{\mu}^\epsilon T^a\gamma^\nu\right)\frac{i}{(k+p)^2}\left(\not{k}+\not{p}\right)\right.$$
$$\left.\cdot\,\frac{\not{\bar{n}}\not{n}}{4}\frac{\not{\bar{n}}}{4}\frac{i}{k^2}\left(-g^{\mu\nu}+\frac{\bar{n}^\mu k^\nu+\bar{n}^\nu k^\mu}{\bar{n}\cdot k}\right)\right], \tag{6.1.2}$$

where we have included powers of $\tilde{\mu}^2 = \frac{\mu^2 e^{\gamma_E}}{4\pi}$ to restore the correct mass dimension and signify that we work in the $\overline{\mathrm{MS}}$ scheme. We assume that all propagators are accompanied by a $+i\epsilon$ prescription. In order to proceed, we want to point out that we are in the regime where $Q \gg m_q$ and thus, all on-shell particles are massless. Therefore the invariant mass is $s \equiv (k+p)^2 = 2k\cdot p$. Finally, we use Cutkosky's cutting rules [118] in order to calculate the discontinuity of the diagram. The cutting rules are

1. Cut through the diagram in any way that can put all of the cut propagators on-shell without violating momentum conservation.

2. For each cut, replace $\frac{1}{p^2-m^2+i\epsilon} \to -2i\pi\delta\left(p^2-m^2\right)\theta\left(p^0\right)$.

3. Sum over all cuts.

4. The result is the discontinuity of the diagram, where $\text{Disc}\left(i\mathcal{M}\right) = -2\text{Im}\mathcal{M}$.

In the end, we can relate the discontinuity of the diagram to the collinear matrix element via the optical theorem. Thus we arrive at the following expression for the collinear matrix element at NLO:

$$\sigma_2^{c,q} = \frac{2g_s^2\tilde{\mu}^{2\epsilon}C_F}{s\left(\bar{n}\cdot k\right)}\left(\left(\bar{n}\cdot k\right)^2\left(1-\epsilon\right)+2\left(\bar{n}\cdot p\right)\left(\left(\bar{n}\cdot k\right)+\left(\bar{n}\cdot p\right)\right)\right), \tag{6.1.3}$$

where we have defined $\sigma^{c,q} = \langle 0|\,\chi(0)\,|X\rangle\,\langle X|\,\bar{\chi}(0)\,|0\rangle$. Note that the additional factors from the cuts are left out of this expression and are shifted to the phase-space integration for convenience.

We can now compute the formula for the quark jet function at NLO

$$\begin{aligned} J_{q,1}(\tau,\mu,Q) = \frac{(2\pi)^d}{\pi}\int\frac{\mathrm{d}^d k}{(2\pi)^{d-1}}\delta(k^2)\theta(k^0)\int\frac{\mathrm{d}^d p}{(2\pi)^{d-1}}\delta(p^2)\theta(p^0)\delta\left(Q-k_- - p_-\right) \\ \times\,\delta^{d-2}\left(k_\perp+p_\perp\right)\mathcal{M}\left(\tau;\{k_i\}\right)\left(\frac{2g_s^2\tilde{\mu}^{2\epsilon}C_F}{s\,k_-}\left(k_-^2(1-\epsilon)+2p_-(k_-+p_-)\right)\right), \end{aligned} \tag{6.1.4}$$

where we have used the definition of $\bar{n}\cdot k = k_-$ and $\bar{n}\cdot p = p_-$. For the phase-space integrals we use

$$\begin{aligned} \int \mathrm{d}^d k\delta(k^2)\theta(k^0) =& \frac{1}{2}\int \mathrm{d}k_-\,\mathrm{d}k_+\,\mathrm{d}^{d-2}k_\perp\delta(k_-k_+ + k_\perp^2)\theta(k_-+k_+) \\ =& \frac{1}{2}\int \mathrm{d}^{d-3}\Omega_T\int_0^\infty \mathrm{d}k_-\,\mathrm{d}k_+\,\mathrm{d}k_T\delta(k_-k_+ - k_T^2)k_T^{d-3}, \end{aligned} \tag{6.1.5}$$

where we transitioned to light-cone coordinates in the first line, switched from Minkowski vector $k_\perp$ to Euclidean $\vec{k}_T$ and immediately continued to spherical coordinates in the second line.

Let us discuss, how we parameterise the phase-space to simplify the calculation. Note that by comparing the number of integrations with the number of δ-functions, we can see that we only have two kinematic integrals and one angular integration to perform; all other integrals are accompanied by a δ-function. Note further that by using the delta distributions $\delta\left(Q-k_- - p_-\right)$ and $\delta(k_-k_+ - k_T^2)$ we can define the following

substitutions:

$$z_k = \frac{k_-}{Q}, \qquad k_T = \sqrt{k_- k_+}, \tag{6.1.6}$$

of which z_k behaves similarly to an energy fraction. Additionally, we observe that the quark with momentum p is entirely determined by the phase-space restrictions from the definition of the jet function. Thus the inverse transformations are given by

$$\begin{aligned} k_- =& z_k Q, \qquad k_+ = \frac{k_T^2}{z_k Q}, \qquad k_T = k_T, \\ p_- =& (1-z_k)Q, \qquad p_+ = \frac{k_T^2}{(1-z_k)Q}, \qquad p_T = k_T. \end{aligned}$$

Finally, before implementing the parametrisation and completing the calculation of the quark jet function, we have to return to the measurement function. In eq. (5.3.9) we have assumed that the measurement function can be written as an exponential, however we have not given the specific form of $\omega(\{k_i\})$.

The specific form of $\omega(\{k_i\})$ is motivated by the NLO soft function calculation shown in [42]. The ansatz for the one-emission measurement function is:

$$\mathcal{M}_1^{\text{soft}}(\tau; k) = \exp\left[-\tau k_T y_k^{n/2} f(y_k, t_k)\right], \tag{6.1.7}$$

where $y_k = k_+/k_-, k_T$ is the same as in eq. (6.1.6) and t_k parametrises the azimuthal dependence around the jet axis. The power n of y_k is fixed by the requirement that the function $f(y_k, t_k)$ is finite and non-zero in the limit $y_k \to 0$. Therefore, the observable is characterised by the parameter $n \in \mathbb{R}$ and a function $f(y_k, t_k)$ that encodes the angular and rapidity dependence.

In order to construct an ansatz for the jet function, we first note that in contrast to the soft function, the dependence on k_T is not fixed since the jet function depends on k_T and Q. On dimensional grounds, we factor out a linear dependence on k_T; we also have to factor out a non-trivial dependence on the dimensionless quantity k_T/Q. Notice that one divergence in the jet function arises due to $z_k \to 0$, so similar to y_k in the soft function, we have to factor out some power of z_k, such that the function $f_{gq}(z_k, t_k)$ is finite and non-zero in the critical limit. Therefore we find the following ansatz for the jet function measurement

$$\mathcal{M}_{1,gq}^{\text{jet}}(\tau; k) = \exp\left[-\tau k_T z_k^{m_1} \left(\frac{k_T}{Q}\right)^{m_2} f_{gq}(z_k, t_k)\right]. \tag{6.1.8}$$

In order to fix m_1 and m_2 we consider the collinear limit of the soft function $y_k \to 0$ and the soft limit of the jet function $z_k \to 0$. In these limits, the soft and jet measurement functions must be equal; therefore, we find

$$\begin{aligned}
\mathcal{M}_1^{\text{soft}}(\tau;k) &\overset{y_k\to 0}{\longrightarrow} \exp\left[-\tau k_T y_k^{n/2} f_c(0,t_k)\right] \\
\mathcal{M}_{1,gq}^{\text{jet}}(\tau;k) &\overset{z_k\to 0}{\longrightarrow} \exp\left[-\tau k_T z_k^{m_1}\left(\frac{k_T}{Q}\right)^{m_2} f_{gq,s}(0,t_k)\right] \\
&\Longrightarrow y_k^{n/2} = z_k^{m_1}\left(\frac{k_T}{Q}\right)^{m_2} \quad \text{and} \quad f_c(0,t_k) = f_{gq,s}(0,t_k).
\end{aligned}$$

If we transform y_k in our parametrisation from eq. (6.1.6) then we can compare the powers with each other and find that $m_1 = -n$ and $m_2 = n$. So finally we can fix our ansatz to be

$$\mathcal{M}_{1,gq}^{\text{jet}}(\tau;k) = \exp\left[-\tau k_T \left(\frac{k_T}{z_k Q}\right)^n f_{gq}(z_k,t_k)\right]. \tag{6.1.9}$$

Now that we have defined an ansatz for the measurement function, we can include it into the jet function and arrive at the following formula:

$$\begin{aligned}
J_{q,1}(\tau,\mu,Q) = \frac{\alpha_s}{4\pi} C_F \left(\mu^2 e^{\gamma_E}\right)^\epsilon \frac{8}{\sqrt{\pi}\Gamma\left(\frac{1}{2}-\epsilon\right)} \int_0^1 \mathrm{d}z_k\, \mathrm{d}t_k\, (4t_k\bar{t}_k)^{-\frac{1}{2}-\epsilon} \frac{(1-\epsilon)z_k^2 + 2\bar{z}_k}{z_k} \\
\int_0^\infty \mathrm{d}k_T\, k_T^{-1-2\epsilon} \exp\left[-\tau k_T \left(\frac{k_T}{z_k Q}\right)^n f_{gq}(z_k,t_k)\right],
\end{aligned} \tag{6.1.10}$$

here we integrated all but one of the angles in the transverse plane via

$$\int \mathrm{d}^{d-3}\Omega_T = \frac{4\pi^{\frac{1}{2}-\epsilon}}{\Gamma\left(\frac{1}{2}-\epsilon\right)} \int_0^1 \mathrm{d}t_k\, (4t_k\bar{t}_k)^{-\frac{1}{2}-\epsilon}, \tag{6.1.11}$$

where $\cos\theta_k = 1 - 2t_k$, $\bar{t}_k = 1 - t_k$. In the end, we can analytically integrate over the transverse momentum k_T and subsequently find the final master formula for the NLO quark jet function:

$$\begin{aligned}
J_{q,1}(\tau,\mu,Q) = \frac{\alpha_s C_F}{4\pi}\left(\frac{\mu\bar{\tau}^{\frac{1}{n+1}}}{Q^{\frac{n}{n+1}}}\right)^{2\epsilon}\left(\frac{\nu}{Q}\right)^\alpha \frac{8}{1+n}\frac{\Gamma(\frac{-2\epsilon}{1+n})}{\sqrt{\pi}\Gamma(\frac{1}{2}-\epsilon)} \exp\left[\gamma_E\epsilon\left(1-\frac{2}{1+n}\right)\right] \\
\times \int_0^1 \mathrm{d}z_k z_k^{-1-2\frac{n}{1+n}\epsilon-\alpha}[(1-\epsilon)z_k^2 + 2\bar{z}_k] \int_0^1 \mathrm{d}t_k (4t_k\bar{t}_k)^{-\frac{1}{2}-\epsilon} f_{gq}(z_k,t_k)^{\frac{2\epsilon}{1+n}},
\end{aligned} \tag{6.1.12}$$

where we used $\bar{\tau} = \tau e^{\gamma_E}$ and inserted $(\nu/zQ)^\alpha$ as additional regulator in the SCET_II case. Note that for non-zero n the z_k integral is well defined so we can set $\alpha = 0$. If $n = 0$, then α must stay non-zero, otherwise the z_k-integration is unregularised. Therefore we can associate non-zero n values with SCET_I observables and $n = 0$ with SCET_II observables. This scaling behaviour was more closely investigated in [42]. Furthermore, the correct value of n is important, because the z_k-divergence is written as

$$z_k^{-1-\frac{2n}{1+n}\epsilon} = -\frac{\delta(z_k)}{\left(\frac{2n}{1+n}\epsilon\right)} + \left[\frac{1}{z_k}\right]_+ + \ldots, \tag{6.1.13}$$

so we would get the pole structure wrong if we did not capture the full leading scaling. Similarly, note that the exponent of $f_{gq}(z_k, t_k)$ depends purely on ϵ. The regulator expansion therefore only produces terms of the type $\ln^m f_{gq}(z_k, t_k)$. Acting with the plus-distributions on such a term will produce expressions of the kind $\ln^m f_{gq}(0, t_k)$ over the entire domain, and these should not diverge.

At NLO, we expect the quark jet function to generate two divergences; the collinear divergence is encoded in $\Gamma(\frac{-2\epsilon}{1+n})$ and the soft divergence is explicit in the z_k monomial. Therefore the divergences are fully accounted for in our master formula. Both the Γ-function and the z_k-structure produce a $\frac{1}{\epsilon}$-pole for SCET_I observables, so the leading contribution is a $\frac{1}{\epsilon^2}$-divergence. In the SCET_II case, the Γ function still produces a $\frac{1}{\epsilon}$ while the z_k contributes to an $\frac{1}{\alpha}$-pole at leading order. Therefore the jet function has an $\frac{1}{\alpha\epsilon}$-leading pole behaviour at NLO in the SCET_II case. One important remark for the SCET_II case is that to get the correct result, the expansion in α must be performed before the ϵ expansion.

In order to conclude the section on the quark jet function, observe that the remaining integral is well-behaved and integrable over the domain. There are integrable singularities[1] at $t_k = \{0, 1\}$. Furthermore, if $f_{gq}(z_k, t_k)$ vanishes in any non-divergent limit, this would contribute to a integrable logarithmic divergence and therefore poses no problem.

After finishing the quark jet function, we turn to the gluon jet function. Here we note that we have to calculate two different contributions, as seen in figures 6.1.1(e) and 6.1.1(i). In order to perform the computations, we close the open indices by contracting J_g with $\frac{g_{\perp,\mu\nu}}{2-d}$, so it reads

$$\frac{g_{\perp,\mu\nu}}{2-d}\left(-g_\perp^{\mu\nu}\right)\frac{\pi}{Q}\delta^{ab}g_s^2 J_g(\tau,\mu,Q) = \frac{\pi}{Q}\delta^{ab}g_s^2 J_g(\tau,\mu,Q). \tag{6.1.14}$$

[1] These will be investigated in section 7.

We start calculating the gluon jet function by evaluating the quark-antiquark final state in figure 6.1.1(i). The calculation generally follows the same method as in the quark function case. The only difference concerns our ansatz for the measurement function. In the previous ansatz, we had to factor out some power of z_k such that $f_{gq}(z_k, t_k)$ stays finite in the limit $z_k \to 0$, due to this limit being the divergence when the gluon becomes soft. However, in the current contribution from figure 6.1.1(i), z_k corresponds to the energy fraction of the antiquark and thus it cannot produce a soft divergence at leading power in SCET [119]. Similarly, this is also true for the quark, and thus we modify our ansatz for this contribution to be

$$\mathcal{M}^{\text{jet}}_{1,q\bar{q}}(\tau; k) = \exp\left[-\tau k_T \left(\frac{k_T}{Q}\right)^n f_{q\bar{q}}(z_k, t_k)\right]. \tag{6.1.15}$$

So we arrive at the following master formula for this colour structure of the gluon jet function contribution

$$\begin{aligned} J_{g\to q\bar{q},1}(\tau, \mu, Q) = \frac{\alpha_s T_F n_f}{4\pi} \left(\frac{\mu \bar{\tau}^{\frac{1}{n+1}}}{Q^{\frac{n}{n+1}}}\right)^{2\epsilon} \left(\frac{\nu}{Q}\right)^{2\alpha} \frac{8}{1+n} \frac{\Gamma(\frac{-2\epsilon}{1+n})}{(1-\epsilon)\sqrt{\pi}\Gamma(\frac{1}{2}-\epsilon)} \\ \times \exp\left[\gamma_E \epsilon \left(1 - \frac{2}{1+n}\right)\right] \int_0^1 \mathrm{d}z_k \, (\bar{z}_k z_k)^{-\alpha} \left[z_k^2 + \bar{z}_k^2 - \epsilon\right] \\ \times \int_0^1 \mathrm{d}t_k (4 t_k \bar{t}_k)^{-\frac{1}{2}-\epsilon} f_{q\bar{q}}(z_k, t_k)^{\frac{2\epsilon}{1+n}}, \end{aligned} \tag{6.1.16}$$

where we included the additional regulator for both the quark and the antiquark.

In case of the contribution with two gluons in the final state, we can see that we now have soft divergences in the case of $z_k \to \{0, 1\}$, and therefore we have to change our ansatz for this contribution again. Here we use

$$\mathcal{M}^{\text{jet}}_{1,gg}(\tau; k) = \exp\left[-\tau k_T \left(\frac{k_T}{z_k \bar{z}_k Q}\right)^n f_{gg}(z_k, t_k)\right]. \tag{6.1.17}$$

By performing the same steps as before we arrive at the following master formula for

$J_{g\to gg,1}(\tau,\mu,Q)$:

$$J_{g\to gg,1}(\tau,\mu,Q) = \frac{\alpha_s C_A}{4\pi}\left(\frac{\mu\bar{\tau}^{\frac{1}{n+1}}}{Q^{\frac{n}{n+1}}}\right)^{2\epsilon}\left(\frac{\nu}{Q}\right)^{2\alpha}\frac{8}{1+n}\frac{\Gamma(\frac{-2\epsilon}{1+n})}{\sqrt{\pi}\Gamma(\frac{1}{2}-\epsilon)}\exp\left[\gamma_E\epsilon\left(1-\frac{2}{1+n}\right)\right]$$
$$\times\int_0^1 \mathrm{d}z_k(\bar{z}_k z_k)^{-1-2\frac{n}{1+n}\epsilon-\alpha}[1-z_k\bar{z}_k]^2\int_0^1 \mathrm{d}t_k(4t_k\bar{t}_k)^{-\frac{1}{2}-\epsilon}f_{gg}(z_k,t_k)^{\frac{2\epsilon}{1+n}}. \tag{6.1.18}$$

Here we observe another complication. Namely, divergences arise in the same variable z_k at both endpoints of the integration domain. However, the regular plus distribution is only defined with one divergence in mind. Thus we have to disentangle the divergences. This could be achieved by including a selector function of the form $1 = z_k + \bar{z}_k$, where we allow in each term only a specific divergence. So, in the end, each term will only have divergences at one endpoint. The downside of this approach would be that we have two pieces to calculate. This will be one of the methods in calculating NNLO real-real contributions. In $J_{g\to gg,1}(\tau,\mu,Q)$ we can use a different technique. First, observe that the contribution from the collinear matrix element is symmetric under the $z_k \leftrightarrow \bar{z}_k$ exchange. Additionally, the only other dependence on z_k is within the measurement function $f_{gg}(z_k,t_k)$; however, as the measurement function cannot differentiate between particles, it must be symmetric under this exchange. Thus we can write the z_k-integral as

$$\int_0^1 \mathrm{d}z_k(\bar{z}_k z_k)^{-1-y\epsilon-\alpha}g(z_k), \tag{6.1.19}$$

where $g(z_k)$ is a function symmetric under the $z_k \leftrightarrow \bar{z}_k$ exchange and $y = 2\frac{n}{1+n}$. So we can perform the following substitution

$$\int_0^1 \mathrm{d}z_k(\bar{z}_k z_k)^{-1-y\epsilon-\alpha}g(z_k) = \underbrace{\int_0^{\frac{1}{2}} \mathrm{d}z_k(\bar{z}_k z_k)^{-1-y\epsilon-\alpha}g(z_k)}_{z_k=\frac{1}{2}u} + \underbrace{\int_{\frac{1}{2}}^1 \mathrm{d}z_k(\bar{z}_k z_k)^{-1-y\epsilon-\alpha}g(z_k)}_{z_k=1-\frac{1}{2}u}$$
$$= 4^{1+y\epsilon+\alpha}\int_0^1 \mathrm{d}u\,\underbrace{u^{-1-y\epsilon-\alpha}}_{\text{pole at } u=0}\underbrace{(2-u)^{-1-y\epsilon-\alpha}}_{\text{pole at } u=2}g(u). \tag{6.1.20}$$

By employing this method, we can shift one pole outside of the integration domain ($u = 2$), so we are left with a divergence only at one endpoint inside the domain ($u = 0$); thus, we can use our standard +-distribution expansion. In terms of the

variable u, we find that the master formula takes the form:

$$J_{g\to gg,1}(\tau,\mu,Q) = \frac{\alpha_s C_A}{4\pi}\left(\frac{\mu\bar{\tau}^{\frac{1}{n+1}}}{Q^{\frac{n}{n+1}}}\right)^{2\epsilon}\left(\frac{\nu}{Q}\right)^{2\alpha}\frac{2^{1+2\alpha+4\frac{n}{1+n}\epsilon}}{1+n}\frac{\Gamma(\frac{-2\epsilon}{1+n})}{\sqrt{\pi}\Gamma(\frac{1}{2}-\epsilon)}$$
$$\times\exp\left[\gamma_E\epsilon\left(1-\frac{2}{1+n}\right)\right]\int_0^1 \mathrm{d}u\, u^{-1-2\frac{n}{1+n}\epsilon-\alpha}(2-u)^{-1-2\frac{n}{1+n}\epsilon-\alpha}(4+u(2-u))^2$$
$$\times\int_0^1 \mathrm{d}t_k(4t_k\bar{t}_k)^{-\frac{1}{2}-\epsilon}f_{gg}(u,t_k)^{\frac{2\epsilon}{1+n}}. \tag{6.1.21}$$

In order to complete the section on the NLO calculation, we point out one observation. The collinear matrix elements of any jet function in our setup can be related to the standard collinear splitting functions [120]. The splitting functions which we require for our calculation are already present in the literature and can be found in [121–126]. This allows us to validate our calculation of the collinear matrix elements. More importantly, it allows us to write the collinear matrix elements in a much more compact form to simplify the master formulae for the jet functions.

In the case of the collinear matrix element for the quark jet function we can relate it to the $q\to gq$ splitting function via

$$\sigma_2^{c,q} = \tilde{\mu}^{2\epsilon}\frac{2g_s^2}{s}QP^{(0)}_{q\to gq}(s,z_k), \tag{6.1.22}$$

where $P^{(0)}_{q\to gq}(s,z_k)$, is the $q\to gq$ splitting function [126]. The prefactor for the gluon jet function is now slightly different, it reads

$$\sigma_2^{c,g} = \tilde{\mu}^{2\epsilon}\frac{2g_s^2}{s}\left(P^{(0)}_{g\to q\bar{q}}(s,z_k)+P^{(0)}_{g\to gg}(s,z_k)\right), \tag{6.1.23}$$

where $P^{(0)}_{g\to q\bar{q}}$ is the $g\to q\bar{q}$ splitting function and $P^{(0)}_{g\to gg}$ is the $g\to gg$ splitting function [126].

6.2 The NNLO case

The NNLO case follows in general the NLO case, although with additional complications in the form of more integrations and non-trivial divergence structures.

We first note that for the NNLO case, the number of diagrams that can contribute is larger than at NLO. In general, we can split the NNLO calculation into two different

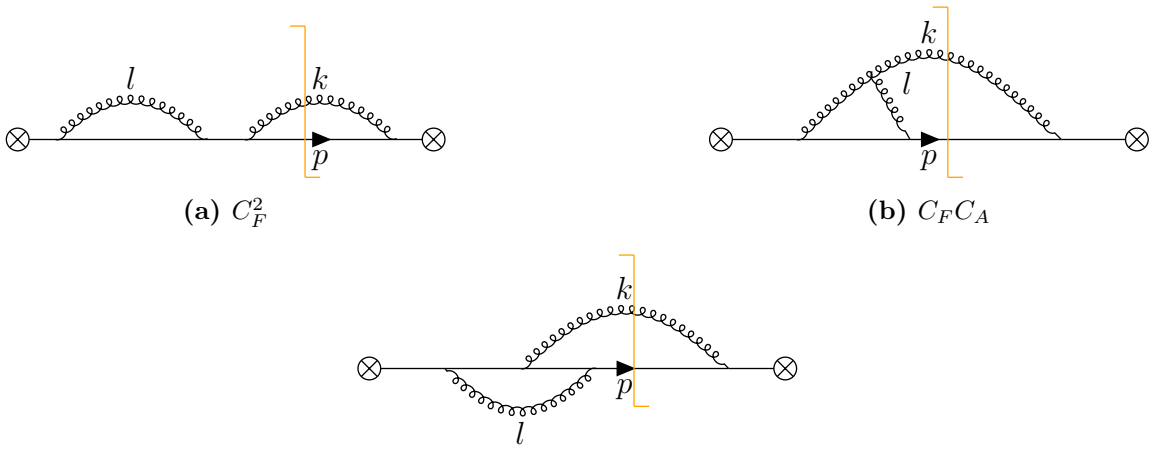

(a) C_F^2 **(b)** $C_F C_A$ **(c)** $C_F\left(C_F - \frac{C_A}{2}\right)$

Figure 6.2.1: Diagrams contributing to the NNLO real-virtual correction to the quark jet function and their respective colour factors. All other diagrams give rise to scaleless integrals. The loop momentum is labeled l and for the on-shell particles the momentum labelling is the same as in the NLO case.

contributions. The first are the 2-particle cut or real-virtual contributions, and the second ones are the 3-particle cut or real-real contributions. It is convenient to treat different colour structures of the real-real contributions separately.

6.2.1 NNLO: Real-virtual contribution

The real-virtual (RV) corrections to the quark jet function are shown in figure 6.2.1. They are structurally identical to the NLO case; the only difference is the matrix element. The subtleties that arise in calculating the collinear matrix element for the RV corrections are present in all diagrams in figure 6.2.1. Therefore we can pick one diagram as a reference on how we compute them. As a guideline to the calculation of the RV contributions we consider the diagram in figure 6.2.1(a). We start by writing down the expression of the matrix element

$$\begin{aligned}\tilde{\sigma}^{c,q}_{2,\mathrm{RV}-a} = \mathrm{Tr}\Bigg[&\frac{\bar{\not{n}}\not{n}}{4}\frac{i\left(\not{p}+\not{k}\right)}{s}\left(ig_s\tilde{\mu}^{\epsilon}T^a\gamma_\mu\right)\not{p}\left(ig_s\tilde{\mu}^{\epsilon}T^a\gamma_\nu\right)\frac{i\left(\not{p}+\not{k}\right)}{s}\left(ig_s\tilde{\mu}^{\epsilon}T^b\gamma_\rho\right)\\ &\times\int\frac{\mathrm{d}^d l}{(2\pi)^d}\frac{i\left(\not{p}+\not{k}+\not{l}\right)}{(p+k+l)^2}\left(ig_s\tilde{\mu}^{\epsilon}T^b\gamma_\sigma\right)\frac{i\left(\not{p}+\not{k}\right)}{s}\frac{\bar{\not{n}}\not{n}}{4}\left[-g^{\mu\nu}+\frac{\bar{n}^\mu k^\nu+\bar{n}^\nu k^\mu}{k_-}\right]\\ &\times\frac{i}{l^2}\left[-g^{\rho\sigma}+\frac{\bar{n}^\rho l^\sigma+\bar{n}^\sigma l^\rho}{\bar{n}\cdot l}\right]\frac{\bar{\not{n}}}{4}\Bigg],\end{aligned} \tag{6.2.1}$$

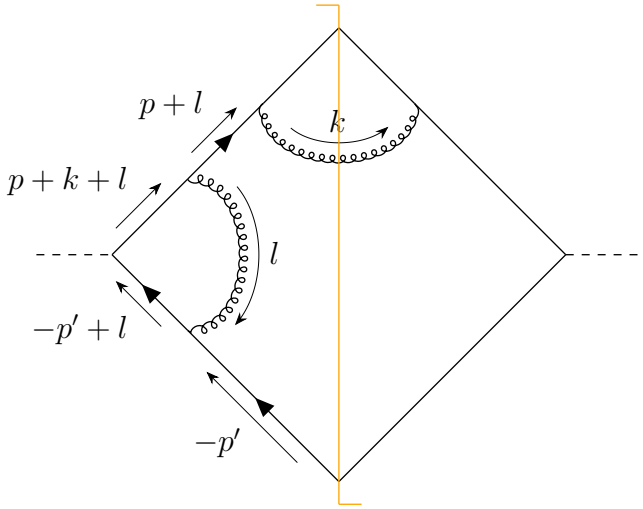

Figure 6.2.2: Full QCD diagram of the quark jet function contribution in figure 6.2.1(a).

where we have already used the cutting rules and shifted the additional factors into the phase-space integration. The first subtlety arises in the next step. We have, until now, mostly neglected to write the $i\epsilon$-prescription of the propagators. However, they were always assumed to be written with an additional $+i\epsilon$. In the case of the real-virtual corrections, this must not be true anymore because of the linear propagator $\bar{n}\cdot l$ where l is the loop momentum. The correct sign must be reconstructed from the full QCD diagram, shown in figure 6.2.2. The propagator of interest is now $(-p'+l)$ where $p'=Q\frac{\bar{n}}{2}$. Thus we find

$$(-p'+l)^2+i\epsilon=-Q\bar{n}\cdot l+i\epsilon\sim-\bar{n}\cdot l+i\epsilon. \tag{6.2.2}$$

So the matrix element $\tilde{\sigma}^{c,q}_{2,\mathrm{RV}-a}$ has the following expression

$$\tilde{\sigma}^{c,q}_{2,\mathrm{RV}-a}=\frac{(-i)(4\pi\alpha_s)^2C_F^2\tilde{\mu}^{4\epsilon}}{s^3}\int\frac{\mathrm{d}^dl}{(2\pi)^d}\frac{N(k\cdot l,p\cdot l,\bar{n}\cdot l,n\cdot l,s,z_k,Q)}{\left[(p+k+l)^2+i\epsilon\right]\left[l^2+i\epsilon\right]\left[-\bar{n}\cdot l+i\epsilon\right]}, \tag{6.2.3}$$

where $N(k\cdot l,p\cdot l,\bar{n}\cdot l,n\cdot l,s,z_k,Q)$ is the numerator of the matrix element. We can now evaluate the loop integral by employing Feynman parameters. We note that it is convenient to use the representation

$$\frac{1}{ab}=\int_0^\infty\mathrm{d}y\,\frac{1}{(a+by)^2}, \tag{6.2.4}$$

to combine linear and quadratic propagators, in the cases where a is a standard propagator, and b is linear in the loop momentum. Thus we obtain

$$\tilde{\sigma}^{c,q}_{2,\mathrm{RV}-a} = \frac{2(-i)(4\pi\alpha_s)^2 C_F^2 \tilde{\mu}^{4\epsilon}}{s^3} \int_0^1 \mathrm{d}x \int_0^\infty \mathrm{d}y \int \frac{\mathrm{d}^d l}{(2\pi)^d} \frac{\tilde{N}(k\cdot l, p\cdot l, \bar{n}\cdot l, n\cdot l, s, z_k, x, y)}{\left[l^2-\Delta\right]^3}, \tag{6.2.5}$$

where $\Delta = [x\bar{x}s + xyQ]\, e^{-i\pi}$. Finally, we can integrate over the loop momentum and the Feynman parameters. In the end, we have to add the complex conjugate in order to get the collinear matrix element,

$$\sigma^{c,q}_{2,\mathrm{RV}-a} = \tilde{\sigma}^{c,q}_{2,\mathrm{RV}-a} + \tilde{\sigma}^{c,q,\dagger}_{2,\mathrm{RV}-a} = \frac{\alpha_s C_F}{4\pi} \left(\mu e^{\gamma_E}\right)^\epsilon s^{-\epsilon} \cos(\pi\epsilon) \frac{4^\epsilon \sqrt{\pi}(4-\epsilon)\Gamma(\epsilon)\Gamma(2-\epsilon)}{\epsilon\Gamma\left(\frac{3}{2}-\epsilon\right)} \sigma^{c,q}_2, \tag{6.2.6}$$

where $\sigma^{c,q}_2$ is its one-loop contribution.

The diagrams in figures 6.2.1(b) and 6.2.1(c) can be calculated along the same lines. In order to write the result as compact as possible, we use the definition of the one-loop correction to the double splitting function in [126]. There we find that the splitting function $P^{(1)}_{q\to gq}(s, z_k)$ is

$$\begin{aligned} P^{(1)}_{q\to gq}(s,z_k) = \left(\frac{\mu^2 e^{\gamma_E}}{s}\right)^\epsilon \frac{2g_s^2}{(4\pi)^2} \frac{\pi\Gamma(1-\epsilon)}{\epsilon\tan(\pi\epsilon)\Gamma(1-2\epsilon)} C_F \Bigg\{ \left[\frac{(1-\epsilon)z_k^2 + 2\bar{z}_k}{z_k}\right] \Bigg[C_F \\ + (C_F - C_A)\left(1 - \frac{\epsilon^2}{1-2\epsilon}\right) + (C_A - 2C_F)\, {}_2F_1\left(1, -\epsilon; 1-\epsilon; \frac{z_k}{z_k-1}\right) \\ - C_A\, {}_2F_1\left(1, -\epsilon; 1-\epsilon; \frac{z_k-1}{z_k}\right) \Bigg] + (C_F - C_A)\frac{\bar{z}_k(2-z_k)}{z_k}\frac{\epsilon^2}{1-2\epsilon^2} \Bigg\}. \end{aligned} \tag{6.2.7}$$

The jet function master formula for the RV contribution at NNLO is then obtained by performing the phase-space steps shown in the NLO case and therefore we find the

following master formula:

$$J_{q,2}^{\mathrm{RV}}(\tau,\mu,Q) = \left(\frac{\alpha_s}{4\pi}\right)^2 \left(\frac{\mu\bar{\tau}^{\frac{1}{n+1}}}{Q^{\frac{n}{n+1}}}\right)^{4\epsilon} \left(\frac{\nu}{Q}\right)^{\alpha} \frac{16}{1+n} \frac{\Gamma(\frac{-4\epsilon}{1+n})}{\sqrt{\pi}\Gamma(\frac{1}{2}-\epsilon)} \frac{\pi\Gamma(1-\epsilon)}{\epsilon\tan(\pi\epsilon)\Gamma(1-2\epsilon)}$$
$$\exp\left[2\gamma_E\epsilon\left(1-\frac{2}{1+n}\right)\right] \int_0^1 \mathrm{d}z_k\,\mathrm{d}t_k\, z_k^{-1-4\frac{n}{1+n}\epsilon+\epsilon-\alpha} \bar{z}_k^{\epsilon} \left(4t_k\bar{t}_k\right)^{-\frac{1}{2}-\epsilon} f_{gq}(z_k,t_k)^{\frac{4\epsilon}{1+n}}$$
$$\left\{C_F^2\left[\frac{\bar{z}_k(2-z_k)\epsilon^2}{1-2\epsilon^2} + \left[(1-\epsilon)z_k^2+2\bar{z}_k\right]\left[\frac{2-\epsilon(\epsilon+4)}{1-2\epsilon} - 2F_1\right]\right]\right.$$
$$\left. + C_F C_A\left[\frac{\bar{z}_k(2-z_k)\epsilon^2}{2\epsilon^2-1} + \left[(1-\epsilon)z_k^2+2\bar{z}_k\right]\left[\frac{1-\epsilon(\epsilon+2)}{2\epsilon-1} + F_1 - F_2\right]\right]\right\}, \quad (6.2.8)$$

where F_1 and F_2 are shorthand notations for the hypergeometric functions,

$$F_1 \coloneqq {}_2F_1\left(1,-\epsilon;1-\epsilon;\frac{z_k}{z_k-1}\right), \qquad F_2 \coloneqq {}_2F_1\left(1,-\epsilon;1-\epsilon;\frac{z_k-1}{z_k}\right).$$

In eq. (6.2.8), we again see the two divergences that were already present in the NLO case. The collinear divergence is again encoded in the Γ-function $\Gamma(\frac{-4\epsilon}{1+n})$, while the soft divergence is present as an explicit z_k monomial. Additionally, we find two divergences from the $(\epsilon\tan(\pi\epsilon))^{-1}$-term originating from the loop integral. Therefore, the leading pole structure of the RV-contribution is ϵ^{-4} for $\mathrm{SCET_I}$ and $\epsilon^{-3}\alpha^{-1}$ for $\mathrm{SCET_{II}}$ observables. Another subtlety we want to highlight concerns $\mathrm{SCET_{II}}$ observables. In eq. (6.2.8) it seems that z_k is regularised in the limit $n=0$ because of the additional $+\epsilon$ in the exponent. This is true for most terms in the master formula; only in the term where z_k is multiplied by F_2 it becomes unregularised. The easiest way to see this is by writing the hypergeometric function in its integral representation,[2]

$$\begin{aligned} z_k^{-1-4\frac{n}{1+n}\epsilon+\epsilon-\alpha} F_2 &= z_k^{-1-4\frac{n}{1+n}\epsilon+\epsilon-\alpha}\, {}_2F_1\left(1,-\epsilon;1-\epsilon;\frac{z_k-1}{z_k}\right) \\ &= z_k^{-1-4\frac{n}{1+n}\epsilon+\epsilon-\alpha}\left(-\epsilon z_k^{-\epsilon}\int_0^1 \mathrm{d}x\, x^{-1-\epsilon}\left(1-\bar{z}_k x\right)^{\epsilon}\right) \\ &= -\epsilon\int_0^1 \mathrm{d}x\, z_k^{-1-4\frac{n}{1+n}\epsilon-\alpha} x^{-1-\epsilon}\left(1-\bar{z}_k x\right)^{\epsilon}, \end{aligned} \quad (6.2.9)$$

here we can clearly see that z_k is unregularised in the limit $n=0$ without the additional regulator.

The calculation of the RV-contribution to the gluon jet function follows the same logic as in the quark jet function case, and therefore we simply write down the corre-

[2] In our computation we always use the integral representations of hypergeometric functions.

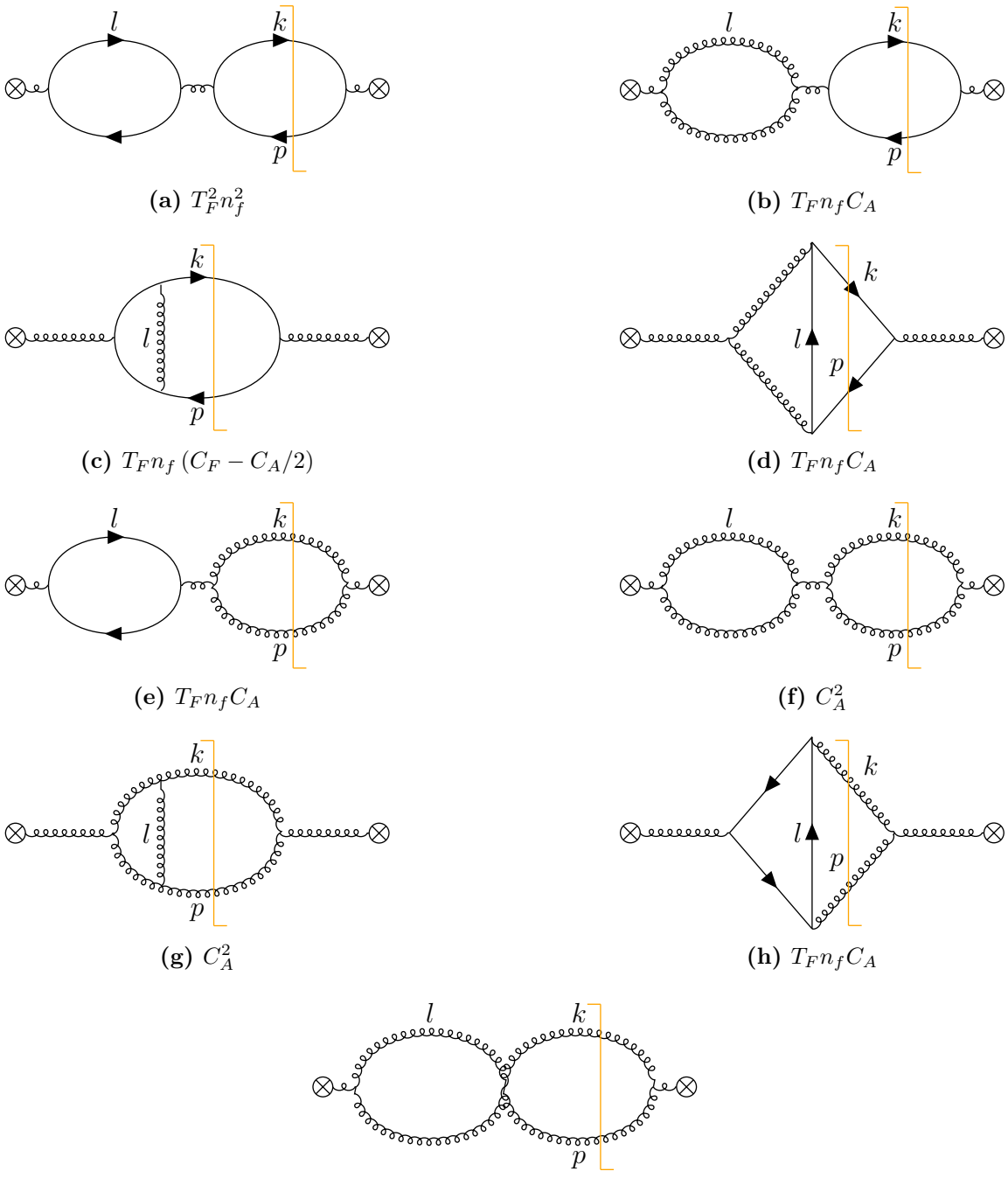

(a) $T_F^2 n_f^2$ **(b)** $T_F n_f C_A$

(c) $T_F n_f \left(C_F - C_A/2\right)$ **(d)** $T_F n_f C_A$

(e) $T_F n_f C_A$ **(f)** C_A^2

(g) C_A^2 **(h)** $T_F n_f C_A$

(i) C_A^2

Figure 6.2.3: Diagrams contributing to the NNLO real-virtual correction to gluon jet function and their respective colour structure. All other diagrams give rise to scaleless integrals. The diagrams (a) through (d) belong to the $P^{(1)}_{g\to q\bar{q}}$ splitting function and the diagrams (e) through (i) belong to the $P^{(1)}_{g\to gg}$ splitting function. The loop momentum is labeled l and for the on-shell particles the momentum labelling is the same as in the NLO case.

sponding double collinear splitting function and the master formulae. The diagrams which have to be computed are shown in figure 6.2.3, where figures 6.2.3(a) through 6.2.3(d) belong to the $P^{(1)}_{g\to q\bar{q}}$ splitting function and the diagrams 6.2.3(e) through 6.2.3(i) belong to the $P^{(1)}_{g\to gg}$ splitting function. We use again the compact form of the splitting functions from [126]. The $P^{(1)}_{g\to q\bar{q}}$ splitting function reads,

$$P^{(1)}_{g\to q\bar{q}}(s,z_k) = \left(\frac{\mu^2 e^{\gamma_E}}{s}\right)^{\epsilon} \frac{2g_s^2}{(4\pi)^2} \frac{\pi\Gamma(1-\epsilon)}{\epsilon\tan(\pi\epsilon)\Gamma(1-2\epsilon)} T_F n_f \Bigg\{ \left[\frac{z_k^2+\bar{z}_k^2-\epsilon}{1-\epsilon}\right] \left[\frac{4(\epsilon-1)\epsilon}{4(\epsilon-2)\epsilon+3} T_F n_f + \frac{\epsilon(3(1-\epsilon)+2\epsilon^2)-2}{(\epsilon-1)(2\epsilon-1)} C_F + \left(2 - F_1 - F_2 + \frac{3+\epsilon^2(2(\epsilon-2)+(1+2(\epsilon-2)\epsilon))}{(\epsilon-1)(3-2\epsilon)(2\epsilon-1)}\right) C_A\right]\Bigg\}, \quad (6.2.10)$$

and $P^{(1)}_{g\to gg}$ is given by

$$P^{(1)}_{g\to gg}(s,z_k) = \left(\frac{\mu^2 e^{\gamma_E}}{s}\right)^{\epsilon} \frac{2g_s^2}{(4\pi)^2} \frac{\pi\Gamma(1-\epsilon)}{\epsilon\tan(\pi\epsilon)\Gamma(1-2\epsilon)} C_A \Bigg\{ \left[\frac{(1-z_k\bar{z}_k)^2}{z_k\bar{z}_k} C_A\right] [1 - F_1 - F_2] + \left(\frac{\epsilon^2(1-2\epsilon z_k\bar{z}_k)(C_A(\epsilon-1)+2T_F n_f)}{2(1-\epsilon)(\epsilon-1)(2\epsilon-3)(2\epsilon-1)}\right)\Bigg\}, \quad (6.2.11)$$

where we used the shorthand notation F_1 and F_2 for the hypergeometric functions again. We are therefore able to write the master formulae for the RV-contribution of the gluon jet function as

$$J^{\mathrm{RV}}_{g\to q\bar{q},2}(\tau,\mu,Q) = \left(\frac{\alpha_s}{4\pi}\right)^2 \left(\frac{\mu\bar{\tau}^{\frac{1}{n+1}}}{Q^{\frac{n}{n+1}}}\right)^{4\epsilon} \left(\frac{\nu}{Q}\right)^{2\alpha} \frac{16}{1+n} \frac{\Gamma(\frac{-4\epsilon}{1+n})}{\sqrt{\pi}\Gamma(\frac{1}{2}-\epsilon)} \frac{\pi\Gamma(1-\epsilon)}{\epsilon\tan(\pi\epsilon)\Gamma(1-2\epsilon)} \exp\left[2\gamma_E\epsilon\left(1-\frac{2}{1+n}\right)\right] \int_0^1 \mathrm{d}z_k\,\mathrm{d}t_k\,(z_k\bar{z}_k)^{\epsilon-\alpha}\,(4t_k\bar{t}_k)^{-\frac{1}{2}-\epsilon}\, f_{q\bar{q}}(z_k,t_k)^{\frac{4\epsilon}{1+n}} \Bigg\{ T_F^2 n_f^2 \left[\frac{4(\epsilon-1)\epsilon\,(z_k^2+\bar{z}_k^2-\epsilon)}{(1-\epsilon)(4(\epsilon-2)\epsilon+3)}\right] + T_F n_f C_F \left[\frac{(\epsilon(3(1-\epsilon)+2\epsilon^2)-2)(z_k^2+\bar{z}_k^2-\epsilon)}{(1-\epsilon)(\epsilon-1)(2\epsilon-1)}\right] + T_F n_f C_A \left[2 - F_1 - F_2 + \frac{3+\epsilon^2(2(\epsilon-2)+(1+2(\epsilon-2)\epsilon))}{(\epsilon-1)(3-2\epsilon)(2\epsilon-1)}\right]\Bigg\}, \quad (6.2.12)$$

and

$$J^{\mathrm{RV}}_{g\to gg,2}(\tau,\mu,Q) = \left(\frac{\alpha_s}{4\pi}\right)^2 \left(\frac{\mu\bar{\tau}^{\frac{1}{n+1}}}{Q^{\frac{n}{n+1}}}\right)^{4\epsilon} \left(\frac{\nu}{Q}\right)^{2\alpha} \frac{16}{1+n} \frac{\Gamma(\frac{-4\epsilon}{1+n})}{\sqrt{\pi}\Gamma(\frac{1}{2}-\epsilon)} \frac{\pi\Gamma(1-\epsilon)}{\epsilon\tan(\pi\epsilon)\Gamma(1-2\epsilon)}$$
$$\exp\left[2\gamma_E\epsilon\left(1-\frac{2}{1+n}\right)\right] \int_0^1 \mathrm{d}z_k\,\mathrm{d}t_k\,(z_k\bar{z}_k)^{-1-4\frac{n}{1+n}\epsilon+\epsilon-\alpha}\,(4t_k\bar{t}_k)^{-\frac{1}{2}-\epsilon}\,f_{gg}(z_k,t_k)^{\frac{4\epsilon}{1+n}}$$
$$\left\{C_A^2\left[(1-z_k\bar{z}_k)^2\,(1-F_1-F_2)+\frac{\epsilon^2(1-2\epsilon z_k\bar{z}_k)z_k\bar{z}_k}{2(1-\epsilon)(2\epsilon-3)(2\epsilon-1)}\right]\right.$$
$$\left.+\,C_A T_F n_f\left[\frac{\epsilon^2(1-2\epsilon z_k\bar{z}_k)z_k\bar{z}_k}{(1-\epsilon)(\epsilon-1)(2\epsilon-3)(2\epsilon-1)}\right]\right\}. \tag{6.2.13}$$

6.2.2 NNLO: Real-real collinear matrix elements

After computing the RV corrections to the jet function, we turn to the real-real (RR) contributions. We start the computation, as we did in the other sections, by evaluating the collinear matrix elements.

The computation of the matrix elements follows the same way as in the NLO case; the only difference is that we have three particles in the final state instead of two. Therefore we will use the fact that they can be related to the triple collinear splitting functions given below. In order to be consistent, we use the following notation for the splitting functions

$$z_1 = \frac{k_-}{Q}, \quad z_2 = \frac{l_-}{Q}, \quad z_3 = \frac{p_-}{Q},$$
$$s_{12} = (k+l)^2, \quad s_{13} = (k+p)^2, \quad s_{23} = (l+p)^2, \quad s_{123} = (k+l+p)^2,$$

where the momenta k, l, p are chosen in reference to the splitting, $q \to p_1(k)p_2(l)p_3(p)$. At NNLO we have to consider five splitting functions which contribute to the jet functions. In the case of the quark jet function the collinear matrix element is given by[3]

$$\sigma_3^{c,q} = \tilde{\mu}^{4\epsilon}\frac{4Qg_s^4}{s_{123}^2}\left(P^{(0)}_{q\to\bar{q}'q'q} + P^{(0)}_{q\to\bar{q}qq} + P^{(0)}_{q\to ggq}\right), \tag{6.2.14}$$

where the primed quark(antiquark) represents a quark(antiquark) of different flavour

[3]In the literature the splitting function $P^{(0)}_{q\to\bar{q}qq}$ is given as $\left(P^{(0)}_{q\to\bar{q}'q'q} + 2\to 3\right) + P^{id,(0)}_{q\to\bar{q}qq}$, however the first two terms can be absorbed into $P^{(0)}_{q\to\bar{q}'q'q}$. Thus we will use $P^{(0)}_{q\to\bar{q}qq} = P^{id,(0)}_{q\to\bar{q}qq}$.

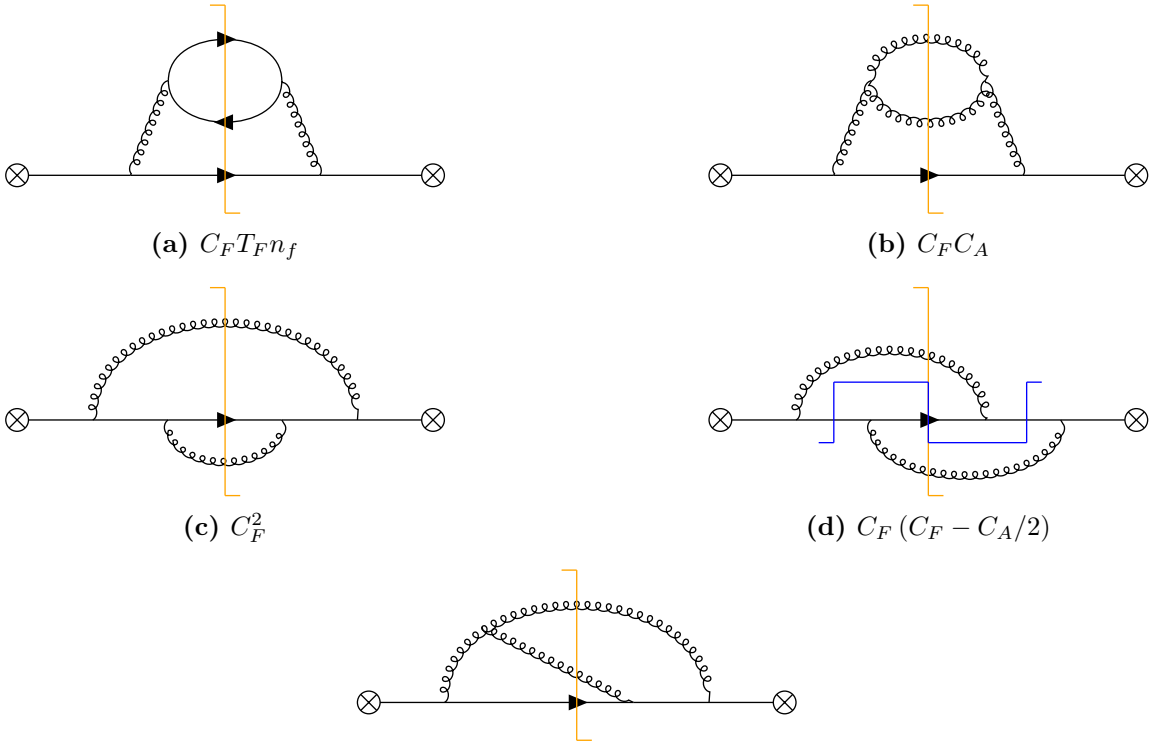

(a) $C_F T_F n_f$ **(b)** $C_F C_A$

(c) C_F^2 **(d)** $C_F\,(C_F - C_A/2)$

(e) $C_F C_A$

Figure 6.2.4: Topologies contributing to NNLO real-real quark jet function and their respective colour structure. The topology in figure (a) corresponds to the $P^{(0)}_{q\to\bar{q}'q'q}$ splitting function. The blue cut in figure (d) belongs to the $P^{(0)}_{q\to\bar{q}qq}$ splitting function and the orange cut in figure (d), as well as the rest of the figures, to $P^{(0)}_{q\to ggq}$. The diagrams with two identical particles in the final state correspond to two diagrams where the momentum labels are switched.

than the parent quark(antiquark). The matrix element for the gluon jet function is

$$\sigma_3^{c,g} = \tilde{\mu}^{4\epsilon}\frac{4g_s^4}{s_{123}^2}\left(P^{(0)}_{g\to gq'\bar{q}'} + P^{(0)}_{g\to ggg}\right). \tag{6.2.15}$$

The topologies that enter the collinear matrix element calculation of the quark jet function are depicted in figure 6.2.4. The leading order triple collinear splitting functions were calculated in [121, 122]. They read

$$P^{(0)}_{q\to\bar{q}'q'q} = C_F T_F n_f \frac{s_{123}}{2s_{12}}\left[-\frac{\left[z_1(s_{12}+2s_{23}) - z_2(s_{12}+2s_{13})\right]^2}{(z_1+z_2)^2 s_{12}s_{123}} + \frac{4z_3 + (z_1-z_2)^2}{z_1+z_2} + (1-2\epsilon)\left(z_1+z_2-\frac{s_{12}}{s_{123}}\right)\right], \tag{6.2.16}$$

$$
\begin{aligned}
P^{(0)}_{q\to\bar{q}qq} =& C_F\left(C_F-\frac{C_A}{2}\right)\left\{(1-\epsilon)\left(\frac{2s_{23}}{s_{12}}-\epsilon\right)+\frac{s_{123}}{s_{12}}\left[\frac{1+z_1^2}{1-z_2}-\frac{2z_2}{1-z_3}\right.\right.\\
&\left.-\epsilon\left(\frac{(1-z_3)^2}{1-z_2}+1+z_1-\frac{2z_2}{1-z_3}\right)-\epsilon^2(1-z_3)\right]\\
&\left.-\frac{s_{123}^2}{2s_{12}s_{13}}z_1\left[\frac{1+z_1^2}{(1-z_2)(1-z_3)}-\epsilon\left(1+2\frac{1-z_2}{1-z_3}\right)-\epsilon^2\right]\right\}+(2\leftrightarrow 3)\,,
\end{aligned}
\tag{6.2.17}
$$

$$
\begin{aligned}
P^{(0)}_{q\to ggq} =& C_F^2\left\{\frac{s_{123}^2}{2s_{13}s_{23}}z_3\left[\frac{1+z_3^2}{z_1z_2}-\epsilon\frac{z_1^2+z_2^2}{z_1z_2}-\epsilon(1+\epsilon)\right]+(1-\epsilon)\left[\epsilon-(1-\epsilon)\frac{s_{23}}{s_{13}}\right]\right.\\
&\left.+\frac{s_{123}}{s_{13}}\left[\frac{z_3(1-z_1)+(1-z_2)^3}{z_1z_2}-\epsilon(z_1^2+z_1z_2+z_2^2)\frac{1-z_2}{z_1z_2}+\epsilon^2(1+z_3)\right]\right\}\\
&+C_FC_A\left\{(1-\epsilon)\left(\frac{1}{4}-\frac{\epsilon}{2}+\frac{\left[z_1(s_{12}+2s_{23})-z_2(s_{12}+2s_{13})\right]^2}{4(z_1+z_2)^2s_{12}s_{123}}\right)+\frac{s_{123}^2}{2s_{12}s_{13}}\right[\\
&\frac{2z_3+(1-\epsilon)(1-z_3)^2}{z_2}+\frac{2(1-z_2)+(1-\epsilon)z_2^2}{1-z_3}\left]-\frac{s_{123}^2}{4s_{13}s_{23}}z_3\right[\epsilon(1-\epsilon)\\
&+\frac{2z_3+(1-\epsilon)(1-z_3)^2}{z_1z_2}\left]+\frac{s_{123}}{2s_{12}}\right[2\epsilon\frac{z_3(z_1-2z_2)-z_2}{z_2(1-z_3)}\\
&+(1-\epsilon)\frac{z_1(2-2z_1+z_1^2)-z_2(6-6z_2+z_2^2)}{z_2(1-z_3)}\left]+\frac{s_{123}}{2s_{13}}\right[\frac{z_3(z_1-1)-(1-z_2)^3}{z_1z_2}\\
&+(1-\epsilon)\frac{(1-z_2)^3+z_3^2-z_2}{z_2(1-z_3)}-\epsilon(\frac{2(1-z_2)(z_2-z_3)}{z_2(1-z_3)}-z_1+z_2)\\
&\left.\left.+\epsilon(1-z_2)\left(\frac{z_1^2+z_2^2}{z_1z_2}-\epsilon\right)\right]\right\}+(1\leftrightarrow 2)\,.
\end{aligned}
\tag{6.2.18}
$$

The $P^{(0)}_{g\to gq'\bar{q}'}$ splitting function can be decomposed into the colour structures

$$
P^{(0)}_{g\to gq'\bar{q}'} = C_FT_Fn_FP_1 + C_AT_Fn_FP_2, \tag{6.2.19}
$$

where

$$
\begin{aligned}
P_1 =& -2-(1-\epsilon)s_{23}\left(\frac{1}{s_{12}}+\frac{1}{s_{13}}\right)+2\frac{s_{123}^2}{s_{12}s_{13}}\left(1+z_1^2-\frac{z_1+2z_2z_3}{1-\epsilon}\right)\\
&-\frac{s_{123}}{s_{12}}\left(1+2z_1+\epsilon-2\frac{z_1+z_2}{1-\epsilon}\right)-\frac{s_{123}}{s_{13}}\left(1+2z_1+\epsilon-2\frac{z_1+z_3}{1-\epsilon}\right),
\end{aligned}
\tag{6.2.20}
$$

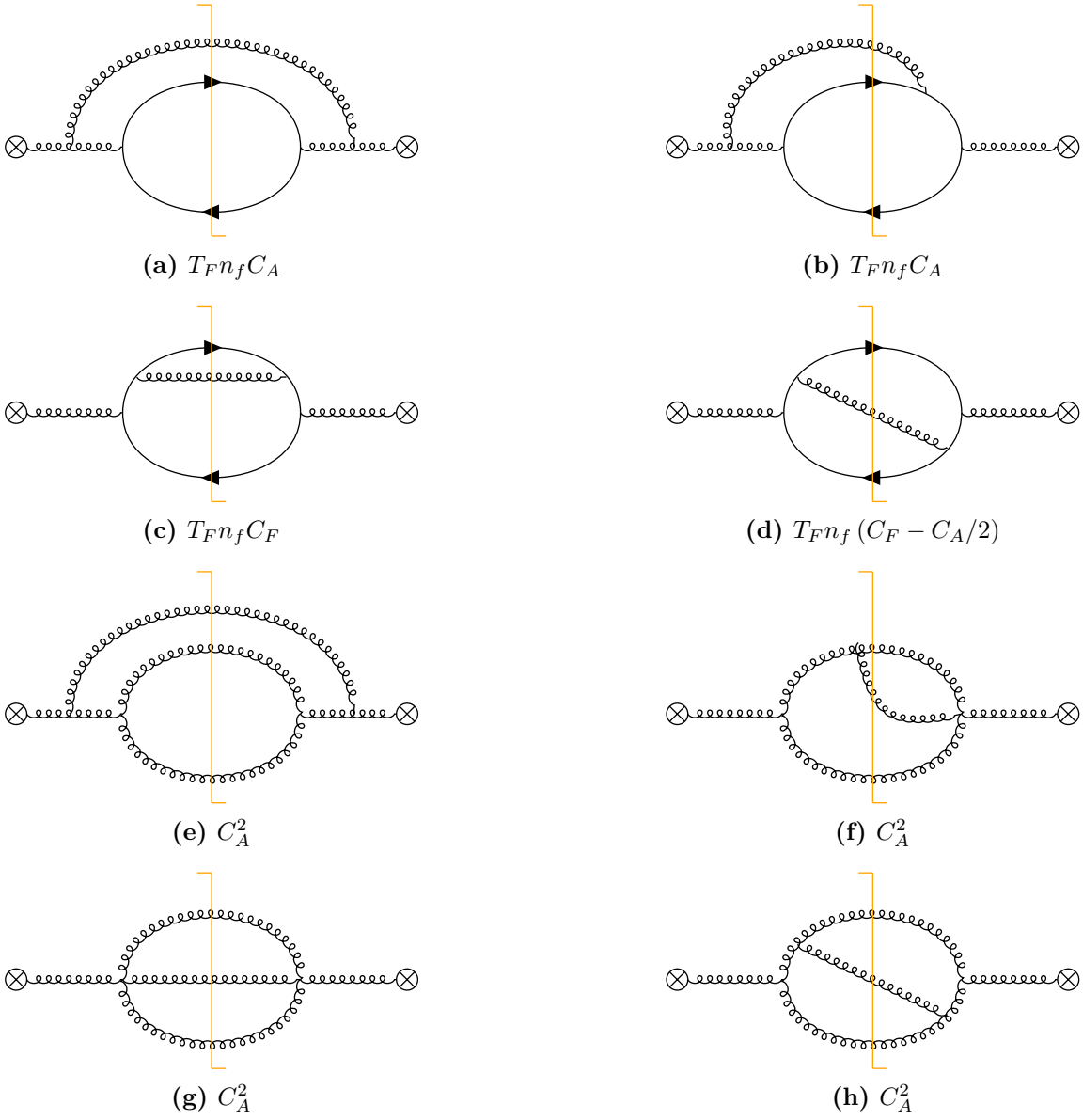

(a) $T_F n_f C_A$ **(b)** $T_F n_f C_A$

(c) $T_F n_f C_F$ **(d)** $T_F n_f \left(C_F - C_A/2\right)$

(e) C_A^2 **(f)** C_A^2

(g) C_A^2 **(h)** C_A^2

Figure 6.2.5: Topologies contributing to NNLO real-real gluon jet function and their respective colour structure. The topology in figures (a) through (d) corresponds to the $P^{(0)}_{g\to gq'\bar{q}'}$ splitting function and figures (e) through (h) to $P^{(0)}_{g\to ggg}$.The diagrams with two(three) identical particles in the final state correspond to two(six) diagrams where the momentum labels are switched.

and

$$
\begin{aligned}
P_2 = \Bigg[& \frac{-t_{23,1}^2}{4s_{23}^2} + \frac{s_{123}^2}{2s_{13}s_{23}} z_3 \left(\frac{(1-z_1)^3 - z_1^3}{z_1(1-z_1)} - \frac{2z_3(1-z_3-2z_1z_2)}{(1-\epsilon)z_1(1-z_1)} \right) \\
& + \frac{s_{123}}{2s_{13}}(1-z_2) \left(1 + \frac{1}{z_1(1-z_1)} - \frac{2z_2(1-z_2)}{(1-\epsilon)z_1(1-z_1)} \right) \\
& + \frac{s_{123}}{2s_{23}} \left(\frac{1+z_1^3}{z_1(1-z_1)} + \frac{z_1(z_2-z_3)^2 - 2z_2z_3(1+z_1)}{(1-\epsilon)z_1(1-z_1)} \right) \\
& - \frac{s_{123}^2}{2s_{12}s_{13}} \left(1 + z_1^2 - \frac{z_1+2z_2z_3}{1-\epsilon} \right) - \frac{1}{4} + \frac{\epsilon}{2} \Bigg] + (2 \leftrightarrow 3).
\end{aligned} \tag{6.2.21}
$$

The last splitting function we need for the gluon jet function is $P^{(0)}_{g\to ggg}$ given as,

$$
\begin{aligned}
P^{(0)}_{g\to ggg} = C_A^2 \Bigg[& \frac{(1-\epsilon)}{4} \frac{t_{12,3}^2}{s_{12}^2} + \frac{3}{4}(1-\epsilon) + \frac{s_{123}}{s_{12}} \Bigg(4\frac{z_1z_2-1}{1-z_3} + \frac{z_1z_2-2}{z_3} \\
& + \frac{3}{2} + \frac{5}{2}z_3 + \frac{(1-z_3(1-z_3))^2}{z_3z_1(1-z_1)} \Bigg) + \frac{s_{123}^2}{s_{12}s_{13}} \Bigg(\frac{z_1z_2(1-z_2)(1-2z_3)}{z_3(1-z_3)} + z_2z_3 - 2 \\
& + \frac{z_1(1+2z_1)}{2} + \frac{1+2z_1(1+z_1)}{2(1-z_2)(1-z_3)} + \frac{1-2z_1(1-z_1)}{2z_2z_3} \Bigg) \Bigg] + 5 \text{ Permutations}.
\end{aligned} \tag{6.2.22}
$$

The diagrams for the splitting functions are shown in figure 6.2.5, and the compact form is taken from [122]. In eqs. (6.2.19) and (6.2.22) we used

$$
t_{ij,k} = 2\frac{z_i s_{jk} - z_j s_{ik}}{z_i + z_j} + \frac{z_i - z_j}{z_i + z_j} s_{ij}.
$$

Note that the splitting functions with identical particles in the final state come with an additional symmetry factor. In our calculation, we will, most of the time, cancel the symmetry factor against the additional permutations. Therefore, we only have to use the shown form of the splitting functions in calculating the jet function master formulae.

As a last note on the splitting functions, observe that the triple collinear splitting functions have a rich divergence structure. Therefore it is convenient to split these further into structures with similar divergent behaviour. This decomposition of the splitting functions is shown in appendix B.

Before we introduce the phase-space parametrisation, we show the colour decomposition of the quark and gluon jet function, along with some prefactors, so that we

can simplify the notation. The decomposition reads

$$J_q^{\mathrm{RR}} = \left(\frac{\alpha_s}{4\pi}\right)^2 \left(\frac{\mu\bar{\tau}^{\frac{1}{1+n}}}{Q^{\frac{n}{1+n}}}\right)^{4\epsilon} \left(\frac{\nu}{Q}\right)^{2\alpha} \left[C_F T_F n_f J_q^{\mathrm{Ff}} + C_F^2 J_q^{\mathrm{FF}} + C_F C_A J_q^{\mathrm{FA}} + C_F \left(C_F - \frac{C_A}{2}\right) J_q^{\mathrm{ID}}\right], \quad (6.2.23)$$

$$J_g^{\mathrm{RR}} = \left(\frac{\alpha_s}{4\pi}\right)^2 \left(\frac{\mu\bar{\tau}^{\frac{1}{1+n}}}{Q^{\frac{n}{1+n}}}\right)^{4\epsilon} \left(\frac{\nu}{Q}\right)^{3\alpha} \left[T_F n_f C_F J_g^{\mathrm{fF}} + T_F n_f C_A J_g^{\mathrm{fA}} + C_A^2 J_g^{\mathrm{AA}}\right], \quad (6.2.24)$$

where the coefficients J_i are integrals of the collinear matrix elements.

6.2.3 NLO quark jet function: $\mathbf{C_F T_F n_f}$

One of the simplest structures for the 3-particle phase-space cut is the $C_F T_F n_f$ colour structure for the quark jet function. It arises from diagrams that involve cutting a fermion bubble, depicted in figure 6.2.4(a). The associated splitting function is given in eq. (6.2.16).

The collinear matrix element can be further separated into two different structures according to its dependence on the triple invariant mass s_{123}.

$$\sigma^{c,q}_{3,C_F T_F n_f} = \left(\frac{1}{s_{123}^2}\sigma_A + \frac{1}{s_{123}}\sigma_B\right) C_F T_F n_f, \quad (6.2.25)$$

where

$$\sigma_A = -4\tilde{\mu}^{4\epsilon} g_s^4 \left[\frac{\left[z_1(s_{12}+2s_{23}) - z_2(s_{12}+2s_{13})\right]^2}{2(z_1+z_2)^2 s_{12}^2} + \frac{(1-2\epsilon)}{2}\right], \quad (6.2.26)$$

and

$$\sigma_B = \frac{2\tilde{\mu}^{4\epsilon} g_s^4}{s_{12}} \left[\frac{4z_3 + (z_1-z_2)^2}{z_1+z_2} + (1-2\epsilon)(z_1+z_2)\right]. \quad (6.2.27)$$

Here we can already see that the divergence structure is more complicated than in the 2-particle cut cases discussed above. In particular, the collinear divergence due to

$$s_{12} = \frac{k_-}{l_-} k_T^2 + \frac{l_-}{k_-} l_T^2 - 2 k_T l_T \cos\theta_{kl}, \quad (6.2.28)$$

requires some attention and a direct factorisation of the divergences seems impossible.

Like in the 2-particle-cut case, we transform to light-cone coordinates and use the

on-shell conditions and the additional phase-space constraints to eliminate the integrations associated with the third particle and the plus-components of the remaining two particles. The remaining integrations are then the remaining light-cone components k_-, k_T and l_-, l_T, as well as the corresponding angular integrations.

We introduce the physical parametrisation in terms of the sum of light-cone coordinate variables q_T and z_{12}, as well as relative variables a_{12} and b_{12} as follows:

$$q_T = \sqrt{(k_- + l_-)\left(\frac{k_T^2}{k_-} + \frac{l_T^2}{l_-}\right)}, \qquad z_{12} = \frac{k_- + l_-}{Q}, \tag{6.2.29}$$

$$a_{12} = \frac{k_- l_T}{k_T l_-}, \qquad b_{12} = \frac{k_T}{l_T}. \tag{6.2.30}$$

As mentioned in the previous sections, this is not the parametrisation we ultimately use in our numerical approach; though, it is similar. It is far more intuitive than the actual computational parametrisation, so understanding our setup is more straightforward, and the expressions are much shorter.

Now that we have fixed our parametrisation for the light-cone coordinates, we turn to the angular variables. We stated that we allow dependence on one angle per particle measured with respect to a shared reference vector in the transverse plane per final-state particle. However, one angle is always fixed by phase-space constraints. Thus, we technically only allow $i-1$ independent angles for i final-state particles. So, in the case of the NNLO real-real calculation, we need two independent angles in the transverse plane. This is the same case as in the soft function calculation. Thus, we can use the setup from [42].

We parameterise the transverse plane in $(d-2)$ dimensions as

$$\begin{aligned}
\vec{l_\perp} &= \left|\vec{l_\perp}\right|(1, 0, 0, \dots 0), \\
\vec{k_\perp} &= \left|\vec{k_\perp}\right|(\cos\theta_{kl}, \sin\theta_{kl}, 0, \dots, 0), \\
\vec{v_\perp} &= |\vec{v_\perp}|(\cos\theta_l, \sin\theta_l \sin\theta_5, \sin\theta_l \cos\theta_5, 0, \dots, 0),
\end{aligned}$$

where $\theta_k = \measuredangle(\vec{k}_\perp, \vec{v}_\perp), \theta_l = \measuredangle(\vec{l}_\perp, \vec{v}_\perp)$ and $\theta_{kl} = \measuredangle(\vec{k}_\perp, \vec{l}_\perp)$. This arrangement can be seen in figure 6.2.6. This setup ensures that the invariant mass s_{12} has a simple dependence on the angle θ_{kl}. For the angular integration measure we have

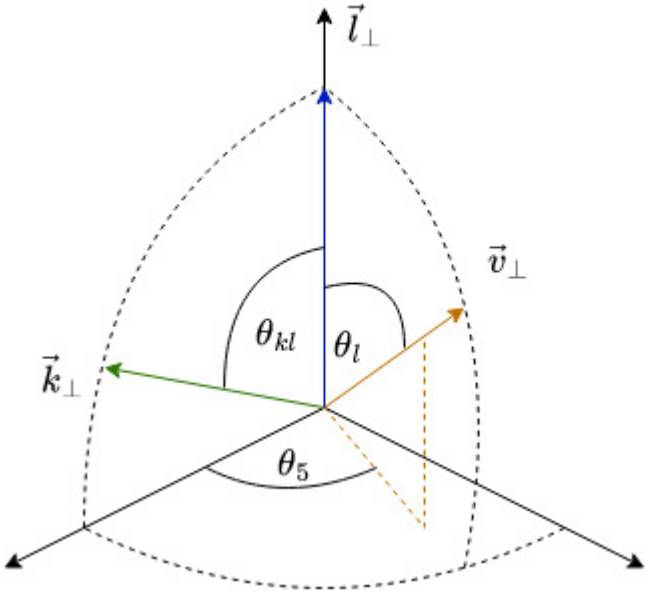

Figure 6.2.6: The angular parametrisation of the transverse space.

$$\begin{aligned}\int \mathrm{d}^{d-3}\Omega_k \mathrm{d}^{d-3}\Omega_l &= \int \mathrm{d}^{d-4}\Omega \mathrm{d}^{d-5}\Omega \int_0^\pi \mathrm{d}\theta_{kl}\mathrm{d}\theta_l \mathrm{d}\theta_5 \sin^{d-4}\theta_{kl} \sin^{d-4}\theta_l \sin^{d-5}\theta_5 \\ &= \frac{32\pi^{\frac{1}{2}-2\epsilon}}{\Gamma(1/2-\epsilon)\Gamma(-\epsilon)} \int_0^1 \mathrm{d}t_{kl}\mathrm{d}t_l\mathrm{d}t_5 (4t_{kl}\bar{t}_{kl})^{-\frac{1}{2}-\epsilon}(4t_l\bar{t}_l)^{-\frac{1}{2}-\epsilon}(4t_5\bar{t}_5)^{-1-\epsilon},\end{aligned} \tag{6.2.31}$$

which is almost the final expression. The t_5 integration suffers from spurious divergences in limit $t_5 \to \{0,1\}$. These divergences are unphysical, and they cancel against the $\frac{1}{\Gamma(-\epsilon)}$ in the prefactor. The origin is that we are resolving more angles in the transverse plane than exist in four space-time dimensions. The divergences in both endpoints again forbids a naive ϵ-expansion on the integrand level. Therefore, we will disentangle them by splitting the integration domain at $t_5 = 1/2$. This leads to two contributions, which after subsequent rescaling, yield

$$\begin{aligned}&\int \mathrm{d}^{d-3}\Omega_k \mathrm{d}^{d-3}\Omega_l = \\ &\frac{16\pi^{\frac{1}{2}-2\epsilon}}{\Gamma(1/2-\epsilon)\Gamma(-\epsilon)} \int_0^1 \mathrm{d}t_{kl}\mathrm{d}t_l\mathrm{d}t_5' (4t_{kl}\bar{t}_{kl})^{-\frac{1}{2}-\epsilon}(4t_l\bar{t}_l)^{-\frac{1}{2}-\epsilon}(t_5'(2-t_5'))^{-1-\epsilon}.\end{aligned} \tag{6.2.32}$$

Notice that we integrate over two copies of the actual integrand, one with the substitution $t_5 \to t_5'/2$ and the second one with $t_5 \to 1 - t_5'/2$. However, the integrand

can only depend implicitly on t_5 through

$$t_k = t_l + t_{kl} - 2t_l t_{kl} - 2\sqrt{t_l \bar{t}_l t_{kl} \bar{t}_{kl}}(1 - 2t_5) \tag{6.2.33}$$

and therefore we only have to sum over two contributions in which the angle θ_k is resolved as

$$t_k^{\pm} = t_l + t_{kl} - 2t_l t_{kl} \pm 2\sqrt{t_l \bar{t}_l t_{kl} \bar{t}_{kl}}(1 - t_5'). \tag{6.2.34}$$

As a last comment on the angular parametrisation, we show how we can express the angles involving the third particle via the other angles. Let us start by looking at the angles θ_{kp} and θ_{lp}, which are required for the invariant masses s_{13} and s_{23}, respectively. We note that from the $(d-2)$-dimensional delta function, we find

$$\vec{p}_T = -\vec{k}_T - \vec{l}_T. \tag{6.2.35}$$

Thus, we can write for $\cos\theta_{kp}$

$$\begin{aligned} \vec{p}_T \cdot \vec{k}_T &= -k_T^2 - k_T l_T \cos\theta_{kl}, \\ p_T k_T \cos\theta_{kp} &= -k_T^2 - k_T l_T \cos\theta_{kl}, \\ \cos\theta_{kp} &= \frac{-k_T^2 - k_T l_T \cos\theta_{kl}}{p_T k_T}, \end{aligned} \tag{6.2.36}$$

and similarly for $\cos\theta_{lp}$ we find

$$\cos\theta_{lp} = \frac{-l_T^2 - k_T l_T \cos\theta_{kl}}{p_T l_T}. \tag{6.2.37}$$

The final angle we require is the angle θ_p between the third particle and the reference vector $\vec{v}_\perp$. This can be computed from the scalar product between $\vec{p}_T$ and the reference vector, using the phase-space restriction on the transverse component. Thus we find

$$\cos\theta_p = -\frac{k_T}{p_T}\cos\theta_k - \frac{l_T}{p_T}\cos\theta_l. \tag{6.2.38}$$

We are now close to writing down the master formula for the $C_F T_F n_f$-colour structure of the quark jet function. The last ingredient we have to specify is the measurement function. At the NLO level, we assumed that the measurement function could

be written in the form

$$\mathcal{M}^{\text{jet}}_{1,gq}(\tau;k) = \exp\left[-\tau k_T \left(\frac{k_T}{z_k Q}\right)^n f(z_k,t_k)\right]. \tag{6.2.39}$$

If we extend this to the NNLO RR contribution, we can see that our new variable q_T is taking the place of k_T as the dimensionful variable. Thus we replace k_T by q_T in the previous equation. Next, we look at the factor z_k^{-n}. We have factored out this term to ensure that $f(z_k,t_k)$ is finite. Similarly, in the RR structure, we have to factor out terms such that the remaining function stays finite and non-zero. The question now arises: What kind of divergences can be present in the RR contribution?

We observe that we can have two different kinds of divergences; one obeys IRC safety, and the other one does not obey it. Therefore we know that if the divergence obeys IRC safety, the measurement function reduces to the NLO measurement function and thus stays finite. If we turn to our parametrisation, we see that the divergences which obey IRC safety are

$$\begin{aligned} b_{12} \to 0 &\;\widehat{=}\; k^\mu \text{ is soft,} \\ b_{12} \to \infty &\;\widehat{=}\; l^\mu \text{ is soft,} \\ a_{12} \to 1 \;\&\; t_{kl} \to 0 &\;\widehat{=}\; k^\mu \text{ is collinear to } l^\mu. \end{aligned}$$

So we never have to factor out these limits, since we are guaranteed that the measurement function is non-zero in this case automatically. All other limits could lead to remainder functions that tend to infinity or are zero in the singular limits of the matrix element. Therefore, we first have to check the divergence structure of the matrix element and then the behaviour of a general measurement function in these singular limits. Note that we do not have to be as general as possible because the divergences are related to the double soft limits and are therefore universal. So we can use a generic event-shape variable, which we will define later. We will denote Ω as a placeholder for those factors which have to be pulled out of the measurement function. The final piece we have to adapt for the NNLO RR structure is $f(z_k,t_k)$. This new function must depend on every variable in our parametrisation except q_T. In particular, it is the only part of our computation that depends on the angles between the transverse component and our reference vector. Thus, we need two versions of this function which we denote

as F:

$$F(a_{12},b_{12},z_{12},t_{kl},t_k^{\pm},t_l) = F_+(a_{12},b_{12},z_{12},t_{kl},t_k^{+},t_l) + F_-(a_{12},b_{12},z_{12},t_{kl},t_k^{-},t_l), \tag{6.2.40}$$

where $t_k^{\pm} = t_k^{\pm}(t_{kl},t_l,t_5')$ was given in (6.2.34). Therefore, our ansatz for the measurement function for the NNLO RR contribution is

$$\mathcal{M}_2^{\text{jet}}(\tau;\{k,l,p\}) = \exp\left[-\tau q_T \left(\frac{q_T}{Q}\right)^n \Omega\, F(a_{12},b_{12},z_{12},t_{kl},t_k^{\pm},t_l)\right]. \tag{6.2.41}$$

Note that this ansatz will be used for all structures in both quark and gluon jet function, with the only difference being the dependence on the kinematic variables and angles in F and the exact form of Ω.

With all the ingredients determined we are now able to write down our master formulae for this colour structure:

$$\begin{aligned}
J_{q,A}^{\text{Ff}} =& \frac{2^{3-6\epsilon}\Gamma\left(\frac{-4\epsilon}{1+n}\right)}{(1+n)\pi^2\Gamma(-2\epsilon)} e^{2\epsilon\gamma_E\frac{n-1}{n+1}} \int_0^\infty \mathrm{d}a_{12}\mathrm{d}b_{12}\int_0^1 \mathrm{d}z_{12}\mathrm{d}t_{kl}\mathrm{d}t_l\mathrm{d}t_5' \\
& (t_{kl}\bar{t}_{kl})^{-\frac{1}{2}-\epsilon}(t_l\bar{t}_l)^{-\frac{1}{2}-\epsilon}(t_5'(2-t_5'))^{-1-\epsilon} a_{12}^{1-2\epsilon-\alpha} b_{12}^{1-2\epsilon-\alpha} z_{12}^{-1-2\alpha}\Omega^{\frac{4\epsilon}{1+n}} F^{\frac{4\epsilon}{1+n}} \\
& \frac{\bar{z}_{12}(a_{12}+b_{12})^{2\epsilon}(1+a_{12}b_{12})^{-2+2\epsilon+2\alpha}}{((1-a_{12})^2+4a_{12}t_{kl})^2((1+a_{12}b_{12})(a_{12}+b_{12})\bar{z}_{12}+z_{12}((1-b_{12})^2+4b_{12}\bar{t}_{kl}))^2} \\
& \big[-2(1-a_{12}^2)^2(1+a_{12}b_{12})^2 + 2(1-a_{12}^2)(1-a_{12}^2b_{12}^2)z_{12}((1-a_{12})^2+4a_{12}t_{kl}) \\
& -(1+a_{12}^2b_{12}^2)z_{12}^2((1-a_{12})^2+4a_{12}t_{kl})^2 + \epsilon\big\{(1+a_{12}b_{12})^2 z_{12}^2((1-a_{12})^2 \\
& +4a_{12}t_{kl})^2\big\}\big],
\end{aligned} \tag{6.2.42}$$

and

$$\begin{aligned}
J_{q,B}^{\text{Ff}} =& \frac{2^{3-6\epsilon}\Gamma\left(\frac{-4\epsilon}{1+n}\right)}{(1+n)\pi^2\Gamma(-2\epsilon)} e^{2\epsilon\gamma_E\frac{n-1}{n+1}} \int_0^\infty \mathrm{d}a_{12}\mathrm{d}b_{12}\int_0^1 \mathrm{d}z_{12}\mathrm{d}t_{kl}\mathrm{d}t_l\mathrm{d}t_5' \\
& (t_{kl}\bar{t}_{kl})^{-\frac{1}{2}-\epsilon}(t_l\bar{t}_l)^{-\frac{1}{2}-\epsilon}(t_5'(2-t_5'))^{-1-\epsilon} a_{12}^{1-2\epsilon-\alpha} b_{12}^{-2\epsilon-\alpha} z_{12}^{-1-2\alpha}\Omega^{\frac{4\epsilon}{1+n}} F^{\frac{4\epsilon}{1+n}} \\
& (a_{12}+b_{12})^{2\epsilon}(1+a_{12}b_{12})^{-2+2\epsilon+2\alpha} \\
& \frac{2+4a_{12}b_{12}\bar{z}_{12}-(2-z_{12})z_{12}+a_{12}^2b_{12}^2(2-(2-z_{12})z_{12})-\epsilon\left\{z_{12}^2(1+a_{12}b_{12})^2\right\}}{((1-a_{12})^2+4a_{12}t_{kl})((1+a_{12}b_{12})(a_{12}+b_{12})\bar{z}_{12}+z_{12}((1-b_{12})^2+4b_{12}\bar{t}_{kl}))},
\end{aligned} \tag{6.2.43}$$

where we abbreviated $F(a_{12},b_{12},z_{12},t_{kl},t_k^{\pm},t_l) = F$. The subscript $J_{q,A}^{\text{Ff}}(J_{q,B}^{\text{Ff}})$ correspond to the structure $\sigma_A(\sigma_B)$ in eq. (6.2.25).

In the formulae for the $C_FT_Fn_f$-contribution, we see that they still require some

work due to three problems. The first problem is that we want to work on the unit hypercube; thus, all integration must have a domain of 0 to 1. This is true for all angular integration and z_{12}, but a_{12} and b_{12} have still unbounded upper limits. The second problem is that we have not yet determined the explicit form of Ω for these structures, and the last problem is that we still have an overlapping singularity between a_{12} and t_{kl} from the collinear limit. Let us solve these problems one by one, starting with the remapping onto the hypercube.

Let us write our integrand as $I(a_{12}, b_{12})$ and assume we only want to integrate over a_{12} and b_{12}. Therefore, we can remap $I(a_{12}, b_{12})$ onto the hypercube in the following way:

$$\begin{aligned}
\int_0^\infty \mathrm{d}a_{12}\mathrm{d}b_{12}\, I(a_{12}, b_{12}) &= \int_0^1 \mathrm{d}a_{12}\mathrm{d}b_{12}\, I(a_{12}, b_{12}) + \int_0^1 \mathrm{d}a_{12} \int_1^\infty \mathrm{d}b_{12}\, I(a_{12}, b_{12}) \\
&+ \int_1^\infty \mathrm{d}a_{12} \int_0^1 \mathrm{d}b_{12}\, I(a_{12}, b_{12}) + \int_1^\infty \mathrm{d}a_{12}\mathrm{d}b_{12}\, I(a_{12}, b_{12}) \\
&= \int_0^1 \mathrm{d}a_{12}\mathrm{d}b_{12}\, I(a_{12}, b_{12}) + \int_0^1 \mathrm{d}a_{12}\mathrm{d}b_{12}\, b_{12}^{-2} I(a_{12}, 1/b_{12}) \\
&+ \int_0^1 \mathrm{d}a_{12}\mathrm{d}b_{12}\, a_{12}^{-2} I(1/a_{12}, b_{12}) + \int_0^1 \mathrm{d}a_{12}\mathrm{d}b_{12}\, a_{12}^{-2} b_{12}^{-2} I(1/a_{12}, 1/b_{12}) \\
&= \int_0^1 \mathrm{d}a_{12}\mathrm{d}b_{12}\, \left(I_A(a_{12}, b_{12}) + I_B(a_{12}, b_{12}) + I_C(a_{12}, b_{12}) + I_D(a_{12}, b_{12})\right).
\end{aligned} \tag{6.2.44}$$

In eq. (6.2.44) we see that, in general, we have to calculate four different sectors in order to recover the total integration domain. We can reduce the number of sectors for some structures by exploiting the underlying $k \leftrightarrow l$ symmetry. This symmetry states that the integral cannot differentiate between the exchange of two particles. In terms of our parametrisation, this implies that

$$a_{12} \to \frac{1}{a_{12}},\ b_{12} \to \frac{1}{b_{12}},\ z_{12} \to z_{12},\ t_l \to t_k,\ t_k \to t_l,\ t_{kl} \to t_{kl}. \tag{6.2.45}$$

In the case of the $C_F T_F n_f$-contribution this symmetry holds and thus we can simplify the remapping to

$$\int_0^\infty \mathrm{d}a_{12}\mathrm{d}b_{12}\, I(a_{12}, b_{12}) = 2 \int_0^1 \mathrm{d}a_{12}\mathrm{d}b_{12}\, \left(I_A(a_{12}, b_{12}) + I_B(a_{12}, b_{12})\right). \tag{6.2.46}$$

Note that this assures that the integral is symmetric under $k \leftrightarrow l$ exchange, but the

integrand can be different.

On the level of the matrix elements, this symmetry holds only for specific splitting functions. However, for the measurement function, this symmetry always holds because it cannot distinguish between the exchange of any particles. The only subtlety arises in the $t_k \to t_l$ exchange because technically t_k is a function of t_l; however, we can simply relabel the angles such that t_l becomes a function of t_k. Then the symmetry still holds.

Now that all the integrations are mapped onto the unit hypercube, we come to the overlapping singularity that arises in the collinear limit. The structure which gives rise to the overlapping singularity is $1/((1-a_{12})^2+4a_{12}t_{kl})$. In order to cure the overlapping singularity, we define a non-linear transformation:

$$a_{12} = 1 - u(1-v), \qquad t_{kl} = \frac{u^2 v}{1-u(1-v)}. \tag{6.2.47}$$

To see what is happening to the collinear divergence let us consider the structure

$$\int_0^1 \mathrm{d}a_{12}\mathrm{d}t_{kl} \frac{(t_{kl}\bar{t}_{kl})^{-\frac{1}{2}-\epsilon}}{(1-a_{12})^2+4a_{12}t_{kl}} \tag{6.2.48}$$

$$= \int_0^1 \mathrm{d}u\mathrm{d}v \underbrace{\frac{u^2(1+v)}{(1-u(1-v))}}_{\text{Jacobian}} \frac{1}{u^2(1+v)^2} \left(\frac{(1-u)u^2v(1+uv)}{(1-u(1-v))^2}\right)^{-\frac{1}{2}-\epsilon}$$

$$= \int_0^1 \mathrm{d}u\mathrm{d}v \frac{u^{-1-2\epsilon}}{1+v}(1-u(1-v))^{2\epsilon} \left(v(1-u)(1+uv)\right)^{-\frac{1}{2}-\epsilon}. \tag{6.2.49}$$

Here we can clearly see that the divergence is now in a monomial form in u and will only give rise to divergences in ϵ. The rest of the expression is either finite or, at most gives rise to integrable square root or logarithmic divergences.

Finally, we arrive at a master formula where all divergences are of monomial type, and therefore we can finally identify Ω for the $C_F T_F n_f$ contribution. In eqs. (6.2.42) and (6.2.43) we can see that the only divergent limits are $z_{12} \to 0$ and $u \to 0$ after using our non-linear transformation. However, we know that the collinear divergence u is protected by IRC and therefore the measurement function stays finite and non-zero in the limit $u \to 0$. In order to see which power of z_{12} we have to factor out; let us create a generic observable which obeys all our previously stated assumptions.

A toy measurement[4] which obeys all our assumptions is

$$\omega(\{k_i\}) = \sum_i k_{-,i}^{\frac{1-n}{2}} k_{+,i}^{\frac{1+n}{2}} . \tag{6.2.50}$$

If we introduce our parametrisation for the 3-particle phase-space and only keep terms related to z_{12} and q_T, then we can compare the result to our ansatz in eq. (6.2.41).

$$k_-^{\frac{1-n}{2}} k_+^{\frac{1+n}{2}} + l_-^{\frac{1-n}{2}} l_+^{\frac{1+n}{2}} + p_-^{\frac{1-n}{2}} p_+^{\frac{1+n}{2}} = q_T \left(\frac{q_T}{Q}\right)^n \left[\frac{G_1(a_{12}, b_{12}, n)}{z_{12}^n} + \frac{G_2(a_{12}, b_{12}, t_{kl}, n)}{\bar{z}_{12}^n}\right], \tag{6.2.51}$$

where G_1 and G_2 are finite functions in the limit $z_{12} \to 0$. Thus, we can see that we have to extract a factor of z_{12}^{-n} from the measurement to make sure that the rest of the expression is finite and non-zero in any of the divergences of the matrix element. So in the case of the $C_F T_F n_f$-structure we find that $\Omega = z_{12}^{-n}$. Therefore, we solved the three problems mentioned above.

Now we are at a point where we could show the master formulae in all their glory. However, as this is not the parametrisation that is passed to the numerical integrator we only show the complete structure for the region A of $J_{q,B}^{\mathrm{Ff}}$ and only the divergence structure of region B. In the case of region A, we find

$$\begin{aligned} J_{q,B,\mathrm{A}}^{\mathrm{Ff}} =& \frac{2^{4-6\epsilon}\Gamma\left(\frac{-4\epsilon}{1+n}\right)}{(1+n)\pi^2\Gamma(-2\epsilon)} e^{2\epsilon\gamma_E \frac{n-1}{n+1}} \int_0^1 \mathrm{d}z_{12}\mathrm{d}u\mathrm{d}b_{12}\mathrm{d}v\mathrm{d}t_l\mathrm{d}t_5' \, u^{-1-2\epsilon} z_{12}^{-1-\frac{4n\epsilon}{1+n}-2\alpha} (t_5')^{-1-\epsilon} \\ & (t_l\bar{t}_l)^{-\frac{1}{2}-\epsilon} (2-t_5')^{-1-\epsilon} (1+v)^{-1} b_{12}^{-2\epsilon-\alpha} (1-u(1-v))^{1-\alpha} ((1-u)v(1+uv))^{-\frac{1}{2}-\epsilon} \\ & \frac{(1-u(1-v)+b_{12})^{2\epsilon}(1+(1-u(1-v))b_{12})^{-2+2\epsilon+2\alpha} F^{\frac{4\epsilon}{1+n}}}{(1+b_{12}^2(1-u\bar{v})-u\bar{v}+b_{12}(2-u((2-u\bar{v})\bar{v}+u(1+v)^2 z_{12})))} \\ & \big[2+4(1-u(1-v))b_{12}\bar{z}_{12} - (2-z_{12})z_{12} + (1-u(1-v))^2 b_{12}^2 (2-(2-z_{12})z_{12}) \\ & \qquad - \epsilon\left\{z_{12}^2(1+(1-u(1-v))b_{12})^2\right\}\big], \end{aligned} \tag{6.2.52}$$

and in region B we find

$$J_{q,B,\mathrm{B}}^{\mathrm{Ff}}(\tau, \mu, Q) \sim \Gamma\left(\frac{-4\epsilon}{1+n}\right) \int_0^1 \mathrm{d}\Pi \, u^{-1-2\epsilon} z_{12}^{-1-\frac{4n\epsilon}{1+n}-2\alpha} \mathcal{W}, \tag{6.2.53}$$

where $\mathcal{W}$ is a function which does not give rise to any divergences. We can see that both

[4] This measurement is actually the precise definition of the angularity measurement. We will treat those more carefully in section 8.2.

regions give rise to the same kind of divergences, namely via the Γ-function and through the monomials in u and z_{12}. Moreover, we find the same divergence structure for the term proportional to $1/s_{123}^2$. Therefore we see that for $\mathrm{SCET_I}$ observables, $C_F T_F n_f$ produces a leading term proportional to ϵ^{-3} and in the case of a $\mathrm{SCET_{II}}$ observable, the leading structure is $\alpha^{-1}\epsilon^{-2}$.

6.2.4 NNLO quark jet function: Identical flavour structure

The next structure we look at is the structure that corresponds to the splitting function $P^{(0)}_{q\to\bar{q}qq}$ in eq. (6.2.17). We can again split the collinear matrix element into different structures according to its dependence on the triple invariant mass s_{123}:

$$\sigma^{c,q}_{3,\text{identical}} = \frac{1}{s_{123}^2}\sigma_C + \frac{1}{s_{123}}\sigma_D + \sigma_E, \tag{6.2.54}$$

where σ_C and σ_D can be calculated in a similar way as the $C_F T_F n_f$ structure. The interesting structure is σ_E because it does not depend on s_{123}, but on two different invariant masses:

$$\sigma_E = \frac{z_1\mathcal{N}}{s_{12}s_{13}(1-z_2)(1-z_3)}, \tag{6.2.55}$$

where $\mathcal{N}$ is the numerator of the expression, however for understanding the difficulty of this structure the exact form of it is irrelevant.

The challenge is that even though we have a parametrisation that perfectly captures the collinear divergence between particles 1 and 2, this is not true for the collinear divergence between particles 1 and 3. This becomes apparent when we write s_{13} in our parametrisation:

$$s_{13} = \frac{b(\bar{z}_{12}^2 + 2a_{12}\bar{z}_{12}(b_{12}+z_{12}(1-2t_{kl})) + a_{12}^2(b_{12}^2 + 2b_{12}z_{12}(1-2t_{kl}) + z_{12}^2))}{(a_{12}+b_{12})(1+a_{12}b_{12})\bar{z}_{12}z_{12}}q_T^2, \tag{6.2.56}$$

here we can see that this structure can become zero in many different singular limits. If these limits lie on the endpoints, they would still be manageable. However, there are also zeros in the middle of the integration domain. Therefore we can see the first massive drawback of our parametrisation in this case. Namely, it can only correctly disentangle the collinear divergence of one invariant mass. Specifically, we used the invariant mass of two particles to define our parametrisation. In the case of the $C_F T_F n_f$-structure we used the particles with momentum label k and l to define our parametrisation. Therefore, we can only correctly describe the collinear divergence

of s_{12}.

Here we have to separate both invariant masses. We achieve this by implementing a selector function $\mathbb{S}$. The selector function is supposed to suppress one divergence without creating new divergences. [5] These selector functions are in the same spirit as those introduced in [127]. The selector function we use for the structure σ_3 has the form

$$\mathbb{S} = z_3 s_{13} + z_2 s_{12}. \tag{6.2.57}$$

The additional z-factors are actually not required for this structure, however they become important for later contributions. Thus the can rewrite structure σ_3 as

$$\begin{aligned}\sigma_3 &= \frac{z_1\mathcal{N}}{s_{12}s_{13}(1-z_2)(1-z_3)}\frac{\mathbb{S}}{\mathbb{S}} \\ &= \frac{z_1\mathcal{N}}{s_{12}s_{13}(1-z_2)(1-z_3)}\frac{z_3 s_{13}}{\mathbb{S}} + \frac{z_1\mathcal{N}}{s_{12}s_{13}(1-z_2)(1-z_3)}\frac{z_2 s_{12}}{\mathbb{S}} \\ &= \frac{z_1 z_3\mathcal{N}}{s_{12}(1-z_2)(1-z_3)\mathbb{S}} + \frac{z_1 z_2\mathcal{N}}{s_{13}(1-z_2)(1-z_3)\mathbb{S}}.\end{aligned} \tag{6.2.58}$$

Now that we have disentangled the two invariant masses, we can introduce for each term their own parametrisation. For the first term, we use the same parametrisation as before because the invariant mass is still s_{12}. In the second term, we now exchange particles 2 and 3 in the parametrisation. So the light-cone parametrisation becomes

$$q_T = \sqrt{(k_- + p_-)\left(\frac{k_T^2}{k_-} + \frac{p_T^2}{p_-}\right)}, \qquad z_{13} = \frac{k_- + p_-}{Q}, \tag{6.2.59}$$

$$a_{13} = \frac{k_- p_T}{k_T p_-}, \qquad b_{13} = \frac{k_T}{p_T}. \tag{6.2.60}$$

and the angles are now t_{kp}, t_p and $t_k(t_{kp}, t_p, t_5')$.

The procedure of finding the proper physical parametrisation of the jet function contributions is as follows. We first identify the invariant mass in the structure and then choose the proper parametrisation accordingly such that the collinear divergence is simple. Note that from now on, we will drop the indices that determine which particles are used in the definition and only use the variables $\{q_T, z, a, b, t, t_l, t_5'\}$ as placeholders. The relabeling can also be thought of as changing the momentum definition of the splitting function such that only s_{12} appears as a collinear divergence.[6]

[5] We will see in the next section that we can allow new divergences, but only if they lie on the endpoints of the integration domain.

[6] In case no invariant mass appears in the structure we will use the parametrisation defined in

One benefit of structure σ_E is that the numerator $\mathcal{N}$ turns out to be symmetric under $2 \leftrightarrow 3$ exchange. Therefore, we can combine the two structures in eq. (6.2.58), simply by exchanging the 2 and 3 labels in the second term. Note that we must include the symmetry factor for two identical particles. So we arrive at the following matrix element for this structure

$$\sigma_E = \frac{z_1 z_3 \tilde{\mathcal{N}}}{s_{12}(1-z_2)(1-z_3)\mathbb{S}}, \tag{6.2.61}$$

where $\tilde{\mathcal{N}}$ is again symmetric under the $2 \leftrightarrow 3$ exchange.

We can now apply the same steps as in the $C_F T_F n_f$ structure to get to the final master formula for σ_3. The only difference is that this structure is symmetric under $2 \leftrightarrow 3$ interchange. However, to calculate only two sectors, it should have been symmetric under $1 \leftrightarrow 2$ exchange. Therefore we have to calculate all four regions. Explicitly, we find the following master formula in region A for this structure

$$\begin{aligned} J^{\mathrm{ID}}_{q,E,A} = &- \frac{2^{2-6\epsilon}\Gamma\left(\frac{-4\epsilon}{1+n}\right) e^{2\epsilon\gamma_E \frac{n-1}{n+1}}}{(1+n)\pi^2\Gamma(-2\epsilon)} \int_0^1 \mathrm{d}a\mathrm{d}b\mathrm{d}z\mathrm{d}t\mathrm{d}t_l\mathrm{d}t_5' \, (t\bar{t})^{-\frac{1}{2}-\epsilon}(t_l\bar{t}_l)^{-\frac{1}{2}-\epsilon}(t_5'(2-t_5'))^{-1-\epsilon} \\ &\frac{a^{2-2\epsilon-\alpha}b^{-2\epsilon-\alpha}z^{-2\alpha}(a+b)^{2\epsilon}(1+ab)^{-1+2\epsilon+2\alpha}(1+ab-z)^{-1}\Omega^{\frac{4\epsilon}{1+n}}F^{\frac{4\epsilon}{1+n}}}{((1-a)^2+4at)((1+ab)^2-2(1+ab)(1-a(1-2t))z+2((1-a^2)+4at)z^2)} \\ &\big[1+ab(2+ab(1+z^2)) - \epsilon\{1-\bar{z}z+ab(2+z^2)+a^2b^2(1+z(1+z))\} \\ &\qquad - \epsilon^2\{(1+ab)(1+ab-z)z\}\big], \end{aligned} \tag{6.2.62}$$

from this expression, we can see that the only divergence is the collinear divergence. We use the previously introduced non-linear transformation, such that the only divergence then lies at $u \to 0$. Therefore, $\Omega = 1$ such that, no term has to be factored out of F. So this structure only contributes to ϵ^{-2} for both $\mathrm{SCET_I}$ and $\mathrm{SCET_{II}}$ observables.

The other three regions have the same divergence structure. We do not list them here but in the appendix C together with all the other master formulae in the physical parametrisation.

6.2.5 NNLO quark jet function: $\mathbf{C_F^2}$

The next colour structure which introduces new challenges is the C_F^2 structure of the $P^{(0)}_{q\to ggq}$ splitting function. Similar to the previous examples, we split this structure into

eq. (6.2.29).

different divergence structures depending on the denominator:

$$\sigma^{c,q}_{3,C_F^2} = \frac{1}{z_1 z_2 s_{13} s_{23}}\sigma_F + \frac{1}{z_1 z_2 s_{13} s_{123}}\sigma_G + \frac{1}{s_{123} s_{13}}\sigma_H, \tag{6.2.63}$$

while the third structure σ_H is now similar to the cases we have already encountered, the other two structures are new. We explain in detail the steps to arrive at the master formulae for the structure σ_F and outline the steps for σ_G.

To start the computation, we relabel 2 and 3 and then use a selector function of the form

$$\mathbb{S} = z_1 s_{12} + z_3 s_{23}. \tag{6.2.64}$$

Since σ_F is now symmetric under 1 and 3 interchange, we can add the two terms such that we arrive at

$$\frac{1}{z_1 z_3 s_{12} s_{23}}\sigma_F \frac{\mathbb{S}}{\mathbb{S}} \Longrightarrow \frac{\mathcal{N}}{s_{12} z_1 (z_1 s_{12} + z_3 s_{23})}, \tag{6.2.65}$$

where $\mathcal{N}$ is again the numerator of the expression. We now have one invariant mass, and can choose the proper physical parametrisation in this case accordingly.

Hence we arrive at the master formula for this structure in region A:

$$\begin{aligned} J^{\mathrm{FF}}_{q,F,A} =& \frac{8^{1-2\epsilon}\Gamma\left(\frac{-4\epsilon}{1+n}\right) e^{2\epsilon\gamma_E \frac{n-1}{n+1}}}{(1+n)\pi^2\Gamma(-2\epsilon)} \int_0^1 \mathrm{d}a\mathrm{d}b\mathrm{d}z\mathrm{d}t\mathrm{d}t_l\mathrm{d}t_5' \, (t\bar{t})^{-\frac{1}{2}-\epsilon}(t_l\bar{t}_l)^{-\frac{1}{2}-\epsilon}(t_5'(2-t_5'))^{-1-\epsilon} \\ & \frac{a^{-1-2\epsilon-\alpha} b^{-1-2\epsilon-\alpha} z^{-\alpha}\bar{z}^{-1-\alpha}(a+b)^{2\epsilon}(1+ab)^{-1+2\epsilon+2\alpha}\Omega^{\frac{4\epsilon}{1+n}} F^{\frac{4\epsilon}{1+n}}\widetilde{\mathcal{N}}(a,b,z,\epsilon)}{((1-a)^2+4at)((1+ab)^2+2b(1+ab)(1-a-2t)z+2((1-a^2)+4at)z^2b^2)}, \end{aligned} \tag{6.2.66}$$

where $\widetilde{\mathcal{N}}(a,b,z,\epsilon)$ is the numerator and has no influence on the divergence structure of this expression. We can see in eq. (6.2.66) that we obtain divergences in monomial form in the limits $a \to 0$, $b \to 0$, and $z \to 1$. On top of that we also see the collinear divergence for $a \to 1$ and $t \to 0$. So as a first step, we have to disentangle the divergences in a, such that we obtain expressions with one divergence per variable. The simplest solution for this problem is to multiply the expression by $1 = a + (1-a)$, where the first(second) term is free of divergences for $a \to 0 (a \to 1)$.

In the first term, we thus find the divergences at $b \to 0$, $z \to 1$, and the collinear divergence. So we can again apply our method for disentangling the overlapping singularity and write the divergence structure in terms of monomials in $b, \bar{z}$ and u. We will determine the correct form of Ω after looking at the second term.

The second term seems more straightforward than the first one because all diver-

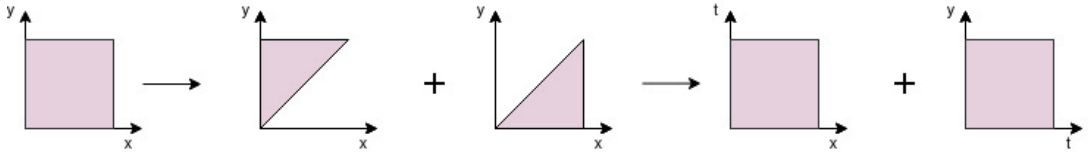

Figure 6.2.7: Sector decomposition represented schematically. The integration domain of each variable is $[0, 1]$.

gences are already in the monomial form. However, a problem arises due to the factors

$$a^{-1-2\epsilon} b^{-1-2\epsilon} (a+b)^{2\epsilon}, \tag{6.2.67}$$

where we dropped the additional regulators as the problem already appears in the $\mathrm{SCET_I}$ case. Even though it seems that this structure has no overlapping singularity, it poses a problem because if we expand in the regulator ϵ, we see that we get terms of the form

$$\frac{1}{2\epsilon} \ln(a+b)\, \delta(a)\delta(b) + \mathcal{O}(\epsilon^0). \tag{6.2.68}$$

If we now evaluated the integral, we would encounter $\ln 0$-terms that are not well defined. Thus, we need to separate the limit of a and b going to 0 simultaneously. In order to separate this limit, we use sector decomposition [128–130].[7]

Let us introduce the basic concept of sector decomposition via a simple two-dimensional example. Consider the integral

$$I = \int_0^1 \mathrm{d}x\mathrm{d}y\, x^{-1-\epsilon} y^{-\epsilon} \left(x + (1-x)y\right)^{-1}, \tag{6.2.69}$$

where we have a divergence at $x \to 0$ and on top an overlapping singularity at $x \to 0$ and $y \to 0$. The goal of sector decomposition is to factorise the divergences. To accomplish that, we separate the integration domain into two sectors where x and y are ordered, according to figure 6.2.7, leading to

$$I = \int_0^1 \mathrm{d}x\mathrm{d}y\, x^{-1-\epsilon} y^{-\epsilon} \left(x + (1-x)y\right)^{-1} [\underbrace{\theta(x-y)}_{\text{sector 1}} + \underbrace{\theta(y-x)}_{\text{sector 2}}]. \tag{6.2.70}$$

In sector 1 we substitute $y = xt$ and in sector 2 we substitute $x = yt$. Therefore, we

[7] We could have also used additional non-linear transformations. Their downside is that they increase the numerical complexity of the integrand.

find

$$\begin{aligned} I &= \int_0^1 \mathrm{d}x\mathrm{d}y\, x^{-1-\epsilon} y^{-\epsilon} \left(x + (1-x)y\right)^{-1} [\underbrace{\theta(x-y)}_{\text{sector 1}} + \underbrace{\theta(y-x)}_{\text{sector 2}}] \\ &= \int_0^1 \mathrm{d}x \int_0^x \mathrm{d}y\, x^{-1-\epsilon} y^{-\epsilon} \left(x + (1-x)y\right)^{-1} \\ &+ \int_0^1 \mathrm{d}y \int_0^y \mathrm{d}x\, x^{-1-\epsilon} y^{-\epsilon} \left(x + (1-x)y\right)^{-1} \\ &= \int_0^1 \mathrm{d}x\mathrm{d}t\, x^{-1-2\epsilon} t^{-\epsilon} \left(1 + (1-x)t\right)^{-1} \\ &+ \int_0^1 \mathrm{d}y\mathrm{d}t\, t^{-1-\epsilon} y^{-1-2\epsilon} \left(1 + (1-y)t\right)^{-1}. \end{aligned} \tag{6.2.71}$$

Note that the final expression has no overlapping singularity anymore. Thus, we can evaluate the integrals in the usual way. More steps of sector decompositions are needed to disentangle the singularities for more complex overlapping singularities.

By performing a sector decomposition between the variables a and b in our expression, we find that

$$\begin{aligned} \int_0^1 \mathrm{d}a\mathrm{d}b\, a^{-1-2\epsilon} b^{-1-2\epsilon} (a+b)^{2\epsilon} \to \int_0^1 \mathrm{d}h\mathrm{d}b\, h^{-1-2\epsilon} b^{-1-2\epsilon} (1+h)^{2\epsilon} \\ + \int_0^1 \mathrm{d}a\mathrm{d}h\, a^{-1-2\epsilon} h^{-1-2\epsilon} (1+h)^{2\epsilon}, \end{aligned} \tag{6.2.72}$$

where in the first term, we used $a = bh$ and in the second term, $b = ah$. Thus we cured the expression of the $\ln 0$-terms in the integrals.

In some cases where we perform sector decomposition and substitute $a = bh$, there is still an overlapping singularity present at the point $h \to 0$ and $z \to 1$. Thus, we have to perform another sector decomposition step in order to disentangle the overlapping singularity.

Finally, we arrive at four master formulae for the region A contribution to σ_F, which

are given with respect to their divergence structure by

$$\begin{aligned}
J^{\mathrm{FF}}_{q,F,A} =& \frac{8^{1-2\epsilon}\Gamma\left(\frac{-4\epsilon}{1+n}\right)e^{2\epsilon\gamma_E\frac{n-1}{n+1}}}{(1+n)\pi^2\Gamma(-2\epsilon)}\int_0^1 \mathrm{d}\Pi\,(S_1+S_2+S_3+S_4)\\
S_1 =& u^{-1-2\epsilon}b^{-1-2\epsilon}(1-z)^{-1-\alpha}\Omega_1^{\frac{4\epsilon}{1+n}}F_1^{\frac{4\epsilon}{1+n}}\mathcal{N}_1, \qquad (6.2.73)\\
S_2 =& a^{-1-2\epsilon-2\alpha}h^{-1-2\epsilon-\alpha}(1-z)^{-1-\alpha}\Omega_2^{\frac{4\epsilon}{1+n}}F_2^{\frac{4\epsilon}{1+n}}\mathcal{N}_2, \qquad (6.2.74)\\
S_3 =& h^{-1-2\epsilon-2\alpha}b^{-1-2\epsilon-2\alpha}g^{-1-\alpha}\Omega_3^{\frac{4\epsilon}{1+n}}F_3^{\frac{4\epsilon}{1+n}}\mathcal{N}_3, \qquad (6.2.75)\\
S_4 =& g^{-1-2\epsilon-\alpha}b^{-1-2\epsilon-2\alpha}(1-z)^{-1-2\epsilon-2\alpha}\Omega_4^{\frac{4\epsilon}{1+n}}F_4^{\frac{4\epsilon}{1+n}}\mathcal{N}_4, \qquad (6.2.76)
\end{aligned}$$

where the functions $\mathcal{N}_i$ contain no additional divergences.

Before we determine the factors Ω_i, let us recap what we have done to get to these divergence structures.[8] In order to get to S_1 we multiplied our original expression by the factor a and then used the non-linear transformation in eq. (6.2.47) to disentangle the overlapping singularity. For the structures S_2 , S_3 and S_4 we multiplied our original expression by $(1-a)$. Afterwards we performed a sector decomposition between a and b where S_2 is obtained from the sector $b = ah$, and S_3 and S_4 from the sector $a = bh$. Finally in the sector where we used $a = bh$, we perform an additional sector decomposition step between h and $1-z$, where S_3 is obtained from the sector $z = 1-hg$ and S_4 from $h = (1-z)g$.

As a final step to complete the master formulae, we require the correct factors Ω_i. Thus we again look at our toy example in eq. (6.2.50). For structure S_1, the factor is simply $\Omega_1 = \bar{z}^{-n}$ because $\bar{z}$ is the only singularity in this contribution that IRC does not protect.

In the case of S_2, we must first identify how the measurement function behaves after the sector decomposition step. We have

$$\left[\frac{G_1(a,b,n)}{z^n}+\frac{G_2(a,b,t,n)}{\bar{z}^n}\right]\underbrace{=}_{b=ah}(1+a^{1-n}h)\tilde{G}_1+(1-z)^{-n}\tilde{G}_2. \qquad (6.2.77)$$

Note that we have dropped the dependence on q_T and Q because they are not relevant for this discussion and $\tilde{G}_{1,2}$ are finite in the singular limits. First, we have to factor out $(1-z)^{-n}$; otherwise, the measurement function would tend to infinity in the divergent

[8] All of these sector decomposition steps and insertions are listed completely in appendix D for all structures of the jet function.

$z \to 1$ limit. After factoring out this term, the measurement function becomes

$$(1 + a^{1-n}h)(1-z)^n \tilde{G}_1 + \tilde{G}_2. \tag{6.2.78}$$

If $n \leq 1$ then we see that the measurement function is finite in the singular limits of the matrix element, however if $n > 1$ then in the limit $a \to 0$ the measurement function tends to infinity. Therefore, we also have to factor out a^{1-n}. After factoring out this term, the measurement function is

$$(a^{n-1} + h)(1-z)^n \tilde{G}_1 + a^{n-1}\tilde{G}_2 = a^{n-1}(\underbrace{\tilde{G}_2 + (1-z)^n \tilde{G}_1}_{\tilde{G}_3}) + h(1-z)^n \tilde{G}_1, \tag{6.2.79}$$

where the new function $\tilde{G}_3$ is again finite in the critical limits. We notice that this measurement function becomes zero in the limits $a \to 0 + h \to 0$ and $a \to 0 + z \to 1$. Therefore, we have to perform another sector decomposition on top between a and h, followed by a sector decomposition between a and $\bar{z}$ to ensure that the measurement stays non-zero. The problem, however, is that all contributions scale differently, but a one-step sector decomposition requires that the two terms in which the decomposition is performed scale homogeneously.

In order to cure this, we scale up all variables such that their exponents are identical. In our example, this requires the rescaling:

$$h \to h^{n(n-1)},\ a \to a^n,\ \bar{z} \to \bar{z}^{n-1}. \tag{6.2.80}$$

On the level of the matrix element, the rescaling and additional sector decomposition only effects the ϵ and α exponents of the monomials but leaves the power of the singularity unchanged.

Rescaling and the subsequent sector decompositions lead to different measurement functions

$$\text{Sector 1} \xrightarrow{h=ag} \left\{\Omega_{\text{Sector 1}} = \bar{z}^{-n(n-1)},\ F_{\text{Sector 1}} = \tilde{G}_3 + g^{n(n-1)}\bar{z}^{n(n-1)}\tilde{G}_1\right\}, \tag{6.2.81}$$

$$\text{Sector 2} \xrightarrow{a=hg,\bar{z}=gf} \left\{\Omega_{\text{Sector 2}} = g^{n(1-n)}f^{-n(n-1)},\ F_{\text{Sector 2}} = \tilde{G}_3 + f^{n(n-1)}\tilde{G}_1\right\}, \tag{6.2.82}$$

$$\text{Sector 3} \xrightarrow{a=hg,g=\bar{z}f} \left\{\Omega_{\text{Sector 3}} = f^{n(1-n)}\bar{z}^{-n(n-1)},\ F_{\text{Sector 3}} = f^{n(n-1)}\tilde{G}_3 + \tilde{G}_1\right\}, \tag{6.2.83}$$

where $F_{\text{Sector 1,2,3}}$ are finite in the singular limits of the matrix element.

In the case of S_3, we find a similar picture for Ω_3, namely that in the case of $n \leq 1$,

it is simply given by

$$\Omega_3 = h^{\frac{1-n}{2}} g^{-n}. \tag{6.2.84}$$

However in the case $n > 1$ we have to upscale the variables b and g and afterwards perform a sector decomposition between those, similar to S_2.

Finally let us turn to S_4 where we find that Ω_4 is

$$\Omega_4^{n\geq 1} = \bar{z}^{\frac{1-n}{2}} g^{\frac{1-n}{2}} b^{n-1}, \tag{6.2.85}$$

but only if $n \geq 1$. In the case of $n = 0$ this expression simplifies to

$$\Omega_4^{n=0} = \bar{z}^{\frac{1-n}{2}} g^{\frac{1-n}{2}}. \tag{6.2.86}$$

In the case of $0 < n < 1$, we again have to perform a rescaling and an additional sector decomposition. The exact form of Ω and what kind of rescaling and sector decomposition must be performed to arrive at the final master formulae can be found in appendix D.

Let us look at the divergence structure of the different contributions again. We now include the correct Ω for the two examples $n = 1$ and $n = 0$, such that we can see the leading pole structure for SCET_I and SCET_II observables. In the case of the SCET_I with $n = 1$, we find

$$\text{Div}_1 = u^{-1-2\epsilon} b^{-1-2\epsilon} (1-z)^{-1-2\epsilon} \sim \epsilon^{-3}, \tag{6.2.87}$$
$$\text{Div}_2 = a^{-1-2\epsilon} h^{-1-2\epsilon} (1-z)^{-1-2\epsilon} \sim \epsilon^{-3}, \tag{6.2.88}$$
$$\text{Div}_3 = h^{-1-2\epsilon} b^{-1-2\epsilon} g^{-1-2\epsilon} \sim \epsilon^{-3}, \tag{6.2.89}$$
$$\text{Div}_4 = g^{-1-2\epsilon} b^{-1-2\epsilon} (1-z)^{-1-2\epsilon} \sim \epsilon^{-3}, \tag{6.2.90}$$

and in the case of $n = 0$ we find

$$\text{Div}_1 = u^{-1-2\epsilon} b^{-1-2\epsilon} (1-z)^{-1-\alpha} \sim \epsilon^{-2} \alpha^{-1}, \tag{6.2.91}$$
$$\text{Div}_2 = a^{-1-2\epsilon-2\alpha} h^{-1-2\epsilon-\alpha} (1-z)^{-1-\alpha} \sim \epsilon^{-2} \alpha^{-1}, \tag{6.2.92}$$
$$\text{Div}_3 = h^{-1-\alpha} b^{-1-2\epsilon-2\alpha} g^{-1-2\alpha} \sim \epsilon^{-1} \alpha^{-2}, \tag{6.2.93}$$
$$\text{Div}_4 = g^{-1-\alpha} b^{-1-2\epsilon-2\alpha} (1-z)^{-1-\alpha} \sim \epsilon^{-1} \alpha^{-2}. \tag{6.2.94}$$

Notice that all these divergences have to be multiplied by ϵ^{-1} for the correct leading contribution because of the Γ function in the prefactor. Here we want to point to one

interesting observation, namely the two α-divergences in S_3 and S_4. Let us take S_3 as an example. We can see by comparing the divergence structure of the $\mathrm{SCET_I}$ and $\mathrm{SCET_{II}}$ that the divergence in g is not regularised in the case $n = 0$. Therefore this is our typical α-pole, like in the $C_F T_F n_f$-structure. The other α-pole comes from the monomial in h. The monomial in h is

$$h^{-1-2\epsilon-2\alpha}\Omega_3^{\frac{4}{1+n}} = h^{-1-2\epsilon-2\alpha}h^{2\frac{1-n}{1+n}\epsilon} = h^{-1-\frac{4n}{1+n}\epsilon-\alpha}, \tag{6.2.95}$$

and therefore we recover the standard form of the α-divergence via a subtle cancellation between the phase-space factor and measurement function. In order to understand why this cancellation occurs, we look at how the α^{-2}-poles arise in the soft function.

In order to keep the discussion as short as possible, we only consider observables that follow non-Abelian exponentiation (NAE) [131, 132]. In this case, the α poles are simply given by

$$\mathrm{Div}_{\text{soft function}} \sim \Gamma(-4\epsilon - 2\alpha) y_k^{-1+\alpha/2} y_l^{-1+\alpha/2} b^{-1-2\epsilon-\alpha}, \tag{6.2.96}$$

where the variable b implies that one parton becomes soft with respect to the other, the Γ-function corresponds to the situation in which both emitted partons become soft. The variables y_k and y_l reflect that one parton becomes collinear to the n^μ direction at fixed transverse momenta. In our language, this means that the particles with energy fraction z_1 and z_3 have to vanish with fixed transverse momentum. In this sector, they are given by

$$z_1 \underbrace{\to}_{S_3} = \frac{hb^2(1-gh)Q}{1+b^2h},$$
$$z_3 \underbrace{\to}_{S_3} = ghQ.$$

So $g \to 0$ corresponds to the limit where particle z_3 is collinear to n^μ while $h \to 0$ corresponds to both particles z_1 and z_3 collinear to n^μ.[9] Thus the α-poles correspond to the same physical scenario in both jet and soft functions. This explains the subtle cancellation seen in the divergence structure.

This finishes the discussion on the calculation of σ_F in region A. Regions B, C, and D are very similar to region A. Therefore, we will refer all the required sector decomposition steps and the exact form of the Ω_i factors to appendix D.

[9] The limit where only particle z_1 is collinear to n^μ is part of the structure S_4.

The second structure of the C_F^2 contribution is

$$\frac{1}{z_1 z_2 s_{13} s_{123}} \sigma_G, \tag{6.2.97}$$

where we have just one invariant mass, so we could directly use our parametrisation for this case and arrive at a master formula. The problem would be that because of the piece $z_1 z_2 s_{123}$ we would encounter in the appropriate parametrisation a structure like

$$\sim (1-z)^{-1} a^{-1} ((1+ab)(a+b)(1-z) + az((1-b)^2 + 4b(1-t)))^{-1}. \tag{6.2.98}$$

This has now overlapping singularities at $a, \bar{z} \to 0$ and in addition an overlapping singularity between $\bar{b}, \bar{z}, \bar{t} \to 0$. This singularity is the reason why we do not want to use the direct way because this singularity is present in all of the four regions, and it requires a minimum of two-sector decomposition steps with an additional rescaling on top.[10]

Before we show how we computed this structure, let us first explain why this structure leads to additional complications. We first note that

$$s_{123} = s_{12} + s_{13} + s_{23}. \tag{6.2.99}$$

and there is an additional factor s_{13} in the denominator. Thus, we can properly describe with our parametrisation the soft limits of z_1 and z_3 as well as the collinear limit between particles 1 and 3. The problem in this structure now arises that we somehow need to describe the soft limit of z_2. Further, we need the double soft limit for z_1 and z_2 visible in eq. (6.2.99). In our parametrisation, these two limits cannot be described easily in one variable. Similar to the fact that we can only properly define the collinear limit between the referenced particles, we can only properly describe the single soft or double soft limit of referenced particles.[11]

We compute this structure by using again a selector function of the form

$$\mathbb{S} = z_2 s_{12} + z_3 s_{13}. \tag{6.2.100}$$

[10] In the gluon jet function, we find a similar structure, however, with fewer divergences. In that case we use an additional non-linear transformation, see section 6.2.6.

[11] This is also the reason why we still had overlapping singularities in the previous structure σ_1.

This leads to the following terms

$$\frac{1}{z_1 z_2 s_{13} s_{123}} \sigma_G \frac{\mathbb{S}}{\mathbb{S}} = \Bigg(\underbrace{\frac{z_3}{z_1 z_2 s_{123}(z_2 s_{12} + z_3 s_{13})}}_{S_{F_1}} + \underbrace{\frac{s_{12}}{z_1 s_{13} s_{123}(z_2 s_{12} + z_3 s_{13})}}_{S_{F_2}} \Bigg) \sigma_G. \quad (6.2.101)$$

In the second term we have to use the parametrisation that properly describes the collinear limit between particles 1 and 3. Therefore, we still have overlapping singularities. However, the overlapping limit $\bar{b}, \bar{z}, \bar{t} \to 0$ is now suppressed because of the numerator. In the first term we are free to use any parametrisation because we only need to correctly describe the proper soft limits. Thus we choose the parametrisation to describe the collinear limit between particles 1 and 2.

We want to point out one last observation, which is that even though we can now better describe the occurring limits in the collinear matrix elements, there are still overlapping singularities present in the structure because of general overlapping features in our parametrisation between specific collinear limits and soft limits.[12] These overlapping singularities can be handled in the same fashion as before; therefore, we refer to appendices C and D for further information on this structure.

6.2.6 NNLO gluon jet function: $\mathbf{C_A T_F n_f}$

The final new element in the calculation of the jet functions arises in the colour structure $C_A T_F n_f$ which is part of the gluon jet function. Here we focus on the structure which is proportional to

$$\frac{1}{s_{123} s_{23} z_1 \bar{z}_1}. \quad (6.2.102)$$

If we use the appropriate parametrisation we find the following master formula for it in region A

$$\begin{aligned} J_{g,A}^{\mathrm{Af}} =& \frac{2^{4-6\epsilon}\Gamma\left(\frac{-4\epsilon}{1+n}\right) e^{2\epsilon\gamma_E \frac{n-1}{n+1}}}{(1+n)\pi^2\Gamma(-2\epsilon)} \int_0^1 \mathrm{d}a\mathrm{d}b\mathrm{d}z\mathrm{d}t\mathrm{d}t_l\mathrm{d}t_5' \, (t\bar{t})^{-\frac{1}{2}-\epsilon} (t_l\bar{t}_l)^{-\frac{1}{2}-\epsilon} (t_5'(2-t_5'))^{-1-\epsilon} \\ & \frac{a^{1-2\epsilon-\alpha} b^{-2\epsilon-\alpha} z^{-1-2\alpha} \bar{z}^{-1-\alpha} (a+b)^{2\epsilon} (1+ab)^{-2+2\epsilon+2\alpha} \Omega^{\frac{4\epsilon}{1+n}} F^{\frac{4\epsilon}{1+n}} \widetilde{\mathcal{N}}(a,b,z,\epsilon)}{((1-a)^2+4at)((1+ab)(a+b)(1-z)+az((1-b)^2+4b(1-t)))}, \end{aligned} \quad (6.2.103)$$

where $\widetilde{\mathcal{N}}(a,b,z,\epsilon)$ is the numerator which does not effect the divergence structure.

The divergences of this structure are $(z \to \{0,1\})$, $(\bar{a}, t \to 0)$, and $\left(\bar{b}, \bar{z}, \bar{t} \to 0\right)$.

[12] i.e. $a \to 0$ and $b \to 0$ or $a \to 0$ and $z \to 1$.

Thus as a first step, we introduce $1 = z + \bar{z}$ to disentangle the two divergences of z at different endpoints. The second divergence is the standard collinear divergence $(\bar{a}, t \to 0)$, while the third is the complicated overlapping singularity mentioned in the last section. Here we will use a new non-linear transformation to handle the overlapping singularity rather than introducing a selector function. The reason is that the selector function would increase the number of regions we have to calculate by a factor of four. Additionally, this sector has overall only three divergences. Therefore, it is numerically not that costly to use a non-linear transformation compared to the sectors with four divergences.

Note that the standard collinear divergence and this new divergence exclude each other because of the different endpoint values of t. Therefore we can extend the already included identity by an additional identity of the form $1 = t + \bar{t}$. Thus overall, we have to multiply the contribution by

$$1 = zt + z\bar{t} + \bar{z}, \tag{6.2.104}$$

where the first term only allows the divergences $z \to 1$ and $\bar{z}, \bar{b}, \bar{t} \to 0$, the second term $z \to 1$ and $\bar{a}, t \to 0$ and finally the third term $z \to 0$ and $\bar{a}, t \to 0$. The second and third term can be calculated with the steps outlined in the previous section. Therefore we will only go into detail for the first term.

The non-linear transformation we use to disentangle the overlapping singularity is

$$\begin{aligned} z &= 1 - \tilde{u}^2\tilde{v}, \\ b &= \frac{1 - \tilde{u}(\tilde{u}\tilde{v} + (1-\tilde{v})(1-p))}{1 - \tilde{u}^2\tilde{v}}, \\ t &= \frac{(1-\tilde{u})(1+\tilde{u}\tilde{v})(1-\tilde{u}(\tilde{u}\tilde{v} - p(1-\tilde{v})))}{(1-\tilde{u}^2\tilde{v})(1-\tilde{u}(\tilde{u}\tilde{v} + (1-\tilde{v})(1-p)))}, \end{aligned} \tag{6.2.105}$$

where $\tilde{u} \to 0$ is the overlapping singularity and $\tilde{v} \to 0$ encondes the limit $z \to 1$ for fixed $\tilde{u}$.

In order to see how this non-linear transformation behaves, we consider a toy ex-

ample

$$\begin{aligned}
&\int_0^1 \mathrm{d}a\mathrm{d}b\mathrm{d}z\mathrm{d}t\, \frac{(1-z)^{-1-\epsilon}(1-t)^{-1/2-\epsilon}}{((1+ab)(a+b)(1-z)+az((1-b)^2+4b(1-t)))} \\
\to &\int_0^1 \mathrm{d}a\mathrm{d}\tilde{u}\mathrm{d}\tilde{v}\mathrm{d}p\, \underbrace{\frac{(1+p)\tilde{u}^4(1-\tilde{v})^2(1+\tilde{v})}{(1-\tilde{u}^2\tilde{v})^2(1-\tilde{u}(1-p-\tilde{v}+\tilde{v}(p+\tilde{u})))}}_{\text{Jacobian}} \\
&\frac{\tilde{u}^{-5-4\epsilon}(1-\tilde{v})^{-1-2\epsilon}\tilde{v}^{-1-\epsilon}(1-\tilde{u}^2\tilde{v})^{3/2-\epsilon}p^{-1/2-\epsilon}(1-\tilde{u}(\tilde{u}\tilde{v}+(1-\tilde{v})(1-p)))^{-1/2-\epsilon}}{\mathrm{Den}(a,\tilde{u},\tilde{v},p)}, \\
&= \int_0^1 \mathrm{d}a\mathrm{d}\tilde{u}\mathrm{d}\tilde{v}\mathrm{d}p\, \tilde{u}^{-1-4\epsilon}\tilde{v}^{-1-\epsilon}R(a,\tilde{u},\tilde{v},p), \qquad (6.2.106)
\end{aligned}$$

where $\mathrm{Den}(a,\tilde{u},\tilde{v},p)[R(a,\tilde{u},\tilde{v},p)]$ is a function without zeros[divergences]. As a last step we have to extract the correct factor from the measurement function. By substituting the non-linear transformation into our toy measurement, we find that for the case where $n \geq 1$ the factor we have to pull out of the measurement function is $\Omega = \tilde{u}^{1-n}\tilde{v}^{-n}$ and in the case of $n = 0$ the factor is $\Omega = 1$. In the case of $0 < n < 1$ we have to use rescaling and a sector decomposition step in order to keep the measurement function finite and non-zero.

As a last observation of this structure, notice that this divergence sits at the point $\bar{b}, \bar{z}, \bar{t} \to 0$. Therefore, it is present in both regions of this structure. However, neither the non-linear transformation nor the Ω factor change from region A to region B.

6.2.7 NNLO: Recap

In the previous section, we have shown in detail all the steps that are required to factorise all phase-space divergences in the jet function calculation. In this section, we recap these steps and combine them into a short list for the reader's convenience.

- The first step is to determine the structure for which we want to build the master formulae. The structures used in this work are all shown in appendix B.

- Next, choose the suitable parametrisation, determined by the invariant masses present in the contribution. If two different invariant masses or undesired soft limits are present in the structure, then use a selector function of the form $\mathbb{S} = z_i s_{ij} + z_l s_{ik}$. This selector function should, first of all, cancel or suppress the undesired structures and should not create new complicated divergences.

- Transform the collinear matrix element with the proper parametrisation and

perform the additional angular integrals and integration over the dimensionful variable q_T. Afterwards remap the integration region onto the unit hypercube. Check if the integral has some kind of particle exchange symmetry such that the number of regions can be reduced. In our decomposition, these structures are shown in appendix C.

- Check that every divergence is in monomial form. If there are still overlapping singularities present in the expressions, choose either sector decomposition steps or non-linear transformations to disentangle them. In the present work we only used non-linear transformation for the collinear divergences [eq. (6.2.47)] and triple-overlapping divergence [eq. (6.2.105)]. For all other overlapping singularities, we used sector decomposition steps.

- Finally, determine the Ω factors in each structure through some sample measurement function. In this work, we have assumed a measurement function of the form in eq. (6.2.50). Notice that we sometimes had to distinguish between different n-values: $n > 1$, $n < 1$ and $n = \{0, 1\}$. In case that nothing can be factored out to make the measurement function finite in the critical limits, we perform rescaling of the variables and afterwards sector decomposition steps until the measurement function stays finite. The last two steps for our master formulae are shown schematically in appendix D.

6.3 Renormalisation

In this section we show how to extract the resummation ingredients from the bare jet function for both SCET_I and SCET_II observables. It is easier and more straightforward to consider the renormalisation procedure of SCET_I observables before the SCET_II case.

6.3.1 $\mathbf{SCET_I}$ observables

In this section, we label the bare quantities with the subscript 'bare'. Upon expansion in the dimensional regulator, we assume that the bare jet function takes the form

$$J_{\text{bare}}(\tau,Q) = 1 + \left(\frac{\alpha_{s,\text{bare}}}{4\pi}\right)\left(\frac{\mu\bar{\tau}^{\frac{1}{1+n}}}{Q^{\frac{n}{1+n}}}\right)^{2\epsilon}\left[\frac{x_2}{\epsilon^2}+\frac{x_1}{\epsilon}+x_0+x_{-1}\epsilon+x_{-2}\epsilon^2+\mathcal{O}(\epsilon^3)\right] + \left(\frac{\alpha_{s,\text{bare}}}{4\pi}\right)^2\left(\frac{\mu\bar{\tau}^{\frac{1}{1+n}}}{Q^{\frac{n}{1+n}}}\right)^{4\epsilon}\left[\frac{y_4}{\epsilon^4}+\frac{y_4}{\epsilon^3}+\frac{y_2}{\epsilon^2}+\frac{y_1}{\epsilon}+y_0+\mathcal{O}(\epsilon)\right]+\mathcal{O}(\alpha_{s,\text{bare}}^3), \tag{6.3.1}$$

where the x_i and y_i are NLO and NNLO coefficients of the ϵ^{-i} term, respectivly.

In order to renormalise α_s, we use

$$Z_{\alpha_s}\alpha_s\mu^{2\epsilon} = e^{-\gamma_E}(4\pi)^\epsilon\alpha_{s,\text{bare}}, \qquad \text{with} \qquad Z_{\alpha_s} = 1-\frac{\alpha_s}{4\pi}\frac{\beta_0}{\epsilon}+\mathcal{O}(\alpha_s^2), \tag{6.3.2}$$

and introduce a Z_J-factor to absorb all remaining ϵ-poles in the bare jet function, we find for the renormalised jet function:

$$\begin{aligned} J(\tau,\mu,Q) &= Z_J J_{\text{bare}}(\tau,Q) \\ &= 1+\left(\frac{\alpha_s}{4\pi}\right)\left[2x_2L^2+2x_1L+x_0\right]+\left(\frac{\alpha_s}{4\pi}\right)^2\left[\frac{32}{3}y_4L^4+\frac{32y_3-4x_2\beta_0}{3}L^3\right. \\ &\quad +\left(8(y_2-x_0x_2)-2\beta_0x_1\right)L^2+\left(4(y_1-x_0x_1-x_2x_{-1})-2\beta_0x_0\right)L \\ &\quad \left.+y_0-x_2x_{-2}-x_{-1}(x_1+\beta_0)\right]+\mathcal{O}(\alpha_s^3), \end{aligned} \tag{6.3.3}$$

where $L=\ln\left(\frac{\mu\bar{\tau}^{\frac{1}{1+n}}}{Q^{\frac{n}{1+n}}}\right)$. We can find a similar expression for the counterterm Z_J which reads

$$\begin{aligned} Z_J =& 1-\left(\frac{\alpha_s}{4\pi}\right)\left[\frac{x_2}{\epsilon^2}+\frac{2x_2L+x_1}{\epsilon}\right]-\left(\frac{\alpha_s}{4\pi}\right)^2\left[\frac{y_4}{\epsilon^4}+\frac{4y_4L+y_3-x_2\beta_0}{\epsilon^3}\right. \\ &+\frac{8y_4L^2+2(2y_3-\beta_0x_2)L+y_2-x_0x_2+\beta_0x_1}{\epsilon^2}+\frac{32y_4L^3+6(4y_3-\beta_0x_2)L^2}{3\epsilon} \\ &\left.+\frac{2(2y_2-2x_0x_2-\beta_0x_1)L+(y_1-x_0(\beta_0+x_1)-x_2x_{-1})}{\epsilon}\right]+\mathcal{O}(\alpha_s^3). \end{aligned} \tag{6.3.4}$$

The jet function fulfils an RGE. In terms of anomalous dimensions the RGE is written

as

$$\frac{\mathrm{d}J(\tau,\mu,Q)}{\mathrm{d}\ln\mu} = 2\left[\frac{1+n}{n}\Gamma_{\mathrm{Cusp}}L + \gamma_J\right]J(\tau,\mu,Q), \tag{6.3.5}$$

where we take similar definitions for Γ_{Cusp} and γ_J as eq. (4.5.8)

$$\Gamma_{\mathrm{Cusp}}(\alpha_s) = \sum_{n=0}^{\infty}\left(\frac{\alpha_s}{4\pi}\right)\Gamma_n, \tag{6.3.6}$$

$$\gamma_J(\alpha_s) = \sum_{n=0}^{\infty}\left(\frac{\alpha_s}{4\pi}\right)\gamma_n. \tag{6.3.7}$$

The argument of the logarithm L is the same as in previous equations and n is the exponent of the scaling behaviour of the soft-collinear limit.

This RGE can now be solved, its NNLO solution is

$$\begin{aligned} J(\tau,\mu,Q) = 1 &+ \left(\frac{\alpha_s}{4\pi}\right)\left[\frac{1+n}{n}\Gamma_0 L^2 + 2\gamma_0 L + c_1\right] + \left(\frac{\alpha_s}{4\pi}\right)^2\left[\frac{1}{2}\left(\frac{1+n}{n}\right)^2\Gamma_0^2 L^4\right. \\ &+ \left(2\frac{1+n}{n}\Gamma_0\gamma_0 + \frac{2}{3}\frac{1+n}{n}\beta_0\Gamma_0\right)L^3 + \left(\frac{1+n}{n}\left(\Gamma_1 + \Gamma_0 c_1\right)\right. \\ &\left.\left. + 2\gamma_0(\gamma_0+\beta_0)\right)L^2 + 2\left(\gamma_1 + c_1(\gamma_0+\beta_0)\right)L + c_2\right] + \mathcal{O}(\alpha_s^3), \end{aligned} \tag{6.3.8}$$

and similarly for the counterterm we find

$$\begin{aligned} Z_J = 1 &- \left(\frac{\alpha_s}{4\pi}\right)\left[\frac{1+n}{2n}\Gamma_0\frac{1}{\epsilon^2} + \left(\frac{1+n}{n}\Gamma_0 L + \gamma_0\right)\frac{1}{\epsilon}\right] - \left(\frac{\alpha_s}{4\pi}\right)^2\left[\left(\frac{(1+n)\Gamma_0}{\sqrt{8}n}\right)^2\frac{1}{\epsilon^4}\right. \\ &+ \left(\left(\frac{(1+n)\Gamma_0}{\sqrt{2}n}\right)^2 L + \left(\frac{1+n}{n}\right)\Gamma_0\left(\frac{3\beta_0}{8} + \frac{\gamma_0}{2}\right)\right)\frac{1}{\epsilon^3} + \left(\left(\frac{(1+n)\Gamma_0}{\sqrt{2}n}\right)^2 L^2\right. \\ &+ \left(\frac{1+n}{n}\right)\Gamma_0\left(\frac{\beta_0}{2} + \gamma_0\right)L - \frac{1+n}{8n}\Gamma_1 + \frac{\gamma_0}{2}\left(\gamma_0+\beta_0\right)\Bigg)\frac{1}{\epsilon^2} \\ &\left.\left. + \left(-\frac{1+n}{2n}\Gamma_1 L - \frac{\gamma_1}{2}\right)\frac{1}{\epsilon}\right] + \mathcal{O}(\alpha_s^3). \end{aligned} \tag{6.3.9}$$

Comparing coefficients between the eqs. (6.3.3) and (6.3.8) allows us to determine the quantities $\gamma_{0,1}$ and $c_{1,2}$, which need to be determined for NNLL′ resummation. We also determine the cusp anomalous dimension which provides a strong check of our computation. If we compare eqs. (6.3.4) and (6.3.9), we can construct relations for the pole cancellation between the RGE and our result.

The expression for the anomalous dimensions and matching coefficients are

$$\begin{aligned}
&\text{NLO expressions :}\\
&\Gamma_0 = \frac{2n}{1+n} x_2,\\
&\gamma_0 = x_1,\\
&c_1 = x_0,\\
&\text{NNLO expressions :}\\
&\Gamma_1 = \frac{4n}{1+n}\left(y_2 - 2x_0x_2 - x_1(\beta_0 + x_1)\right),\\
&\gamma_1 = 2\left(y_1 - x_0(\beta_0 + x_1) - x_{-1}x_2\right),\\
&c_2 = y_0 - x_{-1}(\beta_0 + x_1) - x_{-2}x_2.
\end{aligned}$$

From the pole cancellation we find two additional equations which are not present in the previous set, they are

$$\begin{aligned}
y_4 &= \frac{(1+n)^2}{8n^2}\Gamma_0^2,\\
y_3 &= \frac{1+n}{8n}\Gamma_0\left(4\gamma_0 + \beta_0\right).
\end{aligned}$$

6.3.2 $\mathrm{SCET_{II}}$ observables

The occurrence of the collinear anomaly [95] introduces additional challenges for $\mathrm{SCET_{II}}$ observables, namely the second regulator α and the ties between soft and jet functions.

Let us start by writing the jet function in the following form, similar to eq. (6.3.1):

$$\begin{aligned}
J_{\text{bare}}(\tau,Q) &= 1+\left(\frac{\alpha_{s,\text{bare}}}{4\pi}\right)(\mu\bar{\tau})^{2\epsilon}\left(\frac{Q^2}{\nu^2}\right)^{-\frac{1}{2}\alpha}\left[\frac{1}{\alpha}\left(\frac{x_{11}}{\epsilon}+x_{10}+x_{1-1}\epsilon+x_{1-2}\epsilon^2+x_{1-3}\epsilon^3\right)\right.\\
&\quad+\left(\frac{x_{02}}{\epsilon^2}+\frac{x_{01}}{\epsilon}+x_{00}+x_{0-1}\epsilon+x_{0-2}\epsilon^2\right)+\alpha\left(\frac{x_{-13}}{\epsilon^3}+\frac{x_{-12}}{\epsilon^2}+\frac{x_{-11}}{\epsilon}+x_{-10}\right.\\
&\quad\left.\left.+x_{-1-1}\epsilon\right)\right]+\left(\frac{\alpha_{s,\text{bare}}}{4\pi}\right)^2(\mu\bar{\tau})^{4\epsilon}\left\{\left(\frac{Q^2}{\nu^2}\right)^{-\frac{1}{2}\alpha}\left[\frac{1}{\alpha}\left(\frac{z_{13}}{\epsilon^3}+\frac{z_{12}}{\epsilon^2}+\frac{z_{11}}{\epsilon}+z_{10}\right)\right.\right.\\
&\quad+\frac{z_{04}}{\epsilon^4}+\frac{z_{03}}{\epsilon^3}+\frac{z_{02}}{\epsilon^2}+\frac{z_{01}}{\epsilon}+z_{00}\left.\right]+\left(\frac{Q^2}{\nu^2}\right)^{-\alpha}\left[\frac{1}{\alpha^2}\left(\frac{y_{22}}{\epsilon^2}+\frac{y_{21}}{\epsilon}+y_{20}\right)\right.\\
&\quad\left.\left.+\frac{1}{\alpha}\left(\frac{y_{13}}{\epsilon^3}+\frac{y_{12}}{\epsilon^2}+\frac{y_{11}}{\epsilon}+y_{10}\right)+\left(\frac{y_{04}}{\epsilon^4}+\frac{y_{03}}{\epsilon^3}+\frac{y_{02}}{\epsilon^2}+\frac{y_{01}}{\epsilon}+y_{00}\right)\right]\right\}\\
&\quad+\mathcal{O}(\alpha_{s,\text{bare}}^3) \qquad (6.3.10)\\
&= 1+\left(\frac{\alpha_{s,\text{bare}}}{4\pi}\right)(\mu\bar{\tau})^{2\epsilon}\left(\frac{Q^2}{\nu^2}\right)^{-\frac{1}{2}\alpha}\left[\frac{H_J^1}{\alpha}+H_J^0+H_J^{-1}\alpha\right]\\
&\quad+\left(\frac{\alpha_{s,\text{bare}}}{4\pi}\right)^2(\mu\bar{\tau})^{4\epsilon}\left\{\left(\frac{Q^2}{\nu^2}\right)^{-\frac{1}{2}\alpha}\left[\frac{G_J^1}{\alpha}+G_J^0\right]+\left(\frac{Q^2}{\nu^2}\right)^{-\alpha}\left[\frac{P_J^2}{\alpha^2}+\frac{P_J^1}{\alpha}\right.\right.\\
&\quad\left.\left.+P_J^0\right]\right\}+\mathcal{O}(\alpha_{s,\text{bare}}^3), \qquad (6.3.11)
\end{aligned}$$

where we needed to separate the 2-particle cut contributions z_{ij} from those of the 3-particle cuts y_{ij} and the NLO x_{ij} coefficients, because the analytic regulator modifies the contributions differently depending on the number of particles in the final state. In the second equation the functions H_J^i , G_J^i and P_J^i represent the ϵ structure of the α^{-i} contribution.

Similarly, we can write down the form of the bare soft function as

$$\begin{aligned}
S_{\text{bare}}(\tau) &= 1+\left(\frac{\alpha_{s,\text{bare}}}{4\pi}\right)(\mu\bar{\tau})^{2\epsilon}\left(\nu^2\bar{\tau}^2\right)^{\frac{1}{2}\alpha}\left[\frac{H_S^1}{\alpha}+H_S^0+H_S^{-1}\alpha\right]\\
&\quad+\left(\frac{\alpha_{s,\text{bare}}}{4\pi}\right)^2(\mu\bar{\tau})^{4\epsilon}\left\{\left(\nu^2\bar{\tau}^2\right)^{-\frac{1}{2}\alpha}\left[\frac{G_S^1}{\alpha}+G_S^0\right]+\left(\nu^2\bar{\tau}^2\right)^{-\alpha}\left[\frac{P_S^2}{\alpha^2}+\frac{P_S^1}{\alpha}+P_S^0\right]\right\}\\
&\quad+\mathcal{O}(\alpha_{s,\text{bare}}^3), \qquad (6.3.12)
\end{aligned}$$

where the exact form of the functions H_S^i, G_S^i and P_S^i can be taken from [42].

In order to extract the required quantities, we look again at eq. (4.6.3). We see that in order for the exponentiation to take place, the jet and soft functions must be

written as

$$J(\tau) = \left(\frac{Q^2}{\nu^2}\right)^{-\frac{1}{2}F(\tau)} W_J(\tau), \tag{6.3.13}$$

$$S(\tau) = \left(\nu^2\bar{\tau}^2\right)^{-F(\tau)} W_S(\tau), \tag{6.3.14}$$

because the dependence on the additional scale ν must cancel in the product of jet and soft functions. This implies that the anomaly exponent F can be determined independently from either the jet function or soft function for any observable. However, the remainder function $W(\tau) = W_J(\tau)W_J(\tau)W_S(\tau)$ requires that both jet and soft functions are known.

Now we define $P(\tau) = J\bar{J}S$ and write it in terms of the functions H^i, G^i and P^i as:

$$\begin{aligned}
P(\tau) = 1 &+ \left(\frac{\alpha_{s,\text{bare}}}{4\pi}\right)(\mu\bar{\tau})^{2\epsilon}\left[\frac{1}{\alpha}\left(H_S^1 + 2H_J^1\right) - H_J^1 L_J + \frac{1}{2}H_S^1 L_S + 2H_J^0 + H_S^0\right] \\
&+ \left(\frac{\alpha_{s,\text{bare}}}{4\pi}\right)^2(\mu\bar{\tau})^{4\epsilon}\left[\frac{1}{\alpha^2}\left(P_S^2 + 2P_J^2 + 2H_J^1 H_S^1 + \left(H_J^1\right)^2\right) + \frac{1}{\alpha}\Bigg(\right. \\
&- \left[\left(H_J^1\right)^2 + H_J^1 H_S^1 + 2P_J^2\right] L_J + \left[H_J^1 H_S^1 + P_S^2\right] L_S + 2G_J^1 + G_S^1 + 2H_J^0 H_J^1 \\
&+ 2H_J^1 H_S^0 + 2H_J^0 H_S^1 + 2P_J^1 + P_S^1\Bigg) + \Bigg(\left[\frac{H_J^1}{2} + \frac{H_J^1 H_S^1}{4} + P_J^2\right] L_J^2 \\
&+ \left[\frac{H_J^1 H_S^1}{4} + \frac{P_S^2}{2}\right] L_S^2 - \frac{1}{2}H_J^1 H_S^1 L_S L_J - \Bigg[G_J^1 + 2H_J^0 H_J^1 + H_J^1 H_S^0 + H_J^0 H_S^1 \\
&+ 2P_J^1\Bigg] L_J + \left[\frac{G_S^1}{2} + H_J^1 H_S^0 + H_J^0 H_S^1 + P_S^1\right] L_S + 2G_J^0 + G_S^0 + \left(H_J^0\right)^2 \\
&+ 2H_J^1 H_J^{-1} + 2H_J^0 H_S^0 + H_J^{-1} H_S^1 + 2H_J^1 H_S^{-1} + 2P_J^0 + P_S^0\Bigg] + \mathcal{O}(\alpha_{s,\text{bare}}^3),
\end{aligned} \tag{6.3.15}$$

where we expanded in α and used $L_J = \ln\left(\frac{Q^2}{\nu^2}\right)$ and $L_S = \ln\left(\nu^2\bar{\tau}^2\right)$. We know that the function $P(\tau)$ must be independent of the additional regulator α and the scale ν. Thus the α poles in eq. (6.3.15) must cancel and the logarithms L_J and L_S recombine to $L_H = \ln\left(\bar{\tau}^2 Q^2\right)$. This leads to relations between the different functions. At NLO we find that

$$H_S^1 = -2H_J^1, \tag{6.3.16}$$

and at NNLO we find

$$P_S^2 = -2P_J^2 + 3\left(H_J^1\right)^2, \tag{6.3.17}$$
$$P_S^1 = -2G_J^1 - G_S^1 + 2H_J^0 H_J^1 - 2H_J^1 H_S^0 - 2P_J^1, \tag{6.3.18}$$
$$P_J^2 = \frac{1}{2}\left(H_J^1\right)^2, \tag{6.3.19}$$
$$G_S^1 = -2G_J^1. \tag{6.3.20}$$

By employing all of these relations the function $P(\tau)$ simplifies to

$$\begin{aligned} P(\tau) = 1 &+ \left(\frac{\alpha_{s,\text{bare}}}{4\pi}\right)(\mu\bar{\tau})^{2\epsilon}\left[2H_J^0 + H_S^0 - H_J^1 L_H\right] \\ &+ \left(\frac{\alpha_{s,\text{bare}}}{4\pi}\right)^2 (\mu\bar{\tau})^{4\epsilon}\left[\frac{1}{2}\left(H_J^1\right)^2 L_H^2 - \left(G_J^1 + H_J^1 H_S^0 + 2P_J^1\right) L_H\right. \\ &\left. + 2G_J^0 + G_S^0 + \left(H_J^0\right)^2 - 2H_J^1 H_J^{-1} + 2H_J^0 H_S^0 + 2H_J^1 H_S^{-1} + 2P_J^0 + P_S^0\right] \\ &+ \mathcal{O}(\alpha_{s,\text{bare}}^3). \end{aligned} \tag{6.3.21}$$

Let us now see how $P(\tau)$ is written in terms of the anomaly exponent and remainder function. We have

$$\begin{aligned} P(\tau) = J\bar{J}S &= \left[\left(\frac{Q^2}{\nu^2}\right)^{-\frac{1}{2}F(\tau)} W_J(\tau)\right]\left[\left(\frac{Q^2}{\nu^2}\right)^{-\frac{1}{2}F(\tau)} W_{\bar{J}}(\tau)\right]\left[\left(\nu^2\bar{\tau}^2\right)^{-F(\tau)} W_S(\tau)\right] \\ &= \left(Q^2\bar{\tau}^2\right)^{-F(\tau)} W(\tau) \\ &= \left(Q^2\bar{\tau}^2\right)^{-\sum_{i=1}\left(\frac{\alpha_{s,\text{bare}}}{4\pi}\right)^i (\mu\bar{\tau})^{2i\epsilon} F_{i,\text{bare}}}\left(1 + \sum_{i=1}\left(\frac{\alpha_{s,\text{bare}}}{4\pi}\right)^i (\mu\bar{\tau})^{2i\epsilon} W_{i,\text{bare}}\right) \\ &= 1 + \left(\frac{\alpha_{s,\text{bare}}}{4\pi}\right)(\mu\bar{\tau})^{2\epsilon}\left[W_{1,\text{bare}} - F_{1,\text{bare}} L_H\right] \\ &\quad + \left(\frac{\alpha_{s,\text{bare}}}{4\pi}\right)^2 (\mu\bar{\tau})^{4\epsilon}\left[\frac{1}{2}F_{1,\text{bare}}^2 L_H^2 - \left(F_{1,\text{bare}} W_{1,\text{bare}} + F_{2,\text{bare}}\right) L_H + W_{2,\text{bare}}\right] \\ &\quad + \mathcal{O}(\alpha_{s,\text{bare}}^3) \end{aligned} \tag{6.3.22}$$

where we expanded in $\alpha_{s,\text{bare}}$ in the fourth line. In order to extract the anomaly exponent and the remainder expression we now compare eqs. (6.3.21) and (6.3.22). Up to NNLO we find the following forms for the bare anomaly exponent and remainder

expression

$$F_{\text{bare}}(\tau) = \left(\frac{\alpha_{s,\text{bare}}}{4\pi}\right)(\mu\bar{\tau})^{2\epsilon} H_J^1 + \left(\frac{\alpha_{s,\text{bare}}}{4\pi}\right)^2 (\mu\bar{\tau})^{4\epsilon} \left(G_J^1 + 2P_J^1 - 2H_J^0 H_J^1\right) + \mathcal{O}(\alpha_{s,\text{bare}}^3), \tag{6.3.23}$$

$$\begin{aligned} W_{\text{bare}}(\tau) = 1 + \left(\frac{\alpha_{s,\text{bare}}}{4\pi}\right)(\mu\bar{\tau})^{2\epsilon} \left(2H_J^0 + H_S^0\right) + \left(\frac{\alpha_{s,\text{bare}}}{4\pi}\right)^2 (\mu\bar{\tau})^{4\epsilon} \Bigg(2G_J^0 + G_S^0 + \left(H_J^0\right)^2 \\ - 2H_J^1 H_J^{-1} + 2H_J^0 H_S^0 + 2H_J^1 H_S^{-1} + 2P_J^0 + P_S^0\Bigg) + \mathcal{O}(\alpha_{s,\text{bare}}^3). \end{aligned} \tag{6.3.24}$$

From the bare anomaly exponent, it is visible that only jet function determines the coefficients. Notice that if we choose to eliminate the jet function expressions in eq. (6.3.15) instead, the anomaly exponent would purely depend on the soft function inputs. On the other hand, the remainder expression will always depend on both jet and soft function pieces.

We now have to renormalise both the anomaly exponent and the remainder expression. We first start with the anomaly exponent. From the form of $P(\tau)$, and the RGE of the hard function, it follows [95] that the anomaly exponent fulfills the RGE

$$\frac{\mathrm{d}F(\tau,\mu)}{\mathrm{d}\ln\mu} = 2\Gamma_{\text{Cusp}}, \tag{6.3.25}$$

where $F = F_{\text{bare}} - Z_F$ because the anomaly exponent renormalises additively in Laplace space. The NNLO solution to this RGE is given by

$$F(\tau,\mu) = \left(\frac{\alpha_s}{4\pi}\right)(2\Gamma_0 L + d_1) + \left(\frac{\alpha_s}{4\pi}\right)^2 \left(2\beta_0\Gamma_0 L^2 + 2\left(\Gamma_1 + \beta_0 d_1\right)L + d_2\right) + \mathcal{O}(\alpha_s^3) \tag{6.3.26}$$

and the corresponding counterterm, which satisfies a similar RGE, is given by

$$Z_F = \left(\frac{\alpha_s}{4\pi}\right)\left(\frac{\Gamma_0}{\epsilon}\right) + \left(\frac{\alpha_s}{4\pi}\right)^2 \left(-\frac{\beta_0\Gamma_0}{2\epsilon^2} + \frac{\Gamma_1}{2\epsilon}\right) + \mathcal{O}(\alpha_s^3), \tag{6.3.27}$$

with $L = \ln(\mu\bar{\tau})$. We can now extract the coefficients d_1 and d_2 and find consistency relations by reintroducing in F_{bare} the proper definitions of H, G, and P and finally

expand in ϵ. At NLO we find the following relations

$$\Gamma_0 = x_{11},$$
$$d_1 = x_{10}.$$

In the case of NNLO we find the following consistency relations

$$z_{13} = 2\left(-y_{13} + x_{02}x_{11}\right),$$
$$z_{12} = \frac{1}{2}\left(-4y_{12} + 4x_{02}x_{10} + x_{11}\left(\beta_0 + 4x_{01}\right)\right),$$

and we can extract the quantities

$$\Gamma_1 = -2\left(-2y_{11} - z_{11} + 2x_{00}x_{11} + 2x_{02}x_{1-1} + x_{10}\left(\beta_0 + 2x_{01}\right)\right),$$
$$d_2 = 2y_{10} + z_{10} - 2\left(x_{00}x_{10} + x_{11}x_{0-1} + x_{02}x_{1-2} + x_{1-1}\left(x_{01} + \frac{\beta_0}{2}\right)\right),$$

where the x_{ij}, y_{ij} and z_{ij} refer purely to the jet quantities. In the final step we have to renormalise the remainder expression. It satisfies the RGE

$$\frac{\mathrm{d}W(\tau,\mu)}{\mathrm{d}\ln\mu} = 2\left[2\Gamma_{\mathrm{Cusp}}L + \gamma_W\right]W(\tau,\mu). \tag{6.3.28}$$

This RGE can now be solved and its NNLO solution in terms of the anomalous dimensions is

$$\begin{aligned} W(\tau,\mu) = 1 + \left(\frac{\alpha_s}{4\pi}\right)\left[2\Gamma_0 L^2 + 2\gamma_0^W L + c_1\right] + \left(\frac{\alpha_s}{4\pi}\right)^2\Bigg[2\Gamma_0^2 L^4 \\ + \left(4\Gamma_0\gamma_0^W + \frac{4}{3}\beta_0\Gamma_0\right)L^3 + \left(2\left(\Gamma_1 + \Gamma_0 c_1\right) + 2\gamma_0^W(\gamma_0^W + \beta_0)\right)L^2 \\ + 2\left(\gamma_1^W + c_1(\gamma_0^W + \beta_0)\right)L + c_2\Bigg] + \mathcal{O}(\alpha_s^3). \end{aligned} \tag{6.3.29}$$

Similarly we find for the counterterm

$$\begin{aligned} Z_W = 1 - \left(\frac{\alpha_s}{4\pi}\right)\left[\Gamma_0\frac{1}{\epsilon^2} + \left(2\Gamma_0 L + \gamma_0^W\right)\frac{1}{\epsilon}\right] - \left(\frac{\alpha_s}{4\pi}\right)^2\left[\frac{\Gamma_0^2}{2}\frac{1}{\epsilon^4}\right. \\ + \left(2\Gamma_0^2 L + \Gamma_0\left(\frac{3\beta_0}{4} + \gamma_0^W\right)\right)\frac{1}{\epsilon^3} + \left(2\Gamma_0^2 L^2 + \Gamma_0\left(\beta_0 + 2\gamma_0^W\right)L\right. \\ \left.\left. - \frac{1}{4}\Gamma_1 + \frac{\gamma_0^W}{2}\left(\gamma_0^W + \beta_0\right)\right)\frac{1}{\epsilon^2} - \left(\Gamma_1 L + \frac{\gamma_1^W}{2}\right)\frac{1}{\epsilon}\right] + \mathcal{O}(\alpha_s^3), \end{aligned} \tag{6.3.30}$$

where $L = \ln(\mu\bar{\tau})$. The expression for the anomalous dimensions and matching corrections can be subsequently derived by inserting the correct values of the functions H, G, and P in eq. (6.3.24) and expanding in ϵ. At NLO we find the following expressions

$$\begin{aligned} \Gamma_0 &= 2x_{02}^J + x_{02}^S, \\ \gamma_0^W &= 2x_{01}^J + x_{01}^S, \\ c_1 &= 2x_{00}^J + x_{00}^S, \end{aligned}$$

and at NNLO

$$\begin{aligned} \Gamma_1 &= -2\big(- 2y_{02}^J - y_{02}^S - 2z_{02}^J - z_{02}^S + 3(x_{01}^J)^2 + 2x_{01}^J x_{01}^S + (x_{01}^S)^2 + \beta_0(2x_{01}^J + x_{01}^S) \\ &\quad + 2x_{02}^J(3x_{00}^J + x_{00}^S) + 2x_{02}^S(x_{00}^J + x_{00}^S) + 2x_{11}^J x_{-11}^J - 2x_{11}^J x_{-11}^S + 2x_{10}^J x_{-12}^J - 2x_{10}^J x_{-12}^S \\ &\quad + 2x_{1-1}^J x_{-13}^J - 2_{x1-1}^J x_{-13}^S\big), \\ \gamma_1^W &= -2\big(- 2y_{01}^J - y_{01}^S - 2z_{01}^J - z_{01}^S + \beta_0(2x_{00}^J + x_{00}^S) + 2x_{00}^J x_{01}^J + x_{00}^S x_{01}^S + 2x_{02}^J x_{0-1}^J \\ &\quad + x_{02}^S x_{0-1}^S + 2x_{11}^J x_{-10}^J - 2x_{11}^J x_{-10}^S + 2x_{10}^J x_{-11}^J - 2x_{10}^J x_{-11}^S + 2x_{1-1}^J x_{-12}^J - 2x_{1-1}^J x_{-12}^S \\ &\quad + 2x_{1-2}^J x_{-13}^J - 2x_{1-2}^J x_{-13}^S\big), \\ c_2 &= 2y_{00}^J + y_{00}^S + 2z_{00}^J + z_{00}^S + (x_{00}^J)^2 + 2x_{00}^J x_{00}^S - 2x_{01}^J x_{0-1}^J - \beta_0(2x_{0-1}^J + x_{0-1}^S) \\ &\quad - x_{01}^S x_{0-1}^S - 2x_{02}^J x_{0-2}^J - x_{02}^S x_{0-2}^S - 2\big(x_{10}^J(x_{-10}^J - x_{-10}^S) + x_{1-1}^J x_{-11}^J - x_{1-1}^J x_{-11}^S \\ &\quad + x_{1-2}^J x_{-12}^J - x_{1-2}^J x_{-12}^S + x_{1-3}^J x_{-13}^J - x_{1-3}^J x_{-13}^S + x_{11}^J x_{-1-1}^J - x_{11}^J x_{-1-1}^S\big). \end{aligned}$$

From the consistency relations we obtain two additional equations which are not present

in the previous set. They are

$$2y^J_{04} + y^S_{04} + 2z^J_{04} + z^S_{04} + (x^J_{02})^2 + 2x^J_{02}x^S_{02} + 2x^J_{11}(x^S_{-13} - x^J_{-13}) = \frac{1}{2}\Gamma_0^2,$$
$$2y^J_{03} + y^S_{03} + 2z^J_{03} + z^S_{03} + 2x^S_{01}x^J_{02} + 2x^J_{01}(x^J_{02} + x^S_{02}) - 2x^J_{11}x^J_{-12} + 2x^J_{11}x^S_{-12} - 2x^J_{10}x^J_{-13} + 2x^J_{10}x^S_{-13} = \Gamma_0\left(\gamma_0 + \frac{1}{4}\beta_0\right).$$

Here we denote the ingredients from the jet function with a superscript J while the soft ingredients are denoted by an S.

Chapter 7

Numerical implementation

In this chapter, we will explore how we implemented the master formulae from chapter 6 into the public program `pySecDec` [133–135] and why a straightforward numerical integration of the master formulae fails, and how to change the integrand in a way to make it work.

7.1 `pySecDec`

The program `pySecDec` is the new version of the `SecDec` [130, 136, 137] program. The algebraic part is written in `python` and `FORM` [138, 139]. The program is completely open source and it allows maximal flexibility due to its modular structure. The `python` code writes `FORM` files to produce optimized `C++` functions which in turn are passed to the numerical integrator `CUBA` [140, 141].

The program flow of `pySecDec` is shown in figure 7.1.1. In this work, we are dealing with general polynomials P_i and not directly with loop integrals; thus, our starting point is 1b) in the figure. The next step is the sector decomposition algorithm, which aims to factorise the polynomials P_i as products of a monomial and a polynomial with a nonzero constant term:

$$P_i(\{x_i\}) \to \prod_j x_j^{\alpha_j} (p_i(\{x_j\}) + \text{const}). \tag{7.1.1}$$

The iterative sector decomposition splits the integral and remaps the integration domain until all polynomials P_i in all arising integrals have the desired form. In our approach, we can skip this step as we already performed all the required sector decom-

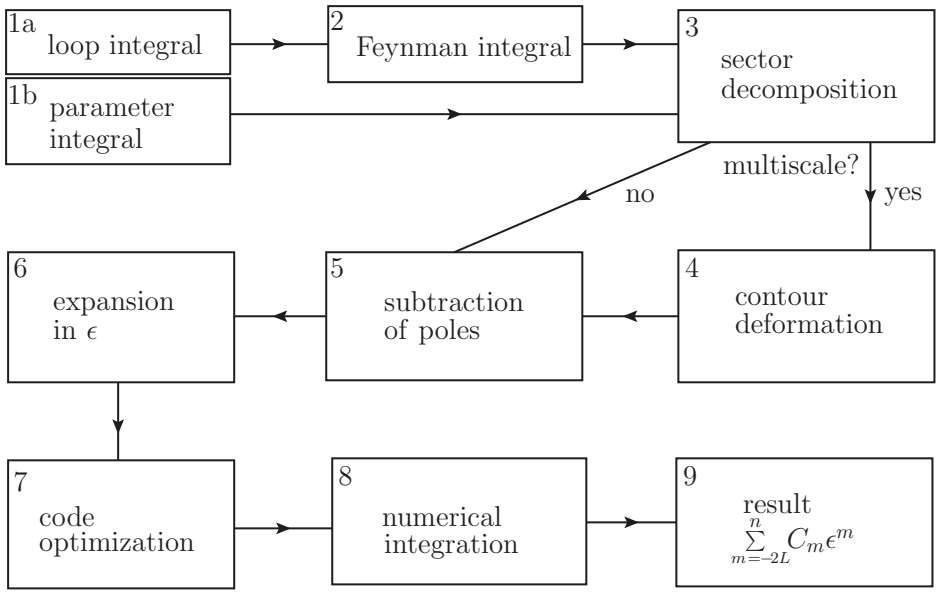

Figure 7.1.1: Flowchart showing the main building blocks of `pySecDec`. Steps 1 – 6 are done in `python`. `FORM` is used in step 7 to produce optimized `C++` code and for step 8 the code is passed onto the `CUBA`-library for the numerical integration. This image was taken from [133]

.

position steps in a `Mathematica` code. Thus, our integrals are always in the form

$$I = \prod_i x_i^{-1+y_i} R, \tag{7.1.2}$$

which is to say that the divergences are already in monomial form and R is a finite remainder expression. If we had dealt with a multiscale problem, we would need to perform an additional contour deformation. However, in our integrals, there is no such explicit mass scale. Therefore, we can again skip this step. Following the flowchart, we arrive at step 5 where the pole subtraction takes place. This routine isolates the divergences in ϵ and α by repeatedly applying integration by parts. In the case of a one-dimensional integral, this becomes

$$\int_0^1 \mathrm{d}x\, x^{a-b\epsilon} I(x,\epsilon) = \sum_{p=0}^{|a|-1} \frac{1}{a+p+1-b\epsilon} \frac{I^{(p)}(0,\epsilon)}{p!} + \int_0^1 \mathrm{d}x\, x^{a-b\epsilon} R(x,\epsilon), \tag{7.1.3}$$

where $I^{(p)}$ denotes the p-th derivative of I with respect to x. The remaining integral over x and the remainder function R are free from divergences. In the subsequent

steps, the expressions are expanded in a Laurent series in the regulators, then passed to the numerical integrator through some internal optimization, and finally integrated.

The numerical integration can either be done by the `CUBA`-libary or, in the newer version of `pySecDec`(v.1.5), by a quasi-Monte Carlo integrator. In this work we will exclusively calculate our master integrals with the routines implemented in `CUBA`. For more details on `pySecDec` we refer to [133–135] and the references therein.

7.2 Error estimation

As mentioned in the previous section, the numerical integration is performed via the `CUBA`-library, which uses Monte Carlo integration. If we perform the integration of our master formulae from section 6, then we find that the convergence rate is low and the error is underestimated. In order to understand how this arises we first need to understand Monte Carlo integration in more detail.

7.2.1 Monte Carlo integration

Let us assume that we have a function $f(x)$ that we want to integrate numerically over some interval G:

$$I[f] = \int_G \mathrm{d}x f(x). \tag{7.2.1}$$

We can approximate this integral by averaging samples of the function $f(x)$ at uniform random points within the interval. Given a set of N uniform random variables $X_i \in G$ with a corresponding probability density function Ω, the Monte Carlo estimator for computing $I[f]$ is

$$\langle I^N[f] \rangle = \frac{|\Omega|}{N} \sum_{i=0}^{N} f(X_i), \tag{7.2.2}$$

where $\langle I^N[f] \rangle$ is an approximation of the $I[f]$ using N samples. We expect to improve the approximation by increasing the number of samples N because as we increase the number of samples N, the estimator $\langle I^N[f] \rangle$ becomes a closer approximation of $I[f]$.

Due to the strong law of large numbers [142], in the limit $N \to \infty$, we can guarantee that we have the exact solution:

$$\Pr\left(\lim_{N\to\infty} \langle I^N[f] \rangle = I[f] \right) = 1, \tag{7.2.3}$$

where Pr is a shorthand notation for probability. From the central limit theorem [143],

we know that the statistical error on how $\langle I^N[f]\rangle$ converges towards $I[f]$ is $\frac{\sigma_f}{\sqrt{N}}$ provided both the expected value $I[f]$ and the variance $\sigma_f^2 = \int_G \mathrm{d}x\, f^2(x) - I^2[f]$ stay finite. If the expected value $I[f]$ is unknown, then it is very likely that the variance is also unknown. However, it can be estimated using sample variance $\sigma_N[f]$:

$$\sigma_N^2[f] = \sum_{i=1}^{N} \frac{|\Omega|}{N-1} \left(f(X_i) - \frac{\langle I^N[f]\rangle}{|\Omega|} \right)^2 . \tag{7.2.4}$$

Therefore we can reduce the expected statistical uncertainty by simply using more samples and thus, in return, improve the quality of the Monte Carlo integration.

However, the increase of samples in the Monte Carlo integration comes at the cost of increasing the runtime. Therefore, it is much better to try and reduce the variance. There exist many different variance-reduction techniques. We will briefly mention one, importance sampling, as this technique is used in the Vegas routine [144, 145] of the `CUBA` library, which we use in this work.

7.2.2 Variance reduction

Importance sampling reduces the variance by noticing that we have the freedom to choose the probability density functions Ω used in the integration. The variance is reduced by choosing samples from a distribution that has a similar shape as the function $f(x)$ being integrated. In simple terms, importance sampling places more samples where the contribution of the integrand is more dominant, than in the regions where the contribution is less dominant.

In a mathematical sense, this can be written as

$$I[f] = \int_G \mathrm{d}x\, f(x) = \int_G \mathrm{d}x\, g(x) \frac{f(x)}{g(x)} = I^g \left[\frac{f}{g} \right] , \tag{7.2.5}$$

where I^g is the expectation value as evaluated with respect to the probability density function $g(x)$.

Let us us assume that $g(x)$ is approximately $f(x)$ such that the ratio of the function $\frac{f(x)}{g(x)}$ is close to being constant. Then we only require a few samples for a good estimate since constant functions are not difficult to estimate. In terms of the variance, this

means that in order to reduce it, we require

$$\sigma^2_{\frac{f}{g}} < \sigma^2_f \tag{7.2.6}$$

$$0 < \sigma^2_f - \sigma^2_{\frac{f}{g}}$$

$$0 < \left(\int_G \mathrm{d}x\, f(x)^2 - I[f]^2\right) - \left(\int_G \mathrm{d}x\, g(x) \left(\frac{f(x)}{g(x)}\right)^2 - I^g\left[\frac{f}{g}\right]^2\right)$$

$$0 < \left(\int_G \mathrm{d}x\, f(x)^2 - I[f]^2\right) - \left(\int_G \mathrm{d}x\, g(x) \left(\frac{f(x)}{g(x)}\right)^2 - I[f]^2\right)$$

$$0 < \int_G \mathrm{d}x\, f(x)^2 \left(1 - \frac{1}{g(x)}\right). \tag{7.2.7}$$

In order to achieve this the probability density function $g(x)$ should behave similar to $f(x)$. From a computational point of view it should also be easy to generate values from $g(x)$.

7.2.3 Integrable divergences

Now that we understand how the numerical integrator tries to reduce the variance of the integrand, we are able to understand why our master formulae in section 6 give us trouble in the numerical integration. If we look at our current master formulae, for example at (6.1.12), we find that the angular parametrisation contributes a factor $(t_k\bar{t}_k)^{-\frac{1}{2}-\epsilon}$, which is divergent at 0 and 1. This divergence is integrable; even at the higher-order expansion of the regulator. The expansion yields

$$\frac{\ln^n(t_k\bar{t}_k)}{\sqrt{t_k\bar{t}_k}}. \tag{7.2.8}$$

We can immediately see that this contribution is not square-integrable. As a result, the corresponding variance σ^2_f diverges. As a consequence of $\sigma^2_f \to \infty$, the central limit theorem requirements are violated and therefore do not apply anymore. This leads to a problem for the Vegas integrator, as on the one hand, the error estimates, which are based on the critical limit theorem, are no longer valid. On the other hand, the importance sampling does not really work because anything is a reduction from ∞. So to regain proper error estimations and variance reduction, we have to transform the square-root divergences into an expression that is square-integrable. We have achieved this transformation by going from our physical parametrisation to another so-called

computational parametrisation.

7.2.4 Computational parametrisation

The source of the square-root divergences are in general the angular integrations t_{kl}, t_l, t_k. On top of that the non-linear transformation variables v and p also give rise to square-root divergences. Let us see how they appear in the master formulae. In the case of the angular integration variables t_{kl}, t_l, t_k they, at worst, appear as

$$(t\bar{t})^{-\frac{1}{2}-\epsilon}, \tag{7.2.9}$$

where t is a place holder for any of the three variables. In the case of the non-linear transformation variable v, p they appear at worst as

$$x^{-\frac{1}{2}-\epsilon}, \tag{7.2.10}$$

where again x is a place holder for either v or p. So, in general, we see that the worst behaviour in terms of square root divergence is coming from the angular variables. Therefore if we cure their behaviour, it is a simple task to cure the other variables as well.

We can use the substitution

$$t = 1 - (1 - \xi^a)^b, \tag{7.2.11}$$

where a, b are determined depending on how t scales at the endpoints. Here we can see that $t \sim \xi^a$ and $\bar{t} \sim \bar{\xi}^b$. This leads to the following expression for the angular integrations

$$(t\bar{t})^{-\frac{1}{2}-\epsilon}\,\mathrm{d}t \sim \xi^{-1+\frac{1}{2}a}\bar{\xi}^{-1+\frac{1}{2}b}\,\mathrm{d}\xi, \tag{7.2.12}$$

for ξ near the endpoints 0 and 1, with the inclusion of the proper Jacobian. We can now choose the proper values for a and b to eliminate the occurrence of the square root divergences. In the case of the angular integration, we use $a = b = 4$ such that

$$\begin{aligned} t &= 1 - (1 - \xi^4)^4, \\ (t\bar{t})^{-\frac{1}{2}-\epsilon}\,\mathrm{d}t &\sim \xi\bar{\xi}\,\mathrm{d}\xi. \end{aligned}$$

We can use different values for a and b such that we cure all the other square root divergences.

By performing these reparamatrisations, we cured the occurrence of all square-root divergences. Therefore we could stop here and use the Vegas integrator to evaluate the master formulae. However, we also choose to use similar transformations to cure the occurrence of any logarithmic divergences to have a better convergence rate.

Finally, we turn to the divergences themselves; they are invariant under these substitutions. However, they still affect the plus distribution. Let us assume that we have a structure like:

$$\begin{aligned}\int_0^1 \mathrm{d}x \left[\frac{\ln x}{x}\right]_+ f(x) &= \int_0^1 \mathrm{d}x \frac{\ln x}{x}\left(f_0 + f_1 x + \frac{f_2}{2}x^2 \ldots - f_0\right) \\ &= \int_0^1 \mathrm{d}x \left(f_1 + \frac{f_2}{2}x \ldots\right)\ln x, \end{aligned} \tag{7.2.13}$$

where we expanded $f(x)$ in a Taylor series. We can see that this expression suffers again from logarithmic divergences. By substituting $x = 1 - (1-\xi^2)^2$ we can again suppress this divergence

$$\int_0^1 \mathrm{d}x \left(f_1 + \frac{f_2}{2}x \ldots\right)\ln x = 4\int_0^1 \mathrm{d}\xi \left(f_1 + \frac{f_2}{2}\xi^2 \ldots\right)\xi\bar{\xi}\ln\xi, \tag{7.2.14}$$

On top of suppressing the logarithmic divergence we also included a suppression term in the limit $\xi \to 1$.

We want to mention the divergence of $\bar{z}^{-1}$ as an additional point. Here we have to change the form of our transformation slightly because we want to remap the divergence to $z \to 0$. Therefore if we encounter such a divergence, we use $z = (1-\xi^2)^2$.

Now we can write a complete list of transformations, which must be applied to the master formulae in section 6 to cure the undesired behaviour. For the NLO and NNLO RV contributions, we use

$$\{z, u\} \to 1 - (1-x^m)^2, \qquad t_k \to 1 - (1-c^4)^4, \qquad r \to 1 - (1-l^2)^2,$$

where we use the same variable for u and z as they can not appear simultaneously, and r is the variable related to the integral representation of the hypergeometric functions. In the case, where the divergence of u or z lies at 1, we use

$$\{z, u\} \to (1-x^m)^2.$$

For the NNLO RR contributions, we can divide the physical parametrisations into

three distinct classes. The first class corresponds to the case where only sector decomposition or upscaling but no non-linear transformations are performed. The second class is where we could still perform sector decomposition but use the non-linear transformation in eq. (6.2.47) and in the last class we used the non-linear transformation of eq. (6.2.105). The three different classes can thus be written as

$$\begin{aligned} \text{I: } &\{\alpha, \beta, \gamma, t, t_l, t_5\}, \\ \text{II: } &\{\alpha, \beta, u, v, t_j, t_5\}, \\ \text{III: } &\{a, \tilde{u}, \tilde{v}, p, t_j, t_5\}, \end{aligned}$$

where α, β, γ denote any variables which are not changed by a non-linear transformation. The variables u, v are from the transformation in eq. (6.2.47), $\tilde{u}$, $\tilde{v}$, p are the variables from the transformation in eq. (6.2.105) and t, t_l, t_5 are the angular variables. In the case of a divergence at $\{\alpha, \beta, \gamma\} \to 0$ we use the substitution

$$\{\alpha, \beta, \gamma\} = 1 - (1 - x^m)^2,$$

and

$$\{\alpha, \beta, \gamma\} = (1 - x^m)^2,$$

whenever a divergence lies $\{\alpha, \beta, \gamma\} \to 1$, where x is a simple placeholder. In case a variable is not contained in the respective Ω of the master formula, we set $m = 2$. If the variable does not give rise to a divergence at any endpoint, we simply transform them like

$$\{\alpha, \beta, \gamma\} = 1 - (1 - x^2)^2.$$

For the angular variables we use the substitutions

$$t = 1 - (1 - s^4)^4, \qquad t_l = 1 - (1 - s_l^4)^4, \qquad t_5 = s_5^2.$$

In the case of parametrisation class II, all the previous substitution rules are still used for the variables that are not affected by the non-linear transformation. The variables affected by the non-linear transformation are substituted via

$$u = 1 - (1 - c^2)^4, \qquad v = 1 - (1 - w^4)^2.$$

Finally in the case of parametrisation class III we use the following parametrisation

$$\begin{aligned} a &= 1-(1-r^2)^2, & \tilde{u} &= 1-(1-c^m)^2, & \tilde{v} &= 1-(1-x^m)^2, \\ p &= 1-(1-w^4)^4, & t_l &= 1-(1-s_l^4)^4, & t_5 &= s_5^2. \end{aligned}$$

These transformation rules allow us to write the master formulae of section 6 in a way that there are no square root, reduce the occurrence of logarithmic divergences and that the integrand vanishes in all non-divergent endpoints.[1]

As the last point, we note that we kept an open parameter, namely m, in most transformations. This variable comes about because of the interplay between plus distributions and integrable divergences. However, this time, because of the measurement function and not the matrix element. Let us assume the measurement function has the following expansion $M(x) \sim M_0 + M_1 x^a + \mathcal{O}(x^a)$, where a can be any real number, after factoring out the proper coefficient. If we now insert the plus distribution, we find that

$$\begin{aligned} \left[x^{-1+n\epsilon}\right]_+ M(x) &\sim \frac{M_0 + M_1 x^a + \mathcal{O}(x^a) - M_0}{x} + n\epsilon \frac{\ln x}{x} \left(M_0 + M_1 x^a + \mathcal{O}(x^a) - M_0\right) \\ &= M_1 \left(x^{a-1} + n\epsilon\, x^{a-1} \ln x\right) + \mathcal{O}(x^a, \epsilon^2). \end{aligned} \tag{7.2.15}$$

We observe that we get integrable divergences when $a < 1$. If we now perform the transformation $x \to 1-(1-y^m)^2$, then the expression changes to

$$\begin{aligned} &\int_0^1 \mathrm{d}x\, M_1 \left(x^{a-1} + n\epsilon\, x^{a-1} \ln x\right) + \mathcal{O}(x^a, \epsilon^2) \to \\ &\int_0^1 \mathrm{d}y\, 2(1-y^m) m (2-y^m)^{-1+a} M_1 \left(y^{-1+ma} + n\epsilon\, y^{-1+ma} \ln\left(y^m(2-y^m)\right)\right) + \mathcal{O}(y^{ma}, \epsilon^2). \end{aligned} \tag{7.2.16}$$

Here we can see that the expression is automatically suppressed in the $y \to 1$ limit. By choosing $m > \frac{2}{a}$ we always eliminate any integrable divergence at $y \to 0$, which would spoil the convergence rate and error estimation. Therefore m needs to be specified according to the observable. In section 8 where we show results for some sample observables for which we either choose $m = 2$ or $m = 4$.

[1] This is not completely true as the limit $t_5 \to 1$ is not suppressed, but this limit is only present in the measurement function and has no effect on the matrix element.

Chapter 8

Results

In this section we show that our automated approach can be used to compute a wide range of jet functions. We choose observables that fall into different categories, which cover most of the structures we can encounter in the calculation of generic observables.

The first category contains observables for which $n = 1$ and there is no dependence on the reference vector $\vec{v}_\perp$ in the transverse plane. The example we choose for this kind is thrust. The second category involves observables where n is neither one nor zero, with still no angular dependence. The example we choose is the class of observables called angularities. The third category of observables has a non-trivial angular dependence, and the example here is transverse thrust. The final category is the SCET_II case with $n = 0$, where we looked at the Winner-take-all axis broadening. We present numerical results for all these observables, some of these results were already presented with this framework in [46].

The general setup for this section is that we first define the observable in light-cone coordinates and in the physical parametrisation at NLO and NNLO. Finally, we give the extracted quantities and the compare them with the literature whenever available.

8.1 Thrust

The first event-shape observable, which we investigate is thrust, which we already introduced in section 3.1. The measurement function in light-cone coordinates is defined as

$$\omega_{\text{Thrust}}(\{k_i\}) = \sum_i k_i^+ \tag{8.1.1}$$

in terms of light-cone coordinates. In the physical parametrisation thrust is written as

$$\omega_{\text{Thrust}}^{\text{NLO}} = k_T \left(\frac{k_T}{Q}\right) \left(\frac{1}{z_k} + \frac{1}{1-z_k}\right), \tag{8.1.2}$$

at NLO and at NNLO we get the following structure

$$\omega_{\text{Thrust}}^{\text{NNLO}} = q_T \left(\frac{q_T}{Q}\right) \left(\frac{1}{z} + \frac{a((1-b)^2 + 4b(1-t))}{(1-z)(a+b)(1+ab)}\right). \tag{8.1.3}$$

We thus have $n = 1$, and the thrust measurement function for Region A, B, C and, D are identical. In order to present the results we choose not to include the colour factors in the numbers. We find for the quark jet function anomalous dimensions:

$$\begin{aligned}
\Gamma_0^{C_F} &= 4 \pm 2 \cdot 10^{-5} && [4], && \gamma_0^{C_F} &= 3 \pm 9 \cdot 10^{-5} && [3], \\
\Gamma_1^{C_F T_F} &= -8.8881(8) && [-8.8889], && \gamma_1^{C_F T_F} &= -13.3495(27) && [-13.3495], \\
\Gamma_1^{C_F^2} &= -0.0066(167) && [0], && \gamma_1^{C_F^2} &= 10.6439(483) && [10.6102], \\
\Gamma_1^{C_F C_A} &= 16.6202(130) && [16.6183], && \gamma_1^{C_F C_A} &= -3.2509(458) && [-3.2602],
\end{aligned} \tag{8.1.4}$$

and the corresponding matching corrections,

$$\begin{aligned}
c_1^{C_F} &= 0.4202(3) && [0.4203], \\
c_2^{C_F T_F} &= -10.7853(92) && [-10.7871], \\
c_2^{C_F^2} &= 4.6633(1199) && [4.6551], \\
c_2^{C_F C_A} &= -2.0920(1352) && [-2.1649].
\end{aligned} \tag{8.1.5}$$

Similarly we calculate the anomalous dimensions for the gluon jet function:

$$\begin{aligned}
\Gamma_0^{C_A} &= 4 \pm 2 \cdot 10^{-5} && [4], && \gamma_0^{C_A} &= 3.6666 \pm 7 \cdot 10^{-6} && [3.6666], \\
\Gamma_0^{T_F} &= 0 && [0], && \gamma_0^{T_F} &= -1.3333 \pm 7 \cdot 10^{-6} && [-1.3333], \\
\Gamma_1^{T_F^2} &= 0 \pm 2 \cdot 10^{-5} && [0], && \gamma_1^{T_F^2} &= 0 \pm 2 \cdot 10^{-4} && [0], \\
\Gamma_1^{C_F T_F} &= 0 \pm 2 \cdot 10^{-3} && [0], && \gamma_1^{C_F T_F} &= -3.9987(128) && [-4], \\
\Gamma_1^{C_A T_F} &= -8.8889(5) && [-8.8889], && \gamma_1^{C_A T_F} &= -9.2422(199) && [-9.2431], \\
\Gamma_1^{C_A^2} &= 16.6180(513) && [16.6183], && \gamma_1^{C_A^2} &= 9.2966(546) && [9.2968],
\end{aligned} \tag{8.1.6}$$

and the matching corrections,

$$\begin{aligned} c_1^{C_A} &= 0.8647(3) && [0.8647], \\ c_1^{T_F} &= -2.2222 \pm 5 \cdot 10^{-5} && [-2.2222], \\ c_2^{T_F^2} &= 2.0139(6) && [2.0139], \\ c_2^{C_F T_F} &= 0.9044(503) && [0.8996], \\ c_2^{C_A T_F} &= -13.7266(689) && [-13.7248], \\ c_2^{C_A^2} &= 3.1948(1677) && [3.1966], \end{aligned} \tag{8.1.7}$$

which are in agreement with the analytic results from [116] for the quark jet function and [146] for the gluon jet function at NNLO shown in the square brackets. We want to point out that all individual sectors have sub-percent accuracy. However, due to the number of sectors and because of large cancellations between different sectors, the total uncertainty of the matching corrections can be at the percent level.

8.2 Angularities

The next observables we looked at are the event-shape angularities [147, 148]. Technically angularities represent a whole class of observables, which can be considered as a generalisation of thrust that depend on a continuous parameter A. According to their standard definition, the angularities are measured with respect to the thrust axis, and they are defined as

$$\omega_{\mathrm{Ang}}(\{k_i\}) = \sum_i \left(k_i^+\right)^{1-A/2} \left(k_i^-\right)^{A/2}, \tag{8.2.1}$$

which reduces to thrust at $A = 0$. In the physical parametrisation they are written as

$$\omega_{\text{Ang}}^{\text{NLO}} = k_T \left(\frac{k_T}{Q}\right)^{1-A} \left(\frac{1}{z_k^{1-A}} + \frac{1}{(1-z_k)^{1-A}}\right), \tag{8.2.2}$$

$$\omega_{\text{Ang,A}}^{\text{NNLO}} = q_T \left(\frac{q_T}{Q}\right)^{1-A} \left(\frac{a^{\frac{A}{2}}\left(a^{1-A}+b\right)}{z_k^{1-A}(1+ab)^{\frac{A}{2}}(a+b)^{1-\frac{A}{2}}} + \frac{a^{1-\frac{A}{2}}}{(1-z_k)^{1-A}} \left(\frac{(1-b)^2+4b(1-t)}{(a+b)(1+ab)}\right)^{1-\frac{A}{2}}\right), \tag{8.2.3}$$

$$\omega_{\text{Ang,B}}^{\text{NNLO}} = q_T \left(\frac{q_T}{Q}\right)^{1-A} \left(\frac{a^{\frac{A}{2}}\left(1+ba^{1-A}\right)}{z_k^{1-A}(a+b)^{\frac{A}{2}}(1+ab)^{1-\frac{A}{2}}} + \frac{a^{1-\frac{A}{2}}}{(1-z_k)^{1-A}} \left(\frac{(1-b)^2+4b(1-t)}{(a+b)(1+ab)}\right)^{1-\frac{A}{2}}\right). \tag{8.2.4}$$

For values of $A < 1$ considered in this work, the angularities fall into the SCET_I class with $n = 1-A$. The non-cusp anomalous dimension can be checked via the consistency relation as both hard and soft anomalous dimensions are known. In [149] even the matching coefficients for quark jet function were extracted, using an `EVENT2` [150, 151] fixed-order calculation.[1]

In figures 8.2.1(a) and 8.2.2(a) we can see that the two-loop non-cusp anomalous dimension from our calculation agrees well with the expected value from the consistency relation. Similarly, in the case of the quark jet function c_1 matching correction, in figure 8.2.1(b), we find that our computation is in agreement with the numerical calculation in [149]. The two loop matching coefficient for the quark case is known approximately through an `EVENT2` extraction [149]. We compare these against our direct calculation for $A = [-1, -0.75, -0.5, -0.25, 0, 0.25, 0.5]$ and find a deviation as large as 3.9σ for $C_F T_F$ color structure as shown in figure 8.2.1(c). In the case of the C_F^2 colour structure, shown in figure 8.2.1(d), we find that most values lie within 1σ. The values for $A = -0.75$ and $A = 0.25$ have a larger deviation of 1.6σ. While the value for $A = 0.5$ has a deviation of 4.7σ. Finally, in the case of the $C_F C_A$ colour structure we observe deviations of as large as 3σ for $A < 0.5$ and even 5.5σ for $A = 0.5$. These results are shown in 8.2.1(e). The source of the large deviation for $A = 0.5$ for all colour structures lies in the extraction of the matching corrections from the `EVENT2` fit. The source of this problem is discussed in [149]. In general, this shows that the fit extraction in [149] is insufficient to obtain the correct c_2 values, and a direct calculation is essential to obtain the correct result

[1] The values for $c_2^{C_F^2}$ and $c_2^{C_F C_A}$ are updated quad precision numbers of [149]. They were obtained from private correspondence with the authors.

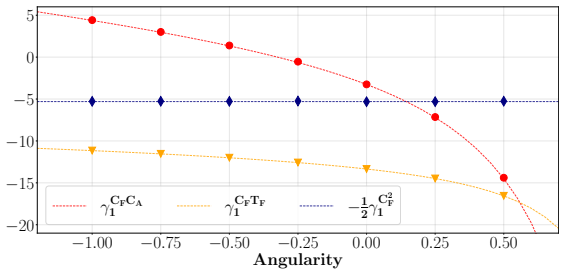

(a) Two-loop non-cusp anomalous dimension compared to the expected value from consistency relation. The uncertainty for the later is negligible.

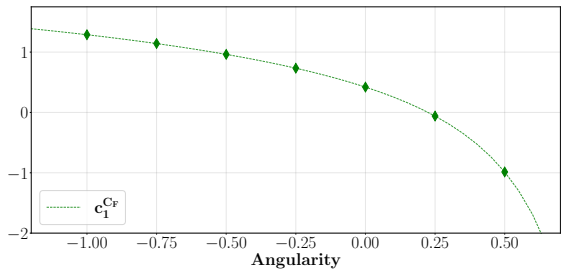

(b) Matching correction c_1 is compared against the numerical calculation in [149]. The uncertainty for the later is negligible.

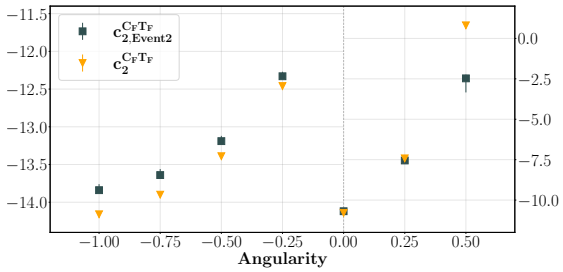

(c) Matching correction $c_2^{C_F T_F}$ compared to the extraction of `EVENT2` fit.

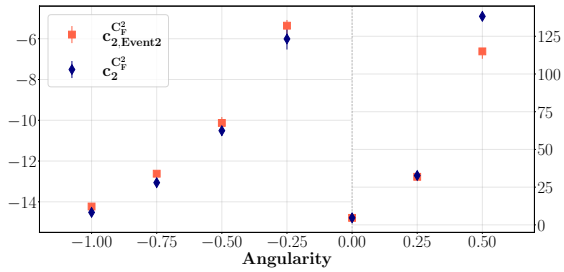

(d) Matching correction $c_2^{C_F^2}$ compared to the extraction of `EVENT2` fit.

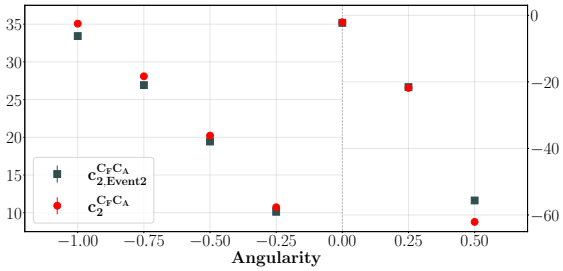

(e) Matching correction $c_2^{C_F C_A}$ compared to the extraction of `EVENT2` fit.

Figure 8.2.1: Two-loop non-cusp anomalous dimension and c_1 and c_2 matching corrections for the angularity quark jet function. The calculations were performed for the angularity values $A = [-1, -0.75, -0.5, -0.25, 0, 0.25, 0.5]$.

as it is done in this work. Finally, we also computed the matching corrections to the gluon jet function angularities which have not been determined before. Our results, are shown in figure 8.2.2(c).

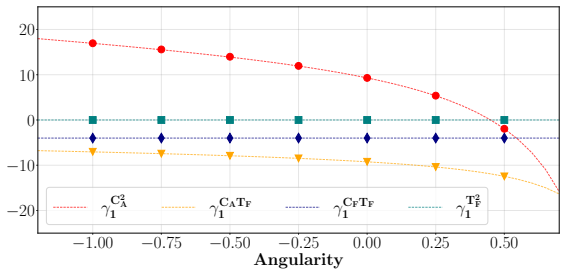

(a) Two-loop non-cusp anomalous dimension compared to the expected value from consistency relation. The uncertainty for the later is negligible.

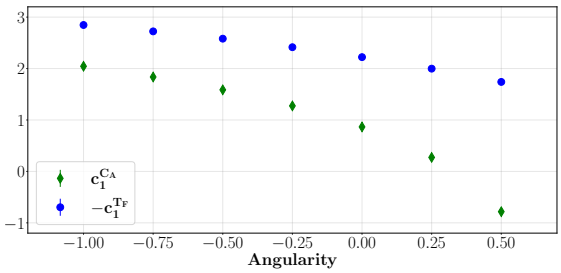

(b) Matching corrections $c_1^{C_A}$ and $c_1^{T_F}$.

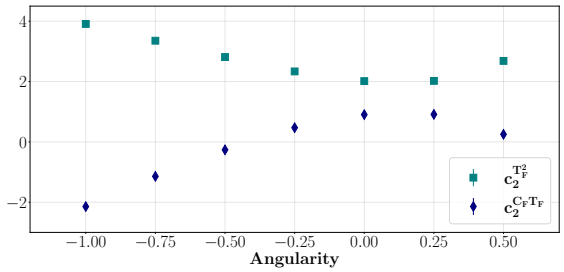

(c) Matching corrections $c_2^{T_F^2}$ and $c_2^{C_F T_F}$.

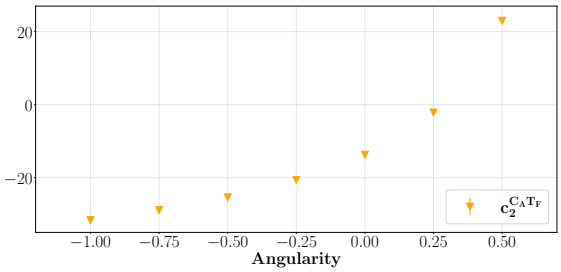

(d) Matching correction $c_2^{C_A T_F}$.

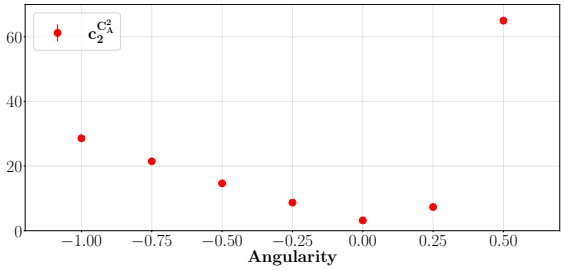

(e) Matching correction $c_2^{C_A^2}$.

Figure 8.2.2: Two-loop non-cusp anomalous dimension and c_1 and c_2 matching corrections for the angularity gluon jet function. The calculations were performed for the angularity values $A = [-1, -0.75, -0.5, -0.25, 0, 0.25, 0.5]$.

8.3 Transverse Thrust

The last SCET_I observable we investigated is the hadronic event-shape variable transverse thrust [152, 153]. The measurement function in light-cone components is given by

$$\omega_{\text{TT}}(\{k_i\}) = 4 s_\theta \sum_i \left(\left| \vec{k}_i^{\top} \right| - \left| \vec{n}_\top \cdot \vec{k}_i^{\top} \right| \right), \tag{8.3.1}$$

where $s_\theta = \sin\theta_B$ describes the angle between the beam and the jet axis. The decomposition into our light-cone coordinates is more involved, since the components $k_\perp^\mu$ transverse to the thrust axis differ from the components $k_\top^\mu$ in eq. (8.3.1) that are

transverse to the beam axis.

We find that in our parametrisation the NLO measurement function is

$$\omega_{\mathrm{TT}}^{\mathrm{NLO}}(\{k_i\}) = k_T \left(\frac{k_T}{Q}\right) \left(\frac{16 s_\theta t_k \bar{t}_k}{z_k(1-z_k)}\right), \tag{8.3.2}$$

such that $n = 1$, and at NNLO we find

$$\begin{aligned}\omega_{\mathrm{TT,A}}^{\mathrm{NNLO}}(\{k_i\}) = q_T \left(\frac{q_T}{Q}\right) \frac{16 s_\theta}{z\bar{z}(1+ab)(a+b)} \Big[& t_k^{\pm}\bar{t}_k^{\pm} b(1+ab-z) + t_l \bar{t}_l a(1+ab\bar{z}) \\ & + (t_k^{\pm} + t_l - t_{kl} - 2t_k^{\pm} t_l) abz \Big],\end{aligned} \tag{8.3.3}$$

$$\begin{aligned}\omega_{\mathrm{TT,B}}^{\mathrm{NNLO}}(\{k_i\}) = q_T \left(\frac{q_T}{Q}\right) \frac{16 s_\theta}{z\bar{z}(1+ab)(a+b)} \Big[& t_k^{\pm}\bar{t}_k^{\pm} ba(a\bar{z}+b) + t_l \bar{t}_l (a+b\bar{z}) \\ & + (t_k^{\pm} + t_l - t_{kl} - 2t_k^{\pm} t_l) abz \Big],\end{aligned} \tag{8.3.4}$$

where $t_k^{\pm} = t_l + t_{kl} - 2t_l t_{kl} \pm 2\sqrt{t_l \bar{t}_l t_{kl} \bar{t}_{kl}}(1 - t_5)$.

Thus we find for the quark jet function:

$$\begin{aligned}
\Gamma_0^{C_F} &= 4 \pm 3 \cdot 10^{-5} && [4], & \gamma_0^{C_F} &= 3 \pm 9 \cdot 10^{-4} && [3], \\
\Gamma_1^{C_F T_F} &= -8.8884(11) && [-8.8889], & \gamma_1^{C_F T_F} &= -21.0857(91) && [-20^{+3}_{-2}][-21.0917(25)], \\
\Gamma_1^{C_F^2} &= -0.0143(435) && [0], & \gamma_1^{C_F^2} &= 10.8048(1690) && [10.6102], \\
\Gamma_1^{C_F C_A} &= 16.6380(364) && [16.6183], & \gamma_1^{C_F C_A} &= 83.6726(1558) && [78^{+30}_{-20}][83.77(3)],
\end{aligned} \tag{8.3.5}$$

and the corresponding matching corrections,

$$\begin{aligned}
c_1^{C_F} &= -6.1595(3) \\
c_2^{C_F T_F} &= -5.9106(340) \\
c_2^{C_F^2} &= 42.5481(5921) \\
c_2^{C_F C_A} &= 116.6630(6068).
\end{aligned} \tag{8.3.6}$$

Similarly we calculate the anomalous dimensions for the gluon jet function:

$$\begin{aligned}
\Gamma_0^{C_A} &= 4 \pm 3 \cdot 10^{-5} \;\; [4], & \gamma_0^{C_A} &= 3.6666 \pm 1 \cdot 10^{-5} \;\; [3.6666], \\
\Gamma_0^{T_F} &= 0 \qquad\qquad\;\; [0], & \gamma_0^{T_F} &= -1.3333 \pm 1 \cdot 10^{-5} [-1.3333], \\
\Gamma_1^{T_F^2} &= 0 \pm 1 \cdot 10^{-4} \;\; [0], & \gamma_1^{T_F^2} &= 0 \pm 6 \cdot 10^{-4} \qquad [0], \\
\Gamma_1^{C_F T_F} &= 0 \pm 4 \cdot 10^{-3} \;\; [0], & \gamma_1^{C_F T_F} &= -3.9966(252) \qquad [-4], \\
\Gamma_1^{C_A T_F} &= -8.8949(85) \; [-8.8889], & \gamma_1^{C_A T_F} &= -16.9532(429) \qquad [-16.3^{+1.5}_{-1.0}] [-16.9853(25)], \\
\Gamma_1^{C_A^2} &= 16.6180(513) [16.6183], & \gamma_1^{C_A^2} &= 96.3293(2079) \qquad [91^{+15}_{-10}] [96.33(3)], \qquad (8.3.7)
\end{aligned}$$

and the matching corrections,

$$\begin{aligned}
c_1^{C_A} &= -5.7150(3), \\
c_1^{T_F} &= -2.2222 \pm 5 \cdot 10^{-5}, \\
c_2^{T_F^2} &= 7.8626(5), \\
c_2^{C_F T_F} &= -47.2099(1162) \\
c_2^{C_A T_F} &= 30.6910(1921), \\
c_2^{C_A^2} &= 172.9177(8147). \qquad (8.3.8)
\end{aligned}$$

In the case of the non-cusp anomalous dimension at NNLO, we can compare our results against two different sources. The first source is [152, 153] where the authors extracted the non-cusp anomalous dimension via a fixed-order code. The second source is to check against the consistency relations from the hard and soft non-cusp anomalous dimension [42].

We find for all cusp and non-cusp anomalous dimensions agreement between our computation and the expected results from the literature. As the matching corrections are still unknown in the literature we present these results for the first time in this work.

8.4 Winner-take-all-axis broadening

The last observable we investigated in this work is the winner-take-all (WTA)-axis broadening. This observable is of the SCET_{II} type and thus $n = 0$. In order to study this observable we first have to understand the WTA axis [93, 154].

The WTA axis $\vec{n}$ is defined by a certain pair-wise recombination scheme, like the k_T-

algorithm. The recombination scheme determines how two pseudo-jets will be merged to form a combined pseudo-jet. The direction of this combined pseudo-jet is given by its most energetic constituent. When used with an IRC safe clustering measure, the WTA scheme is IRC safe [154].

At NLO the most energetic particle will set the axis because we have a two particle final-state and we cannot cluster any particles together. At NNLO this is not true anymore and we have to determine a recombination scheme. The clustering algorithm we choose in our calculation of the WTA axis is the k_T-algorithm for e^+e^- collisions [155] with the distance measure,

$$d_{ij} = \frac{2\min\left(E_i^2, E_j^2\right)\left(1-\cos\hat{\theta}_{ij}\right)}{R}, \tag{8.4.1}$$

where $E_{i,j}$ are the energies of the two particles, $\hat{\theta}_{ij}$ is the physical angle between the particles and R is the radius parameter. In the WTA scheme the parameter R is not important because we only want to find the relative distance between all final-state particles and thus we can set $R = 1$. In light-cone coordinates this distance measure d_{kp} for particles k and p is written as

$$d_{kp} = \min\left(|k_{\perp p}|^2, |p_{\perp k}|^2\right), \tag{8.4.2}$$

where

$$|k_{\perp p}|^2 = \frac{k_-^2 p_T^2 + p_-^2 k_T^2 - 2k_- p_- k_T p_T \cos\theta_{kl}}{p_-^2}, \tag{8.4.3}$$

$$|p_{\perp k}|^2 = \frac{k_-^2 p_T^2 + p_-^2 k_T^2 - 2k_- p_- k_T p_T \cos\theta_{kl}}{k_-^2}. \tag{8.4.4}$$

At NNLO we also require d_{kl} and d_{lp}, which have similar expressions as eq. (8.4.2).

The WTA-axis at NNLO is then determined in the following way. First, we calculate the distance measures d_{kp}, d_{kl} and d_{lp} and take the minimum. Let us suppose that d_{kp} is the minimum. We cluster particles k and p together to create the new pseudo particle q with energy $q_- = k_- + p_-$. We then compare the energies between the new pseudo particle and the remaining particle l. If the energy of l is larger than that of q, it will set the axis $\vec{n}_l$. On the other hand if the energy of q is larger than l, we have to compare the energies of the pseudo particle constituents. The more energetic particle of the two will set the axis. We have shown this setup graphically for NNLO in figure 8.4.1.

The broadening is now determined by the projection of the particles transverse mo-

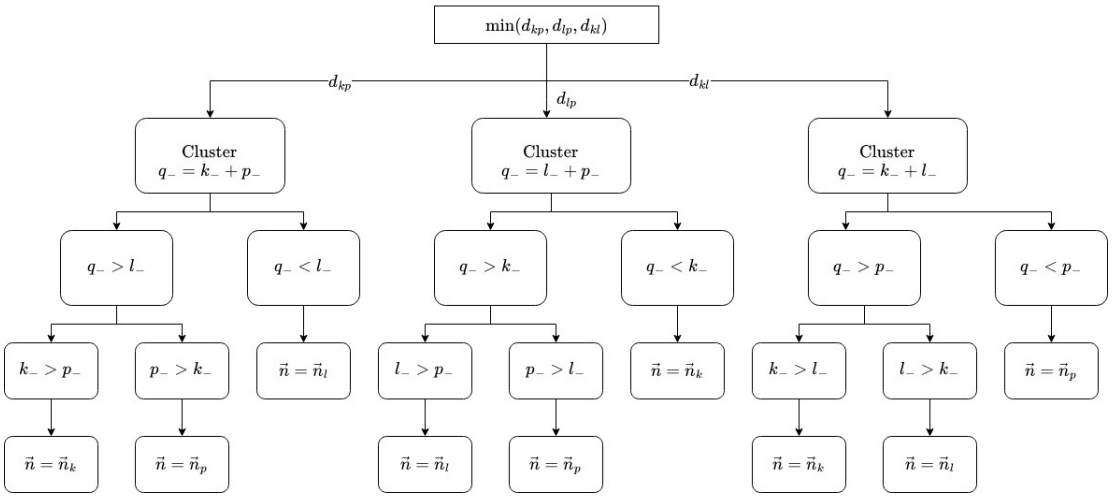

Figure 8.4.1: Determination of WTA axis at NNLO.

mentum onto the corresponding axis. At NLO we find that the measurement function is given by

$$\omega_{\mathrm{WTAB}}^{\mathrm{NLO}}(\{k_i\}) = k_T \min\left(\frac{1}{z}, \frac{1}{\bar{z}}\right), \tag{8.4.5}$$

and at NNLO

$$\omega_{\mathrm{WTAB}}^{\mathrm{NNLO}}(\{k_i\}) = \begin{cases} F_k = |l_{\perp k}| + |p_{\perp k}| & , \vec{n} = \vec{n}_k \\ F_l = |k_{\perp l}| + |p_{\perp l}| & , \vec{n} = \vec{n}_l \\ F_P = |k_{\perp p}| + |l_{\perp p}| & , \vec{n} = \vec{n}_p \end{cases}, \tag{8.4.6}$$

where the expressions are similar to eqs. (8.4.3) and (8.4.4). In the physical parametri-

sation for regions A and D we find

$$\begin{aligned}
F_{k,A} =& \sqrt{\frac{q_T^2}{a(a+b)(1+ab)}} \left(\sqrt{\bar{a}^2 + 4at} \right. \\
&\left. + \frac{1}{z} \sqrt{a^2 z^2 (\bar{b}^2 + 4b\bar{t}) + \bar{z}^2 (1+ab)^2 + 2az\bar{z}(1+ab)(1+b-2t)} \right), \\
F_{l,A} =& \sqrt{\frac{aq_T^2}{(a+b)(1+ab)}} \left(b\sqrt{\bar{a}^2 + 4at} \right. \\
&\left. + \frac{1}{z} \sqrt{z^2 (\bar{b}^2 + 4b\bar{t}) + \bar{z}^2 (1+ab)^2 + 2z\bar{z}(1+ab)(1+b(1-2t))} \right), \\
F_{p,A} =& \sqrt{\frac{aq_T^2}{(a+b)(1+ab)^3}} \frac{b}{\bar{z}} \left(\sqrt{a^2 z^2 (\bar{b}^2 + 4b\bar{t}) + \bar{z}^2 (1+ab)^2 + 2az\bar{z}(1+ab)(1+b-2t)} \right. \\
&\left. + \frac{1}{b} \sqrt{z^2 (\bar{b}^2 + 4b\bar{t}) + \bar{z}^2 (1+ab)^2 + 2z\bar{z}(1+ab)(1+b(1-2t))} \right).
\end{aligned} \tag{8.4.7}$$

Similarly, the measurement function in regions B and C is

$$\begin{aligned}
F_{k,B} =& \sqrt{\frac{q_T^2}{a(a+b)(1+ab)}} \left(b\sqrt{\bar{a}^2 + 4at} \right. \\
&\left. + \frac{1}{z} \sqrt{a^2 z^2 (\bar{b}^2 + 4b\bar{t}) + \bar{z}^2 (a+b)^2 + 2az\bar{z}(a+b)(1+b(1-2t))} \right), \\
F_{l,B} =& \sqrt{\frac{aq_T^2}{(a+b)(1+ab)}} \left(\sqrt{\bar{a}^2 + 4at} \right. \\
&\left. + \frac{1}{z} \sqrt{z^2 (\bar{b}^2 + 4b\bar{t}) + \bar{z}^2 (a+b)^2 + 2z\bar{z}(1+ab)(1+b-2t)} \right), \\
F_{p,B} =& \sqrt{\frac{aq_T^2}{(a+b)(1+ab)^3}} \frac{b}{\bar{z}} \left(\sqrt{z^2 (\bar{b}^2 + 4b\bar{t}) + \bar{z}^2 (a+b)^2 + 2z\bar{z}(a+b)(1+b-2t)} \right. \\
&\left. + \frac{1}{b} \sqrt{a^2 z^2 (\bar{b}^2 + 4b\bar{t}) + \bar{z}^2 (a+b)^2 + 2az\bar{z}(a+b)(1+b(1-2t))} \right).
\end{aligned} \tag{8.4.8}$$

As the WTA broadening is a $\mathrm{SCET_{II}}$ observable, the first quantity we can calculate is the anomaly exponent. This can be checked by comparing our result against the corresponding soft function, which we obtain from `SoftSERVE`. In the case of the quark

jet function, we find

$$\begin{aligned} d_1^{C_F} &= 0 \pm 3 \cdot 10^{-7} && [0], \\ d_2^{C_F T_F} &= -18.7368(8) && [-18.7371(2)], \\ d_2^{C_F^2} &= -0.1175(2303) && [0], \\ d_2^{C_F C_A} &= 15.9504(1540) && [15.9810(13)], \end{aligned} \tag{8.4.9}$$

and for the gluon jet function we obtain

$$\begin{aligned} d_1^{C_A} &= 0 \pm 3 \cdot 10^{-7} && [0], \\ d_1^{T_F} &= 0 && [0], \\ d_2^{T_F^2} &= 0 && [0], \\ d_2^{C_F T_F} &= 0 && [0], \\ d_2^{C_A T_F} &= -18.7365(65) && [-18.7371(2)], \\ d_2^{C_A^2} &= 15.9763(148) && [15.9810(18)]. \end{aligned} \tag{8.4.10}$$

At the level of the remainder function W we can extract the same quantities as for $\mathrm{SCET_I}$ observables. We obtain for the quark remainder function

$$\begin{aligned} \Gamma_0^{C_F} &= 4 \pm 3 \cdot 10^{-8} && [4], && \gamma_0^{C_F} &= 6 \pm 1 \cdot 10^{-5} && [6], \\ \Gamma_1^{C_F T_F} &= -8.8889(2) && [-8.8889], && \gamma_1^{C_F T_F} &= -22.7902(12) && [-22.7891], \\ \Gamma_1^{C_F^2} &= -0.0384(347) && [0], && \gamma_1^{C_F^2} &= 21.3426(1110) && [21.2203], \\ \Gamma_1^{C_F C_A} &= 16.5961(368) && [16.6183], && \gamma_1^{C_F C_A} &= 9.2890(1090) && [9.2742], \end{aligned} \tag{8.4.11}$$

and the matching corrections,

$$\begin{aligned} c_1^{C_F} &= -27.2164 \pm 5 \cdot 10^{-5}, \\ c_2^{C_F T_F} &= 62.9577(33), \\ c_2^{C_F^2} &= 511.0941(2980), \\ c_2^{C_F C_A} &= -240.4355(2738). \end{aligned} \tag{8.4.12}$$

Similarly, we calculated the following anomalous dimensions for the gluon remainder

function:

$$\begin{aligned}
\Gamma_0^{C_A} &= 4 \pm 3 \cdot 10^{-8} \quad [4], & \gamma_0^{C_A} &= 7.3333 \pm 5 \cdot 10^{-6} \quad [7.3333], \\
\Gamma_0^{T_F} &= 0 \quad [0], & \gamma_0^{T_F} &= -2.6667 \pm 2 \cdot 10^{-6} \quad [-2.6667], \\
\Gamma_1^{T_F^2} &= 0 \pm 3 \cdot 10^{-5} \quad [0], & \gamma_1^{T_F^2} &= 0 \pm 3 \cdot 10^{-4} \quad [0], \\
\Gamma_1^{C_F T_F} &= 0.0004(97) \quad [0], & \gamma_1^{C_F T_F} &= -7.9967(401) \quad [-8], \\
\Gamma_1^{C_A T_F} &= -8.8891(48) \quad [-8.8889], & \gamma_1^{C_A T_F} &= -14.5780(257) \quad [14.5765], \\
\Gamma_1^{C_A^2} &= 16.6280(201) \quad [16.6183], & \gamma_1^{C_A^2} &= 34.3346(260) \quad [34.3882], \qquad (8.4.13)
\end{aligned}$$

and matching corrections,

$$\begin{aligned}
c_1^{C_A} &= -28.5093(1), \\
c_1^{T_F} &= -0.0810(1), \\
c_2^{T_F^2} &= 17.4352(1), \\
c_2^{C_F T_F} &= -85.2223(576) \\
c_2^{C_A T_F} &= 135.9650(214), \\
c_2^{C_A^2} &= 293.9550(708). \qquad (8.4.14)
\end{aligned}$$

8.5 Possible extensions

By implementing our master formulae into `pySecDec` we are capable of computing jet functions for a wide range of observables. Nevertheless some areas where we can extend our framework are :

- A standalone `C++` code. `pySecDec` is tailored to factorise divergences from generic products of polynomials by sector decomposition. However we perform all sector decomposition steps in a `Mathematica` code and only feed factorised divergences into the program. So we only use `pySecDec` for its Laurent expansion and subsequent numerical integration. Thus a standalone `C++` code with already Laurent expanded master formulae will reduce the evaluation time. Additionally, we can manipulate the expression in a way that the subsequent numerical integration can be done faster and with better rate of convergence.

- Other collinear resummation ingredients. In this work, we exclusively dealt with jet functions that describe final-state collinear radiation. However, there are other

collinear resummation ingredients like beam functions, which describe initial-state collinear radiation. The corresponding matrix element is related to the splitting function via crossing symmetries. The divergence structure of the beam functions are similar to the ones for the jet functions and we already developed a similar framework for the computation of beam functions. We have already presented first results for the beam functions within this framework in [46–48].

Chapter 9

Conclusion

Precision measurements in collider experiments are very important in the search for new physics and the validation of the SM. From a theoretical point of view, many collider observables suffer from large Sudakov logarithms due to the radiation of soft and collinear particles. The occurrence of these logarithms spoils the convergence of perturbation theory and must therefore be resummed to all orders.

The computation of jet anomalous dimensions and matching coefficients, which can be extracted from NNLO jet functions, is an essential step for the resummation of Sudakov logarithms to NNLL$'$ accuracy within the SCET framework. So far most of these calculations were performed analytically on a case-by-case basis.

In this thesis, we have constructed a new formalism for the automated numerical computation of NNLO quark and gluon jet functions for a broad class of observables. This formalism is based on the fact that the origin of all occurring divergences is linked only to the matrix element describing the emission of collinear radiation.

We set up a generic framework for NNLO jet functions starting from their operator definitions. In the process, we checked that the matrix elements are proportional to the standard double- and triple-collinear splitting functions. By comparing to the soft functions, we have identified the restrictions that an observable needs to obey to be computable in our approach. Due to the complicated divergence structure of the underlying collinear matrix elements, we encountered many overlapping singularities in the real-real contribution, which we disentangled with the help of a mixed strategy based on sector decomposition, non-linear transformations, and selector functions. As a result, we formulated master formulae in which all poles are exposed in monomial form.

On the level of the measurement function, we discussed some of the implications of

infrared-collinear safety. Additionally, we have also shown the challenges induced by the measurement function when the momentum modes scale non-homogeneously and provided a solution to this problem.

We have implemented the master formulae in the open-source program `pySecDec` for both SCET_I and SCET_II observables. We have furthermore shown why our ansatz for the parametrisation fails in a numerical integrator due to integrable divergences and provided a strategy to cure this problem by introducing more suitable parametrisations.

Finally, we validated our approach by recomputing the thrust jet functions, which are known analytically for both the quark and the gluon case. We furthermore applied the novel framework to various classes of observables, which include SCET_I and SCET_II jet functions, observables with a non-trivial azimuthal dependence and those that involve the action of a jet algorithm. While the anomalous dimensions for all of these observables were known, our predictions for the finite matching corrections are new. Due to the breadth of our approach, we expect that many further jet functions will be computed with our framework in the future.

This thesis represents a step towards the complete automation of resummations at NNLL$'$ accuracy, as it shows how to compute one of the last important and computationally challenging ingredients, which may finally result in automated computational tools to be used for precision phenomenological analyses at the LHC.

Appendix A

Anomalous Dimensions

The coefficients of the beta function up to two-loop order in $\overline{\text{MS}}$ scheme are given by [98, 99]

$$\beta_0 = \frac{11}{3}C_A - \frac{4}{3}T_F n_f, \tag{A.0.1}$$

$$\beta_1 = \frac{34}{3}C_A^2 - \left(\frac{20}{3}C_A + 4C_F\right)T_F n_f. \tag{A.0.2}$$

The cusp anomalous dimension coefficients are given up to two-loop order [97, 109]

$$\Gamma^q_{\text{Cusp}} = \Gamma_n C_F, \quad \Gamma^g_{\text{Cusp}} = \Gamma_n C_A, \quad (\text{for } n = 0, 1),$$

$$\Gamma_0 = 4, \tag{A.0.3}$$

$$\Gamma_1 = \frac{4}{3}\left((4-\pi^2)C_A + 5\beta_0\right). \tag{A.0.4}$$

The $\overline{\text{MS}}$ scheme non-cusp anomalous dimensions for the hard functions can be obtained from the infrared divergences of on-shell form factors, which are given up to two-loop order [156, 157],

$$\gamma_0^{q,H} = -6C_F, \tag{A.0.5}$$

$$\gamma_0^{g,H} = -2\beta_0, \tag{A.0.6}$$

$$\gamma_1^{q,H} = -C_F\left[\left(\frac{82}{9} - 52\zeta_3\right)C_A + \left(3 - 4\pi^2 + 48\zeta_3\right)C_F + \left(\frac{65}{9} + \pi^2\right)\beta_0\right], \tag{A.0.7}$$

$$\gamma_1^{g,H} = 2C_A\left[C_A\left(-\frac{59}{9} + 2\zeta_3\right) + \beta_0\left(-\frac{19}{9} + \frac{\pi^2}{6}\right)\right] - 2\beta_1. \tag{A.0.8}$$

The non-cusp anomalous dimensions for the thrust jet function are given [116, 146]

explicitly by

$$\gamma_0^{q,\text{Thrust},J} = 3C_F, \tag{A.0.9}$$

$$\gamma_0^{g,\text{Thrust},J} = \beta_0, \tag{A.0.10}$$

$$\gamma_1^{q,\text{Thrust},J} = C_F\Bigg[\left(\frac{1769}{54}+\frac{11}{9}\pi^2-40\zeta_3\right)C_A+\frac{1}{2}\left(3-4\pi^2+48\zeta_3\right)C_F - \frac{2}{27}\left(121+6\pi^2\right)T_F n_f\Bigg], \tag{A.0.11}$$

$$\gamma_1^{g,\text{Thrust},J} = \left(\frac{1096}{27}-\frac{11}{9}\pi^2-16\zeta_3\right)C_A^2+\left(-\frac{368}{27}+\frac{4}{9}\pi^2\right)C_A T_F n_f - 4C_F T_F n_f. \tag{A.0.12}$$

The non-cusp soft anomalous dimension is then given by the consistency relation in (4.5.17).

Appendix B

Decomposition of splitting functions

The splitting functions introduced in sections 6 have a rich divergence structure therefore it is easier to separate them further into manageable pieces, according to the divergences and invariant masses present.

Let us start with the $P^{(1)}_{q\to gq}(s,z_k)$ in (6.2.7), we can split it in the following decomposition

$$P^{(1)}_{q\to gq}(s,z_k) = P^{(1),A}_{q\to gq}C_F^2 + P^{(1),B}_{q\to gq}C_F\left(C_F - \frac{C_A}{2}\right) + P^{(1),C}_{q\to gq}C_FC_A + P^{(1),D}_{q\to gq}C_FC_A, \quad \text{(B.0.1)}$$

where the indivual terms are

$$\begin{aligned}
P^{(1),i}_{q\to gq} &= \left(\frac{\mu^2 e^{\gamma_E}}{s}\right)^{\epsilon}\frac{2}{(4\pi)^2}\frac{\pi\Gamma(1-\epsilon)}{\epsilon\tan(\pi\epsilon)\Gamma(1-2\epsilon)}\tilde{P}^{(1),i}_{q\to gq},\\
\tilde{P}^{(1),A}_{q\to gq} &= \left(\frac{1+\bar{z}_k^2-\epsilon z_k^2}{z_k}\right)\left(2-\frac{\epsilon^2}{1-2\epsilon}\right)+\frac{\bar{z}_k(2-z_k)\epsilon^2}{(1-2\epsilon)z_k},\\
\tilde{P}^{(1),B}_{q\to gq} &= -2\left(\frac{1+\bar{z}_k^2-\epsilon z_k^2}{z_k}\right){}_2F_1\left(1,-\epsilon;1-\epsilon;\frac{z_k}{z_k-1}\right),\\
\tilde{P}^{(1),C}_{q\to gq} &= \left(\frac{1+\bar{z}_k^2-\epsilon z_k^2}{z_k}\right)\left(-1+\frac{\epsilon^2}{1-2\epsilon}\right)-\frac{\bar{z}_k(2-z_k)\epsilon^2}{(1-2\epsilon)z_k},\\
\tilde{P}^{(1),D}_{q\to gq} &= -\left(\frac{1+\bar{z}_k^2-\epsilon z_k^2}{z_k}\right){}_2F_1\left(1,-\epsilon;1-\epsilon;\frac{z_k-1}{z_k}\right).
\end{aligned}$$

The splitting functions $P^{(1)}_{g\to q\bar{q}}(s,z_k)$ and $P^{(1)}_{g\to gg}(s,z_k)$ in (6.2.10) and (6.2.11) can be

decomposed in a similar fashion;

$$P^{(1)}_{g\to q\bar{q}}(s,z_k) = P^{(1),A}_{g\to q\bar{q}}T_F^2 n_f^2 + P^{(1),B}_{g\to q\bar{q}}C_F T_F n_f + \left(P^{(1),C}_{g\to q\bar{q}} + P^{(1),D}_{g\to q\bar{q}}\right) C_A T_F n_f, \tag{B.0.2}$$

$$P^{(1)}_{g\to gg}(s,z_k) = \left(P^{(1),A}_{g\to gg} + P^{(1),B}_{g\to gg}\right) C_A^2 + P^{(1),C}_{g\to gg}C_A T_F n_f, \tag{B.0.3}$$

where the terms are given by

$$\begin{aligned}
P^{(1),i}_{g\to kl} &= \left(\frac{\mu^2 e^{\gamma_E}}{s}\right)^{\epsilon} \frac{2}{(4\pi)^2}\frac{\pi\Gamma(1-\epsilon)}{\epsilon\tan(\pi\epsilon)\Gamma(1-2\epsilon)}\tilde{P}^{(1),i}_{g\to kl} \\
,\tilde{P}^{(1),A}_{g\to q\bar{q}} &= \frac{z_k^2+\bar{z}_k^2-\epsilon}{1-\epsilon}\left(2\frac{2(\epsilon-1)\epsilon}{4(\epsilon-2)\epsilon+3}\right), \\
\tilde{P}^{(1),B}_{g\to q\bar{q}} &= \frac{z_k^2+\bar{z}_k^2-\epsilon}{1-\epsilon}\left(\frac{\epsilon(3(1-\epsilon)+2\epsilon^2)-2}{(\epsilon-1)(2\epsilon-1)}\right), \\
\tilde{P}^{(1),C}_{g\to q\bar{q}} &= -2\frac{z_k^2+\bar{z}_k^2-\epsilon}{1-\epsilon}{}_2F_1\left(1,-\epsilon;1-\epsilon;\frac{z_k-1}{z_k}\right), \\
\tilde{P}^{(1),D}_{g\to q\bar{q}} &= \frac{z_k^2+\bar{z}_k^2-\epsilon}{1-\epsilon}\left(2+\frac{3+\epsilon^2(2(\epsilon-2)+(1+2(\epsilon-2)\epsilon))}{(\epsilon-1)(3-2\epsilon)(2\epsilon-1)}\right), \\
\tilde{P}^{(1),A}_{g\to gg} &= \frac{(1-z_k\bar{z}_k)^2}{z_k\bar{z}_k} + \frac{\epsilon^2(1-2\epsilon z_k\bar{z}_k)((\epsilon-1))}{2(1-\epsilon)(\epsilon-1)(2\epsilon-3)(2\epsilon-1)}, \\
\tilde{P}^{(1),B}_{g\to gg} &= -2\frac{(1-z_k\bar{z}_k)^2}{z_k\bar{z}_k}{}_2F_1\left(1,-\epsilon;1-\epsilon;\frac{z_k-1}{z_k}\right), \\
\tilde{P}^{(1),C}_{g\to gg} &= \frac{\epsilon^2(1-2\epsilon z_k\bar{z}_k)}{(1-\epsilon)(\epsilon-1)(2\epsilon-3)(2\epsilon-1)}.
\end{aligned}$$

After showing the decomposition of the splitting functions, which go into the real-virtual structure we turn to the triple collinear splitting functions.

We start with the $C_F T_F n_f$ structure of the quark jet function $P^{(0)}_{q\to\bar{q}'q'q}$ in (6.2.16)

$$P^{(0)}_{q\to\bar{q}'q'q} = P^{A}_{q\to\bar{q}'q'q} + P^{B}_{q\to\bar{q}'q'q}, \tag{B.0.4}$$

where

$$\begin{aligned}
P^{A}_{q\to\bar{q}'q'q} &= -\frac{1}{2}\left(\frac{(z_1(s_{12}+2s_{23})-z_2(s_{12}+2s_{13}))^2}{(z_1+z_2)^2 s_{12}^2 s_{123}^2} + \frac{1-2\epsilon}{s_{123}^2}\right), \\
P^{A}_{q\to\bar{q}'q'q} &= \frac{4z_3+(z_1-z_2)^2}{2s_{12}s_{123}(z_1+z_2)} + (1-2\epsilon)\frac{z_1+z_2}{2s_{12}s_{123}}.
\end{aligned}$$

For the identical piece in (6.2.17) we can decompose it into

$$P^{(0)}_{q\to\bar{q}qq} = P^{A}_{q\to\bar{q}qq} + P^{B}_{q\to\bar{q}qq}, \tag{B.0.5}$$

with

$$\begin{aligned}
P^{A}_{q\to\bar{q}qq} &= \frac{(1-\epsilon)}{s^2_{123}}\left(2\frac{s_{23}}{s_{12}} - \epsilon\right) + \frac{1+z_1^2-\epsilon\bar{z}_3^2}{(1-z_2)s_{123}s_{12}} - \frac{2z_2(1-\epsilon)}{(1-z_3)s_{123}s_{12}} - \frac{\epsilon(1+z_1)-\epsilon^2\bar{z}_3}{s_{123}s_{12}},\\
P^{B}_{q\to\bar{q}qq} &= \frac{-z_1z_3}{s_{12}\bar{z}_2\bar{z}_3(z_3s_{13}+z_2s_{12})}\left(1+z_1^2-\epsilon\left(3z_1+z_2^2+z_2z_3+z_3^2\right)-\epsilon^2\left(z_1+z_2z_3\right)\right).
\end{aligned}$$

The last splitting function for the quark jet function is $P_{q\to ggq}$ in (6.2.18). The decomposition is as follows

$$\begin{aligned}
P^{(0)}_{q\to ggq} = &\left(P^{A}_{q\to ggq} + P^{B}_{q\to ggq} + P^{C}_{q\to ggq}\right)C_F\left(C_F - \frac{C_A}{2}\right) + P^{D}_{q\to ggq}C_F^2\\
&+ \left(P^{E}_{q\to ggq} + P^{F}_{q\to ggq} + P^{G}_{q\to ggq} + P^{H}_{q\to ggq} + P^{I}_{q\to ggq}\right)C_FC_A\\
&- \left(\frac{1-\epsilon}{2}\right)P^{A}_{q\to\bar{q}'q'q}C_FC_A,
\end{aligned} \tag{B.0.6}$$

where we are able to reuse pieces we already calculated before. The individual structures are given by

$$\begin{aligned}
P^{A}_{q\to ggq} &= \frac{z_2}{z_1s_{12}(z_3s_{23}+z_1s_{12})}\left(1+z_2^2-\epsilon(z_1^2+z_3^2)-z_1z_3\epsilon(1+\epsilon)\right),\\
P^{B}_{q\to ggq} &= \frac{z_3}{z_1z_2s_{123}(z_2s_{12}+z_3s_{13})}\left(z_3\bar{z}_1+\bar{z}_2^3-\bar{z}_2(z_1^2+z_1z_2+z_2^2)+z_1z_2(1+z_3)\epsilon^2\right),\\
P^{C}_{q\to ggq} &= \frac{s_{13}}{z_1s_{12}s_{123}(z_3s_{13}+z_2s_{12})}\left(z_2\bar{z}_1+\bar{z}_3^3-\bar{z}_3(z_1^2+z_1z_3+z_3^2)+z_1z_3(1+z_2)\epsilon^2\right),\\
P^{D}_{q\to ggq} &= \frac{1-\epsilon}{s^2_{123}}\left(\epsilon-(1-\epsilon)\frac{s_{12}}{s_{12}}\right),\\
P^{E}_{q\to ggq} &= \frac{1}{2s_{12}\bar{z}_2(z_3s_{13}+z_2s_{12})}\left(\bar{z}_2(2z_2+(1-\epsilon)\bar{z}_2^2)+z_3(2\bar{z}_3+(1-\epsilon)z_3^2)\right),\\
P^{F}_{q\to ggq} &= \frac{z_3}{2s_{12}z_2\bar{z}_3(z_3s_{13}+z_2s_{12})}\left(\bar{z}_3(2z_3+(1-\epsilon)\bar{z}_3^2)+z_2(2\bar{z}_2+(1-\epsilon)z_2^2)\right),\\
P^{G}_{q\to ggq} &= \frac{\left((1-\epsilon)\left(z_1(2-2z_1+z_1^2)-z_2(6-6z_2+z_2^2)\right)+2\epsilon\left(z_3(z_1-2z_2)-z_2\right)\right)}{2s_{12}z_2\bar{z}_3s_{123}},\\
P^{H}_{q\to ggq} &= \frac{z_3\left((1-\epsilon)(\bar{z}_2^3+z_3^2-z_2)-\epsilon(2\bar{z}_2(z_2-z_3))-\epsilon(1-\epsilon)\bar{z}_1\right)}{2s_{123}z_2\bar{z}_3(z_2s_{12}+z_3s_{13})},\\
P^{I}_{q\to ggq} &= \frac{s_{13}\left((1-\epsilon)(\bar{z}_3^3+z_2^2-z_3)-\epsilon(2\bar{z}_3(z_3-z_2))-\epsilon(1-\epsilon)\bar{z}_1\right)}{2s_{12}s_{123}\bar{z}_2(z_2s_{12}+z_3s_{13})}.
\end{aligned}$$

The two splitting functions for the gluon jet function are shown in (6.2.19) and (6.2.22), we decompose them in the following way;

$$P_1 = -2P_1^A + P_1^B + 2P_1^C + P_1^D, \tag{B.0.7}$$

$$P_2 = \left(-\frac{1}{4} + \frac{\epsilon}{2}\right) P_1^A - \frac{1}{4}P_2^A + P_2^B + P_2^C + P_2^D + P_2^E - \frac{1}{2}P_1^C, \tag{B.0.8}$$

$$P^{(0)}_{g\to ggg} = \frac{(1-\epsilon)}{4}P_2^A + \frac{3}{4}(1-\epsilon)P_1^A + P^A_{g\to ggg} + P^B_{g\to ggg} + P^C_{g\to ggg} + P^D_{g\to ggg}. \tag{B.0.9}$$

where the terms are defined via

$$\begin{aligned}
P_1^A &= \frac{1}{s_{123}^2},\\
P_1^B &= -2(1-\epsilon)\frac{s_{23}}{s_{12}s_{123}^2},\\
P_1^C &= \frac{z_3}{s_{12}(z_3 s_{13} + z_2 s_{12})}\left(1 + z_1^2 - \frac{z_1 + 2z_2 z_3}{1-\epsilon}\right),\\
P_1^D &= -2\frac{1}{s_{12}s_{123}}\left(1 + 2z_1 + \epsilon - 2\frac{z_1+z_2}{1-\epsilon}\right),\\
P_2^A &= \frac{t_{21,3}^2}{s_{123}^2 s_{12}^2},\\
P_2^B &= \frac{z_1}{2s_{12}\bar{z}_3(z_3 s_{13} + z_2 s_{12})}\left((1-z_1)^3 - z_1^3 - \frac{2z_1(1-z_1-2z_3z_2)}{(1-\epsilon)}\right),\\
P_2^C &= \frac{z_2 z_3}{2s_{12}\bar{z}_1 z_1(z_1 s_{12} + z_3 s_{23})}\left((1-z_1)^3 - z_1^3 - \frac{2z_2(1-z_2-2z_1z_3)}{(1-\epsilon)}\right),\\
P_2^D &= \frac{\bar{z}_3}{2s_{12}s_{123}}\left(1 + \frac{1}{z_1(1-z_1)} - \frac{2z_3(1-z_3)}{(1-\epsilon)z_1(1-z_1)}\right),\\
P_2^E &= \frac{1}{s_{12}s_{123}}\left(\frac{1+z_3^3}{z_3(1-z_3)} + \frac{z_3(z_2-z_1)^2 - 2z_1z_2(1+z_3)}{(1-\epsilon)z_3(1-z_3)}\right),\\
P^A_{g\to ggg} &= 2\frac{1}{s_{123}s_{12}}\left(4\frac{z_1z_2-1}{1-z_3} + \frac{z_1z_2-2}{z_3} + \frac{3}{2} + \frac{5}{2}z_3\right),\\
P^B_{g\to ggg} &= \frac{z_3}{s_{123}(z_2 s_{12} + z_3 s_{13})}\left(\frac{(1-z_2(1-z_2))^2}{z_2 z_1(1-z_1)}\right),\\
P^C_{g\to ggg} &= \frac{s_{13}}{s_{12}s_{123}(z_2 s_{12} + z_3 s_{13})}\left(\frac{(1-z_3(1-z_3))^2}{z_3 z_1(1-z_1)}\right),\\
P^D_{g\to ggg} &= \frac{z_3}{s_{12}(z_2 s_{12} + z_3 s_{13})}\left(\frac{z_1z_2(1-z_2)(1-2z_3)}{z_3(1-z_3)} + z_2z_3 - 2\right.\\
&\qquad \left. + \frac{z_1(1+2z_1)}{2} + \frac{1+2z_1(1+z_1)}{2(1-z_2)(1-z_3)} + \frac{1-2z_1(1-z_1)}{2z_2z_3}\right) + (2\leftrightarrow 3),
\end{aligned}$$

where we define $t_{ij,k}$ as

$$t_{ij,k} = 2\frac{z_i s_{jk} - z_j s_{ik}}{z_i + z_j} + \frac{z_i - z_j}{z_i + z_j} s_{ij}.$$

Appendix C

Master formulae in physical parametrisation

Here we list the master formulae for the real-real contribution in physical parametrisation. In order to keep the list as compact as possible we will not project the expressions onto the unit hypercube. Thus we can write all expressions in the following way

$$J_i^{\mathrm{RR}}(\tau,\mu,Q) = \left(\frac{\alpha_s}{4\pi}\right)^2 \left(\frac{\mu\bar{\tau}^{\frac{1}{1+n}}}{Q^{\frac{n}{1+n}}}\right)^{4\epsilon} \left(\frac{\nu}{Q}\right)^{2\alpha\delta_{iq}+3\alpha\delta_{ig}} \frac{2^{3-6\epsilon}\Gamma\left(\frac{-4\epsilon}{1+n}\right)}{(1+n)\pi^2\Gamma(-2\epsilon)} e^{2\epsilon\gamma_E\frac{n-1}{n+1}} \int_0^\infty \mathrm{d}a\mathrm{d}b \int_0^1 \mathrm{d}z\mathrm{d}t\mathrm{d}t_l\mathrm{d}t_5' \, (t\bar{t})^{-\frac{1}{2}-\epsilon}(t_l\bar{t}_l)^{-\frac{1}{2}-\epsilon}(t_5'(2-t_5'))^{-1-\epsilon}\Omega^{\frac{4\epsilon}{1+n}}F^{\frac{4\epsilon}{1+n}}\sum_j J_i^{P_j} \tag{C.0.1}$$

where $i \in \{q, g\}$ and $J_i^{P_j}$ are the decompositions of the splitting functions transformed in the physical parametrisation.

So the coefficients for the $C_F T_F n_f$ quark jet functions are

$$J_q^{P^A_{q\to\bar{q}'q'q}} = \frac{(1-z)z^{-1-2\alpha}a^{1-\alpha-2\epsilon}(a+b)^{2\epsilon}b^{1-\alpha-2\epsilon}(1+ab)^{-2+2\alpha+2\epsilon}}{(4at+(1-a)^2)^2\left(az\left(4b(1-t)+(1-b)^2\right)+(1-z)(a+b)(ab+1)\right)^2}$$
$$\Big(2\left(1-a^2\right)z\left(1-a^2b^2\right)\left(4at+(1-a)^2\right)-2\left(1-a^2\right)^2(ab+1)^2$$
$$+\epsilon\left(z^2(ab+1)^2\left(4at+(a-1)^2\right)^2\right)-z^2\left(a^2b^2+1\right)\left(4at+(1-a)^2\right)^2\Big),$$

$$J_q^{P^B_{q\to\bar{q}'q'q}} = \frac{z^{-1-2\alpha}a^{1-\alpha-2\epsilon}(a+b)^{2\epsilon}b^{-\alpha-2\epsilon}(1+ab)^{-2+2\alpha+2\epsilon}}{(4at+(1-a)^2)\left(az\left(4b(1-t)+(1-b)^2\right)+(1-z)(a+b)(ab+1)\right)}$$
$$\left(a^2b^2(2-(2-z)z)-z^2\epsilon(ab+1)^2+4ab(1-z)-(2-z)z+2\right).$$

The coefficients for the identical structure are:

$$J_q^{P^A_{q\to\bar{q}qq}} = \frac{-z^{-2\alpha}a^{1-\alpha-2\epsilon}(a+b)^{2\epsilon}b^{-\alpha-2\epsilon}(1+ab)^{-1+2\alpha+2\epsilon}(1+ab-z)^{-1}}{(4at+(1-a)^2)\left(az\left(4b(1-t)+(1-b)^2\right)+(1-z)(a+b)(ab+1)\right)^2}$$
$$\Big(\left(-a^2b^2\left(z^2+1\right)-2z+1\right)\left(az\left(4b(1-t)+(1-b)^2\right)\right.$$
$$\left.+(1-z)(a+b)(ab+1)\right)-2a(ab-z+1)\left(b^2z^2\left(4at+(a-1)^2\right)\right.$$
$$\left.-2bz(ab+1)(a+2t-1)+(ab+1)^2\right)+\epsilon\Big(\left(a^2b^2\left(z^2+z+1\right)\right.$$
$$\left.+abz^2+z^2+z-1\right)\left(az\left(4b(1-t)+(1-b)^2\right)+(1-z)(a+b)(ab+1)\right)$$
$$\times(ab-z+1)\Big(bz^2(ab-1)\left(4at+(a-1)^2\right)-bz(ab+1)$$
$$\times(a(3a+4t-2)-1)+2a(ab+1)^2\Big)\Big)+\epsilon^2\Big(z(ab+1)(ab-z+1)$$
$$\left.-bz\left(4at+(a-1)^2\right)\Big)+b(z-1)z(ab+1)\left(4at+(a-1)^2\right)(ab-z+1)\Big)\right),$$

$$J_q^{P^B_{q\to\bar{q}qq}} = \frac{-z^{-2\alpha}a^{2-\alpha-2\epsilon}(a+b)^{2\epsilon}b^{-\alpha-2\epsilon}(1+ab)^{-1+2\alpha+2\epsilon}(1+ab-z)^{-1}}{\left(-2z(ab+1)(a(2t-1)+1)+(ab+1)^2+2z^2\left(4at+(a-1)^2\right)\right)}$$
$$\Big(-\epsilon\left(a^2b^2\left(z^2+z+1\right)+ab\left(z^2+2\right)-(1-z)z+1\right)+ab\left(ab\left(z^2+1\right)+2\right)$$
$$-\left(z\epsilon^2(ab+1)(ab-z+1)\right)+1\Big)\left(4at+(1-a)^2\right)^{-1}.$$

The coefficients for the splitting $q \to ggq$ are:

$$
\begin{aligned}
J_q^{P^A_{q\to ggq}} =& \frac{(1-z)^{-1-\alpha} z^{-\alpha} a^{-1-\alpha-2\epsilon}(a+b)^{2\epsilon} b^{-1-\alpha-2\epsilon}(1+ab)^{-1+\alpha+2\epsilon}(4at+(1-a)^2)^{-1}}{2b^2z^2\left(4at+(a-1)^2\right)-2bz(ab+1)(a+2t-1)+(ab+1)^2} \\
& \Big(-\epsilon\left(a^2b^2(1-(1-z)z)+ab(1-z)(2-z)+(1-z)^2\right)-ab(1-z)z \\
& +\epsilon^2(ab+1)+(ab+1)^2+z^2\Big),
\end{aligned}
$$

$$
\begin{aligned}
J_q^{P^B_{q\to ggq}} =& \frac{(1-z)z^{-1-2\alpha} a^{-\alpha-2\epsilon}(a+b)^{2\epsilon} b^{-1-\alpha-2\epsilon}(1+ab)^{2\alpha+2\epsilon}}{az\left(4b(1-t)+(1-b)^2\right)+(1-z)(a+b)(ab+1)} \\
& \left(-2z(ab+1)(a(2t-1)+1)+(ab+1)^2+2z^2\left(4at+(a-1)^2\right)\right)^{-1} \\
& \Big(z^2(ab(ab+1)+3)(ab+1)-2z(ab+2)(ab+1)^2+2(ab+1)^3-z^3 \\
& -\epsilon\Big(z^2(ab(ab+1)+1)(ab-z+1)\Big)+\epsilon^2\Big(ab(2-z)z^2(ab+1)\Big)\Big),
\end{aligned}
$$

$$
\begin{aligned}
J_q^{P^C_{q\to ggq}} =& \frac{(1-z)^{-1-\alpha} z^{-\alpha} a^{-\alpha-2\epsilon}(a+b)^{2\epsilon} b^{-1-\alpha-2\epsilon}(1+ab)^{-1+\alpha+2\epsilon}}{\left(4at+(1-a)^2\right)\left(az\left(4b(1-t)+(1-b)^2\right)+(1-z)(a+b)(ab+1)\right)} \\
& \left(\frac{-2z(ab+1)(a(2t-1)+1)+(ab+1)^2+z^2\left(4at+(a-1)^2\right)}{-2z(ab+1)(a(2t-1)+1)+(ab+1)^2+2z^2\left(4at+(a-1)^2\right)}\right) \\
& \Big(-\epsilon\left(a^2b^2(1-(1-z)z)+ab(1-z)(2-z)+(1-z)^2\right) \\
& +z^2(ab+1)^2+ab(1-z)+1+ab(1-z)\epsilon^2(ab+z+1)\Big),
\end{aligned}
$$

$$
\begin{aligned}
J_q^{P^D_{q\to ggq}} =& \frac{(1-\epsilon)(1-z)^{-\alpha} z^{-\alpha} a^{1-\alpha-2\epsilon}(a+b)^{2\epsilon} b^{-\alpha-2\epsilon}(1+ab)^{-1+\alpha+2\epsilon}}{\left(4at+(1-a)^2\right)\left(az\left(4b(1-t)+(1-b)^2\right)+(1-z)(a+b)(ab+1)\right)^2} \\
& \Big(a\left(-b^2z^2\left(4at+(1-a)^2\right)+2bz(ab+1)(a+2t-1)-(ab+1)^2\right) \\
& +\epsilon\left(\left(1-a^2\right)bz(ab+1)-bz^2\left(4at+(a-1)^2\right)+a(ab+1)^2\right)\Big),
\end{aligned}
$$

$$
\begin{aligned}
J_q^{P^E_{q\to ggq}} =& \frac{(1-z)^{-1-\alpha} z^{-\alpha} a^{1-\alpha-2\epsilon}(a+b)^{2\epsilon} b^{-1-\alpha-2\epsilon}(1+ab)^{\alpha+2\epsilon-1}(1+ab-z)^{-1}}{2\left(-2z(ab+1)(a(2t-1)+1)+(ab+1)^2+2z^2\left(4at+(a-1)^2\right)\right)} \\
& \Big(z^2(ab(ab+2)+2)(ab+1)-z^3(ab+2)(ab(ab+1)+1)-z(ab+2)(ab+1)^2 \\
& +2(ab+1)^3-\epsilon(ab(2-z)+2(1-z))\Big(a^2b^2(1-(1-z)z) \\
& +ab(1-z)(2-z)+(1-z)^2\Big)\left(4at+(1-a)^2\right)^{-1}
\end{aligned}
$$

$$
\begin{aligned}
J_q^{P^F_{q\to ggq}} =& \frac{z^{-1-2\alpha}a^{1-\alpha-2\epsilon}(a+b)^{2\epsilon}b^{-1-\alpha-2\epsilon}(1+ab)^{-1+2\alpha+2\epsilon}\left(4at+(1-a)^2\right)^{-1}}{2\left(-2z(ab+1)(a(2t-1)+1)+(ab+1)^2+2z^2\left(4at+(a-1)^2\right)\right)} \\
&\Big(z^2(ab+2)(ab(ab+1)+1)-2z(ab(ab+2)+2)(ab+1) \\
&+2(ab+2)(ab+1)^2-\left(z^2\epsilon(ab+2)(ab(ab+1)+1)\right)\Big),
\end{aligned}
$$

$$
\begin{aligned}
J_q^{P^G_{q\to ggq}} =& \frac{z^{-1-2\alpha}a^{1-\alpha-2\epsilon}(a+b)^{2\epsilon}b^{-\alpha-2\epsilon}(1+ab)^{-2+2\alpha+2\epsilon}}{2\left(4at+(1-a)^2\right)\left(az\left(4b(1-t)+(1-b)^2\right)+(1-z)(a+b)(ab+1)\right)} \\
&\Big(-z^2\left(1-a^3b^3\right)+2z\left(3-a^2b^2\right)(ab+1)+2(ab-3)(ab+1)^2 \\
&+z\epsilon\left(a^2b^2(2-abz)+z-2\right)\Big),
\end{aligned}
$$

$$
\begin{aligned}
J_q^{P^H_{q\to ggq}} =& \frac{(1-z)z^{-1-2\alpha}a^{1-\alpha-2\epsilon}(a+b)^{2\epsilon}b^{-\alpha-2\epsilon}(1+ab)^{-1+2\alpha+2\epsilon}}{2\left(az\left(4b(1-t)+(1-b)^2\right)+(1-z)(a+b)(ab+1)\right)} \\
&\left(-2z(ab+1)(a(2t-1)+1)+(ab+1)^2+2z^2\left(4at+(a-1)^2\right)\right)^{-1} \\
&\Big(z^2(ab(ab+2)+4)(ab+1)-2z(ab+3)(ab+1)^2+2(ab+1)^3-z^3 \\
&+z^2\epsilon^2(ab+1)(ab(1-z)+1)+z^2\epsilon(ab(ab+1)+1)(ab-z+1)\Big),
\end{aligned}
$$

$$
\begin{aligned}
J_q^{P^I_{q\to ggq}} =& \frac{(1-z)^{-\alpha-1}z^{-\alpha}a^{-\alpha-2\epsilon+1}(a+b)^{2\epsilon}b^{-\alpha-2\epsilon}(ab+1)^{\alpha+2\epsilon-1}}{2\left(4at+(1-a)^2\right)(ab-z+1)} \\
&\left(az\left(4b(1-t)+(1-b)^2\right)+(1-z)(a+b)(ab+1)\right)^{-1} \\
&\left(\frac{-2z(ab+1)(a(2t-1)+1)+(ab+1)^2+z^2\left(4at+(a-1)^2\right)}{-2z(ab+1)(a(2t-1)+1)+(ab+1)^2+2z^2\left(4at+(a-1)^2\right)}\right) \\
&\Big(z^3(ab+1)^2+(z-1)\epsilon^2(ab(z-1)-1)(ab-z+1)+z(ab+1)^2 \\
&-(ab+1)^2+z^2+z\epsilon\left(a^2b^2\left(-z^2+z-1\right)-ab(z-2)(z-1)-(z-1)^2\right)\Big).
\end{aligned}
$$

The coefficients for the $T_F n_f C_F$ colour structure are:

$$J_g^{P_1^A} = \frac{(1-z)^{1-\alpha} z^{1-2\alpha} a^{1-\alpha-2\epsilon} (a+b)^{2\epsilon} b^{1-\alpha-2\epsilon} (1+ab)^{2\alpha+2\epsilon}}{\left(az\left(4b(1-t)+(1-b)^2\right)+(1-z)(a+b)(ab+1)\right)^2},$$

$$J_g^{P_1^B} = -\frac{2(1-\epsilon)(1-z)^{-\alpha} z^{-2\alpha} a^{2-\alpha-2\epsilon} (a+b)^{2\epsilon} b^{-\alpha-2\epsilon} (1+ab)^{2\alpha+2\epsilon-1}}{4at+(1-a)^2} \left(\frac{b^2 z^2\left(4at+(1-a)^2\right)+2bz(ab+1)(-a-2t+1)+(ab+1)^2}{\left(az\left(4b(1-t)+(1-b)^2\right)+(1-z)(a+b)(ab+1)\right)^2}\right),$$

$$\begin{aligned} J_g^{P_1^C} = & \frac{(1-z)^{-\alpha} z^{-2\alpha} a^{1-\alpha-2\epsilon} (a+b)^{2\epsilon} b^{-1-\alpha-2\epsilon} (1+ab)^{-1+2\alpha+2\epsilon}}{(1-\epsilon)\left(4at+(1-a)^2\right)} \\ & \left(-2z(ab+1)(1-a(1-2t))+(ab+1)^2+2z^2\left(4at+(a-1)^2\right)\right)^{-1} \\ & \left(a^2b^2((z-1)z+1)-\epsilon\left(ab\left(ab\left(z^2+1\right)+2\right)+1\right)\right. \\ & \left.+ab(z(2z-3)+2)+2(z-1)z+1\right), \end{aligned}$$

$$J_g^{P_1^D} = -\frac{2(1-z)^{-\alpha} z^{-2\alpha} a^{1-\alpha-2\epsilon} (a+b)^{2\epsilon} b^{-\alpha-2\epsilon} (1+ab)^{-1+2\alpha+2\epsilon}}{(1-\epsilon)\left(4at+(1-a)^2\right)} \left(\frac{-2abz\epsilon-\left(\epsilon^2(ab+1)\right)+ab-2z+1}{az\left(4b(1-t)+(1-b)^2\right)+(1-z)(a+b)(ab+1)}\right).$$

The coefficients for the $T_F n_f C_A$ colour structure are:

$$J_g^{P_2^A} = \frac{(1-z)^{1-\alpha} z^{-1-2\alpha} a^{1-\alpha-2\epsilon} (a+b)^{2\epsilon} b^{1-\alpha-2\epsilon} (1+ab)^{-2+2\alpha+2\epsilon}}{\left(4at+(1-a)^2\right)^2} \left(\frac{\left(2\left(1-a^2\right)(ab+1) - z(1-ab)\left(4at+(1-a)^2\right)\right)^2}{\left(az\left(4b(1-t)+(1-b)^2\right)+(1-z)(a+b)(ab+1)\right)^2} \right),$$

$$\begin{aligned} J_g^{P_2^B} = & -\frac{(1-z)^{-1-\alpha} z^{-2\alpha} a^{2-\alpha-2\epsilon} (a+b)^{2\epsilon} b^{-\alpha-2\epsilon} (1+ab)^{-2+2\alpha+2\epsilon}}{2(1-\epsilon)\left(4at+(1-a)^2\right)} \\ & \left(-2z(ab+1)(a(2t-1)+1)+(ab+1)^2+2z^2\left(4at+(a-1)^2\right)\right)^{-1} \\ & \left(a^2b^2\left(z\left(-2z^2+z-1\right)+1\right)+2ab(z-1)^2+z((3-2z)z-3)+1\right. \\ & \left.+(2z-1)((z-1)z+1)\epsilon(ab+1)^2\right), \end{aligned}$$

$$\begin{aligned} J_g^{P_2^C} = & \frac{(1-z)^{-\alpha} z^{-2\alpha} a^{-1-\alpha-2\epsilon} (a+b)^{2\epsilon} b^{-1-\alpha-2\epsilon} (1+ab)^{-1+2\alpha+2\epsilon}}{2(1-\epsilon)\left(4at+(1-a)^2\right)(1+ab(1-z))} \\ & \left(2b^2z^2\left(4at+(a-1)^2\right)-2bz(ab+1)(a+2t-1)+(ab+1)^2\right)^{-1} \\ & \left((1+ab)^3-(1+ab)^2(2+3ab)z+(1+ab)(2+ab(4+3ab))z^2\right. \\ & -2ab(2+ab(2+ab))z^3+\epsilon\left(ab\left(ab\left(ab(2z-1)((z-1)z+1)-3(z-1)^2\right)\right.\right. \\ & \left.\left.+3(z-1)\right)-1\right), \end{aligned}$$

$$\begin{aligned} J_g^{P_2^D} = & \frac{(1-z)^{-\alpha} z^{-2\alpha} a^{-\alpha-2\epsilon} (a+b)^{2\epsilon} b^{-1-\alpha-2\epsilon} (1+ab)^{2\alpha+2\epsilon}}{2(1-\epsilon)\left(4at+(1-a)^2\right)(ab(1-z)+1)} \\ & \left(az\left(4b(1-t)+(1-b)^2\right)+(1-z)(a+b)(ab+1)\right)^{-1} \\ & \left(a^2b^2((z-1)z+1)+ab(z(4z-3)+2)+2(z-1)z+1\right. \\ & \left.-\epsilon\left(ab\left(ab\left(-z^2+z+1\right)+z+2\right)+1\right)\right), \end{aligned}$$

$$\begin{aligned} J_g^{P_2^E} = & -\frac{(1-z)^{-1-\alpha} z^{-1-2\alpha} a^{1-\alpha-2\epsilon} (a+b)^{2\epsilon} b^{-\alpha-2\epsilon} (1+ab)^{-2+2\alpha+2\epsilon}}{(1-\epsilon)\left(az\left(4b(1-t)+(1-b)^2\right)+(1-z)(a+b)(ab+1)\right)} \\ & \left(-2+z(3+2(-2+z)z)-2ab(2-3z+z^3)+a^2b^2(-2+z(3+2(-2+z)z))\right. \\ & \left.+(2-z)(1-(1-z)z)\epsilon(ab+1)^2\right)\left(4at+(1-a)^2\right)^{-1}. \end{aligned}$$

The final coefficients belong to the C_A^2 colour structure. They are

$$
\begin{aligned}
J_g^{P^A_{g\to ggg}} =& \frac{(1-z)^{-1-\alpha} z^{-1-2\alpha} a^{1-\alpha-2\epsilon} (a+b)^{2\epsilon} b^{-\alpha-2\epsilon} (1+ab)^{-2+2\alpha+2\epsilon}}{4at+(1-a)^2} \\
& \left(az\left(4b(1-t)+(1-b)^2\right)+(1-z)(a+b)(ab+1)\right)^{-1} \\
& \left(z^3(ab(5ab+4)+5)-z^2(ab(13ab+18)+13)+12z(ab+1)^2\right. \\
& \left.-8(ab+1)^2\right),
\end{aligned}
$$

$$
\begin{aligned}
J_g^{P^B_{g\to ggg}} =& \frac{(1-z)^{1-\alpha} z^{-1-2\alpha} a^{-\alpha-2\epsilon} (a+b)^{2\epsilon} b^{-1-\alpha-2\epsilon} (1+ab)^{2\alpha+2\epsilon}}{1+ab(1-z)} \\
& \left(\frac{(-z(ab+1)+(ab+1)^2+z^2)^2}{-2z(ab+1)(1-a(1-2t))+(ab+1)^2+2z^2\left(4at+(1-a)^2\right)}\right) \\
& \left(az\left(4b(1-t)+(1-b)^2\right)+(1-z)(a+b)(ab+1)\right)^{-1},
\end{aligned}
$$

$$
\begin{aligned}
J_g^{P^C_{g\to ggg}} =& \frac{(1-z)^{-1-\alpha} z^{-1-2\alpha} a^{-\alpha-2\epsilon} (a+b)^{2\epsilon} b^{-1-\alpha-2\epsilon} (1+ab)^{2+2\alpha+2\epsilon}}{\left(4at+(1-a)^2\right)(1+ab(1-z))} \\
& \left(\frac{(1-(1-z)z)^2}{az\left(4b(1-t)+(1-b)^2\right)+(1-z)(a+b)(ab+1)}\right) \\
& \left(\frac{(-2z(ab+1)(1-a(1-2t))+(ab+1)^2+z^2\left(4at+(1-a)^2\right))}{-2z(ab+1)(1-a(1-2t))+(ab+1)^2+2z^2\left(4at+(1-a)^2\right)}\right),
\end{aligned}
$$

$$
\begin{aligned}
J_g^{P^D_{g\to ggg}} =& \frac{(1-z)^{-1-\alpha} z^{-1-2\alpha} a^{1-\alpha-2\epsilon} (a+b)^{2\epsilon} b^{-1-\alpha-2\epsilon} (1+ab)^{-2+2\alpha+2\epsilon}}{\left(4at+(1-a)^2\right)(1+ab-z)} \\
& \left(-2z(ab+1)(1-a(1-2t))+(ab+1)^2+2z^2\left(4at+(1-a)^2\right)\right)^{-1} \\
& \left(z^2(ab+2)(ab(3ab+5)+5)(ab+1)^2-2z(ab(ab+3)+3)(ab+1)^3\right. \\
& +(ab+2)(ab+1)^4+z^3(-ab-1)(ab(ab(ab(2ab+11)+21)+20)+10) \\
& \left.+z^4(ab+2)(ab(ab+1)+1)(ab(ab+3)+3)-2z^5(ab(ab+1)+1)^2\right).
\end{aligned}
$$

Appendix D

How to arrive at monomial master formulae?

In the last section we wrote down all real-real master formulae in physical parametrisation. However in order to arrive at the setup we want, we have to project the expression on to the unit hypercube. In this final section we will outline the step to arrive at an expression, where all divergences are in a monomial form. Additionally we will list for all structures the occurring divergences as well as the correct Ω factor. In order to separate all contributions, we divide them by the corresponding jet function coefficient $J_i^{P_j}$.

Let us start with the NLO contribution:

Jet function	Substitutions	Divergences	Ω
$J_{q,1}$	–	z	z^{-n}
$J_{g\to q\bar{q},1}$	–	–	–
$J_{g\to gg,1}$	$z \to \frac{1}{2}u$	u	u^{-n}

In the case of the real-virtual corrections at NNLO we find the following structures:

Jet function	Substitutions	Divergences	Ω
$J_q^{P_{q\to gq}^{(1),A}}$	–	z	z^{-n}
$J_q^{P_{q\to gq}^{(1),B}}$	–	z, l	z^{-n}
$J_q^{P_{q\to gq}^{(1),C}}$	–	z	z^{-n}
$J_q^{P_{q\to gq}^{(1),D}}$	–	z, l	z^{-n}
$J_g^{P_{g\to q\bar{q}}^{(1),A}}$	–	–	–
$J_g^{P_{g\to q\bar{q}}^{(1),B}}$	–	–	–
$J_g^{P_{g\to q\bar{q}}^{(1),C}}$	–	l	–
$J_g^{P_{g\to q\bar{q}}^{(1),D}}$	–	–	–
$J_g^{P_{g\to gg}^{(1),A}}$	$z \to \frac{1}{2}u$	u	u^{-n}
$J_g^{P_{g\to gg}^{(1),B}}$	$z \to \frac{1}{2}u$	u, l	u^{-n}
$J_g^{P_{g\to gg}^{(1),A}}$	–	–	–

The divergence of $l \to 0$ is technically a spurious divergence from the integral representation of the hypergeometric functions. We still list here for the sake of completness.

Let us now turn to the rest of the NNLO contributions. We are proceeding a similar fashion as in previous section and start with the $C_F T_F n_f$ contribution of the quark jet function.

Jet function	Region	Substitutions, Sector decomp.	Divergences	Ω
$J_q^{P^A_{q\to\bar{q}'q'q}}$	Region A	$\{a,t\} \to \{u,v\}$	u, z	z^{-n}
	Region B	$\{a,t\} \to \{u,v\}$	u, z	z^{-n}

Jet function	Region	Substitutions, Sector decomp.	Divergences	Ω
$J_q^{P^B_{q\to\bar{q}'q'q}}$	Region A	$\{a,t\} \to \{u,v\}$	u, z	z^{-n}
	Region B	$\{a,t\} \to \{u,v\}$	u, z	z^{-n}

In the case of the identical structure we find:

Jet function	Region	Substitutions, Sector decomp.	Divergences	Ω
$J_q^{P^A_{q\to\bar{q}qq}}$	Region A	$\{a,t\} \to \{u,v\}$	u	–
	Region B	$\{a,t\} \to \{u,v\}$	u	–
	Region C	$\{a,t\} \to \{u,v\}$	u	–
	Region D	$\{a,t\} \to \{u,v\}$	u	–

Jet function	Region	Substitutions, Sector decomp.	Divergences	Ω
$J_q^{P^B_{q\to\bar{q}qq}}$	Region A	$\{a,t\}\to\{u,v\}$	u	–
	Region B	$\{a,t\}\to\{u,v\}$	u	–
	Region C	$\{a,t\}\to\{u,v\}$	u	–
	Region D	$\{a,t\}\to\{u,v\}$	u	–

Now turn to the contributions to the $q\to ggq$ splitting function. Here we have to separate Ω into three different contributions depending on the value of n. In the case we require additional sector decomposition due to the measurement function singularities we denote the sector by A_j,and write this table at the end of the section.

Jet function	Region	Sub., Sector decomp.	Div.	$\Omega_{n>1}$	$\Omega_{n<1}$	$\Omega_{n=0}$
$J_q^{P^A_{q\to ggq}}$	$a\cdot\mathrm{R_A}$	$\{a,t\}\to\{u,v\}$	$u,b,\bar{z}$	$\bar{z}^{-n}$	$\bar{z}^{-n}$	$\bar{z}^{-n}$
	$\bar{a}\cdot\mathrm{R_A}$	$a\to bh, z\to 1-hg$	h,b,g	A_q	$g^{-n}h^{\frac{1-n}{2}}$	$h^{\frac{1}{2}}$
	$\bar{a}\cdot\mathrm{R_A}$	$a\to bh, h\to\bar{z}g$	$g,b,\bar{z}$	$g^{\frac{1-n}{2}}\bar{z}^{\frac{1-n}{2}}b^{1-n}$	$\tilde{A}_q$	$g^{\frac{1}{2}}\bar{z}^{\frac{1}{2}}$
	$\bar{a}\cdot\mathrm{R_A}$	$b\to ah$	$a,h,\bar{z}$	B_q	$\bar{z}^{-n}$	$\bar{z}^{-n}$
	$a\cdot\mathrm{R_B}$	$\{a,t\}\to\{u,v\}$	$u,\bar{z}$	$\bar{z}^{-n}$	$\bar{z}^{-n}$	$\bar{z}^{-n}$
	$\bar{a}\cdot\mathrm{R_B}$	$a\to h\bar{z}$	$h,\bar{z}$	$h^{\frac{1-n}{2}}\bar{z}^{\frac{1-n}{2}}$	$h^{\frac{1-n}{2}}\bar{z}^{\frac{1-n}{2}}$	$h^{\frac{1}{2}}\bar{z}^{\frac{1}{2}}$
	$\bar{a}\cdot\mathrm{R_B}$	$z\to 1-ah$	a,h	$h^{-n}a^{\frac{1-n}{2}}$	$h^{-n}a^{\frac{1-n}{2}}$	$a^{\frac{1}{2}}$
	$\mathrm{R_C}$	$\{a,t\}\to\{u,v\}$	$u,b,\bar{z}$	$\bar{z}^{-n}$	$\bar{z}^{-n}$	$\bar{z}^{-n}$
	$\mathrm{R_D}$	$\{a,t\}\to\{u,v\}$	$u,\bar{z}$	$\bar{z}^{-n}$	$\bar{z}^{-n}$	$\bar{z}^{-n}$

Jet function	Region	Sub., Sector decomp.	Div.	$\Omega_{n>1}$	$\Omega_{n<1}$	$\Omega_{n=0}$
$J_q^{P^B_{q\to ggq}}$	$\mathrm{R_A}$	$a\to bh$	b,z	$z^{-n}b^{1-n}$	z^{-n}	–
	$\mathrm{R_A}$	$b\to ah$	a,h,z	C_q	z^{-n}	–
	$\mathrm{R_B}$	–	z	z^{-n}	z^{-n}	–
	$\mathrm{R_C}$	$a\to bh, b\to zg$	h,z	$z^{-n}h^{\frac{1-n}{2}}$	$z^{-n}h^{\frac{1-n}{2}}$	$h^{\frac{1}{2}}$
	$\mathrm{R_C}$	$a\to bh, z\to bg$	h,b,g	$b^{-n}g^{-n}h^{\frac{1-n}{2}}$	$b^{-n}g^{-n}h^{\frac{1-n}{2}}$	$h^{\frac{1}{2}}$
	$\mathrm{R_C}$	$b\to ah, a\to zg$	h,z	z^{-n}	z^{-n}	–
	$\mathrm{R_C}$	$b\to ah, z\to ag$	a,h,g	$g^{-n}a^{-n}$	$g^{-n}a^{-n}$	–
	$\mathrm{R_D}$	$a\to bh$	h,b,z	$z^{-n}h^{\frac{1-n}{2}}b^{1-n}$	$\tilde{B}_q$	$h^{\frac{1}{2}}$
	$\mathrm{R_D}$	$b\to ah$	a,z	$z^{-n}a^{1-n}$	z^{-n}	–

Jet function	Region	Sub., Sector decomp.	Div.	$\Omega_{n>1}$	$\Omega_{n<1}$	$\Omega_{n=0}$
$J_q^{P^C_{q\to ggq}}$	$a\cdot\mathrm{R_A}$	$\{a,t\}\to\{u,v\}$	$u,b,\bar{z}$	$\bar{z}^{-n}$	$\bar{z}^{-n}$	–
	$\bar{a}\cdot\mathrm{R_A}$	$a\to bh$	$b,\bar{z}$	D_q	$\bar{z}^{-n}$	–
	$\bar{a}\cdot\mathrm{R_A}$	$b\to ah$	$a,h,\bar{z}$	B_q	$\bar{z}^{-n}$	–
	$\mathrm{R_B}$	$\{a,t\}\to\{u,v\}$	$u,\bar{z}$	$\bar{z}^{-n}$	$\bar{z}^{-n}$	–
	$\mathrm{R_C}$	$\{a,t\}\to\{u,v\}$	$u,b,\bar{z}$	$\bar{z}^{-n}$	$\bar{z}^{-n}$	–
	$\mathrm{R_D}$	$\{a,t\}\to\{u,v\}$	$u,\bar{z}$	$\bar{z}^{-n}$	$\bar{z}^{-n}$	–

Jet function	Region	Sub., Sector decomp.	Div.	$\Omega_{n>1}$	$\Omega_{n<1}$	$\Omega_{n=0}$
$J_q^{P^D_{q\to ggq}}$	$\mathrm{R_A}$	$\{a,t\}\to\{u,v\}$	u	–	–	–
	$\mathrm{R_B}$	$\{a,t\}\to\{u,v\}$	u	–	–	–
	$\mathrm{R_C}$	$\{a,t\}\to\{u,v\}$	u	–	–	–
	$\mathrm{R_D}$	$\{a,t\}\to\{u,v\}$	u	–	–	–

Jet function	Region	Sub., Sector decomp.	Div.	$\Omega_{n>1}$	$\Omega_{n<1}$	$\Omega_{n=0}$
$J_q^{P^E_{q\to ggq}}$	$\mathrm{R_A}$	$\{a,t\}\to\{u,v\}, b\to\bar{z}h$	$u,h,\bar{z}$	$\bar{z}^{-n}$	$\bar{z}^{-n}$	–
	$\mathrm{R_A}$	$\{a,t\}\to\{u,v\}, z\to 1-bh$	u,b,h	$b^{-n}h^{-n}$	$b^{-n}h^{-n}$	–
	$\mathrm{R_B}$	$\{a,t\}\to\{u,v\}$	$u,\bar{z}$	$\bar{z}^{-n}$	$\bar{z}^{-n}$	–
	$\mathrm{R_C}$	$\{a,t\}\to\{u,v\}, b\to\bar{z}h$	$u,h,\bar{z}$	$\bar{z}^{-n}$	$\bar{z}^{-n}$	–
	$\mathrm{R_C}$	$\{a,t\}\to\{u,v\}, z\to 1-bh$	u,b,h	$b^{-n}h^{-n}$	$b^{-n}h^{-n}$	–
	$\mathrm{R_D}$	$\{a,t\}\to\{u,v\}$	$u,\bar{z}$	$\bar{z}^{-n}$	$\bar{z}^{-n}$	–

Jet function	Region	Sub., Sector decomp.	Div.	$\Omega_{n>1}$	$\Omega_{n<1}$	$\Omega_{n=0}$
$J_q^{P^F_{q\to ggq}}$	$\mathrm{R_A}$	$\{a,t\}\to\{u,v\}$	u,b,z	z^{-n}	z^{-n}	–
	$\mathrm{R_B}$	$\{a,t\}\to\{u,v\}$	u,b,z	z^{-n}	z^{-n}	–
	$a\cdot\mathrm{R_C}$	$\{a,t\}\to\{u,v\}$	u,b,z	z^{-n}	z^{-n}	–
	$\bar{a}\cdot\mathrm{R_C}$	$a\to bh, b\to zg$	h,z	$z^{-n}h^{\frac{\Gamma-\bar{n}}{2}}$	$z^{-n}h^{\frac{\Gamma-\bar{n}}{2}}$	$h^{\frac{1}{2}}$
	$\bar{a}\cdot\mathrm{R_C}$	$a\to bh, z\to bg$	h,b,g	$b^{-n}g^{-n}h^{\frac{\Gamma-\bar{n}}{2}}$	$b^{-n}g^{-n}h^{\frac{\Gamma-\bar{n}}{2}}$	$h^{\frac{1}{2}}$
	$\bar{a}\cdot\mathrm{R_C}$	$b\to ah, a\to zg$	h,z	z^{-n}	z^{-n}	–
	$\bar{a}\cdot\mathrm{R_C}$	$b\to ah, z\to ag$	h,a,g	$a^{-n}g^{-n}$	$a^{-n}g^{-n}$	–
	$a\cdot\mathrm{R_D}$	$\{a,t\}\to\{u,v\}$	u,b,z	z^{-n}	z^{-n}	–
	$\bar{a}\cdot\mathrm{R_D}$	$a\to bh$	h,b,z	$z^{-n}h^{\frac{1-\bar{n}}{2}}b^{1-n}$	$\tilde{C}_q$	$h^{\frac{1}{2}}$
	$\bar{a}\cdot\mathrm{R_D}$	$b\to ah$	a,h,z	C_q	z^{-n}	–

Jet function	Region	Sub., Sector decomp.	Div.	$\Omega_{n>1}$	$\Omega_{n<1}$	$\Omega_{n=0}$
$J_q^{P^G_{q\to ggq}}$	$\mathrm{R_A}$	$\{a,t\}\to\{u,v\}$	u,z	z^{-n}	z^{-n}	–
	$\mathrm{R_B}$	$\{a,t\}\to\{u,v\}$	u,b,z	z^{-n}	z^{-n}	–
	$\mathrm{R_C}$	$\{a,t\}\to\{u,v\}$	u,z	z^{-n}	z^{-n}	–
	$a\cdot\mathrm{R_D}$	$\{a,t\}\to\{u,v\}$	u,b,z	z^{-n}	z^{-n}	–
	$\bar{a}\cdot\mathrm{R_D}$	$a\to bh$	b,z	$z^{-n}b^{1-n}$	z^{-n}	–
	$\bar{a}\cdot\mathrm{R_D}$	$b\to ah$	a,h,z	C_q	z^{-n}	–

Jet function	Region	Sub., Sector decomp.	Div.	$\Omega_{n>1}$	$\Omega_{n<1}$	$\Omega_{n=0}$
$J_q^{P^H_{q\to ggq}}$	$\mathrm{R_A}$	–	z	z^{-n}	z^{-n}	–
	$\mathrm{R_B}$	–	z	z^{-n}	z^{-n}	–
	$\mathrm{R_C}$	$a\to bh, b\to zg$	h,z	$z^{-n}h^{\frac{\Gamma-\bar{n}}{2}}$	$z^{-n}h^{\frac{\Gamma-\bar{n}}{2}}$	$h^{\frac{\Gamma}{2}}$
	$\mathrm{R_C}$	$a\to bh, z\to bg$	h,b,g	$b^{-n}g^{-n}h^{\frac{\Gamma-\bar{n}}{2}}$	$b^{-n}g^{-n}h^{\frac{\Gamma-\bar{n}}{2}}$	$h^{\frac{\Gamma}{2}}$
	$\mathrm{R_C}$	$b\to ah, a\to zg$	z	z^{-n}	z^{-n}	–
	$\mathrm{R_C}$	$b\to ah, z\to ag$	ag	$a^{-n}g^{-n}$	$a^{-n}g^{-n}$	–
	$\mathrm{R_D}$	$a\to bh$	h,b,z	$z^{-n}h^{\frac{1-\bar{n}}{2}}b^{1-n}$	$\tilde{C}_q$	$h^{\frac{\Gamma}{2}}$
	$\mathrm{R_D}$	$b\to ah$	a,z	$z^{-n}a^{1-n}$	z^{-n}	–

Jet function	Region	Sub., Sector decomp.	Div.	$\Omega_{n>1}$	$\Omega_{n<1}$	$\Omega_{n=0}$
$J_q^{P^I_{q\to ggq}}$	$\mathrm{R_A}$	$\{a,t\}\to\{u,v\}, b\to\bar{z}h$	$u,h,\bar{z}$	$\bar{z}^{-n}$	$\bar{z}^{-n}$	–
	$\mathrm{R_A}$	$\{a,t\}\to\{u,v\}, z\to 1-bh$	u,b,h	$b^{-n}h^{-n}$	$b^{-n}h^{-n}$	–
	$\mathrm{R_B}$	$\{a,t\}\to\{u,v\}$	$u,\bar{z}$	$\bar{z}^{-n}$	$\bar{z}^{-n}$	–
	$\mathrm{R_C}$	$\{a,t\}\to\{u,v\}, b\to\bar{z}h$	$u,h,\bar{z}$	$\bar{z}^{-n}$	$\bar{z}^{-n}$	–
	$\mathrm{R_C}$	$\{a,t\}\to\{u,v\}, z\to 1-bh$	u,b,h	$b^{-n}h^{-n}$	$b^{-n}h^{-n}$	–
	$\mathrm{R_D}$	$\{a,t\}\to\{u,v\}$	$u,\bar{z}$	$\bar{z}^{-n}$	$\bar{z}^{-n}$	–

We now give similar tables for the gluon jet function.

Jet function	Region	Sub., Sector decomp.	Div.	$\Omega_{n>1}$	$\Omega_{n<1}$	$\Omega_{n=0}$
$J_g^{P_1^A}$	$\mathrm{R_A}$	–	–	–	–	–
	$\mathrm{R_B}$	–	–	–	–	–

Jet function	Region	Sub., Sector decomp.	Div.	$\Omega_{n>1}$	$\Omega_{n<1}$	$\Omega_{n=0}$
$J_g^{P_1^B}$	$\mathrm{R_A}$	$\{a,t\}\to\{u,v\}$	u	–	–	–
	$\mathrm{R_B}$	$\{a,t\}\to\{u,v\}$	u	–	–	–
	$\mathrm{R_C}$	$\{a,t\}\to\{u,v\}$	u	–	–	–
	$\mathrm{R_D}$	$\{a,t\}\to\{u,v\}$	u	–	–	–

Jet function	Region	Sub., Sector decomp.	Div.	$\Omega_{n>1}$	$\Omega_{n<1}$	$\Omega_{n=0}$
$J_g^{P_1^C}$	$\mathrm{R_A}$	$\{a,t\}\to\{u,v\}$	u	–	–	–
	$\mathrm{R_B}$	$\{a,t\}\to\{u,v\}$	u	–	–	–
	$\mathrm{R_C}$	$\{a,t\}\to\{u,v\}$	u	–	–	–
	$\mathrm{R_D}$	$\{a,t\}\to\{u,v\}$	u	–	–	–

Jet function	Region	Sub., Sector decomp.	Div.	$\Omega_{n>1}$	$\Omega_{n<1}$	$\Omega_{n=0}$
$J_g^{P_1^D}$	$\mathrm{R_A}$	$\{a,t\}\to\{u,v\}$	u	–	–	–
	$\mathrm{R_B}$	$\{a,t\}\to\{u,v\}$	u	–	–	–
	$\mathrm{R_C}$	$\{a,t\}\to\{u,v\}$	u	–	–	–
	$\mathrm{R_D}$	$\{a,t\}\to\{u,v\}$	u	–	–	–

Jet function	Region	Sub., Sector decomp.	Div.	$\Omega_{n>1}$	$\Omega_{n<1}$	$\Omega_{n=0}$
$J_g^{P_2^A}$	$\mathrm{R_A}$	$\{a,t\}\to\{u,v\}$	u,z	z^{-n}	z^{-n}	–
	$\mathrm{R_B}$	$\{a,t\}\to\{u,v\}$	u,z	z^{-n}	z^{-n}	–

Jet function	Region	Sub., Sector decomp.	Div.	$\Omega_{n>1}$	$\Omega_{n<1}$	$\Omega_{n=0}$
$J_g^{P_2^B}$	$\mathrm{R_A}$	$\{a,t\}\to\{u,v\}$	$u,\bar{z}$	$\bar{z}^{-n}$	$\bar{z}^{-n}$	–
	$\mathrm{R_B}$	$\{a,t\}\to\{u,v\}$	$u,\bar{z}$	$\bar{z}^{-n}$	$\bar{z}^{-n}$	–
	$\mathrm{R_C}$	$\{a,t\}\to\{u,v\}$	$u,\bar{z}$	$\bar{z}^{-n}$	$\bar{z}^{-n}$	–
	$\mathrm{R_D}$	$\{a,t\}\to\{u,v\}$	$u,\bar{z}$	$\bar{z}^{-n}$	$\bar{z}^{-n}$	–

Jet function	Region	Sub., Sector decomp.	Div.	$\Omega_{n>1}$	$\Omega_{n<1}$	$\Omega_{n=0}$
$J_g^{P_2^C}$	$a\cdot\mathrm{R_A}$	$\{a,t\}\to\{u,v\}$	u,b	–	–	–
	$\bar{a}\cdot\mathrm{R_A}$	$a\to bh$	h,b	$h^{\frac{1-\bar{n}}{2}}b^{1-n}$	$\tilde{A}_g$	$h^{\frac{1}{2}}$
	$\bar{a}\cdot\mathrm{R_A}$	$b\to ah$	h,a	A_g	–	–
	$a\cdot\mathrm{R_B}$	$\{a,t\}\to\{u,v\}$	u	–	–	–
	$\bar{a}\cdot\mathrm{R_B}$	–	a	$a^{\frac{1-\bar{n}}{2}}$	$a^{\frac{1-\bar{n}}{2}}$	$a^{\frac{1}{2}}$
	$\mathrm{R_C}$	$\{a,t\}\to\{u,v\}$	u,b	–	–	–
	$\mathrm{R_D}$	$\{a,t\}\to\{u,v\}$	u	–	–	–

Jet function	Region	Sub., Sector decomp.	Div.	$\Omega_{n>1}$	$\Omega_{n<1}$	$\Omega_{n=0}$
$J_g^{P_2^D}$	$a\cdot\mathrm{R_A}$	$\{a,t\}\to\{u,v\}$	u,b	–	–	–
	$\bar{a}\cdot\mathrm{R_A}$	$a\to bh$	b	b^{1-n}	–	–
	$\bar{a}\cdot\mathrm{R_A}$	$b\to ah$	h,a	A_g	–	–
	$\mathrm{R_B}$	$\{a,t\}\to\{u,v\}$	u	–	–	–
	$\mathrm{R_C}$	$\{a,t\}\to\{u,v\}$	u,b	–	–	–
	$\mathrm{R_D}$	$\{a,t\}\to\{u,v\}$	u	–	–	–

Jet function	Region	Sub., Sector decomp.	Div.	$\Omega_{n>1}$	$\Omega_{n<1}$	$\Omega_{n=0}$
$J_g^{P_2^E}$	$zt\cdot\mathrm{R_A}$	$\{z,b,t\}\to\{\tilde{u},\tilde{v},p\}$	$\tilde{u},\tilde{v}$	$\tilde{u}^{1-n}\tilde{v}^{-n}$	$\tilde{B}_g$	–
	$z\bar{t}\cdot\mathrm{R_A}$	$\{a,t\}\to\{u,v\}$	$u,\bar{z}$	$\bar{z}^{-n}$	$\bar{z}^{-n}$	–
	$\bar{z}\cdot\mathrm{R_A}$	$\{a,t\}\to\{u,v\}$	u,z	z^{-n}	z^{-n}	–
	$zt\cdot\mathrm{R_B}$	$\{z,b,t\}\to\{\tilde{u},\tilde{v},p\}$	$\tilde{u},\tilde{v}$	$\tilde{u}^{1-n}\tilde{v}^{-n}$	$\tilde{B}_g$	–
	$z\bar{t}\cdot\mathrm{R_B}$	$\{a,t\}\to\{u,v\}$	$u,\bar{z}$	$\bar{z}^{-n}$	$\bar{z}^{-n}$	–
	$\bar{z}\cdot\mathrm{R_B}$	$\{a,t\}\to\{u,v\}$	u,z	z^{-n}	z^{-n}	–

Jet function	Region	Sub., Sector decomp.	Div.	$\Omega_{n>1}$	$\Omega_{n<1}$	$\Omega_{n=0}$
$J_g^{P^A_{g\to ggg}}$	$zt\cdot \mathrm{R_A}$	$\{z,b,t\}\to\{\tilde{u},\tilde{v},p\}$	$\tilde{u},\tilde{v}$	$\tilde{u}^{1-n}\tilde{v}^{-n}$	$\tilde{B}_g$	–
	$z\bar{t}\cdot \mathrm{R_A}$	$\{a,t\}\to\{u,v\}$	$u,\bar{z}$	$\bar{z}^{-n}$	$\bar{z}^{-n}$	–
	$\bar{z}\cdot \mathrm{R_A}$	$\{a,t\}\to\{u,v\}$	u,z	z^{-n}	z^{-n}	–
	$zt\cdot \mathrm{R_B}$	$\{z,b,t\}\to\{\tilde{u},\tilde{v},p\}$	$\tilde{u},\tilde{v}$	$\tilde{u}^{1-n}\tilde{v}^{-n}$	$\tilde{B}_g$	–
	$z\bar{t}\cdot \mathrm{R_B}$	$\{a,t\}\to\{u,v\}$	$u,\bar{z}$	$\bar{z}^{-n}$	$\bar{z}^{-n}$	–
	$\bar{z}\cdot \mathrm{R_B}$	$\{a,t\}\to\{u,v\}$	u,z	z^{-n}	z^{-n}	–

Jet function	Region	Sub., Sector decomp.	Div.	$\Omega_{n>1}$	$\Omega_{n<1}$	$\Omega_{n=0}$
$J_g^{P^B_{g\to ggg}}$	$\mathrm{R_A}$	$a\to bh$	b,z	$z^{-n}b^{1-n}$	z^{-n}	–
	$\mathrm{R_A}$	$b\to ah$	a,h,z	B_g	z^{-n}	–
	$\mathrm{R_B}$	–	z	z^{-n}	z^{-n}	–
	$z\cdot \mathrm{R_C}$	$b\to ah$	h	–	–	–
	$z\cdot \mathrm{R_C}$	$a\to bh, h\to \bar{z}g$	$g,\bar{z}$	$\bar{z}^{\frac{1-n}{2}}g^{\frac{1-n}{2}}$	$\bar{z}^{\frac{1-n}{2}}g^{\frac{1-n}{2}}$	$\bar{z}^{\frac{1}{2}}g^{\frac{1}{2}}$
	$z\cdot \mathrm{R_C}$	$a\to bh, z\to 1-hg$	h	$h^{\frac{1-n}{2}}$	$h^{\frac{1-n}{2}}$	$h^{\frac{1}{2}}$
	$\bar{z}\cdot \mathrm{R_C}$	$a\to bh, b\to zg$	h,z	$z^{-n}h^{\frac{1-n}{2}}$	$z^{-n}h^{\frac{1-n}{2}}$	$h^{\frac{1}{2}}$
	$\bar{z}\cdot \mathrm{R_C}$	$a\to bh, z\to bg$	h,b,g	$b^{-n}g^{-n}h^{\frac{1-n}{2}}$	$b^{-n}g^{-n}h^{\frac{1-n}{2}}$	$h^{\frac{1}{2}}$
	$\bar{z}\cdot \mathrm{R_C}$	$b\to ah, a\to zg$	h,z	z^{-n}	z^{-n}	–
	$\bar{z}\cdot \mathrm{R_C}$	$b\to ah, z\to ag$	a,h,g	$a^{-n}g^{-n}$	$a^{-n}g^{-n}$	–
	$z\cdot \mathrm{R_D}$	$b\to ah$	a	a^{1-n}	–	–
	$z\cdot \mathrm{R_D}$	$a\to bh, h\to \bar{z}g$	$g,b,\bar{z}$	$\bar{z}^{\frac{1-n}{2}}g^{\frac{1-n}{2}}b^{1-n}$	$\tilde{C}_g$	$\bar{z}^{\frac{1}{2}}g^{\frac{1}{2}}$
	$z\cdot \mathrm{R_D}$	$a\to bh, z\to 1-hg$	h,b	$h^{\frac{1-n}{2}}b^{1-n}$	$h^{\frac{1-n}{2}}$	$h^{\frac{1}{2}}$
	$\bar{z}\cdot \mathrm{R_D}$	$a\to bh$	h,b,z	$z^{-n}h^{\frac{1-n}{2}}b^{1-n}$	$\tilde{D}_g$	$h^{\frac{1}{2}}$
	$\bar{z}\cdot \mathrm{R_D}$	$b\to ah$	a,z	$z^{-n}a^{1-n}$	z^{-n}	–

Jet func.	Region	Sub., Sector decomp.	Div.	$\Omega_{n>1}$	$\Omega_{n<1}$	$\Omega_{n=0}$
$J_g^{P_{g\to ggg}^C}$	$z\bar{a}\cdot \mathrm{R_A}$	$\{a,t\}\to\{u,v\}$	$b,\bar{z},u$	$\bar{z}^{-n}$	$\bar{z}^{-n}$	–
	$\bar{z}a\cdot \mathrm{R_A}$	$\{a,t\}\to\{u,v\}$	b,z,u	z^{-n}	z^{-n}	–
	$z\bar{a}\cdot \mathrm{R_A}$	$b\to ah$	$a,h,\bar{z}$	C_g	$\bar{z}^{-n}$	–
	$z\bar{a}\cdot \mathrm{R_A}$	$a\to bh,h\to \bar{z}g$	$b,\bar{z}$	$\bar{z}^{\frac{1-n}{2}}b^{1-n}$	$\bar{z}^{\frac{1-n}{2}}$	$\bar{z}^{1/2}$
	$z\bar{a}\cdot \mathrm{R_A}$	$a\to bh,z\to 1-hg$	h,b,g	D_g	$g^{-n}h^{\frac{1-n}{2}}$	$h^{1/2}$
	$z\bar{a}\cdot \mathrm{R_A}$	$a\to bh$	b,z	$z^{-n}b^{1-n}$	z^{-n}	–
	$z\bar{a}\cdot \mathrm{R_A}$	$b\to ah$	a,h,z	B_g	z^{-n}	–
	$\bar{z}\cdot \mathrm{R_B}$	$\{a,t\}\to\{u,v\}$	z,u	z^{-n}	z^{-n}	–
	$z\cdot \mathrm{R_B}$	$\{a,t\}\to\{u,v\},b\to \bar{z}h$	$\bar{z},u$	$\bar{z}^{-n}$	$\bar{z}^{-n}$	–
	$z\cdot \mathrm{R_B}$	$\{a,t\}\to\{u,v\},z\to 1-bh$	b,h,u	$b^{-n}h^{-n}$	$b^{-n}h^{-n}$	–
	$za\cdot \mathrm{R_C}$	$\{a,t\}\to\{u,v\}$	$b,\bar{z},u$	$\bar{z}^{-n}$	$\bar{z}^{-n}$	–
	$z\bar{a}\cdot \mathrm{R_C}$	$a\to \bar{z}h,b\to \bar{z}g$	g	–	–	–
	$z\bar{a}\cdot \mathrm{R_C}$	$a\to \bar{z}h,z\to 1-bg$	g	$g^{\frac{1-n}{2}}$	$g^{\frac{1-n}{2}}$	$g^{1/2}$
	$z\bar{a}\cdot \mathrm{R_C}$	$z\to 1-ah,a\to bg$	g,h	$g^{\frac{1-n}{2}}h^{-n}$	$g^{\frac{1-n}{2}}h^{-n}$	$g^{1/2}$
	$z\bar{a}\cdot \mathrm{R_C}$	$z\to 1-ah,b\to ag$	g,h	h^{-n}	h^{-n}	–
	$a\bar{z}\cdot \mathrm{R_C}$	$\{a,t\}\to\{u,v\}$	b,z,u	z^{-n}	z^{-n}	–
	$\bar{z}\cdot \mathrm{R_D}$	$\{a,t\}\to\{u,v\}$	z,u	z^{-n}	z^{-n}	–
	$za\cdot \mathrm{R_D}$	$\{a,t\}\to\{u,v\},b\to \bar{z}h$	$\bar{z},u$	$\bar{z}^{-n}$	$\bar{z}^{-n}$	–
	$za\cdot \mathrm{R_D}$	$\{a,t\}\to\{u,v\},z\to 1-bh$	b,h,u	$b^{-n}h^{-n}$	$b^{-n}h^{-n}$	–
	$z\bar{a}\cdot \mathrm{R_D}$	$a\to \bar{z}h$	$\bar{z}$	$\bar{z}^{\frac{1-n}{2}}$	$\bar{z}^{\frac{1-n}{2}}$	$\bar{z}^{1/2}$
	$z\bar{a}\cdot \mathrm{R_D}$	$z\to 1-ah,b\to hg,a\to hf$	f,h	$h^{-2n}f^{\frac{1-n}{2}}$	$h^{-2n}f^{\frac{1-n}{2}}$	$f^{1/2}$
	$z\bar{a}\cdot \mathrm{R_D}$	$z\to 1-ah,b\to hg,h\to af$	a,f	$a^{-2n}f^{-n}$	$a^{-2n}f^{-n}$	–
	$z\bar{a}\cdot \mathrm{R_D}$	$z\to 1-ah,h\to bg,a\to bf$	f,b,g	$b^{-2n}g^{-n}f^{\frac{1-n}{2}}$	$b^{-2n}g^{-n}f^{\frac{1-n}{2}}$	$f^{1/2}$
	$z\bar{a}\cdot \mathrm{R_D}$	$z\to 1-ah,h\to bg,b\to af$	a,f,g	$a^{-2n}g^{-n}f^{-n}$	$a^{-2n}g^{-n}f^{-n}$	–

Jet func.	Region	Sub., Sector decomp.	Div.	$\Omega_{n>1}$	$\Omega_{n<1}$	$\Omega_{n=0}$
$J_g^{P_{g\to ggg}^D}$	$z\cdot \mathrm{R_A}$	$\{a,t\}\to\{u,v\}$,$b\to \bar{z}h$	$h,\bar{z},u$	$\bar{z}^{-n}$	$\bar{z}^{-n}$	–
	$z\cdot \mathrm{R_A}$	$\{a,t\}\to\{u,v\}$,$z\to 1-bh$	b,h,u	$b^{-n}h^{-n}$	$b^{-n}h^{-n}$	–
	$\bar{z}\cdot \mathrm{R_A}$	$\{a,t\}\to\{u,v\}$	b,z,u	z^{-n}	z^{-n}	–
	$z\cdot \mathrm{R_B}$	$\{a,t\}\to\{u,v\}$	$b,\bar{z},u$	$\bar{z}^{-n}$	$\bar{z}^{-n}$	–
	$\bar{z}\cdot \mathrm{R_B}$	$\{a,t\}\to\{u,v\}$	b,z,u	z^{-n}	z^{-n}	–
	$za\cdot \mathrm{R_C}$	$\{a,t\}\to\{u,v\}$,$b\to \bar{z}h$	$h,\bar{z},u$	$\bar{z}^{-n}$	$\bar{z}^{-n}$	–
	$za\cdot \mathrm{R_C}$	$\{a,t\}\to\{u,v\}$,$z\to 1-bh$	b,h,u	$b^{-n}h^{-n}$	$b^{-n}h^{-n}$	–
	$z\bar{a}\cdot \mathrm{R_C}$	$a\to bh$,$h\to \bar{z}g$	$g,\bar{z}$	$\bar{z}^{\frac{1-n}{2}}g^{\frac{1-n}{2}}$	$\bar{z}^{\frac{1-n}{2}}g^{\frac{1-n}{2}}$	$\bar{z}^{1/2}g^{1/2}$
	$z\bar{a}\cdot \mathrm{R_C}$	$a\to bh$,$z\to 1-hg$	h,g	$h^{\frac{1-n}{2}}g^{-n}$	$h^{\frac{1-n}{2}}g^{-n}$	$h^{1/2}$
	$z\bar{a}\cdot \mathrm{R_C}$	$b\to ah$,$h\to \bar{z}g$	$\bar{z}$	$\bar{z}^{-n}$	$\bar{z}^{-n}$	–
	$z\bar{a}\cdot \mathrm{R_C}$	$b\to ah$,$z\to 1-hg$	g,h	$g^{-n}h^{-n}$	$g^{-n}h^{-n}$	–
	$a\bar{z}\cdot \mathrm{R_C}$	$\{a,t\}\to\{u,v\}$	b,z,u	z^{-n}	z^{-n}	–
	$\bar{a}\bar{z}\cdot \mathrm{R_C}$	$a\to bh$,$b\to zg$	h,z	$h^{\frac{1-n}{2}}z^{-n}$	$h^{\frac{1-n}{2}}z^{-n}$	$h^{1/2}$
	$\bar{a}\bar{z}\cdot \mathrm{R_C}$	$a\to bh$,$z\to bg$	h,b,z	$h^{\frac{1-n}{2}}b^{-n}g^{-n}$	$h^{\frac{1-n}{2}}b^{-n}g^{-n}$	$h^{1/2}$
	$\bar{a}\bar{z}\cdot \mathrm{R_C}$	$b\to ah$,$a\to zg$	h,z	z^{-n}	z^{-n}	–
	$\bar{a}\bar{z}\cdot \mathrm{R_C}$	$b\to ah$,$z\to ag$	a,h,z	$a^{-n}g^{-n}$	$a^{-n}g^{-n}$	–
	$az\cdot \mathrm{R_D}$	$\{a,t\}\to\{u,v\}$	$b,\bar{z},u$	$\bar{z}^{-n}$	$\bar{z}^{-n}$	–
	$a\bar{z}\cdot \mathrm{R_D}$	$\{a,t\}\to\{u,v\}$	b,z,u	z^{-n}	z^{-n}	–
	$z\bar{a}\cdot \mathrm{R_D}$	$a\to bh$,$h\to \bar{z}g$	$b,\bar{z},g$	$\bar{z}^{\frac{1-n}{2}}g^{\frac{1-n}{2}}b^{1-n}$	$\tilde{C}_g$	$\bar{z}^{1/2}g^{1/2}$
	$z\bar{a}\cdot \mathrm{R_D}$	$a\to bh$,$z\to 1-hg$	b,g,h	D_g	$h^{\frac{1-n}{2}}g^{-n}$	$h^{1/2}$
	$z\bar{a}\cdot \mathrm{R_D}$	$b\to ah$	$h,\bar{z},a$	C_g	$\bar{z}^{-n}$	–
	$\bar{a}\bar{z}\cdot \mathrm{R_D}$	$a\to bh$	h,b,z	$z^{-n}h^{\frac{1-n}{2}}b^{1-n}$	$\tilde{D}_g$	$h^{1/2}$
	$\bar{a}\bar{z}\cdot \mathrm{R_D}$	$b\to ah$	h,a,z	B_g	z^{-n}	–

Let us start with additional sectors for the quark jet function in the case where $n > 1$:

Region	Upscale	Sector decomp.	Ω
A_q	$b \to b^n, g \to g^{n-1}$	$b \to gf$	$h^{\frac{1-n}{2}} f^{n(1-n)} g^{n(1-n)}$
		$g \to bf$	$h^{\frac{1-n}{2}} f^{n(1-n)} b^{n(1-n)}$
B_q	$a \to a^n, h \to h^{n-1}, \bar{z} \to \bar{z}^{n-1}$	$z \to 1 - ag$	$a^{n(1-n)} g^{n(1-n)}$
		$a \to \bar{z}g, h \to gf$	$\bar{z}^{n(1-n)}$
		$a \to \bar{z}g, g \to hf$	$\bar{z}^{n(1-n)} f^{n(1-n)}$
C_q	$h \to h^{n-1}$	$a \to gh$	$z^{-n} g^{1-n}$
		$h \to ga$	z^{-n}
D_q	$b \to b^n, \bar{z} \to \bar{z}^{n-1}$	$z \to 1 - bg$	$b^{n(1-n)} g^{n(1-n)}$
		$b \to \bar{z}g$	$\bar{z}^{n(1-n)} g^{n(1-n)}$

Similar we find for $n > 1$ in the case of gluon jet function,

Region	Upscale	Sector decomp.	Ω
A_g	$h \to h^{n-1}$	$h \to af$	–
		$a \to hf$	f^{1-n}
B_g	$h \to h^{n-1}$	$h \to af$	z^n
		$a \to hf$	$z^n f^{n(1-n)}$
C_g	$a \to a^n, h \to h^{n-1}, \bar{z} \to \bar{z}^{n-1}$	$h \to af$	$\bar{z}^{n(1-n)}$
		$a \to hf, f \to \bar{z}g$	$\bar{z}^{n(1-n)} g^{n(1-n)}$
		$a \to hf, z \to 1 - gf$	$f^{n(1-n)} g^{n(1-n)}$
D_g	$b \to b^n, g \to g^{n-1}$	$b \to gf$	$f^{n(1-n)} g^{n(1-n)} h^{\frac{1-n}{2}}$
		$g \to bf$	$f^{n(1-n)} b^{n(1-n)} h^{\frac{1-n}{2}}$

Finally, we write the additional sectors for $n < 1$. First, in the case of the quark jet function followed by the gluon jet function.

Region	Upscale	Sector decomp.	Ω
$\tilde{A}_q$	$b \to b^n, g \to g^{1-n}$	$b \to gf$	$\bar{z}^{\frac{1-n}{2}} g^{\frac{1-n^2}{2}}$
		$g \to bf$	$\bar{z}^{\frac{1-n}{2}} f^{\frac{(1-n)^2}{2}} b^{\frac{1-n^2}{2}}$
$\tilde{B}_q$	$b \to b^n, h \to h^{1-n}, z \to z^{1-n}$	$h \to bg, b \to zf$	$f^{\frac{1-n^2}{2}} g^{\frac{(1-n)^2}{2}} z^{\frac{(1-n)^2}{2}}$
		$h \to bg, z \to bf$	$f^{n(n-1)} g^{\frac{(1-n)^2}{2}} b^{\frac{(1-n)^2}{2}}$
		$b \to hg, h \to zf$	$f^{\frac{1-n^2}{2}} z^{\frac{(1-n)^2}{2}}$
		$b \to hg, z \to hf$	$f^{n(n-1)} h^{\frac{(1-n)^2}{2}}$
$\tilde{C}_q$	$b \to b^n, h \to h^{n-1}$	$h \to bg$	$z^{-n} g^{\frac{(1-n)^2}{2}} b^{\frac{1-n^2}{2}}$
		$b \to hg$	$z^{-n} h^{\frac{1-n^2}{2}}$

Region	Upscale	Sector decomp.	Ω
$\tilde{A}_g$	$b \to b^n, h \to h^{n-1}$	$h \to bf$	$b^{\frac{1-n^2}{2}} f^{\frac{(1-n)^2}{2}}$
		$b \to hf$	$h^{\frac{1-n^2}{2}}$
$\tilde{B}_g$	$\tilde{u} \to \tilde{u}^n, \tilde{v} \to \tilde{v}^{1-n}$	$\tilde{u} \to \tilde{v} f$	–
		$\tilde{v} \to \tilde{u} f$	$f^{-n(1-n)}$
$\tilde{C}_g$	$b \to b^n, g \to g^{1-n}$	$b \to gf$	$\bar{z}^{\frac{1-n}{2}} g^{\frac{1-n^2}{2}}$
		$g \to bf$	$\bar{z}^{\frac{1-n}{2}} b^{\frac{1-n^2}{2}} f^{\frac{(1-n)^2}{2}}$
$\tilde{D}_g$	$b \to b^n, h \to h^{1-n}$	$h \to bf$	$z^{-n} f^{\frac{(1-n)^2}{2}} b^{\frac{1-n^2}{2}}$
		$b \to hf$	$z^{-n} h^{\frac{1-n^2}{2}}$

Bibliography

[1] *ATLAS*. „Observation of a new particle in the search for the Standard Model Higgs boson with the ATLAS detector at the LHC“. In: *Phys. Lett. B* 716 (2012), pp. 1–29. DOI: 10.1016/j.physletb.2012.08.020. arXiv: 1207.7214 [hep-ex]. №: CERN-PH-EP-2012-218.

[2] *CMS*. „Observation of a New Boson at a Mass of 125 GeV with the CMS Experiment at the LHC“. In: *Phys. Lett. B* 716 (2012), pp. 30–61. DOI: 10.1016/j.physletb.2012.08.021. arXiv: 1207.7235 [hep-ex]. №: CMS-HIG-12-028 and CERN-PH-EP-2012-220.

[3] O. S. Brüning, P. Collier, P. Lebrun, S. Myers, R. Ostojic, J. Poole, and P. Proudlock. *LHC Design Report*. CERN Yellow Reports: Monographs. Geneva: CERN, 2004. DOI: 10.5170/CERN-2004-003-V-1. URL: cds.cern.ch/record/782076.

[4] S. Fartoukh et al. *LHC Configuration and Operational Scenario for Run 3*. Tech. rep. 1. Geneva: CERN, Nov. 2021. URL: cds.cern.ch/record/2790409. №: CERN-ACC-2021-0007.

[5] A. G., B. A. I., B. O., F. P., L. M., R. L., and T. L. *High-Luminosity Large Hadron Collider (HL-LHC): Technical Design Report V. 0.1*. CERN Yellow Reports: Monographs. Geneva: CERN, 2017. DOI: 10.23731/CYRM-2017-004. URL: cds.cern.ch/record/2284929.

[6] D. J. Gross and F. Wilczek. „Ultraviolet Behavior of Non-Abelian Gauge Theories“. In: *Phys. Rev. Lett.* 30 (26 June 1973), pp. 1343–1346. DOI: 10.1103/PhysRevLett.30.1343. URL: link.aps.org/doi/10.1103/PhysRevLett.30.1343.

[7] H. D. Politzer. „Reliable Perturbative Results for Strong Interactions?“ In: *Phys. Rev. Lett.* 30 (26 June 1973), pp. 1346–1349. DOI: 10.1103/PhysRevLett.30.1346. URL: link.aps.org/doi/10.1103/PhysRevLett.30.1346.

[8] J. C. Collins, D. E. Soper, and G. F. Sterman. „Factorization of Hard Processes in QCD“. In: *Adv. Ser. Direct. High Energy Phys.* 5 (1989), pp. 1–91. DOI: 10.1142/9789814503266_0001. arXiv: hep-ph/0409313. №: ITP-SB-89-31.

[9] J. R. Gaunt. „Glauber Gluons and Multiple Parton Interactions“. In: *JHEP* 07 (2014), p. 110. DOI: 10.1007/JHEP07(2014)110. arXiv: 1405.2080 [hep-ph]. №: DESY-14-067.

[10] C. F. Berger et al. „An Automated Implementation of On-Shell Methods for One-Loop Amplitudes“. In: *Phys. Rev. D* 78 (2008), p. 036003. DOI: 10.1103/PhysRevD.78.036003. arXiv: 0803.4180 [hep-ph]. №: SLAC-PUB-13161, UCLA-08-TEP-10, MIT-CTP-3937, NSF-KITP-08-48, and SACLAY-IPHT-T08-054.

[11] R. K. Ellis, W. T. Giele, Z. Kunszt, K. Melnikov, and G. Zanderighi. „One-loop amplitudes for W^+ 3 jet production in hadron collisions“. In: *JHEP* 01 (2009), p. 012. DOI: 10.1088/1126-6708/2009/01/012. arXiv: 0810.2762 [hep-ph]. №: FERMILAB-PUB-08-436-T and OUTP-08-17P.

[12] F. Cascioli, P. Maierhofer, and S. Pozzorini. „Scattering Amplitudes with Open Loops“. In: *Phys. Rev. Lett.* 108 (2012), p. 111601. DOI: 10.1103/PhysRevLett.108.111601. arXiv: 1111.5206 [hep-ph]. №: ZU-TH-23-11 and LPN11-66.

[13] G. Bevilacqua et al. „HELAC-NLO“. In: *Comput. Phys. Commun.* 184 (2013), pp. 986–997. DOI: 10.1016/j.cpc.2012.10.033. arXiv: 1110.1499 [hep-ph]. №: DEMO-INP-HEPP-2011-4, WUB-11-13, TTK-11-43, and IFJPAN-IV-2011-7.

[14] S. Badger, B. Biedermann, P. Uwer, and V. Yundin. „Numerical evaluation of virtual corrections to multi-jet production in massless QCD“. In: *Comput. Phys. Commun.* 184 (2013), pp. 1981–1998. DOI: 10.1016/j.cpc.2013.03.018. arXiv: 1209.0100 [hep-ph]. №: HU-EP-12-29.

[15] G. Cullen et al. „G*OSAM*-2.0: a tool for automated one-loop calculations within the Standard Model and beyond“. In: *Eur. Phys. J. C* 74.8 (2014), p. 3001. DOI: 10.1140/epjc/s10052-014-3001-5. arXiv: 1404.7096 [hep-ph]. №: DESY-14-061 and MPP-2014-145.

[16] M. Czakon, M. Krämer, and M. Worek. „Automated NLO/NLL Monte Carlo programs for the LHC“. In: *Nucl. Part. Phys. Proc.* 261-262 (2015). Ed. by J. Blümlein, K. Jansen, M. Krämer, and J. H. Kühn, pp. 93–114. DOI: 10.1016/j.nuclphysbps.2015.03.009. arXiv: 1502.01521 [hep-ph]. №: TTK-15-03.

[17] B. Biedermann, S. Bräuer, A. Denner, M. Pellen, S. Schumann, and J. M. Thompson. „Automation of NLO QCD and EW corrections with Sherpa and Recola“. In: *Eur. Phys. J. C* 77 (2017), p. 492. DOI: 10.1140/epjc/s10052-017-5054-8. arXiv: 1704.05783 [hep-ph].

[18] M. Bahr et al. „Herwig++ Physics and Manual“. In: *Eur. Phys. J. C* 58 (2008), pp. 639–707. DOI: 10.1140/epjc/s10052-008-0798-9. arXiv: 0803.0883 [hep-ph]. №: CERN-PH-TH-2008-038, CAVENDISH-HEP-08-03, KA-TP-05-2008, DCPT-08-22, IPPP-08-11, and CP3-08-05.

[19] T. Gleisberg, S. Hoeche, F. Krauss, M. Schonherr, S. Schumann, F. Siegert, and J. Winter. „Event generation with SHERPA 1.1“. In: *JHEP* 02 (2009), p. 007. DOI: 10.1088/1126-6708/2009/02/007. arXiv: 0811.4622 [hep-ph]. №: FERMILAB-PUB-08-477-T, SLAC-PUB-13420, ZU-TH-17-08, DCPT-08-138, IPPP-08-69, EDINBURGH-2008-30, and MCNET-08-14.

[20] T. Sjöstrand et al. „An introduction to PYTHIA 8.2“. In: *Comput. Phys. Commun.* 191 (2015), pp. 159–177. DOI: 10.1016/j.cpc.2015.01.024. arXiv: 1410.3012 [hep-ph]. №: LU-TP-14-36, MCNET-14-22, CERN-PH-TH-2014-190, FERMILAB-PUB-14-316-CD, DESY-14-178, and SLAC-PUB-16122.

[21] J. M. Campbell, R. K. Ellis, and W. T. Giele. „A Multi-Threaded Version of MCFM“. In: *Eur. Phys. J. C* 75.6 (2015), p. 246. DOI: 10.1140/epjc/s10052-015-3461-2. arXiv: 1503.06182 [physics.comp-ph]. №: FERMILAB-PUB-15-043-T.

[22] P. Stienemeier et al. „WHIZARD 3.0: Status and News“. *International Workshop on Future Linear Colliders*. Apr. 2021. arXiv: 2104.11141 [hep-ph]. №: DESY-21-050.

[23] S. Frixione and B. R. Webber. „Matching NLO QCD computations and parton shower simulations“. In: *JHEP* 06 (2002), p. 029. DOI: 10.1088/1126-6708/2002/06/029. arXiv: hep-ph/0204244. №: CAVENDISH-HEP-02-01, LAPTH-905-02, and GEF-TH-2-2002.

[24] P. Nason. „A New method for combining NLO QCD with shower Monte Carlo algorithms“. In: *JHEP* 11 (2004), p. 040. DOI: 10.1088/1126-6708/2004/11/040. arXiv: hep-ph/0409146. №: BICOCCA-FT-04-11.

[25] M. Dasgupta, F. A. Dreyer, K. Hamilton, P. F. Monni, G. P. Salam, and G. Soyez. „Parton showers beyond leading logarithmic accuracy“. In: *Phys. Rev. Lett.* 125.5 (2020), p. 052002. DOI: 10.1103/PhysRevLett.125.052002. arXiv: 2002.11114 [hep-ph]. №: CERN-TH-2020-026.

[26] A. Banfi, G. P. Salam, and G. Zanderighi. „Principles of general final-state resummation and automated implementation“. In: *JHEP* 03 (2005), p. 073. DOI: 10.1088/1126-6708/2005/03/073. arXiv: hep-ph/0407286. №: FERMILAB-PUB-04-116-T, LPTHE-04-16, and NIKHEF-2004-005.

[27] A. Banfi, H. McAslan, P. F. Monni, and G. Zanderighi. „A general method for the resummation of event-shape distributions in e^+e annihilation“. In: *JHEP* 05 (2015), p. 102. DOI: 10.1007/JHEP05(2015)102. arXiv: 1412.2126 [hep-ph]. №: OUTP-14-18P.

[28] S. Catani, L. Trentadue, G. Turnock, and B. R. Webber. „Resummation of large logarithms in e+ e- event shape distributions“. In: *Nucl. Phys. B* 407 (1993), pp. 3–42. DOI: 10.1016/0550-3213(93)90271-P. №: CERN-TH-6640-92 and CAVENDISH-HEP-91-11.

[29] C. W. Bauer, S. Fleming, D. Pirjol, and I. W. Stewart. „An Effective field theory for collinear and soft gluons: Heavy to light decays“. In: *Phys. Rev. D* 63 (2001), p. 114020. DOI: 10.1103/PhysRevD.63.114020. arXiv: hep-ph/0011336. №: UCSD-PTH-00-28.

[30] C. W. Bauer, D. Pirjol, and I. W. Stewart. „Soft collinear factorization in effective field theory“. In: *Phys. Rev. D* 65 (2002), p. 054022. DOI: 10.1103/PhysRevD.65.054022. arXiv: hep-ph/0109045. №: UCSD-PTH-01-15.

[31] C. W. Bauer, S. Fleming, D. Pirjol, I. Z. Rothstein, and I. W. Stewart. „Hard scattering factorization from effective field theory“. In: *Phys. Rev. D* 66 (2002), p. 014017. DOI: 10.1103/PhysRevD.66.014017. arXiv: hep-ph/0202088. №: UCSD-PTH-02-03.

[32] M. Beneke, A. P. Chapovsky, M. Diehl, and T. Feldmann. „Soft collinear effective theory and heavy to light currents beyond leading power“. In: *Nucl. Phys. B* 643 (2002), pp. 431–476. DOI: 10.1016/S0550-3213(02)00687-9. arXiv: hep-ph/0206152. №: PITHA-02-09.

[33] T. Becher and M. D. Schwartz. „A precise determination of α_s from LEP thrust data using effective field theory“. In: *JHEP* 07 (2008), p. 034. DOI: 10.1088/1126-6708/2008/07/034. arXiv: 0803.0342 [hep-ph]. №: FERMILAB-PUB-08-048-T.

[34] Y.-T. Chien and M. D. Schwartz. „Resummation of heavy jet mass and comparison to LEP data“. In: *JHEP* 08 (2010), p. 058. DOI: 10.1007/JHEP08(2010)058. arXiv: 1005.1644 [hep-ph].

[35] R. Abbate, M. Fickinger, A. H. Hoang, V. Mateu, and I. W. Stewart. „Thrust at N^3LL with Power Corrections and a Precision Global Fit for $\alpha_s(mZ)$“. In: *Phys. Rev. D* 83 (2011), p. 074021. DOI: 10.1103/PhysRevD.83.074021. arXiv: 1006.3080 [hep-ph]. №: MIT-CTP-4101 and MPP-2010-7.

[36] W. Bizon, P. F. Monni, E. Re, L. Rottoli, and P. Torrielli. „Momentum-space resummation for transverse observables and the Higgs $p_\perp$ at N^{3}LL+NNLO“. In: *JHEP* 02 (2018), p. 108. DOI: 10.1007/JHEP02(2018)108. arXiv: 1705.09127 [hep-ph]. №: OUTP-17-05P, CERN-TH-2017-111, and LAPTH-018-17.

[37] G. Das, S.-O. Moch, and A. Vogt. „Soft corrections to inclusive deep-inelastic scattering at four loops and beyond“. In: *JHEP* 03 (2020), p. 116. DOI: 10.1007/JHEP03(2020)116. arXiv: 1912.12920 [hep-ph]. №: SI-HEP-2019-21, DESY 19-088, LTH 1205, and DESY-19-088.

[38] G. Das, S. Moch, and A. Vogt. „Approximate four-loop QCD corrections to the Higgs-boson production cross section“. In: *Phys. Lett. B* 807 (2020), p. 135546. DOI: 10.1016/j.physletb.2020.135546. arXiv: 2004.00563 [hep-ph]. №: SI-HEP-2020-07, DESY 20-037, DESY-20-037, and LTH 1230.

[39] C. Duhr, B. Mistlberger, and G. Vita. „The Four-Loop Rapidity Anomalous Dimension and Event Shapes to Fourth Logarithmic Order“ (May 2022). arXiv: 2205.02242 [hep-ph]. №: BONN-TH-2022-11 and SLAC-PUB-17675.

[40] I. Moult, H. X. Zhu, and Y. J. Zhu. „The Four Loop QCD Rapidity Anomalous Dimension“ (May 2022). arXiv: 2205.02249 [hep-ph].

[41] G. Bell, R. Rahn, and J. Talbert. „Two-loop anomalous dimensions of generic dijet soft functions“. In: *Nucl. Phys. B* 936 (2018), pp. 520–541. DOI: 10.1016/j.nuclphysb.2018.09.026. arXiv: 1805.12414 [hep-ph]. №: SI-HEP-2018-16, QFET-2018-10, DESY 18-078, and DESY-18-078.

[42] G. Bell, R. Rahn, and J. Talbert. „Generic dijet soft functions at two-loop order: correlated emissions“. In: *JHEP* 07 (2019), p. 101. DOI: 10.1007/JHEP07(2019)101. arXiv: 1812.08690 [hep-ph]. №: DESY-18-209.

[43] G. Bell, R. Rahn, and J. Talbert. „Generic dijet soft functions at two-loop order: uncorrelated emissions“. In: *JHEP* 09 (2020), p. 015. DOI: 10.1007/JHEP09(2020)015. arXiv: 2004.08396 [hep-ph]. №: SI-HEP-2020-11, QFET-2020-01, NIKHEF 2020-007, and DESY-19-157.

[44] K. Brune. „NLO calculation of jet and beam functions in Soft-Collinear Effective Theory“. MA thesis. Universität Siegen, 2019.

[45] A. Basdew-Sharma, F. Herzog, S. Schrijnder van Velzen, and W. J. Waalewijn. „One-loop jet functions by geometric subtraction“. In: *JHEP* 10 (2020), p. 118. DOI: 10.1007/JHEP10(2020)118. arXiv: 2006.14627 [hep-ph]. №: NIKHEF 20-009.

[46] G. Bell, K. Brune, G. Das, and M. Wald. „Automation of Beam and Jet functions at NNLO“. In: *SciPost Phys. Proc.* 7 (2022), p. 021. DOI: 10.21468/SciPostPhysProc.7.021. arXiv: 2110.04804 [hep-ph]. №: SI-HEP-2021-25 and P3H-21-069.

[47] G. Bell, K. Brune, G. Das, and M. Wald. „The NNLO quark beam function for jet-veto resummation“ (July 2022). arXiv: 2207.05578 [hep-ph]. №: SI-HEP-2022-13 and P3H-22-064.

[48] G. Bell, K. Brune, G. Das, and M. Wald. „Automated Calculation of Beam Functions at NNLO“. Aug. 2022. arXiv: 2208.04847 [hep-ph]. №: SI-HEP-2022-18 and P3H-22-085.

[49] D. R. Green. *High P(T) physics at hadron colliders*. Vol. 22. 2005.

[50] M. E. Peskin and D. V. Schroeder. *An Introduction to quantum field theory*. Reading, USA: Addison-Wesley, 1995. ISBN: 978-0-201-50397-5.

[51] M. D. Schwartz. *Quantum Field Theory and the Standard Model*. Cambridge University Press, Mar. 2014. ISBN: 978-1-107-03473-0, 978-1-107-03473-0.

[52] *Particle Physics Standard Model Elementary Particle Higgs Boson PNG*. favpng.com.

[53] I. Brivio and M. Trott. „The Standard Model as an Effective Field Theory“. In: *Phys. Rept.* 793 (2019), pp. 1–98. DOI: 10.1016/j.physrep.2018.11.002. arXiv: 1706.08945 [hep-ph].

[54] A. Pich. „The Standard Model of Electroweak Interactions“. In: *CERN-2012-001, pp.1-50* (2012). arXiv: 1201.0537 [hep-ph]. №: IFIC/11-73; FTUV/12-0102.

[55] G. Zweig. „An SU_3 model for strong interaction symmetry and its breaking; Version 2“ (Feb. 1964). Version 1 is CERN preprint 8182/TH.401, Jan. 17, 1964, 80 p. URL: cds.cern.ch/record/570209. №: CERN-TH-412.

[56] O. W. Greenberg. „Spin and Unitary-Spin Independence in a Paraquark Model of Baryons and Mesons“. In: *Phys. Rev. Lett.* 13 (20 Nov. 1964), pp. 598–602. DOI: 10.1103/PhysRevLett.13.598. URL: link.aps.org/doi/10.1103/PhysRevLett.13.598.

[57] M. Gell-Mann. „A Schematic Model of Baryons and Mesons“. In: *Phys. Lett.* 8 (1964), pp. 214–215. DOI: 10.1016/S0031-9163(64)92001-3.

[58] R. Gupta. „Introduction to lattice QCD: Course“. *Les Houches Summer School in Theoretical Physics, Session 68: Probing the Standard Model of Particle Interactions*. July 1997, pp. 83–219. arXiv: hep-lat/9807028. №: LA-UR-98-3271.

[59] A. Khodjamirian. *Hadron Form Factors: From Basic Phenomenology to QCD Sum Rules*. Boca Raton, FL, USA: CRC Press, Taylor & Francis Group, 2020. ISBN: 978-1-138-30675-2, 978-1-315-14200-5.

[60] E. Shuryak. *Lectures on nonperturbative QCD (Nonperturbative Topological Phenomena in QCD and Related Theories)*. 2020. arXiv: 1812.01509 [hep-ph].

[61] H. Haber. „Useful relations among the generators in the defining and adjoint representations of SU(N)“. In: *SciPost Physics Lecture Notes* (Jan. 2021). ISSN: 2590-1990. DOI: 10.21468/scipostphyslectnotes.21. URL: dx.doi.org/10.21468/SciPostPhysLectNotes.21.

[62] J. M. Pendlebury et al. „Revised experimental upper limit on the electric dipole moment of the neutron“. In: *Phys. Rev. D* 92.9 (2015), p. 092003. DOI: 10.1103/PhysRevD.92.092003. arXiv: 1509.04411 [hep-ex].

[63] B. Graner, Y. Chen, E. Lindahl, and B. Heckel. „Reduced Limit on the Permanent Electric Dipole Moment of ^{199}Hg“. In: *Physical Review Letters* 116.16 (Apr. 2016). DOI: 10.1103/physrevlett.116.161601. arXiv: 1601.04339.

[64] J. E. Kim and G. Carosi. „Axions and the Strong CP Problem“. In: *Rev. Mod. Phys.* 82 (2010). [Erratum: Rev.Mod.Phys. 91, 049902 (2019)], pp. 557–602. DOI: 10.1103/RevModPhys.82.557. arXiv: 0807.3125 [hep-ph].

[65] L. D. Faddeev and V. N. Popov. „Feynman Diagrams for the Yang-Mills Field“. In: *Phys. Lett. B* 25 (1967). Ed. by J.-P. Hsu and D. Fine, pp. 29–30. DOI: 10.1016/0370-2693(67)90067-6.

[66] D. F. Litim and J. M. Pawlowski. „On General Axial Gauges for QCD“. In: *Nuclear Physics B - Proceedings Supplements* 74.1–3 (Mar. 1999), pp. 329–332. ISSN: 0920-5632. DOI: 10.1016/s0920-5632(99)00188-7. URL: dx.doi.org/10.1016/S0920-5632(99)00188-7.

[67] D. J. Pritchard and W. J. Stirling. „QCD Calculations in the Light Cone Gauge. 1“. In: *Nucl. Phys. B* 165 (1980), pp. 237–268. DOI: 10.1016/0550-3213(80)90086-3. №: DAMTP-79-1.

[68] P. P. Srivastava and S. J. Brodsky. „Light-front-quantized QCD in the light-cone gauge: The doubly transverse gauge propagator“. In: *Physical Review D* 64.4 (July 2001). ISSN: 1089-4918. DOI: 10.1103/physrevd.64.045006. URL: dx.doi.org/10.1103/PhysRevD.64.045006.

[69] *OPAL*. „Measurement of event shape distributions and moments in e+ e- —> hadrons at 91-GeV - 209-GeV and a determination of alpha(s)“. In: *Eur. Phys. J. C* 40 (2005), pp. 287–316. DOI: 10.1140/epjc/s2005-02120-6. arXiv: hep-ex/0503051. №: CERN-PH-EP-2004-044.

[70] *ATLAS*. „Measurement of event shapes at large momentum transfer with the ATLAS detector in *pp* collisions at $\sqrt{s} = 7$ TeV“. In: *Eur. Phys. J. C* 72 (2012), p. 2211. DOI: 10.1140/epjc/s10052-012-2211-y. arXiv: 1206.2135 [hep-ex]. №: CERN-PH-EP-2012-119 and SLAC-PUB-16021.

[71] *ATLAS*. „Measurement of event-shape observables in $Z \to \ell^+\ell^-$ events in *pp* collisions at $\sqrt{s} = 7$ TeV with the ATLAS detector at the LHC“. In: *Eur. Phys. J. C* 76.7 (2016), p. 375. DOI: 10.1140/epjc/s10052-016-4176-8. arXiv: 1602.08980 [hep-ex]. №: CERN-EP-2016-015.

[72] *Particle Data Group*. „Review of Particle Physics“. In: *PTEP* 2020.8 (2020), p. 083C01. DOI: 10.1093/ptep/ptaa104.

[73] A. H. Hoang, D. W. Kolodrubetz, V. Mateu, and I. W. Stewart. „Precise determination of α_s from the C-parameter distribution“. In: *Phys. Rev. D* 91.9 (2015), p. 094018. DOI: 10.1103/PhysRevD.91.094018. arXiv: 1501.04111 [hep-ph]. №: UWTHPH-2015-1, MIT-CTP-4630, and LPN14-128.

[74] A. Kardos, S. Kluth, G. Somogyi, Z. Tulipánt, and A. Verbytskyi. „Precise determination of $\alpha_S(M_Z)$ from a global fit of energy–energy correlation to NNLO+NNLL predictions“. In: *Eur. Phys. J. C* 78.6 (2018), p. 498. DOI: 10.1140/epjc/s10052-018-5963-1. arXiv: 1804.09146 [hep-ph].

[75] L. Randall and D. Tucker-Smith. „Dijet Searches for Supersymmetry at the LHC“. In: *Phys. Rev. Lett.* 101 (2008), p. 221803. DOI: 10.1103/PhysRevLett.101.221803. arXiv: 0806.1049 [hep-ph].

[76] M. Kramer, E. Popenda, M. Spira, and P. M. Zerwas. „Gluino Polarization at the LHC“. In: *Phys. Rev. D* 80 (2009), p. 055002. DOI: 10.1103/PhysRevD.80.055002. arXiv: 0902.3795 [hep-ph]. №: DESY-09-030, PITHA-09-08, and PSI-PR-09-02.

[77] C. Cesarotti and J. Thaler. „A Robust Measure of Event Isotropy at Colliders“. In: *JHEP* 08 (2020), p. 084. DOI: 10.1007/JHEP08(2020)084. arXiv: 2004.06125 [hep-ph]. №: MIT-CTP 5195.

[78] C. Cesarotti, M. Reece, and M. J. Strassler. „Spheres To Jets: Tuning Event Shapes with 5d Simplified Models“. In: *JHEP* 05 (2021), p. 096. DOI: 10.1007/JHEP05(2021)096. arXiv: 2009.08981 [hep-ph].

[79] C. Cesarotti, M. Reece, and M. J. Strassler. „The efficacy of event isotropy as an event shape observable“. In: *JHEP* 07 (2021), p. 215. DOI: 10.1007/JHEP07(2021)215. arXiv: 2011.06599 [hep-ph].

[80] M. Dasgupta and G. P. Salam. „Event shapes in e+ e- annihilation and deep inelastic scattering“. In: *J. Phys. G* 30 (2004), R143. DOI: 10.1088/0954-3899/30/5/R01. arXiv: hep-ph/0312283. №: CERN-TH-2003-306 and LPTHE-03-40.

[81] A. Banfi, G. P. Salam, and G. Zanderighi. „Phenomenology of event shapes at hadron colliders“. In: *JHEP* 06 (2010), p. 038. DOI: 10.1007/JHEP06(2010)038. arXiv: 1001.4082 [hep-ph].

[82] J. D. Bjorken and S. J. Brodsky. „Statistical Model for Electron-Positron Annihilation into Hadrons“. In: *Phys. Rev. D* 1 (5 Mar. 1970), pp. 1416–1420. DOI: 10.1103/PhysRevD.1.1416. URL: link.aps.org/doi/10.1103/PhysRevD.1.1416.

[83] E. Farhi. „Quantum Chromodynamics Test for Jets“. In: *Phys. Rev. Lett.* 39 (25 Dec. 1977), pp. 1587–1588. DOI: 10.1103/PhysRevLett.39.1587. URL: link.aps.org/doi/10.1103/PhysRevLett.39.1587.

[84] V. D. Barger, J. Ohnemus, and R. J. N. Phillips. „Event shape criteria for single lepton top signals“. In: *Phys. Rev. D* 48 (1993), R3953–R3956. DOI: 10.1103/PhysRevD.48.R3953. arXiv: hep-ph/9308216. №: MAD-PH-777, DTP-93-58, and RAL-93-054.

[85] V. V. Sudakov. „Vertex parts at very high energies in quantum electrodynamics“. In: *Zh. Eksp. Teor. Fiz.* 30 (1956), pp. 87–95. URL: cds.cern.ch/record/478063.

[86] G. Marchesini. „From QCD Lagrangian to Monte Carlo simulation“. In: *Lect. Notes Phys.* 737 (2008), pp. 159–180. arXiv: hep-ph/0701268. №: BICOCCA-FT-07-2.

[87] G. F. Sterman and S. Weinberg. „Jets from Quantum Chromodynamics“. In: *Phys. Rev. Lett.* 39 (1977), p. 1436. DOI: 10.1103/PhysRevLett.39.1436. №: HUTP-77/A044.

[88] B. R. Webber. „Fragmentation and hadronization“. In: *Int. J. Mod. Phys. A* 15S1 (2000). Ed. by J. Jaros and M. E. Peskin, pp. 577–606. DOI: 10.1142/S0217751X00005334. arXiv: hep-ph/9912292. №: CERN-TH-99-387 and CAVENDISH-HEP-99-16.

[89] L. G. Almeida, S. D. Ellis, C. Lee, G. Sterman, I. Sung, and J. R. Walsh. „Comparing and counting logs in direct and effective methods of QCD resummation“. In: *JHEP* 04 (2014), p. 174. DOI: 10.1007/JHEP04(2014)174. arXiv: 1401.4460 [hep-ph]. №: LA-UR-13-28363 and YITP-SB-14-02.

[90] I. W. Stewart. *8.851 Strong Interactions: Effective Field Theories of QCD. Spring 2006. Massachusetts Institute of Technology.* 2006. URL: ocw.mit.edu/courses/physics/8-851-strong-interactions-effective-field-theories-of-qcd-spring-2006/#.

[91] T. Becher, A. Broggio, and A. Ferroglia. *Introduction to Soft-Collinear Effective Theory*. Vol. 896. Springer, 2015. DOI: 10.1007/978-3-319-14848-9. arXiv: 1410.1892 [hep-ph]. №: PSI-PR-14-12.

[92] M. Beneke and V. A. Smirnov. „Asymptotic expansion of Feynman integrals near threshold“. In: *Nucl. Phys. B* 522 (1998), pp. 321–344. DOI: 10.1016/S0550-3213(98)00138-2. arXiv: hep-ph/9711391. №: CERN-TH-97-315.

[93] A. J. Larkoski, D. Neill, and J. Thaler. „Jet Shapes with the Broadening Axis“. In: *JHEP* 04 (2014), p. 017. DOI: 10.1007/JHEP04(2014)017. arXiv: 1401.2158 [hep-ph]. №: MIT–CTP-4512.

[94] T. Becher and G. Bell. „Analytic Regularization in Soft-Collinear Effective Theory“. In: *Phys. Lett. B* 713 (2012), pp. 41–46. DOI: 10.1016/j.physletb.2012.05.016. arXiv: 1112.3907 [hep-ph].

[95] T. Becher and M. Neubert. „Drell-Yan Production at Small q_T, Transverse Parton Distributions and the Collinear Anomaly“. In: *Eur. Phys. J. C* 71 (2011), p. 1665. DOI: 10.1140/epjc/s10052-011-1665-7. arXiv: 1007.4005 [hep-ph]. №: HD-THEP-10-13 and MZ-TH-10-26.

[96] C. W. Bauer and A. V. Manohar. „Shape function effects in B —> X(s) gamma and B —> X(u) l anti-nu decays“. In: *Phys. Rev. D* 70 (2004), p. 034024. DOI: 10.1103/PhysRevD.70.034024. arXiv: hep-ph/0312109. №: CALT-68-2465.

[97] A. Grozin, J. M. Henn, G. P. Korchemsky, and P. Marquard. „The three-loop cusp anomalous dimension in QCD and its supersymmetric extensions“. In: *JHEP* 01 (2016), p. 140. DOI: 10.1007/JHEP01(2016)140. arXiv: 1510.07803 [hep-ph]. №: DESY-15-186, IPHT-T15-174, and MITP-15-088.

[98] F. Herzog, B. Ruijl, T. Ueda, J. A. M. Vermaseren, and A. Vogt. „The five-loop beta function of Yang-Mills theory with fermions“. In: *JHEP* 02 (2017), p. 090. DOI: 10.1007/JHEP02(2017)090. arXiv: 1701.01404 [hep-ph]. №: NIKHEF-2017-001 and LTH-1117.

[99] T. Luthe, A. Maier, P. Marquard, and Y. Schroder. „The five-loop Beta function for a general gauge group and anomalous dimensions beyond Feynman gauge“. In: *JHEP* 10 (2017), p. 166. DOI: 10.1007/JHEP10(2017)166. arXiv: 1709.07718 [hep-ph]. №: BI-TP-2017-13, DESY-17-142, and IPPP-17-68.

[100] L. G. Almeida, S. D. Ellis, C. Lee, G. Sterman, I. Sung, and J. R. Walsh. „Comparing and counting logs in direct and effective methods of QCD resummation“. In: *JHEP* 04 (2014), p. 174. DOI: 10.1007/JHEP04(2014)174. arXiv: 1401.4460 [hep-ph]. №: LA-UR-13-28363 and YITP-SB-14-02.

[101] J.-y. Chiu, A. Fuhrer, A. H. Hoang, R. Kelley, and A. V. Manohar. „Soft-Collinear Factorization and Zero-Bin Subtractions“. In: *Phys. Rev. D* 79 (2009), p. 053007. DOI: 10.1103/PhysRevD.79.053007. arXiv: 0901.1332 [hep-ph].

[102] J.-Y. Chiu, A. Jain, D. Neill, and I. Z. Rothstein. „A Formalism for the Systematic Treatment of Rapidity Logarithms in Quantum Field Theory“. In: *JHEP* 05 (2012), p. 084. DOI: 10.1007/JHEP05(2012)084. arXiv: 1202.0814 [hep-ph]. №: INT-PUB-11-057 and CALT-68-2864.

[103] M. G. Echevarria, I. Scimemi, and A. Vladimirov. „Universal transverse momentum dependent soft function at NNLO“. In: *Phys. Rev. D* 93.5 (2016), p. 054004. DOI: 10.1103/PhysRevD.93.054004. arXiv: 1511.05590 [hep-ph]. №: NIKHEF-2015-34.

[104] Y. Li, D. Neill, and H. X. Zhu. „An exponential regulator for rapidity divergences“. In: *Nucl. Phys. B* 960 (2020), p. 115193. DOI: 10.1016/j.nuclphysb.2020.115193. arXiv: 1604.00392 [hep-ph]. №: FERMILAB-PUB-16-090-PPD-T and MIT-CTP-4795.

[105] M. Beneke and T. Feldmann. „Factorization of heavy to light form-factors in soft collinear effective theory“. In: *Nucl. Phys. B* 685 (2004), pp. 249–296. DOI: 10.1016/j.nuclphysb.2004.02.033. arXiv: hep-ph/0311335. №: PITHA-03-11 and CERN-TH-2003-286.

[106] J.-y. Chiu, F. Golf, R. Kelley, and A. V. Manohar. „Electroweak Sudakov corrections using effective field theory“. In: *Phys. Rev. Lett.* 100 (2008), p. 021802. DOI: 10.1103/PhysRevLett.100.021802. arXiv: 0709.2377 [hep-ph].

[107] R. H. Boels, T. Huber, and G. Yang. „Four-Loop Nonplanar Cusp Anomalous Dimension in N=4 Supersymmetric Yang-Mills Theory“. In: *Phys. Rev. Lett.* 119.20 (2017), p. 201601. DOI: 10.1103/PhysRevLett.119.201601. arXiv: 1705.03444 [hep-th]. №: SI-HEP-2017-10.

[108] J. M. Henn, T. Peraro, M. Stahlhofen, and P. Wasser. „Matter dependence of the four-loop cusp anomalous dimension“. In: *Phys. Rev. Lett.* 122.20 (2019), p. 201602. DOI: 10.1103/PhysRevLett.122.201602. arXiv: 1901.03693 [hep-ph]. №: MPP-2019-3, MITP/19-001, and ZU-TH 01/19.

[109] J. M. Henn, G. P. Korchemsky, and B. Mistlberger. „The full four-loop cusp anomalous dimension in $\mathcal{N} = 4$ super Yang-Mills and QCD“. In: *JHEP* 04 (2020), p. 018. DOI: 10.1007/JHEP04(2020)018. arXiv: 1911.10174 [hep-th]. №: IPhT-T19/155, MIT-CTP/5160, and MPP-2019-233.

[110] T. Huber, A. von Manteuffel, E. Panzer, R. M. Schabinger, and G. Yang. „The four-loop cusp anomalous dimension from the $N = 4$ Sudakov form factor“. In: *Phys. Lett. B* 807 (2020), p. 135543. DOI: 10.1016/j.physletb.2020.135543. arXiv: 1912.13459 [hep-th]. №: MSUHEP-19-030 and P3H-19-061.

[111] A. von Manteuffel, E. Panzer, and R. M. Schabinger. „Cusp and collinear anomalous dimensions in four-loop QCD from form factors“. In: *Phys. Rev. Lett.* 124.16 (2020), p. 162001. DOI: 10.1103/PhysRevLett.124.162001. arXiv: 2002.04617 [hep-ph]. №: MSUHEP-20-002.

[112] A. Chakraborty et al. „The $Hb\bar{b}$ vertex at four loops and hard matching coefficients in SCET for various currents“ (Apr. 2022). arXiv: 2204.02422 [hep-ph]. №: MSUHEP-22-014, P3H-22-034, TTP22-020, and SI-HEP-2022-06.

[113] R. N. Lee, A. von Manteuffel, R. M. Schabinger, A. V. Smirnov, V. A. Smirnov, and M. Steinhauser. „Quark and Gluon Form Factors in Four-Loop QCD“. In: *Phys. Rev. Lett.* 128.21 (2022), p. 212002. DOI: 10.1103/PhysRevLett.128.212002. arXiv: 2202.04660 [hep-ph]. №: MSUHEP-22-003, P3H-22-014, and TTP22-008.

[114] T. Becher, R. Frederix, M. Neubert, and L. Rothen. „Automated NNLL + NLO resummation for jet-veto cross sections“. In: *Eur. Phys. J. C* 75.4 (2015), p. 154. DOI: 10.1140/epjc/s10052-015-3368-y. arXiv: 1412.8408 [hep-ph]. №: CERN-PH-TH-2014-268 and MITP-14-099.

[115] D. Farhi, I. Feige, M. Freytsis, and M. D. Schwartz. „Streamlining resummed QCD calculations using Monte Carlo integration“. In: *JHEP* 08 (2016), p. 112. DOI: 10.1007/JHEP08(2016)112. arXiv: 1507.06315 [hep-ph].

[116] T. Becher and M. Neubert. „Toward a NNLO calculation of the anti-B —> X(s) gamma decay rate with a cut on photon energy. II. Two-loop result for the jet function“. In: *Phys. Lett. B* 637 (2006), pp. 251–259. DOI: 10.1016/j.physletb.2006.04.046. arXiv: hep-ph/0603140. №: CLNS-06-1954 and FERMILAB-PUB-06-057-T.

[117] T. Becher and M. D. Schwartz. „Direct photon production with effective field theory“. In: *JHEP* 02 (2010), p. 040. DOI: 10.1007/JHEP02(2010)040. arXiv: 0911.0681 [hep-ph].

[118] R. E. Cutkosky. „Singularities and discontinuities of Feynman amplitudes“. In: *J. Math. Phys.* 1 (1960), pp. 429–433. DOI: 10.1063/1.1703676.

[119] A. K. Leibovich, Z. Ligeti, and M. B. Wise. „Comment on quark masses in SCET“. In: *Phys. Lett. B* 564 (2003), pp. 231–234. DOI: 10.1016/S0370-2693(03)00565-3. arXiv: hep-ph/0303099. №: FERMILAB-PUB-03-035-T, LBNL-52196, and CALT-68-2432.

[120] G. Altarelli and G. Parisi. „Asymptotic Freedom in Parton Language“. In: *Nucl. Phys. B* 126 (1977), pp. 298–318. DOI: 10.1016/0550-3213(77)90384-4. №: LPTENS-77-6.

[121] J. M. Campbell and E. W. N. Glover. „Double unresolved approximations to multiparton scattering amplitudes“. In: *Nucl. Phys. B* 527 (1998), pp. 264–288. DOI: 10.1016/S0550-3213(98)00295-8. arXiv: hep-ph/9710255. №: DTP-97-82.

[122] S. Catani and M. Grazzini. „Collinear factorization and splitting functions for next-to-next-to-leading order QCD calculations“. In: *Phys. Lett. B* 446 (1999), pp. 143–152. DOI: 10.1016/S0370-2693(98)01513-5. arXiv: hep-ph/9810389. №: CERN-TH-98-325 and ETH-TH-98-27.

[123] D. A. Kosower and P. Uwer. „One loop splitting amplitudes in gauge theory“. In: *Nucl. Phys. B* 563 (1999), pp. 477–505. DOI: 10.1016/S0550-3213(99)00583-0. arXiv: hep-ph/9903515. №: SACLAY-SPH-T-99-032.

[124] Z. Bern, V. Del Duca, W. B. Kilgore, and C. R. Schmidt. „The infrared behavior of one loop QCD amplitudes at next-to-next-to leading order“. In: *Phys. Rev. D* 60 (1999), p. 116001. DOI: 10.1103/PhysRevD.60.116001. arXiv: hep-ph/9903516. №: BNL-HET-99-6, DFTT-16-99, UCLA-99-TEP-11, and MSUHEP-90325.

[125] S. Catani and M. Grazzini. „Infrared factorization of tree level QCD amplitudes at the next-to-next-to-leading order and beyond“. In: *Nucl. Phys. B* 570 (2000), pp. 287–325. DOI: 10.1016/S0550-3213(99)00778-6. arXiv: hep-ph/9908523. №: CERN-TH-99-263 and ETH-TH-99-22.

[126] G. F. R. Sborlini, D. de Florian, and G. Rodrigo. „Double collinear splitting amplitudes at next-to-leading order“. In: *JHEP* 01 (2014), p. 018. DOI: 10.1007/JHEP01(2014)018. arXiv: 1310.6841 [hep-ph]. №: LPN-13-069 and IFIC-13-73.

[127] M. Czakon. „A novel subtraction scheme for double-real radiation at NNLO“. In: *Phys. Lett. B* 693 (2010), pp. 259–268. DOI: 10.1016/j.physletb.2010.08.036. arXiv: 1005.0274 [hep-ph].

[128] T. Binoth and G. Heinrich. „An automatized algorithm to compute infrared divergent multiloop integrals“. In: *Nucl. Phys. B* 585 (2000), pp. 741–759. DOI: 10.1016/S0550-3213(00)00429-6. arXiv: hep-ph/0004013. №: LAPTH-789-00 and LPT-ORSAY-00-37.

[129] G. Heinrich. „Sector Decomposition“. In: *Int. J. Mod. Phys. A* 23 (2008), pp. 1457–1486. DOI: 10.1142/S0217751X08040263. arXiv: 0803.4177 [hep-ph]. №: IPPP-08-16 and DCPT-08-32.

[130] S. Borowka, G. Heinrich, S. P. Jones, M. Kerner, J. Schlenk, and T. Zirke. „SecDec-3.0: numerical evaluation of multi-scale integrals beyond one loop“. In: *Comput. Phys. Commun.* 196 (2015), pp. 470–491. DOI: 10.1016/j.cpc.2015.05.022. arXiv: 1502.06595 [hep-ph]. №: FR-PHENO-2015-001, MPP-2015-27, and ZU-TH-1-15.

[131] J. G. M. Gatheral. „Exponentiation of Eikonal Cross-sections in Nonabelian Gauge Theories“. In: *Phys. Lett. B* 133 (1983), pp. 90–94. DOI: 10.1016/0370-2693(83)90112-0. №: DAMTP 83/3.

[132] J. Frenkel and J. C. Taylor. „NONABELIAN EIKONAL EXPONENTIATION“. In: *Nucl. Phys. B* 246 (1984), pp. 231–245. DOI: 10.1016/0550-3213(84)90294-3. №: DAMTP-84/1.

[133] S. Borowka, G. Heinrich, S. Jahn, S. P. Jones, M. Kerner, J. Schlenk, and T. Zirke. „pySecDec: a toolbox for the numerical evaluation of multi-scale integrals“. In: *Comput. Phys. Commun.* 222 (2018), pp. 313–326. DOI: 10.1016/j.cpc.2017.09.015. arXiv: 1703.09692 [hep-ph]. №: MPP-2017-42, CERN-TH-2017-063, and IPPP-17-24.

[134] S. Borowka, G. Heinrich, S. Jahn, S. P. Jones, M. Kerner, and J. Schlenk. „A GPU compatible quasi-Monte Carlo integrator interfaced to pySecDec“. In: *Comput. Phys. Commun.* 240 (2019), pp. 120–137. DOI: 10.1016/j.cpc.

2019.02.015. arXiv: 1811.11720 [physics.comp-ph]. №: CERN-TH-2018-246, MPP-2018-279, ZU-TH 43/18, and IPPP/18/100.

[135] G. Heinrich et al. „Expansion by regions with pySecDec“. In: *Comput. Phys. Commun.* 273 (2022), p. 108267. DOI: 10.1016/j.cpc.2021.108267. arXiv: 2108.10807 [hep-ph]. №: KA-TP-19-2021, P3H-21-055, MPP-2021-131, IPPP/21/20, ZU-TH 35/21, and PSI-PR-21-17.

[136] J. Carter and G. Heinrich. „SecDec: A general program for sector decomposition“. In: *Comput. Phys. Commun.* 182 (2011), pp. 1566–1581. DOI: 10.1016/j.cpc.2011.03.026. arXiv: 1011.5493 [hep-ph]. №: IPPP-10-94 and DCPT-10-188.

[137] S. Borowka, J. Carter, and G. Heinrich. „Numerical Evaluation of Multi-Loop Integrals for Arbitrary Kinematics with SecDec 2.0“. In: *Comput. Phys. Commun.* 184 (2013), pp. 396–408. DOI: 10.1016/j.cpc.2012.09.020. arXiv: 1204.4152 [hep-ph]. №: IPPP-12-22, DCPT-12-44, and MPP-2012-75.

[138] J. A. M. Vermaseren. „New features of FORM“ (Oct. 2000). arXiv: math-ph/0010025.

[139] J. Kuipers, T. Ueda, and J. A. M. Vermaseren. „Code Optimization in FORM“. In: *Comput. Phys. Commun.* 189 (2015), pp. 1–19. DOI: 10.1016/j.cpc.2014.08.008. arXiv: 1310.7007 [cs.SC]. №: NIKHEF-2013-036, TTP13-031, and SFB-CPP-13-80.

[140] T. Hahn. „CUBA: A Library for multidimensional numerical integration“. In: *Comput. Phys. Commun.* 168 (2005), pp. 78–95. DOI: 10.1016/j.cpc.2005.01.010. arXiv: hep-ph/0404043. №: MPP-2004-40.

[141] T. Hahn. „Concurrent Cuba“. In: *J. Phys. Conf. Ser.* 608.1 (2015). Ed. by L. Fiala, M. Lokajicek, and N. Tumova, p. 012066. DOI: 10.1088/1742-6596/608/1/012066. arXiv: 1408.6373 [physics.comp-ph]. №: MPP-2014-327.

[142] K. Yao and J. Gao. „Law of Large Numbers for Uncertain Random Variables“. In: *IEEE Transactions on Fuzzy Systems* 24 (Jan. 2015), pp. 1–1. DOI: 10.1109/TFUZZ.2015.2466080.

[143] I. Bárány and V. Vu. „Central limit theorems for Gaussian polytopes“. In: *The Annals of Probability* 35.4 (2007), pp. 1593–1621. DOI: 10.1214/009117906000000791. URL: doi.org/10.1214/009117906000000791.

[144] G. P. Lepage. „A New Algorithm for Adaptive Multidimensional Integration“. In: *J. Comput. Phys.* 27 (1978), p. 192. DOI: 10.1016/0021-9991(78)90004-9. №: SLAC-PUB-1839-REV and SLAC-PUB-1839.

[145] G. P. Lepage. „VEGAS: An adaptive multidimensional integration program“ (Mar. 1980). №: CLNS-80/447.

[146] T. Becher and G. Bell. „The gluon jet function at two-loop order“. In: *Phys. Lett. B* 695 (2011), pp. 252–258. DOI: 10.1016/j.physletb.2010.11.036. arXiv: 1008.1936 [hep-ph].

[147] C. F. Berger, T. Kucs, and G. F. Sterman. „Event shape / energy flow correlations“. In: *Phys. Rev. D* 68 (2003), p. 014012. DOI: 10.1103/PhysRevD.68.014012. arXiv: hep-ph/0303051. №: YITP-SB-03-06.

[148] A. Hornig, C. Lee, and G. Ovanesyan. „Effective Predictions of Event Shapes: Factorized, Resummed, and Gapped Angularity Distributions“. In: *JHEP* 05 (2009), p. 122. DOI: 10.1088/1126-6708/2009/05/122. arXiv: 0901.3780 [hep-ph]. №: UCB-PTH-09-03.

[149] G. Bell, A. Hornig, C. Lee, and J. Talbert. „e^+e^- angularity distributions at NNLL′ accuracy“. In: *JHEP* 01 (2019), p. 147. DOI: 10.1007/JHEP01(2019)147. arXiv: 1808.07867 [hep-ph]. №: SI-HEP-2018-19, LA-UR-18-24071, DESY-18-083, and DESY 18-083.

[150] S. Catani and M. H. Seymour. „The Dipole formalism for the calculation of QCD jet cross-sections at next-to-leading order“. In: *Phys. Lett. B* 378 (1996), pp. 287–301. DOI: 10.1016/0370-2693(96)00425-X. arXiv: hep-ph/9602277. №: CERN-TH-96-28.

[151] S. Catani and M. H. Seymour. „A General algorithm for calculating jet cross-sections in NLO QCD“. In: *Nucl. Phys. B* 485 (1997). [Erratum: Nucl.Phys.B 510, 503–504 (1998)], pp. 291–419. DOI: 10.1016/S0550-3213(96)00589-5. arXiv: hep-ph/9605323. №: CERN-TH-96-029 and CERN-TH-96-29.

[152] T. Becher and X. Garcia i Tormo. „Factorization and resummation for transverse thrust“. In: *JHEP* 06 (2015), p. 071. DOI: 10.1007/JHEP06(2015)071. arXiv: 1502.04136 [hep-ph].

[153] T. Becher, X. Garcia i Tormo, and J. Piclum. „Next-to-next-to-leading logarithmic resummation for transverse thrust“. In: *Phys. Rev. D* 93.5 (2016). Erratum: Phys.Rev.D 93, 079905 (2016), p. 054038. DOI: 10.1103/PhysRevD.93.054038. arXiv: 1512.00022 [hep-ph].

[154] D. Bertolini, T. Chan, and J. Thaler. „Jet Observables Without Jet Algorithms“. In: *JHEP* 04 (2014), p. 013. DOI: 10.1007/JHEP04(2014)013. arXiv: 1310.7584 [hep-ph]. №: MIT-CTP-4502.

[155] S. D. Ellis and D. E. Soper. „Successive combination jet algorithm for hadron collisions“. In: *Phys. Rev. D* 48 (1993), pp. 3160–3166. DOI: 10.1103/PhysRevD.48.3160. arXiv: hep-ph/9305266. №: CERN-TH-6860-93.

[156] S. Moch, J. A. M. Vermaseren, and A. Vogt. „The Quark form-factor at higher orders“. In: *JHEP* 08 (2005), p. 049. DOI: 10.1088/1126-6708/2005/08/049. arXiv: hep-ph/0507039. №: SFB-CPP-05-26, DCPT-05-66, IPP-05-33, NIKHEF-05-011, and DESY-05-106.

[157] S. Moch, J. A. M. Vermaseren, and A. Vogt. „Three-loop results for quark and gluon form-factors“. In: *Phys. Lett. B* 625 (2005), pp. 245–252. DOI: 10.1016/j.physletb.2005.08.067. arXiv: hep-ph/0508055. №: DESY-05-138, SFT-CPP-05-34, NIKHEF-05-013, DCPT-05-88, and IPPP-05-44.

Acknowledgements

First, I would like to thank Prof. Dr. Guido Bell for giving me the opportunity to perform my PhD under his supervision. Furthermore, I am grateful for the being patience at explaining everything I did not immediately understand, even if some of those questions in hindsight are blatantly obvious.

I would like to thank PD Dr. Tobias Huber for helpful discussions on fundamental concepts and to be the second referee of this thesis. I would like to thank Prof. Dr. Markus Cristinziani and PD Dr. Matthias Kleinmann for joining my thesis committee.

I would like to thank Dr. Jan Piclum for the intense proofreading and for helpful discussions on the technical details of writing a thesis. Furthermore, I would like to thank Dr. Goutam Das for the encouraging discussions during our regular afternoon coffees and his support in writing this thesis being it proofreading or cross-checking some calculations.

I would like to express my gratitude towards the former and present members of the Theoretical Particle Physics Institute at University Siegen; it was a great pleasure to be part of such an amazing work group. In particular, I would like to thank Lars-Thorben Moos, Kevin Olschewsky, Dr. Simon Braß, Dr. Jan Piclum and Prof. Dr. Wolfgang Kilian for the many entertaining game nights.

Last, but certainly not least, I would like to thank my family and friends, especially, my parents Frank and Heike and my brother Marvin for your incredible support and the solidarity you have given me during my time as PhD student. Without you, I certainly would not have made it.